CRUSTAL STRUCTURE IN THE SOCORRO AREA OF THE RIO GRANDE RIFT FROM TIME-TERM ANALYSIS

by

Paul J. Singer

Submitted in Partial Fulfillment of the
Requirements for the Degree of
Doctor of Philosophy

New Mexico Institute of Mining and Technology
Socorro, New Mexico

May 1989

ABSTRACT

Local and regional earthquakes and explosions recorded by the New Mexico Tech telemetered network were used to examine the travel-time characteristics of P-waves in the central Rio Grande rift around Socorro, New Mexico. The region is well known for its high seismicity and the presence of a thin, extensive magma sill at mid-crustal depths. Unmodified and modified time-term analyses were used to obtain P-wave velocities and station delays for three major refractors: the Phanerozoic-Precambrian contact, the Conrad discontinuity in the mid-crust, and the Mohorovičić discontinuity.

The 265 Pg data from local explosions gave an average velocity of 5.95 ± 0.03 km/s (1 s.d.) for the basement. The Pg velocity, however, showed a distinct dependence on source distance, implying a velocity gradient with depth in the Precambrian.

Existing as a weak first arrival with a narrow distance window, the P* data set contained only 72 quality readings. These data yielded a low sub-Conrad velocity of 6.40 ± 0.16 km/s (1 s.d.). This depressed P* velocity is most likely caused by elevated temperatures resulting from the emplacement of magma at the base of the upper crust.

A sub-Moho velocity of 8.14 ± 0.05 km/s (1 s.d.) resulted from the analysis of 402 Pn data. This velocity precludes the presence of asthenospheric material in direct contact with the base of the crust in this section of the rift. The Moho shows a strong dip to the northwest of 4.6 ± 0.5° and seems to explain the low 7.6 km/s velocity reported by Olsen et al. (1979), from a north-trending refraction profile.

No anisotropy was evident in the upper mantle when the area was con-

sidered as a whole, but when it was subdivided by a north-south bisector, analyses yielded a north-south oriented anisotropy of ~0.25 km/s in the eastern region, and an east-west oriented anisotropy of similar magnitude in the west. While there are a number of possibilities, the observations could be due to movement on the Hot Springs-Montosa fault during Eocene times.

The Pn velocity showed a distance dependence, decreasing with increasing epicentral distance. While this effect is is most likely the result of attenuation, a negative velocity gradient in the upper mantle could also be a factor.

ACKNOWLEDGEMENTS

I would like to thank my principal advisor, Dr. Allan R. Sanford, for his inspiration, assistance, and encouragement during the course of my studies at New Mexico Tech. His technical expertise and guidance greatly improved the quality of the dissertation. I would also like to thank the members of my committee, Dr. John Knapp, Mr. Larry Jaksha, Dr. Allan Gutjahr, and Dr. Antonius Budding, for their suggestions and ideas during the course of numerous discussions, and for reviewing this manuscript. I would also like to thank Dr. Jim Murdock for his technical advice during the course of this project.

Thanks are due for the efforts of many fellow graduate and undergraduate students. I am particularly grateful to Jon Ake for his friendship and constant help over the years. Thanks to Chris Zervas of the University of Washington for providing much of the software used in the time-term analyses, and Annette Schaefer-Perrini, who wrote many of the graphics programs. Special thanks are also due to Cliff Jarman for his assistance in locating many of the earthquakes used in this study.

I would like to express my appreciation to the Geophysical Research Center, the Society of Explorations Geophysics, and the New Mexico Geological Society for providing a major part of the financial support for this work. The staff of the New Mexico Tech Computing Center gave excellent computational support during this project.

Finally, I would like to thank my family and friends for their support and assistance. In particular, very special thanks are due to my parents, Dr. and Mrs. Edward Singer, for their never-ending encouragement and support.

Table of Contents

List of Figures

List of Tables

List of Maps

INTRODUCTION

Purpose and Scope

The Rio Grande rift is one of the major geologic and physiographic structures of the western United States. As such, and because of its unique geologic and geophysical character, the rift has been the subject of extensive research utilizing a variety of techniques. Nevertheless, there still exist many ambiguities and questions about the velocity structure beneath the central rift, the nature of the major seismic boundaries within the crust, and the existence and position of an asthenospheric upwarp beneath the crust.

The study area, the region surrounding Socorro, is one of the major transitional zones within the Rio Grande rift. North of Socorro, the rift is a significant morpho-tectonic feature, a single line of deep, narrow, axially-aligned grabens. To the south, the structure is much less physiographically distinct, resembling the surrounding Basin and Range province. The Socorro region is the most seismically active part of the rift, and is of particular interest since near the depth of the Conrad discontinuity exists a mid-crustal magma body.

This research project involved applying the time-term method to refraction data collected from earthquakes and explosions recorded by the Socorro seismograph network. The general objectives of this study were:

1. to determine the seismic velocities of the major refracting layers within the crust. These are the Paleozoic-Precambrian boundary, the Conrad discontinuity (separating the upper and lower crust), and the Mohorovičić discontinuity (the crust-mantle interface);
2. to establish for each of the refraction layers if velocity varied geographically or azimuthally, or was influenced by dip;

3. to estimate the time terms and thereby the depths to the various refractors beneath the event sites and recording stations, and relate them to the local geology whenever possible.

Secondary objectives included:

1. using kriging to quantify the spatial variability of the depth estimates for each refractor,
2. modelling the refractor surfaces,
3. establishing the absence or presence an asthenospheric upwarp at the base of the crust, and
4. attempting to bring into accord the results of previous studies in the region.

General Outline of Method

In this study, the velocity structure and characteristics of the major refractors in the crust and upper mantle in the central Rio Grande rift were determined from the analysis of earthquake and explosion seismograms recorded at a wide range of distances. The arrival times and epicentral distances of various phases on the seismograms were analyzed using both unmodified and modified time-term techniques, and models for each of the crustal and upper mantle refractors proposed. The models for each refractor were compared to one another and the observed data. The resulting best-fitting models were then compared to models of local and general structure as inferred from other studies in the Rio Grande rift.

Geological and Geophysical Setting

The study area is located in the central Rio Grande rift near Socorro, New Mexico. The Rio Grande rift is characterized by a series of north-northeast trending en echelon grabens extending south from Leadville, Colorado into northern Mexico (Chapin, 1971) (Figure 1). The rift is composed of three distinct segments: (1) the northern rift, extending from Leadville to the Colorado-New Mexico border; (2) the central rift, which begins at the state line and ends near Socorro; (3) the southern rift, extending south from Socorro into Chihuahua, Mexico. The central rift is bounded by the Great Plains to the east, and the Colorado Plateau to the west (Figure 2). Details on the large scale aspects of the rift may be found in Chapin (1971), Chapin and Seager (1975), Sanford et al. (1977), Cordell (1978), the volume *Rio Grande Rift: Tectonics and Magmatism* edited by Riecker (1979), Baldridge et al. (1984), as well as the special section on the rift in the *Journal of Geophysical Research 91* , B6 (1986).

Figure 3 shows the major physiographic features in the Socorro area in addition to the current station locations in the seismic network. The geologic record in the area begins at ~1.7 bya, the age of the oldest exposed Precambrian rocks (Condie and Budding, 1979). The structural grain in the Precambrian generally trends north-northeast and has probably influenced subsequent faulting and structural development (Chapin et al., 1978).

Thick sedimentary sequences were deposited during the Paleozoic and are preserved in the Socorro-Lemitar Mountains and the Magdalena Mountains. During the late Paleozoic, the region experienced tectonic rejuvenation; it underwent broad deformation during the Laramide. A large highland existed in the Eocene along the western margin of the rift, with subsequent erosion remov-

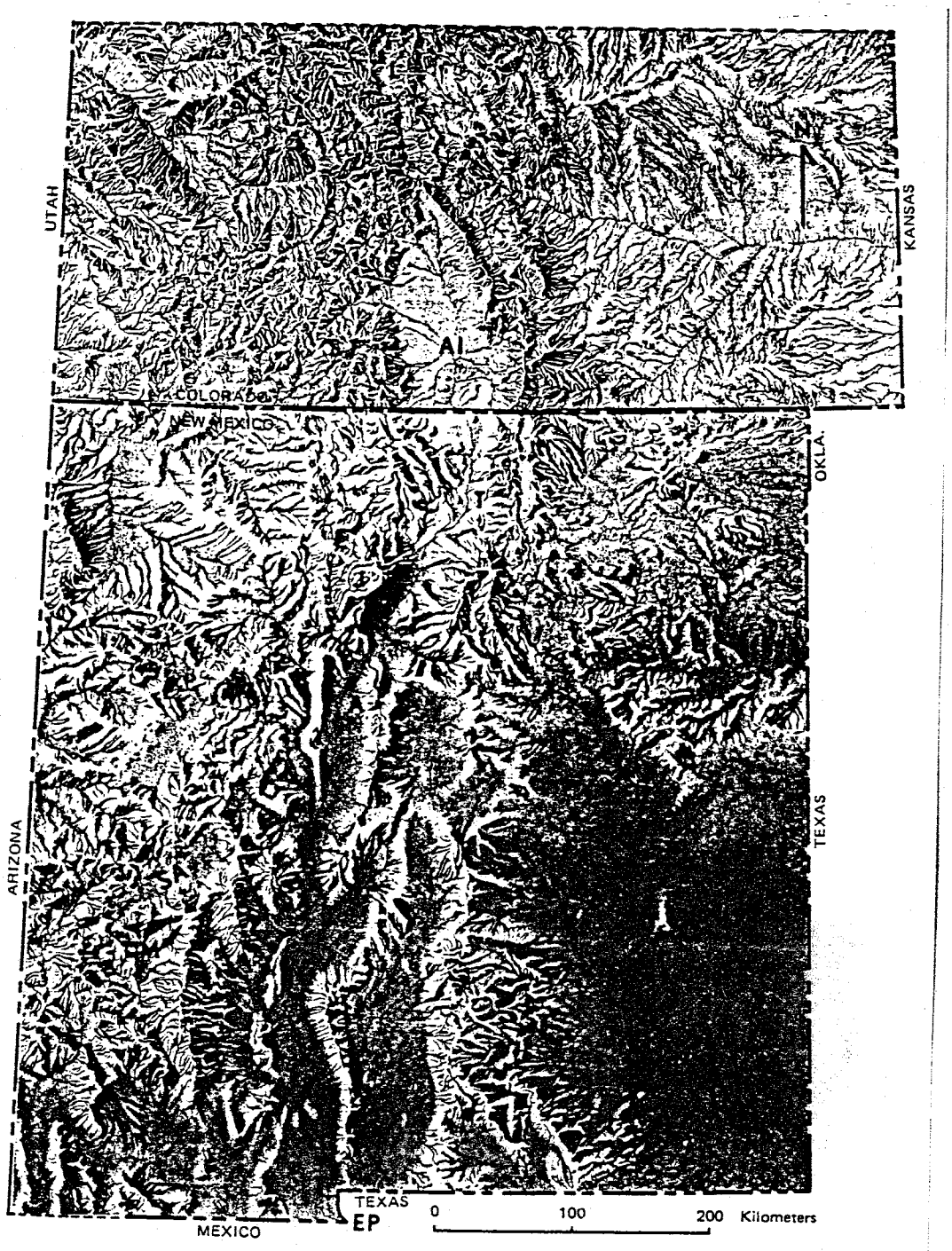

Figure 1: Shaded relief map of the Rio Grande rift. L = Leadville, Al = Alamosa, SJ = San Juan volcanic field, T = Taos, J = Jemez volcanic field, A = Albuquerque, S = Socorro, SA = San Augustine rift, DM = Datil-Mogollon volcanic field, LC = Las Cruces, EP = El Paso (after Chapin, 1979).

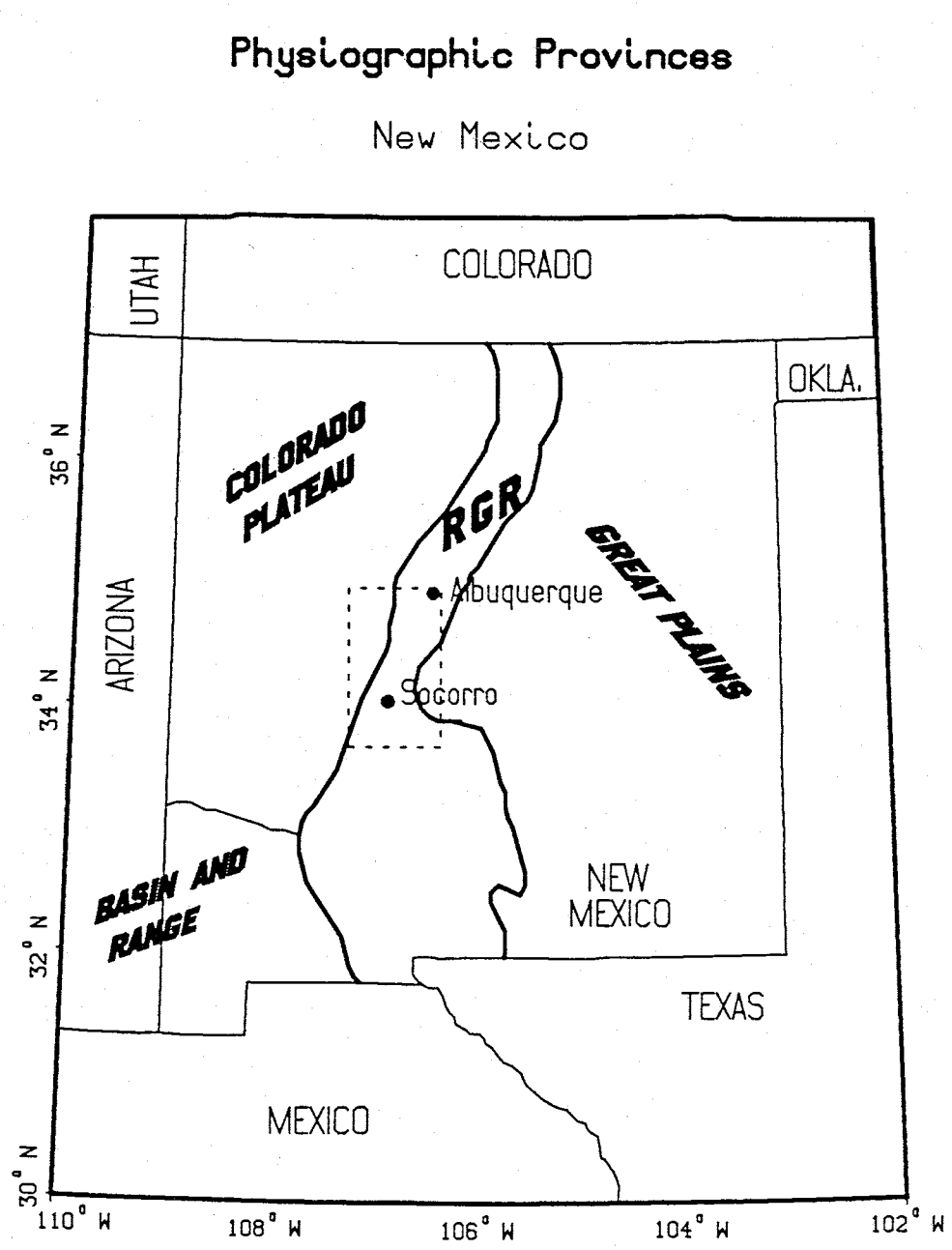

Figure 2: Physiographic provinces within the state of New Mexico (after Sinno et al., 1986). Box indicates area of Figure 3.

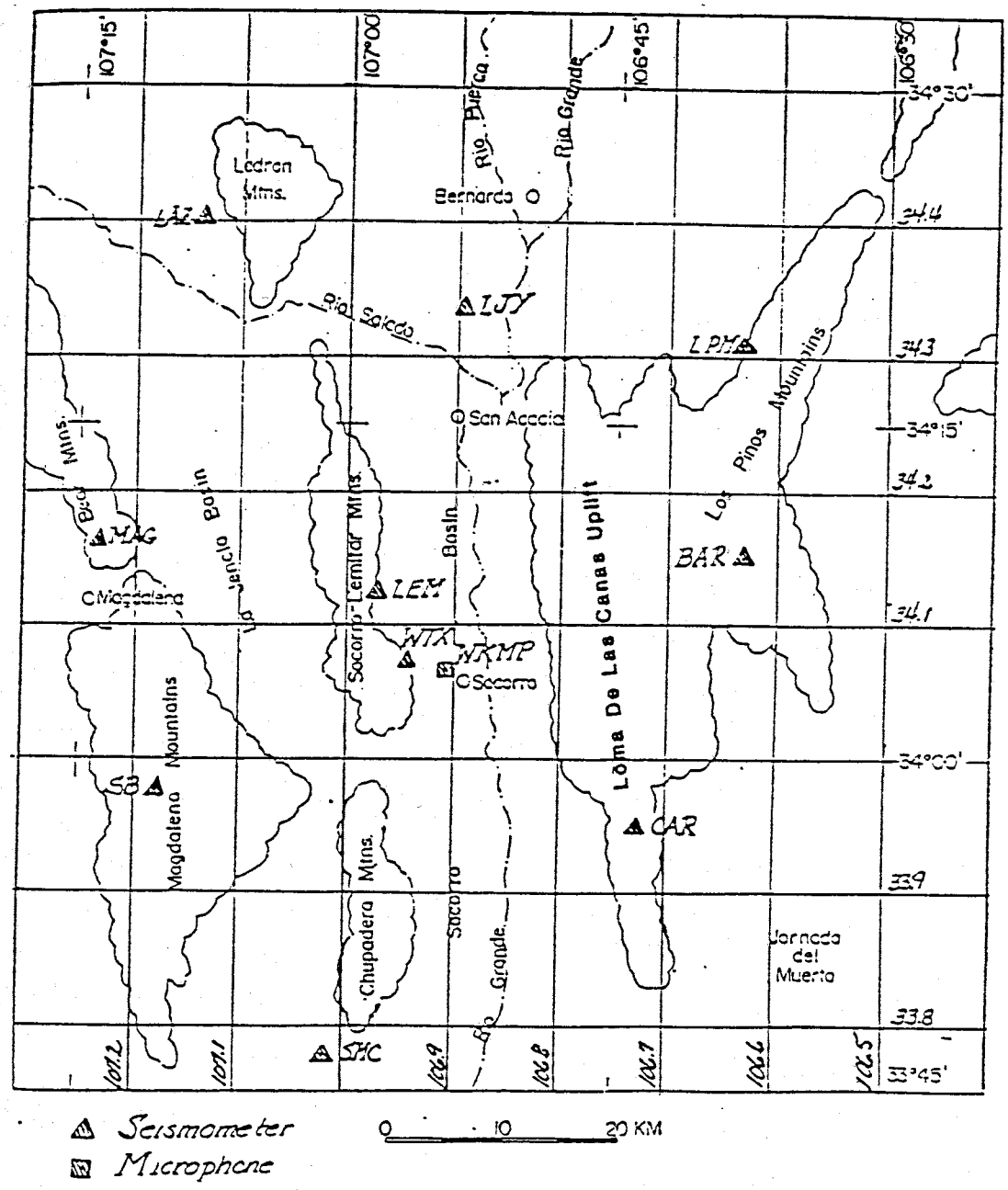

Figure 3: Major physiographic features near Socorro. Also shown are the locations of some of the Socorro network seismograph stations as of mid-1984.

ing much of the Mesozoic section (Cather, 1983). As a result, Tertiary rocks have been deposited directly on late Paleozoic and Precambrian rocks through much of the region.

During Oligocene and Miocene times, that region was covered with calc-alkaline ash flow sheets from the Datil-Mogollon volcanic field, located to the southwest of the study area (Chapin and Seager, 1975). The Socorro cauldron developed about 33 mya as the northeast extension of this volcanic field (Osburn and Chapin, 1983).

Rifting began in the Socorro area about 33 mya (Chapin, 1983), and was contemporaneous with the later stages of cauldron development. Extension proceeded in a generally uniform manner until the mid-Miocene, when a tectonic lull resulted in the filling of large basins with bolson-type sediments. This sedimentation was interrupted by the rhyolitic dome eruptions along the north moat of the Socorro cauldron about 7 to 12 mya (Chapin et al., 1978). Following this, the Socorro-Lemitar and Magdalena mountain blocks were uplifted and rotated (Chamberlin, 1983). At present, tectonic activity continues and has been accompanied by the intrusion and eruption of flood basalts during the last 4 my (Kelley and Kudo, 1978).

The area of interest in this study lies within the central RGR. Here, the rift changes in character from a single line of axially interconnected basins north of Socorro becoming a series of parallel basins with intergraben horst blocks to the south. A transitional zone, the region nevertheless possesses a distinct geological and geophysical character including a large mid-crustal magma body (Sanford et al., 1977; Rinehart et al., 1979), high heat flow (Reiter and Smith, 1977), an area of positive surface uplift (Reilinger et al., 1980; Larsen et al., 1986), a high seismicity level (Sanford et al., 1979), the intersection of two major volcanic

lineaments (Chapin et al., 1978), and extensive north-south trending Quaternary faulting (Machette and McGimsey, 1982; Sanford et al., 1972).

Seismic monitoring in this area began in 1962, and is presently being undertaken using the Socorro seismograph network (Figure 4). This region is the most seismically active portion of the RGR (Sanford and Holmes, 1962; Sanford et al., 1983) with a historical record including major earthquakes and discontinuous microearthquake activity (Sanford et al., 1979). Many of these microearthquakes occur in swarms, and several hundred shocks are located each year. Previous studies (Shuleski, 1976; Johnston, 1978; Ward, 1980; Sanford and Schlue, 1980; Carpenter and Sanford, 1985) have interpreted some of the swarm activity to be related to the intrusion of small amounts of magma into the crust. Such intrusion would contribute to elevated temperatures in the upper crust (Reiter and Smith, 1977).

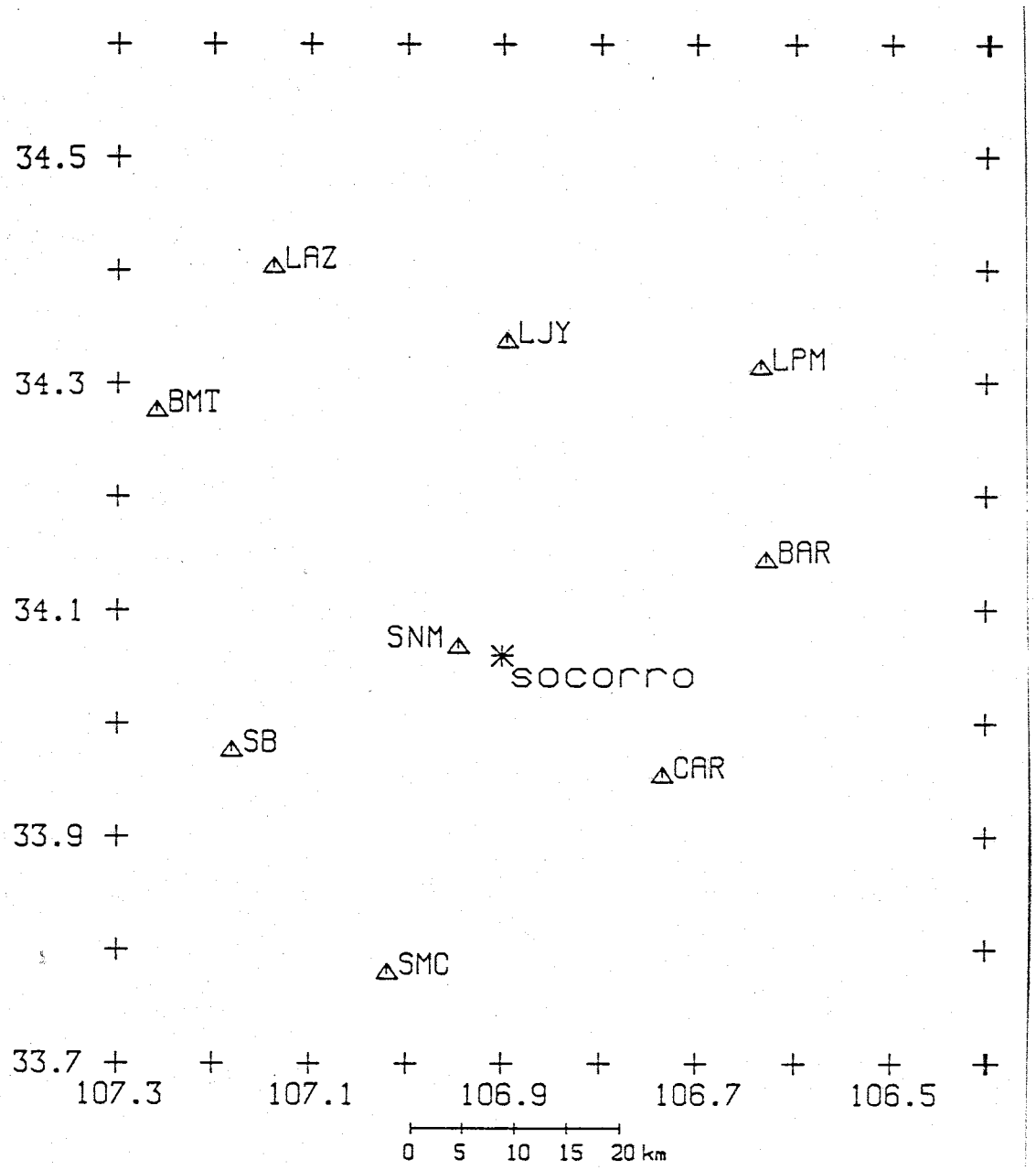

Figure 4: Station locations of the Socorro seismograph network as of mid-1989.

PREVIOUS CRUSTAL STUDIES

Figure 5 is a compilation of crustal models developed from previous crustal studies in the state of New Mexico. A majority of these models were obtained from seismic refraction profiles whose locations are shown in Figure 6. The number on the line refers to the crustal model of the same number in the previous figure.

The 550 km long GASBUGGY profile (Line 1, Figure 6) provided the first published refraction information about the crustal structure of the Rio Grande rift (Toppozada and Sanford, 1976). The initial unreversed profile yielded an inter-rift basement velocity of 5.8 km/s, a 6.5 km/s velocity for the mid-crust, and a sub-Moho velocity of 8.12 km/s. Toppozada (1974) estimated 2° northward dip on the Moho along the profile. Adjusting for this dip yielded an upper mantle velocity of 7.9 km/s (Model 1, Figure 5). An average crustal thickness of 39.9 km was reported along the profile length, with no less than a 30 km thick crust being allowed in the vicinity of Albuquerque. This line, however, included a large area west of the topographic expression of the rift. Thus, the results may well be affected by non-rift structures, specifically the Colorado Plateau.

The earlier refraction lines of Dee (1973) are also not pure rift paths (Lines 6, Figure 6), and traverse at least one other geologic province before entering the rift. Model 6 of Figure 5 shows the inferred crustal model. The 6.2 km/s crustal velocity agrees with the 6.15 km/s extra-rift velocity for the upper crust of Toppozada and Sanford (1976). For surface sources, like the mine blasts used in Dee's study, critical refractions from the mid-crust never appear as first arrivals. Since this study only used first arrival data from surface sources, no mid-crustal layer was seen. The unreversed 8.1 km/s velocity is notably higher

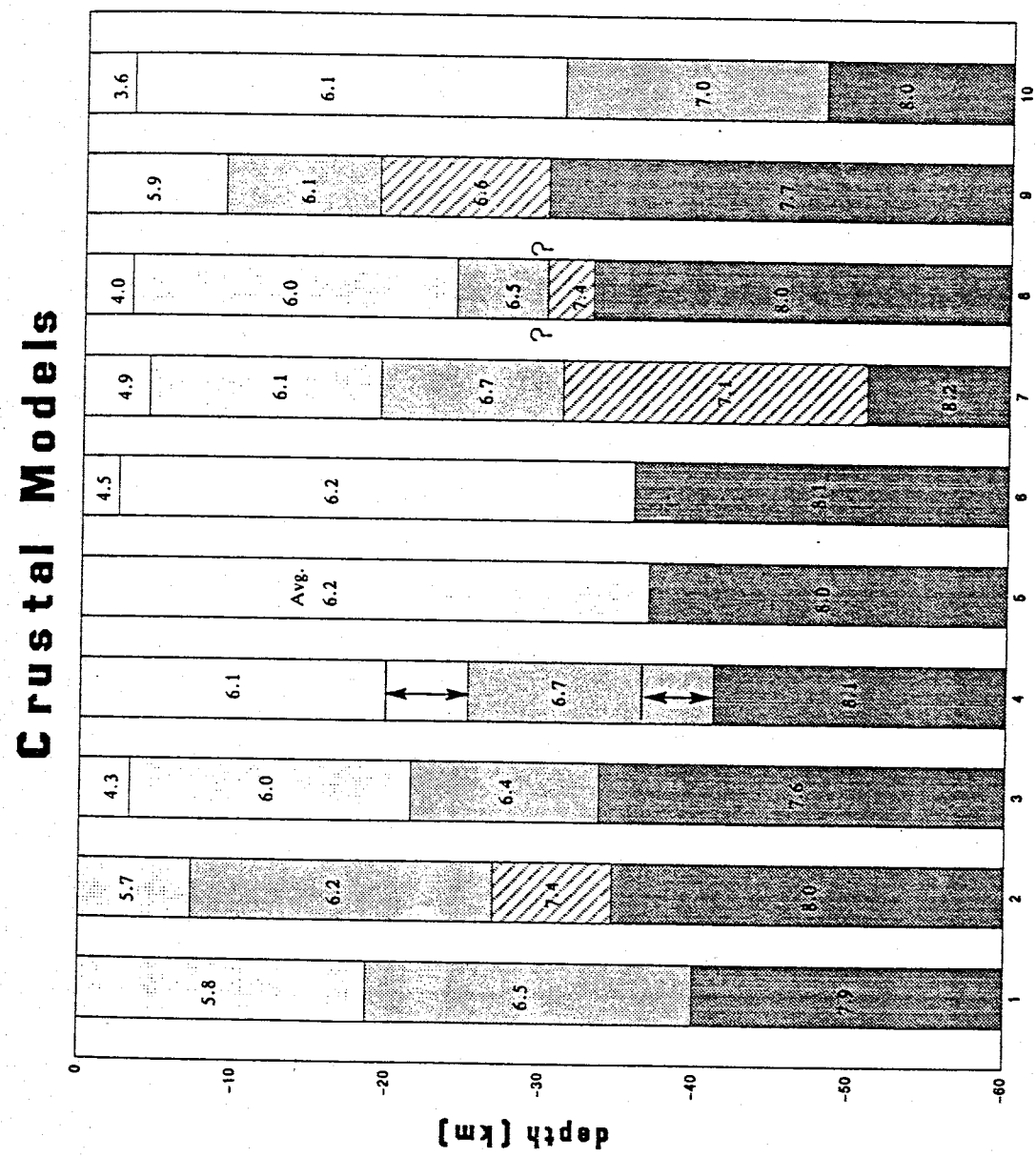

Figure 5: Crustal sections for New Mexico.

References for Crustal Sections

1. Toppozada and Sanford, 1976.

2. Cook, McCullar, Decker, and Smithson, 1979.

3. Olsen, Keller, and Stewart, 1979.

4. Phinney, 1964.

5. Murdock and Jaksha, 1981.

6. Dee, 1973.

7. Stewart and Pakiser, 1962.

8. Jaksha, 1982.

9. Sinno, Daggett, Keller, Morgan, and Harder, 1986.

10. Jaksha and Evans, 1984.

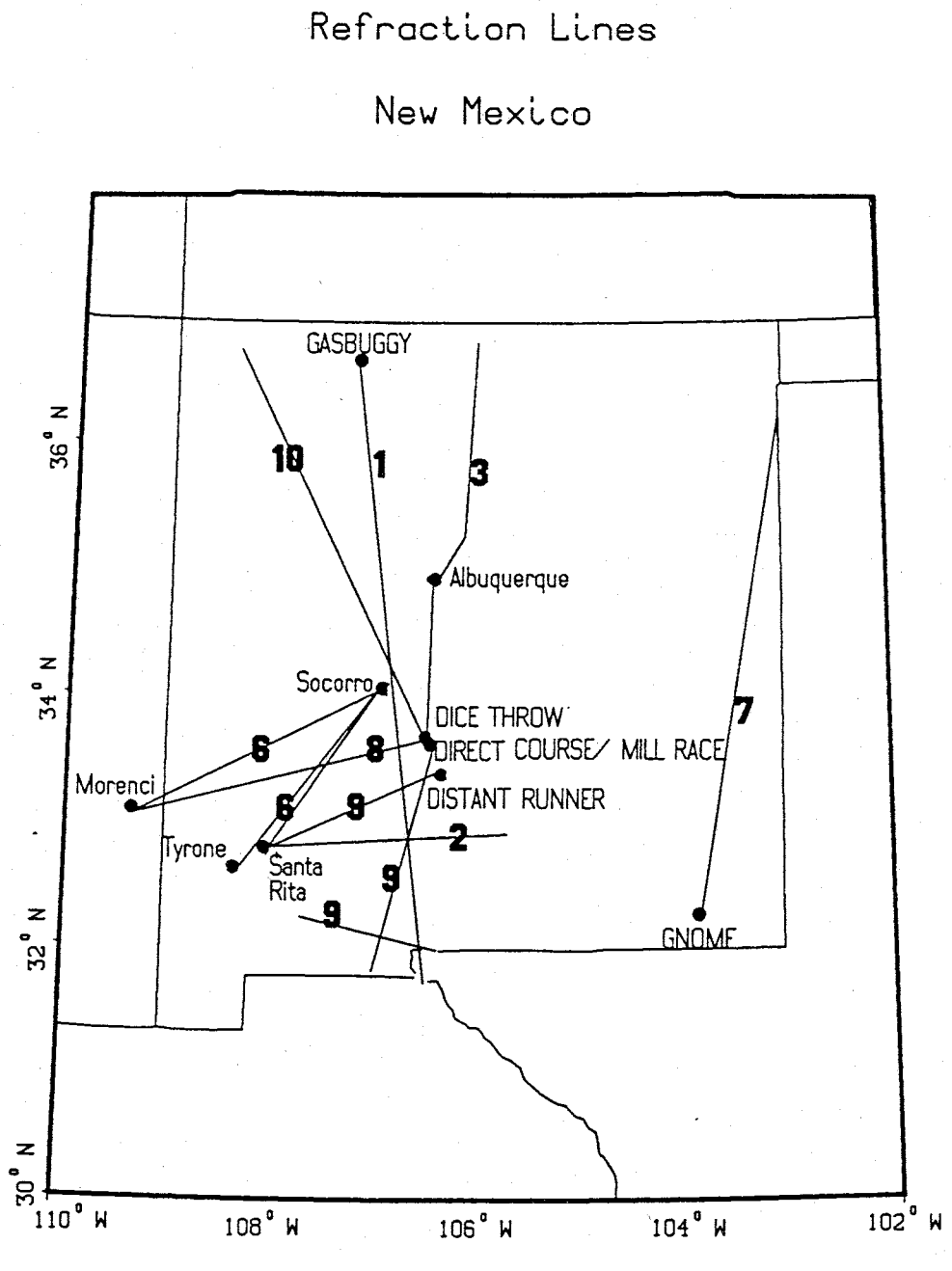

Figure 6: Index map showing position of lines for previous refraction work in New Mexico. The lines are numbered according to Figure 5.

than the final value of Toppozada and Sanford (1976). However, Dee's value may be affected by dip, non-rift structures, or a non-uniform Moho velocity beneath the rift.

In the southern rift, previous refraction surveys present a far from consistent picture, with crustal models showing considerable variation in both layer thicknesses and velocities. The mantle velocity is of particular interest since it is directly related to the nature of the thermal regime and the rock composition at the base of the crust. A depressed mantle velocity is indicative of extremely elevated temperatures below the Moho, and/or asthenospheric rocks in direct contact with the crust. Sinno et al. (1986) (Model 9, Figure 5; Lines 9, Figure 6) report a depressed mantle velocity of 7.7 km/s, while Cook et al. (1979) (Model 2, Figure 5; Line 2, Figure 6) report a normal 8.0 km/s velocity for the same general area. For the unreversed axial (N-S Line 9, Figure 6) and pipeline road (southernmost E-W Line 9, Figure 6) lines of Sinno et al. (1986), a velocity of 7.95 km/s provided the best fit line through the Pn data. The differences between this value and the 7.7 km/s velocity of the reversed E-W line (north E-W Line 9, Figure 6) are interpreted to be the result of crustal thinning, although no dip on the Moho was observed on the reversed E-W line. This seems to require a very complicated crust-mantle interface. Yet even if the upper mantle velocities of Sinno et al. (1986) and Cook et al. (1979) could be reconciled, the the velocities and depths of the major crustal boundaries of the two models would still be in basic disagreement. There does not appear to be a clear picture of the velocity structure of the southern rift at this time.

Similarly, models of the central rift show great variability. The most notable difference centers on the 0.5 km/s range in Pn velocities. Olsen et al. (1979) (Model 3, Figure 5) reported a very low Pn velocity of 7.6 km/s for a north running profile in the central rift (Line 3, Figure 6). It should be noted that much

of this unreversed line was actually outside the physiographic boundaries of the rift (compare Figures 2 and 6). The 7.6 km/s velocity differs distinctly from the 8.0 km/s result of Murdock and Jaksha (1981) from time-term analysis in the north-central rift, and the 8.1 km/s velocity reported by Phinney (1964) at Albuquerque from the analysis of spectral amplitudes. If the differences between the models are dip related, the Moho must dip 3-4° to the north, a value consistent with the time-term results (Murdock and Jaksha, 1981).

Finally, comparing the rift models with those of surrounding provinces, there appears to be basic crustal differences between the Great Plains province (Model 7, Figure 5; Line 7, Figure 6), the Colorado Plateau (Model 10, Figure 5; Line 10, Figure 6), and the Rio Grande rift. The exact nature of these differences is impossible to quantify without a much more constrained velocity/depth structure in each of the provinces, especially with respect to the sub-Moho velocity. Well constrained models will greatly assist in understanding the nature of the rifting process in this region.

THEORY

Typically, given a known source location and origin time, the arrival times of a particular phase recorded by a seismic network are plotted versus horizontal distance travelled. The apparent velocity across the network can then be determined by fitting a least squares line to the data. The equation of this line is of the form

$$t_i = d + \frac{\Delta_i}{V}, \tag{1}$$

where

t_i is the travel time from the source to the ith station,

d is the intercept time,

Δ_i is the epicentral distance between the source and the ith site, and

V is the apparent velocity.

Given a sufficient source distance, the waves arriving at the network will arrive from a narrow range of distances and azimuths. As a result, the apparent velocity computed from these data can be associated with a mean distance and azimuth. By recording data from sources having a wide spatial distribution, apparent velocities can be catalogued for sources located at specific distances and azimuths. Unfortunately, in addition to other complications, variations in crustal thickness, lateral velocity variations, and dip on the refracting interface introduce large errors in the velocities calculated. The analysis technique used in this study is a modified version of this method, but can handle these problems with great facility. Furthermore, the time-term method can be modified to model changes in the refractor velocity caused by a number of different geologic situations.

Unmodified Time-Term Method

The time-term method, proposed by Scheidegger and Willmore (1957) and developed extensively by Willmore and Bancroft (1960) and Berry and West (1966a and b), simultaneously estimates the refractor velocity, time terms for each source and receiver site, and errors in the estimated parameters. This method is particularly well-suited to this study because it allows analysis of fairly complex geologic structures with little dependence on the areal distribution of sources and receivers, although good azimuthal coverage should be utilized whenever possible.

The fundamental principle behind the time-term approach is that travel time may be expressed in terms of the epicentral distance, and two delay times associated with the source and receiver. Thus, t_{ij}, the theoretical travel time between a source i and receiver j, may be written as

$$t_{ij} = a_i + a_j + \frac{\Delta_{ij}}{V}, \tag{2}$$

where

a_i is the time term associated with source i,

a_j is the time term associated with receiver j,

Δ_{ij} is the distance between the ith and jth sites, and

V is the velocity below the refracting interface.

This equation will be referred to as the unmodified time-term equation.

A time term may be thought of as the difference between the time it takes a critically refracted wave to pass through the layers above the refracting interface and the time for the head wave to travel the offset distance (the horizontal distance between the point of critical refraction and the source or receiver) at the sub-interface velocity. For the simplest case of a planar horizontal constant

velocity layer overlying a half-space of higher velocity,

$$a_j = H_j \frac{\cos(\Theta_c)}{V_c}, \tag{3}$$

where

H_j is the depth of the interface below site j,

Θ_c is the angle of critical refraction, and

V_c is the velocity of the layer overlying the half-space.

Given a number of observed travel times, a system of linear equations can be developed. This system of travel time equations is solved, by weighted least squares, for the parameters V, a_i, and a_j, where i=1,2,...,k and k is the number of events, and j=k+1,k+2,...,k+l where l is the number of stations. These equations are most easily solved when expressed in matrix notation of the form

$$\left[c_{ij}\right]\left[a_j\right] = \left[x_i\right]$$

or

$$CA = X, \tag{4}$$

where

C is the coefficient matrix,

A is the vector of parameters to be estimated, and

X is the vector of observations (i.e. travel times).

Assuming the case of more data than parameters, the solution to this equation is

$$A = (C^T C)^{-1} C^T X, \tag{5}$$

where

C^T is the transpose of the coefficient matrix C, and

$(C^T C)^{-1}$ is the inverse of the matrix $C^T C$.

Characterization of the time-term method and its limitations have been dis-

cussed extensively in the literature by Willmore and Bancroft (1960), Berry and West (1966a and b), Smith et al. (1966), O'Brien (1968), Reiter (1970), Bamford (1971, 1973), McCollom and Crosson (1975), Whitcombe and Maguire (1979), and Whitcombe and Rogers(1981). The aforementioned model is valid (Berry and West, 1966) provided:

1. the velocity within the cone of critically refracted ray paths under the shot or station varies only with depth;
2. the velocity of the base refractor beneath the array is essentially constant;
3. the slope of the refracting surface is small (less than 10 degrees);
4. the curvature of the refracting surface is small.

In short, the method assumes that the station and event delays are constant and independent of distance or azimuth (McCollom and Crosson, 1975). Knowledge of the rift structure gained from this as well as previous studies done within the central rift (e.g. Toppozada and Sanford, 1976; Olsen et al., 1979) indicate that the assumptions are not violated, or at worst, not sufficiently violated to invalidate the approach or its conclusions.

Willmore and Bancroft (1960) list four guidelines to follow in designing an time-term experiment:

1. sources and receivers should form extended patterns;
2. the region of interest should be surrounded by either sources or receivers;
3. receivers should record data from many sources;
4. at least one site should be both a source and receiver.

In the case of this study, these guidelines must be considered for each

refractor studied. For the Phanerozoic - Precambrian contact, all the design criteria are met. Furthermore, the overall azimuthal distribution of the data is very good (Figure 7).

The study of the mid-crustal Conrad discontinuity satisfies the first three of the design precepts, including a reasonable azimuthal distribution (Figure 8). The fourth is violated since no seismograph occupied a source site. For this case, an arbitrary constant may be added to the source time terms and subtracted from the receiver time terms without changing the observed travel times. As such, the P* solution is formally indeterminate, i.e. only relative time terms may be calculated. The easiest solution to this problem is to fix the time term for one station making all other time terms relative to that station's value. Outside information gained from previous studies is used in setting the time term of the reference station.

As with the P* data set, no point was occupied by both a source and receiver in the Pn (sub-Moho) data set. As explained above, this presents no major difficulties in doing the analysis. However, the data for this refractor are skewed with respect to azimuth, containing fewer arrivals from the east, the 180 - 360 degrees station to receiver direction interval in Figure 9. Given the generally aseismic nature of the Great Plains, this is not surprising. It is a factor though, that may have bearing on the interpretation of the results of the time-term analysis.

Modified Time-Term Method

The time-term equation may be modified to consider more complicated geologic situations (Raitt et al., 1969; Morris et al., 1969; McCollom and Crosson, 1975; Zervas and Crosson, 1986). Assume the velocity of the base refractor is perturbed by a small amount dV. Doing a Taylor series expansion to the travel

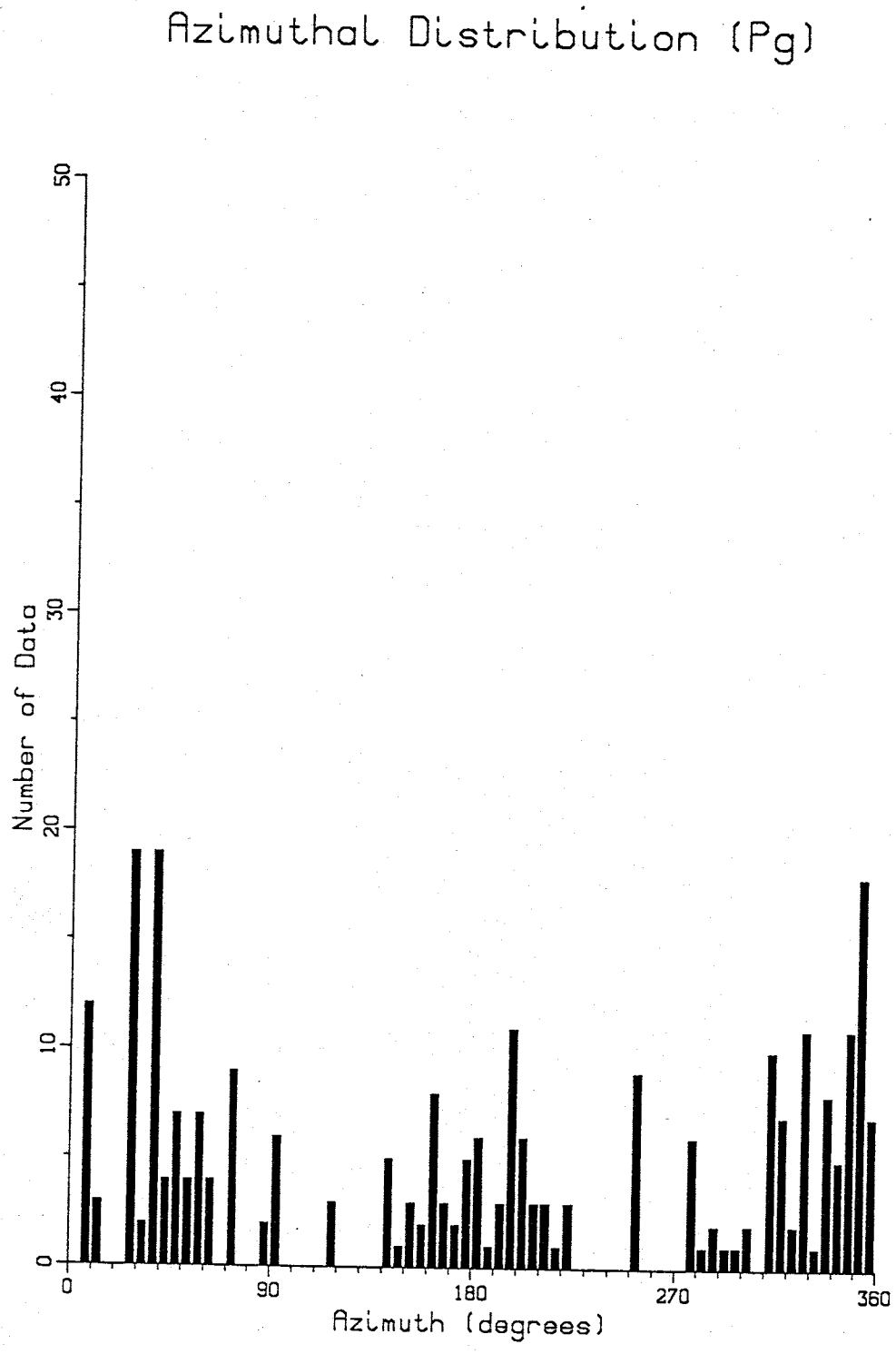

Figure 7: Azimuthal distribution of Pg data. The distribution is well balanced and not skewed toward any one direction.

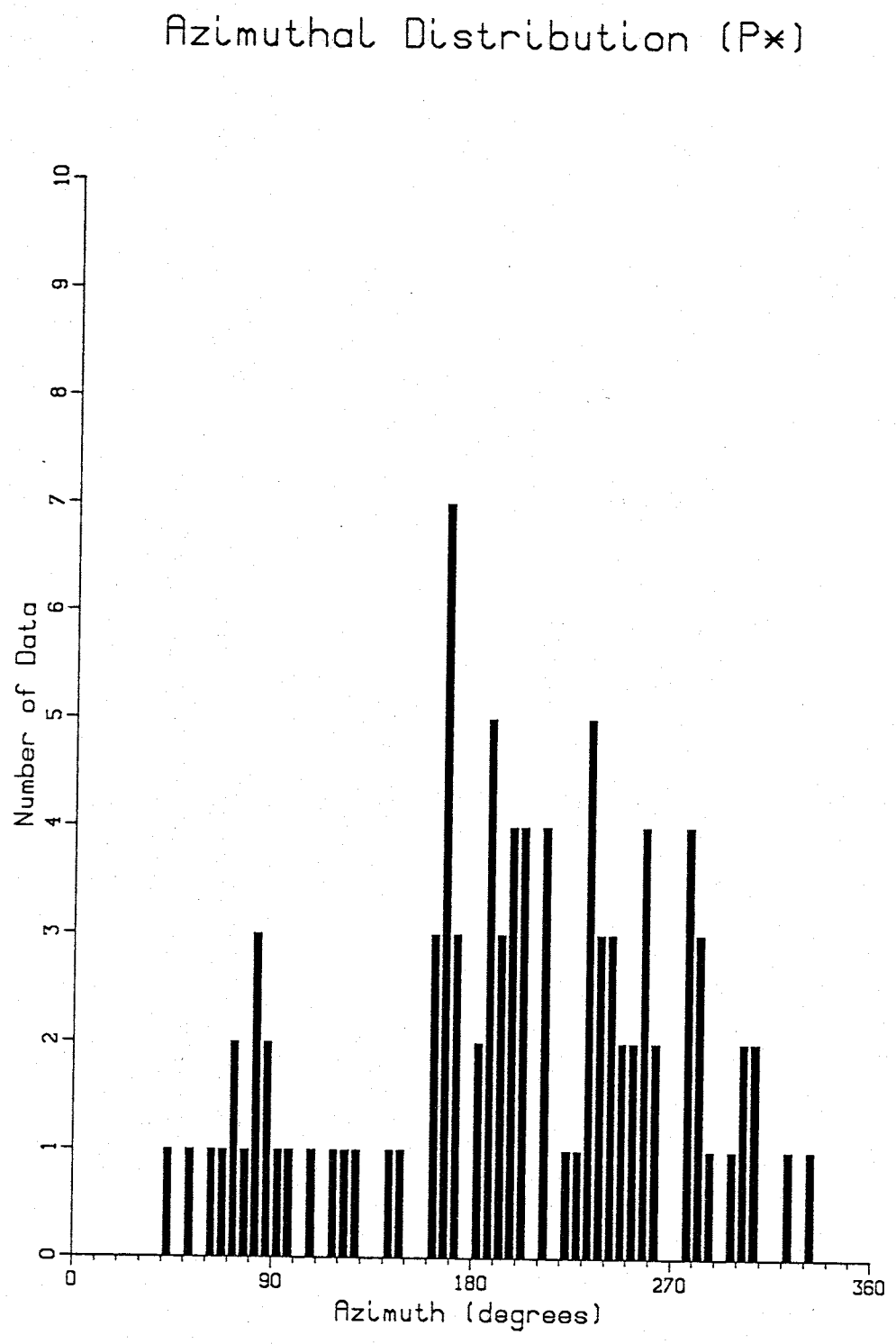

Figure 8: Azimuthal distribution of P* data. The distribution is reasonably good, especially considering the sparsity of data.

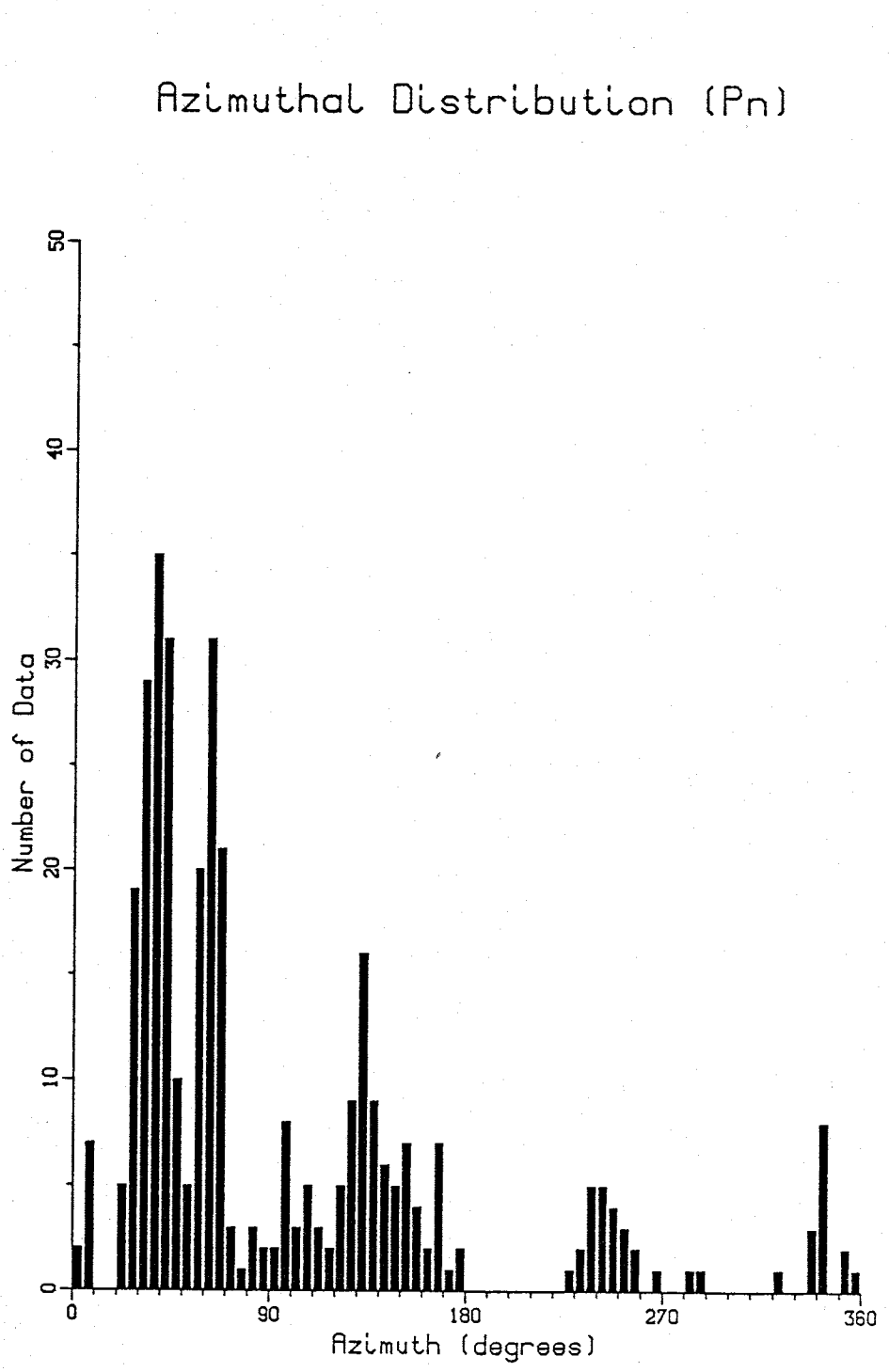

Figure 9: Azimuthal distribution of Pn data. The distribution is skewed, with the majority of events located west of the study area.

time about the velocity $V=V_o$ and keeping only first-order terms, then

$$t_{ij} = a_i + a_j + \frac{\Delta_{ij}}{V_o} + \left[\frac{\partial a_i}{\partial V} + \frac{\partial a_j}{\partial V} - \frac{\Delta_{ij}}{V^2}\right] dV \quad V=V_o. \tag{6}$$

Defining F_j as the offset distance between site j and the point at which the critically refracted ray enters or leaves the refractor, the travel time equation may be written

$$t_{ij} = a_i + a_j + \frac{\Delta_{ij}}{V_o} + \left[\frac{F_i + F_j - \Delta_{ij}}{V_o^2}\right] dV. \tag{7}$$

Generally, this equation is simplified and solved assuming that the offset distances F_i and F_j are equal and known. This is possible since for deep crust and upper mantle refractions, the variations in the offset distances are small in comparison to the source-receiver distances. However, the assumption that F_i and F_j are equal is not appropriate for mid and upper crustal refractors unless the sources are at or near the earth's surface. This problem, specifically with the P* analysis, was resolved by computing an average offset distance from knowledge of the average source depth (7 kilometers) and the approximate depth of the refractor of interest (19.6 kilometers).

The choice of the functional form of dV depends on the specific earth model under consideration. For each of the models in this study, dV was approximated by a linear function with unknown parameters. This allows equation (7) to be treated as a linear equation and solved using normal least squares techniques. The three cases that have been considered are:

1. refractors with azimuthal anisotropy;
2. a velocity gradient with depth;
3. a dipping refractor or equivalently, a lateral gradient in the average crustal velocity across the array.

Considering the first case, that of an azimuthally anisotropic refractor, the velocity perturbation dV from Backus (1965) can be expressed as

$$dv = A\ sin(2\Phi_{ij}) + B\ cos(2\Phi_{ij}) + C\ sin(4\Phi_{ij}) + D\ cos(4\Phi_{ij}), \qquad (8)$$

where Φ_{ij} is the azimuth (clockwise from north) of the travel path from site i to site j. This specific formula was developed for an upper mantle refractor with weak anisotropy, but is valid for the velocity perturbation caused by any nearly isotropic refractor. In general, weak anisotropy implies a total velocity variation of less than ten percent. Substituting equation (8) into equation (7), the expanded travel time equation becomes

$$t_{ij} = a_i + a_j + \frac{\Delta_{ij}}{V_o} + \left[\frac{2F - \Delta_{ij}}{V_o^2}\right](A\ sin(2\Phi_{ij}) + B\ cos(2\Phi_{ij}) + C\ sin(4\Phi_{ij}) + D\ cos(4\Phi_{ij})). \qquad (9)$$

The magnitude and direction of the maxima of the velocity perturbation can be computed from the four parameters of the dV term. The time-term method based on equation (9) will be referred to as anisotropy analysis.

The second model under discussion is a velocity gradient, where rays originating from distant sources will penetrate deeper than those from nearer sources and will emerge at the network with larger apparent velocities. Following Smith et al. (1966), the apparent velocity can be expressed as a linear function of distance,

$$V_{ij} = V_o + W_1\Delta_{ij}. \qquad (10)$$

From inspection, the velocity perturbation dV is $W_1\Delta_{ij}$. The time-term equation for the second model is

$$t_{ij} = a_i + a_j + \frac{\Delta_{ij}}{V_o} + \frac{2F - \Delta_{ij}}{V_o^2} W_1\Delta_{ij}. \qquad (11)$$

The time-term method based on equation (11) will be referred to as distance analysis.

The third and final model considers a dipping refractor. The effect of dip will be absorbed in the station time terms, which will increase in the direction of crustal thickening above the refractor. Following Zervas and Crosson (1986), the dip effect can be modelled as a perturbation in the apparent velocity by assuming:

1. a horizontal refractor;
2. that the average crustal velocity is the same for all stations;
3. that the velocity below the interface varies with azimuth.

For simplicity, all the station time terms are assumed equal and arbitrarily assigned a zero value. As a result, non-linear variations in crustal thickness or crustal velocities above the refractor will become part of the residuals of the travel time equation. Accordingly, this procedure generally causes an increase in the sum of the squares of the weighted residuals. V_o, the apparent velocity computed, will be the velocity of a critically refracted wave travelling along the refractor at an azimuthally dependent apparent dip. Zervas and Crosson (1986) derived a linear velocity perturbation for small dip angles (less than 10 degrees) of

$$dV = -V_o \alpha cot(\Theta_c) \left[cos(\Psi) cos(\Phi_{ij}) + sin(\Psi) sin(\Phi_{ij}) \right], \qquad (12)$$

where

α is the true dip angle,

Θ_c is the critical angle, and

Ψ is the azimuth of the true dip direction.

Combining with equation (7), the travel time equation is

$$t_{ij} = a_i + \frac{\Delta_{ij}}{V_o} - \frac{2F - \Delta_{ij}}{V_o^2} V_o \alpha cot(\Theta_c) \times \left[cos(\Psi) cos(\Phi_{ij}) + sin(\Psi) sin(\Phi_{ij}) \right] \tag{13}$$

When $\Psi = \Phi_{ij}$, dV is a maximum and the magnitude of the true dip will have a value of

$$\alpha = \frac{|dV|}{V_o} tan(\Theta_c). \tag{14}$$

The time-term method based on equation (13) will be referred to as dip analysis. The preceding analysis assumes that there are no lateral velocity gradients in the overlying velocity structure, since such gradients would produce the same effect as a dipping interface.

Error Analysis

Estimates of the goodness of fit of the model (the standard deviation of the solution) and the standard errors of the individual time terms were developed by Berry and West (1966). However, no uncertainty estimates were provided for the refractor velocity, nor were the parameters and the attendant uncertainties of more complex models even considered.

Independently, Murdock and Steppe (1980, and 1974, unpublished data) as well as McCollom and Crosson (1975) applied multiple linear regression techniques to the time-term method to obtain uncertainty estimates. As previously discussed, the normal equations may be written in matrix notation as

$$CA = X, \tag{4}$$

where the symbols are as previously defined. Assuming s^2, the variance of the solution equals σ^2, the true variance, and a conceptually correct initial model, standard errors may be computed for each of the parameters. Following Draper and Smith (1966), the product $(C^T C)^{-1}\sigma^2$ is called the variance-covariance matrix. The main diagonal of this matrix gives the estimated variances of the parameter estimates. The square roots of these variances are the estimated standard errors, while the off-diagonal terms are the estimated covariances. The sum of squares of the residuals, minimized by the linear regression, is

$$S = X^T X - A^T C^T X, \tag{15}$$

and s^2, also called the mean square about regression (Draper and Smith, 1966), is

$$s^2 = \frac{S}{N - P}, \tag{16}$$

where

N is the number of data (i.e. observations);

P is the number of parameters being estimated.

Therefore, s^2 is the sum of squares of the residuals divided by the number of degrees of freedom of the residuals.

CRITICALLY REFRACTED ARRIVALS

The data for this study consist of the travel times, epicentral distances, and azimuths for a series of critically refracted arrivals collected from earthquakes and explosions recorded by the temporary and permanent stations of the Socorro seismic network (Figure 10; Tables 1, 2). Three specific phases are of interest: Pg, P*, and Pn. Pg is the head wave refracted from the Phanerozoic-Precambrian boundary. P* is the critically refracted wave which travels along the Conrad discontinuity, which separates the upper and lower crust. Pn is the head wave generated at the Mohorovičić discontinuity, the crust-mantle interface. Each of these phases is only observed as a first arrival over a specific range of distances. Figures 11, 12, and 13 show reduced travel time plots for all three arrivals for several focal depths using the rift model of Toppozada and Sanford (1976). The depths chosen were for surface explosions (0 km), the average focal depth for earthquakes in the central Rio Grande rift (7 km), and the base of the seismogenic zone in the central Rio Grande rift (12 km) as delineated by King (1986).

Pg Phase

Pg is an impulsive, well-defined phase on the Socorro network records (Figure 14) and is the first arrival in the distance range from a few kilometers to over one hundred kilometers. The Pg data set has the least uncertainty of the three used, because the arrival time is the easiest to pick. Moreover, this set is composed entirely of explosions whose precise locations and origin times are known so errors in the source time terms and the apparent Pg velocity are significantly reduced. Explosion data were particularly important for the Pg data set since several shot points were close to, and inside the array. Location

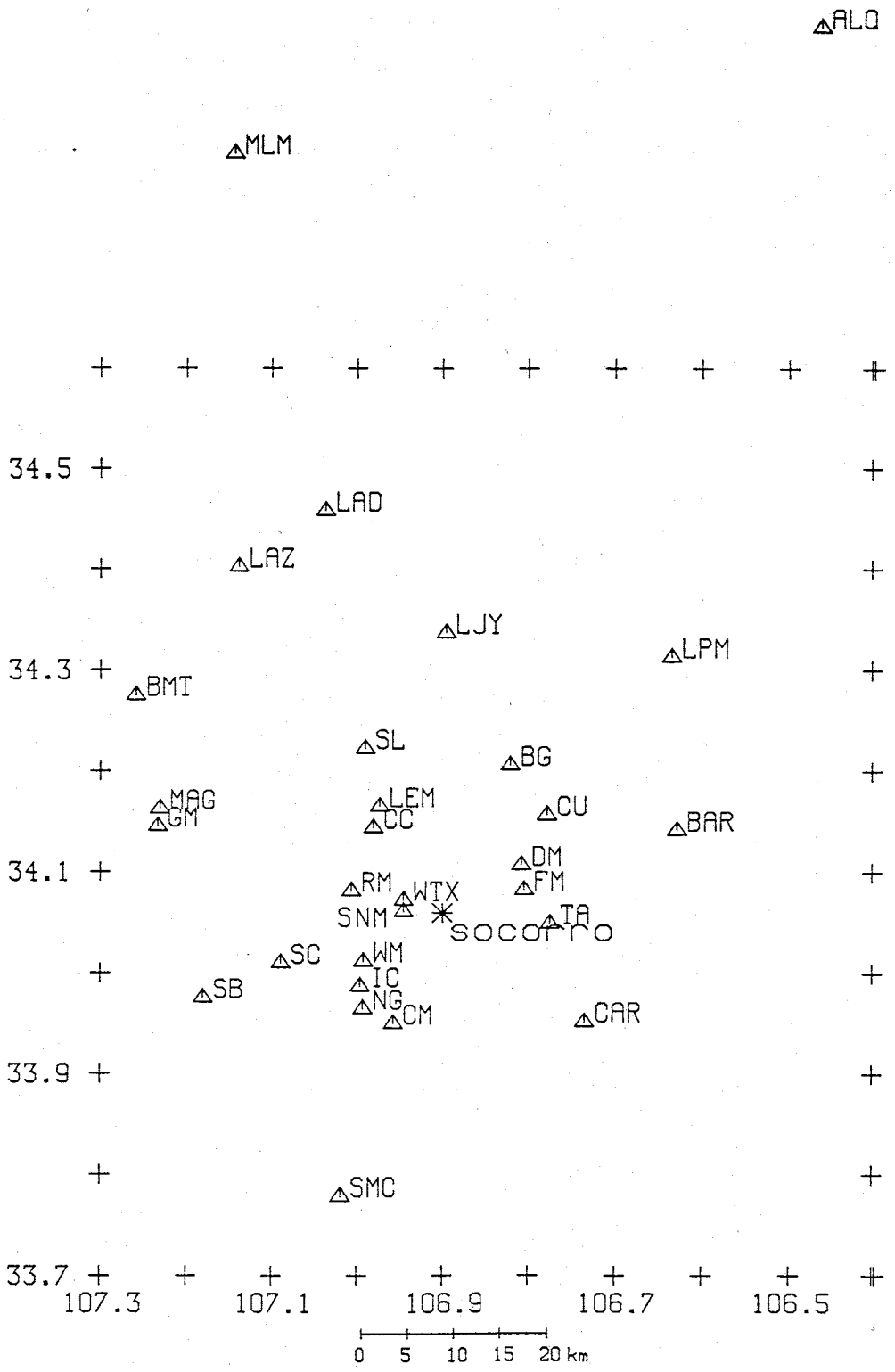

Figure 10: All of the stations of the Socorro seismograph networks used in this study. Permanent stations designated by three-letter names; temporary stations by two-letter names.

Table 1

Station Names

New Mexico Tech Seismic Network

ALQ (USGS)	Albuquerque
BAR	Barren Site
BG	Bowling Green
BMT	Bear Mountain
CAR	Carthage
CC	Corkscrew Canyon
CM	Chupadera Mountains
CU	Chupadera Mine
DM	Duchess Mine
FM	Fluorite Mine
GM	Granite Mountain
IC	Indian Cave
LAD	Ladron Mountain
LAZ	Ladron Mountain
LEM	Lemitar
LJY	LaJoya
LPM	Los Pinos Mountains
MAG	Magdalena
MLM	Mesa Lucero
NG	Nogal Canyon
RM	Rattlesnake Mound

Table 1 (continued)	
SB	South Baldy
SC	South Canyon
SL	San Lorenzo Canyon
SMC	San Marcial
SNM	Socorro
TA	Arroyo del Tajo
WM	Windmills
WTX	Wood's Tunnel

Table 2

Station Locations

New Mexico Tech Seismic Network

Station	Latitude (°N)	Longitude (°W)	Elevation (km)
ALQ (USGS)	34.9416	106.4583	1.853
BAR	34.1420	106.6280	2.120
BG	34.2068	106.8205	1.516
BMT	34.2750	107.2602	1.972
CAR	33.9525	106.7345	1.662
CC	34.1442	106.9812	1.649
CM	33.9501	106.9579	1.640
CU	34.1573	106.7785	1.585
DM	34.1075	106.8079	1.536
FM	34.0829	106.8047	1.570
GM	34.1454	107.2345	1.945
IC	33.9870	106.9967	1.730
LAD	34.4583	107.0375	1.768
LAZ	34.4020	107.1393	1.853
LEM	34.1655	106.9742	1.698
LJY	34.3365	106.8958	1.532
LPM	34.3128	106.6338	1.707
MAG	34.1625	107.2320	1.926
MLM	34.8143	107.1450	2.088
NG	33.9648	106.9933	1.730
RM	34.0812	107.0069	1.719

Table 2 (continued)			
SB	33.9752	107.1807	3.230
SC	34.0100	107.0894	2.073
SL	34.2234	106.9910	1.615
SMC	33.7787	107.0193	1.560
SNM	34.0702	106.9435	1.511
TA	34.0498	106.7751	1.558
WM	34.0120	106.9929	1.673
WTX	34.0722	106.9459	1.555

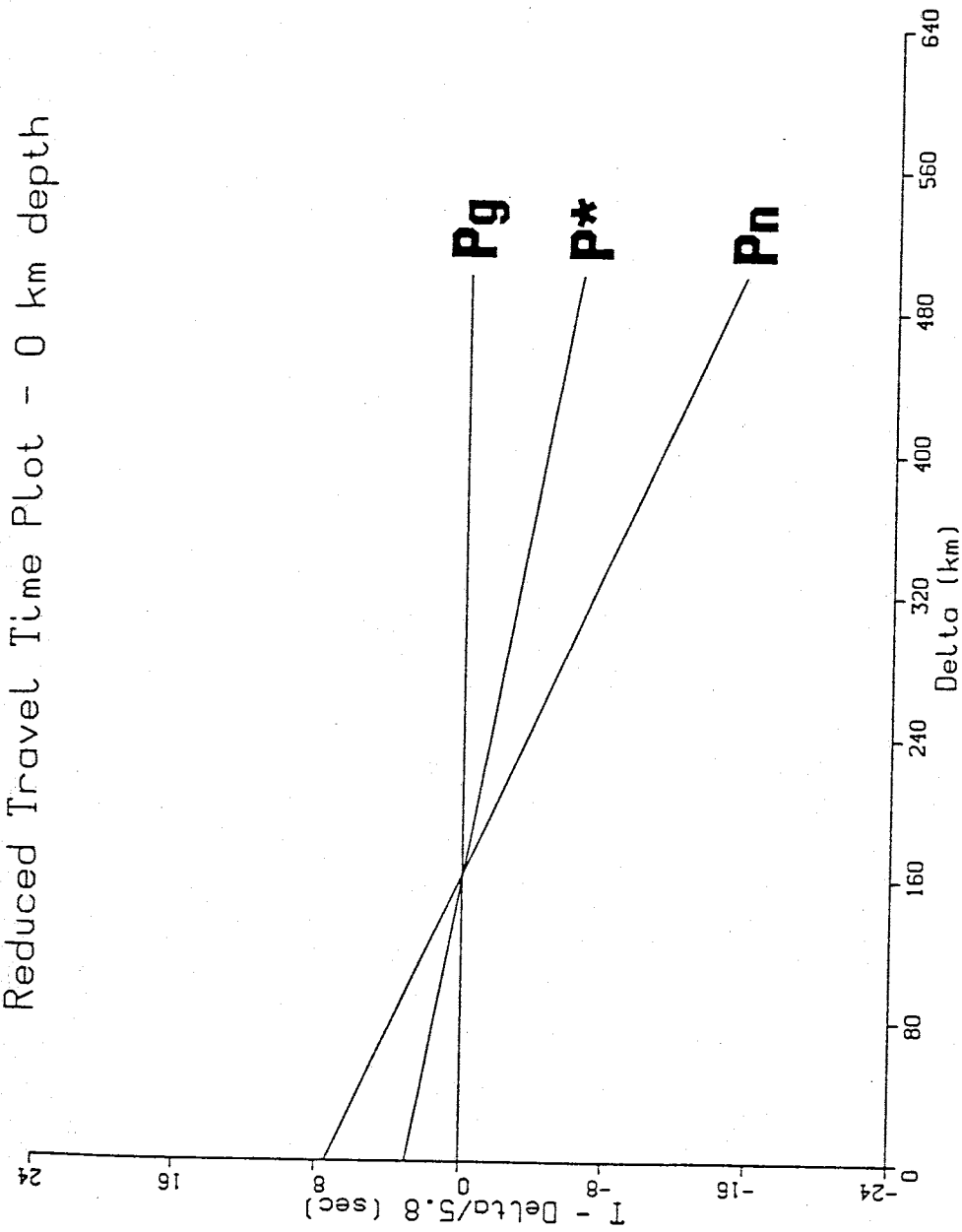

Figure 11: Reduced travel time plot for surface explosions in the central Rio Grande rift. P* phase is never seen as a first arrival. The travel times are based on the crustal structure of Toppozada and Sanford (1976).

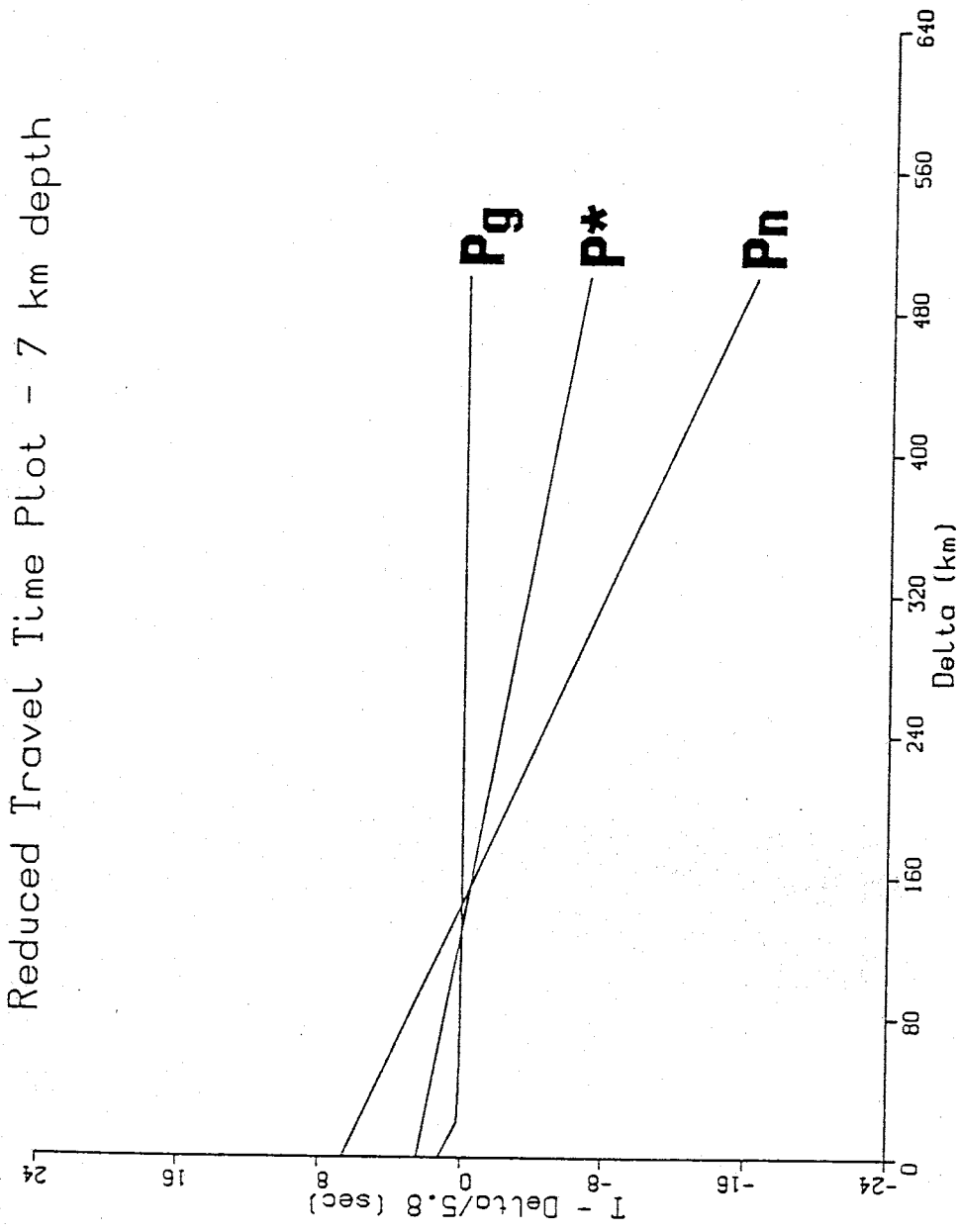

Figure 12: Reduced travel time plot for events at the average focal depth for the Socorro region. P* phase is a first arrival for less than 30 km. The travel times are based on the crustal structure of Toppozada and Sanford (1976).

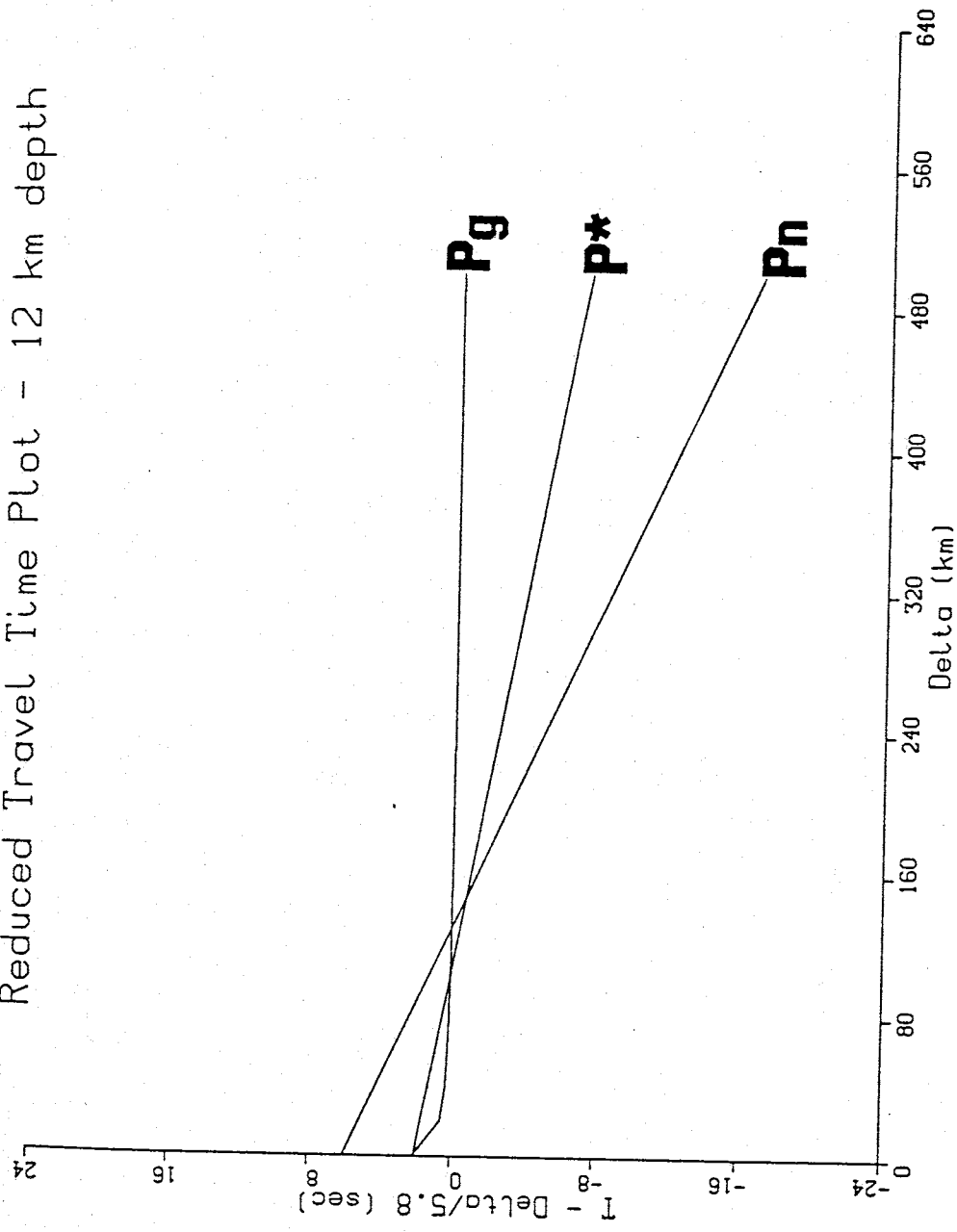

Figure 13: Reduced travel time plot for events at the base of the seimsogenic zone in the Socorro region. P* is a first arrival over ~60 km. The travel times are based on the crustal structure of Toppozada and Sanford (1976).

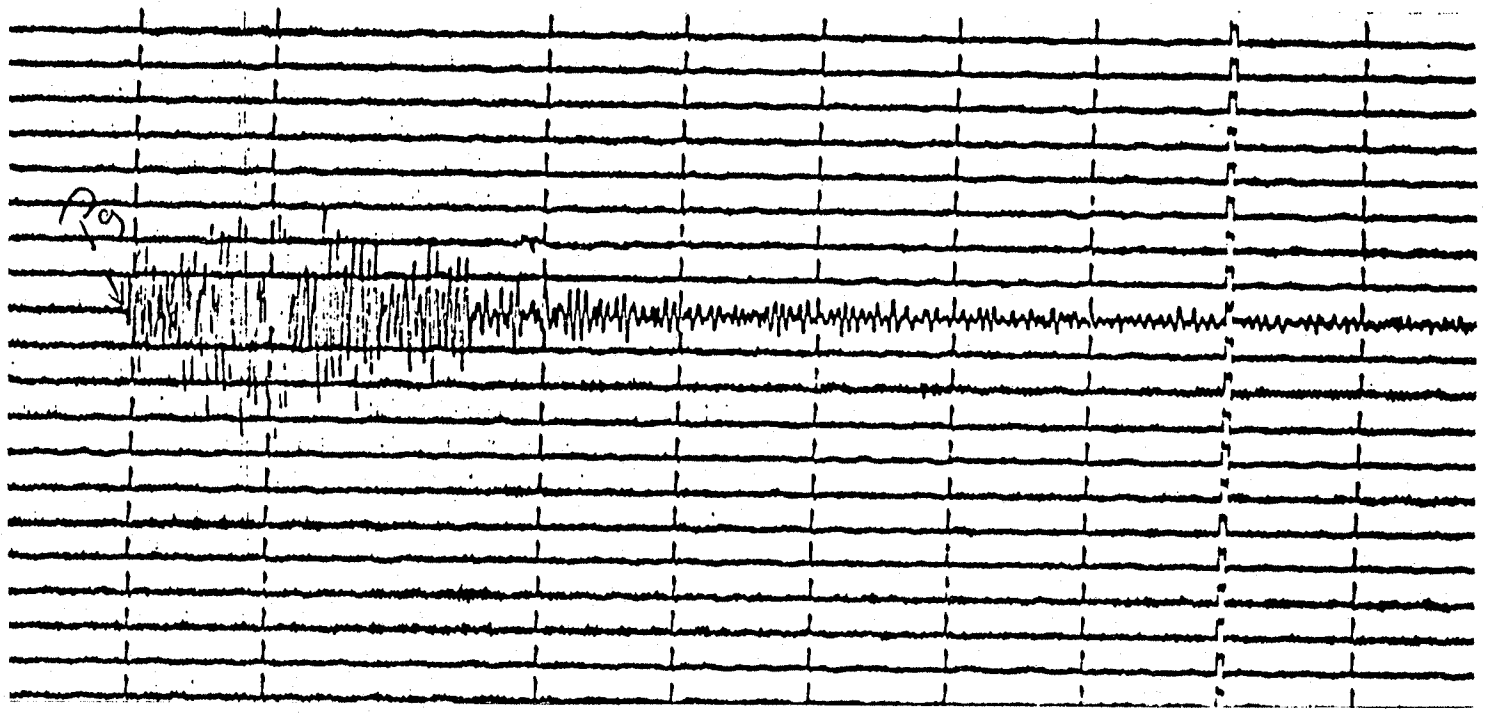

Figure 14: Seismogram from station SMC showing impulsive Pg phase from a local mine explosion.

errors for these near events will affect the station time terms, although a majority of the error would be absorbed in the source time term. For events far outside the array, epicentral errors are less important since they will have only a small effect on the computed intra-station distances. Thus, for P* and Pn, epicentral errors are not a significant factor.

P* Phase

The second principal arrival, P*, is generally weak, indistinct, and emergent, and the most uncertain of the three phases studied (Figure 15). Worse yet, the distance window in which P* appears as a first arrival is extremely narrow due to the crustal velocity structure of the Rio Grande rift and the adjacent provinces. Varying the depth of source through the seismogenic zone and employing a reasonable rift model (Model 1, Figure 5), the maximum window width is on the order of 60 km for a focal depth of 12 km, but less than 30 km for a focal depth of 7 km (Figures 12 and 13). For surface events, the situation is even worse, since P* will never appear as a first arrival (Figure 11). Outside the rift boundaries, the distance window never exceeds 30 km. Because location and depth of focus severely limit the first arrival window for this phase, the number of events for which P* clearly appears on the seismic records is small.

The second problem with the P* phase centers around the fact that the arrival is generally very weak. As a result, it can only be clearly picked from recordings of fairly strong events. While the central New Mexico is a seismically active area, sufficiently strong earthquakes at the right distance are relatively rare.

Pn Phase

Pn, the critically refracted phase below the M discontinuity, is the final

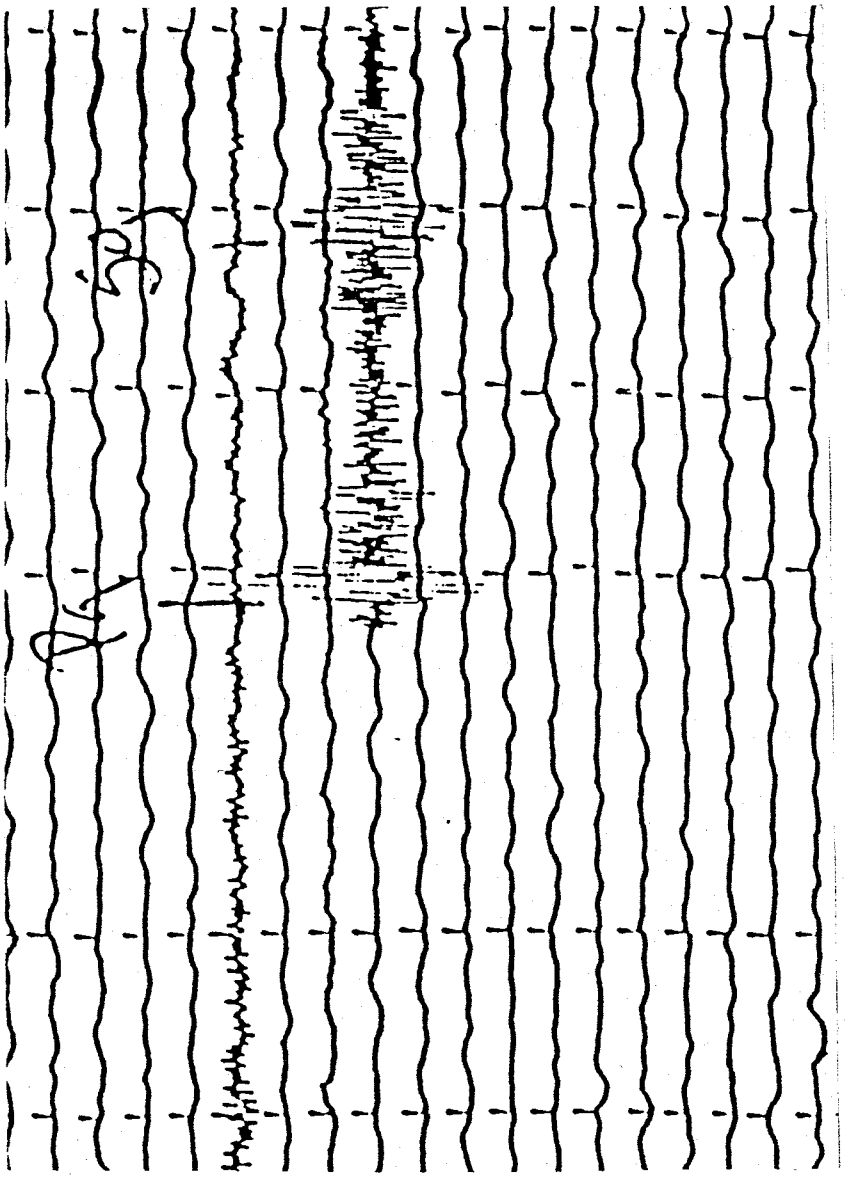

Figure 15: Strong regional event recorded at SMC showing a rare impulsive P* phase.

arrival to be considered. The Pn phase is usually low in amplitude but generally has a sharp, impulsive onset (Figure 16). However, for distant events, the initial cycle is often low frequency in character (Figure 17), possibly the result of unusually high wave attenuation in the Rio Grande rift (Jordan et al., 1965). Pn has the largest distance window of the three phases emerging as a first arrival approximately 180 km away from a source and existing to at least 600 km distance. The large distances often result in large uncertainties in the hypocenters and origin times of the earthquakes and explosions producing the Pn phase. Because of this and the fact that there is no estimate of the P wave velocity between sources and the Socorro network, the source time terms are not accurate. Nevertheless, this does not affect the relative accuracy of either the station time terms or the estimation of the refractor velocity (McCollom and Crosson, 1975).

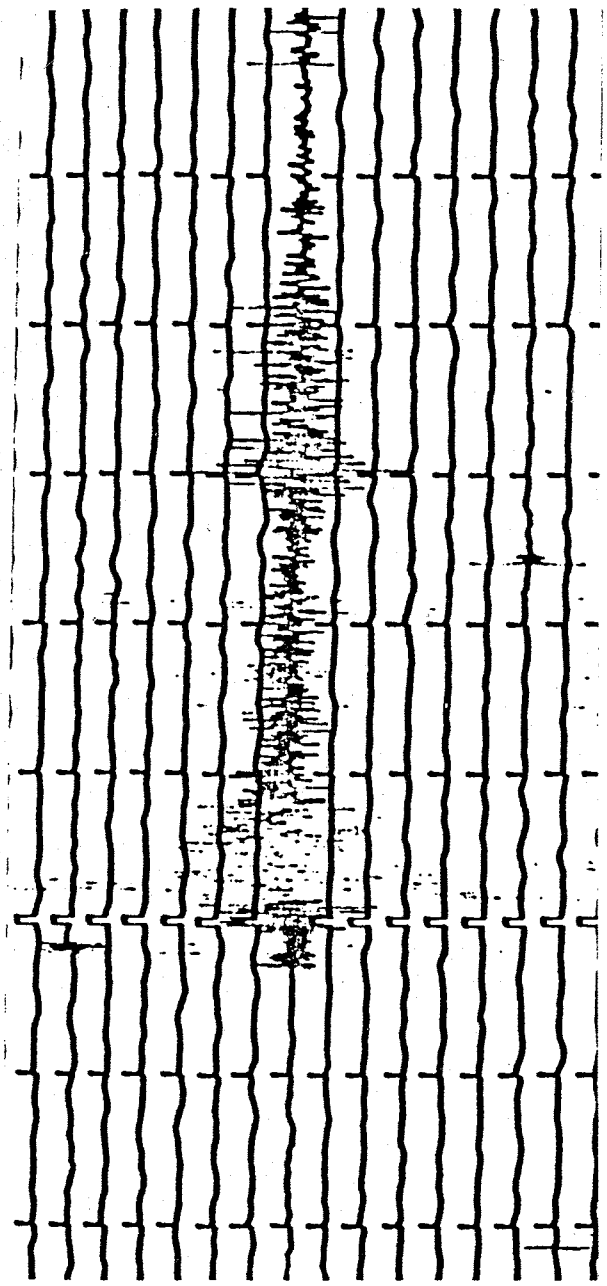

Figure 16: Seismogram showing impulsive Pn phase recorded at station LAZ from large mining explosion in southwestern New Mexico.

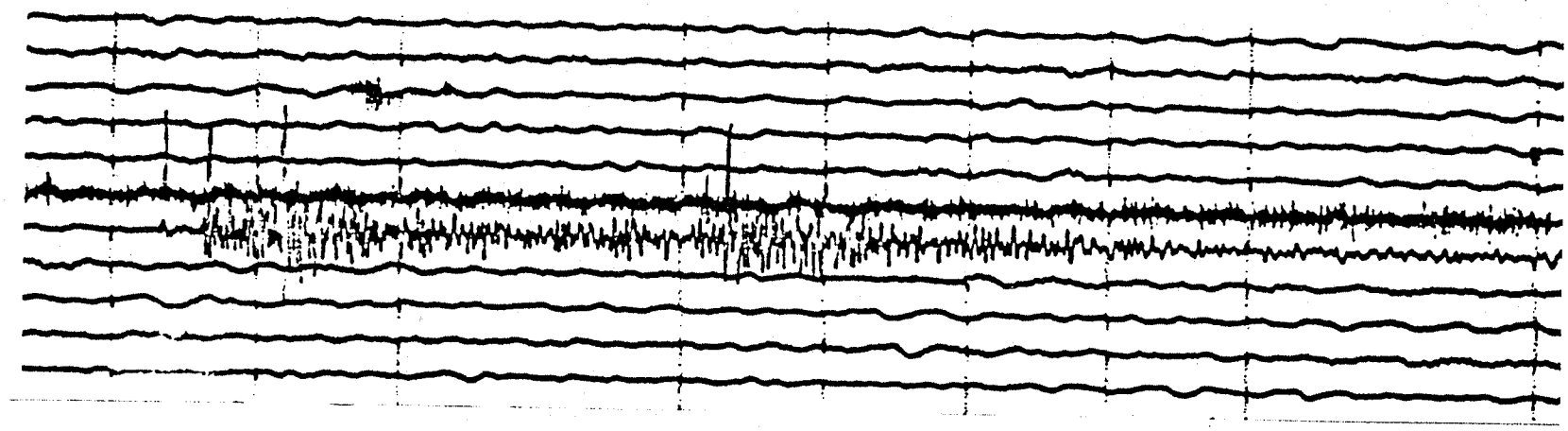

Figure 17: Strong far-regional event recorded at station LPM showing low frequency onset of the Pn phase.

DATA

Seismic monitoring in the Socorro area first began in the early 1960's on a very limited scale. Beginning in 1975, a series of portable seismic stations centered around Socorro was maintained semi-continuously. The locations of these stations, designated by 2 letter station names (Figure 10), were changed periodically to adjust the area of coverage. In early 1982, the United States Geological Survey (USGS) and New Mexico Tech (NMT) began a cooperative program of monitoring seismic activity in the central rift. Since mid-June 1982, signals from six to twelve permanent stations, designated by three letter station names (except for station SB), have been telemetered into the NMT campus (Figure 10). As a result, the data for this study are composed of two essentially mutually exclusive parts, the data from the small, portable net prior to June 1982, and the data from the larger, more widely dispersed permanent net from June 1982 to the present. This does not present any problems for this study, but it does explain the lack of data continuity and the time variations in station locations (Appendices 1,2,3). The P* data set is the only one of the three data sets which does not contain any data prior to 1982. Hypocentral locations of near-regional events were not well-constrained prior to this time and it is extremely difficult to distinguish between P* arrivals and poor quality Pn arrivals based on their waveform characteristics alone. Therefore, to avoid contamination of the P* data set with Pn arrivals, only well located events, those recorded since 1982, were used.

All data were acquired with vertical component, 1 second natural period seismometers. At temporary stations, MEQ-800 analog recorders operating with a drum speed of 2 mm/sec recorded the data. Corrections for clock drift were computed and applied, which reduced timing errors in these data to

approximately 10 to 20 milliseconds. At permanent stations, data were recorded at the New Mexico Tech seismic observatory by Geotech Helicorders operating at a drum speed of 1 mm/sec. Because the observatory clock is reset daily, differences between WWV standard time and observatory time were generally on the order of 10 to 20 milliseconds. Thus, no time corrections needed to be applied.

For each of the three data sets, Pg, P*, and Pn, only the readings from first arrivals were used. Arrival times and reading uncertainties were determined for each event for as many stations as possible. In the least squares calculations, each observation was weighted by the inverse of the uncertainty for that pick (Wolberg, 1967; Zervas and Crosson, 1986). Uncertainties ranged from 0.03 to 0.30 seconds. For each ray path, a distance and azimuth was calculated using an elliptical earth model, with the azimuth of each path measured clockwise from north from the source to each station.

Time distance plots were then constructed for each data set. A best fit line was passed through the data using least squares. The arrival times for those data lying greater than two standard deviations outside this line were rechecked and some were removed. This yielded a Pg data set of 265 arrivals from 43 events (Table 3) recorded at 27 stations (Figure 18), a P* data set of 72 arrivals from 24 events (Table 4) recorded at 11 stations (Figure 19), and a Pn data set of 402 arrivals from 79 events (Table 5) recorded at 23 stations (Figure 20).

Table 3

List of Events

Pg Phase

Date	Time	Latitude	Longitude
07/23/75	16:51:51.26	34.0422 ° N	106.9640 ° W
08/12/75	16:59:59.80	33.3788 ° N	106.3650 ° W
04/20/76	18:56:12.81	34.0422 ° N	106.9640 ° W
04/21/76	19:16:43.96	34.0422 ° N	106.9640 ° W
04/22/76	19:45:27.82	34.0422 ° N	106.9640 ° W
10/06/76	14:00:00.50	33.6790 ° N	106.5210 ° W
02/14/77	23:31:43.80	35.1110 ° N	107.3930 ° W
02/22/77	18:47:54.25	34.0422 ° N	106.9640 ° W
02/23/77	18:48:58.70	34.0422 ° N	106.9640 ° W
05/10/77	23:48:25.06	34.0422 ° N	106.9640 ° W
05/11/77	20:43:26.29	34.0422 ° N	106.9640 ° W
05/14/77	19:50:28.55	34.0422 ° N	106.9640 ° W
05/19/77	22:49:51.48	34.0422 ° N	106.9640 ° W
06/02/77	19:59:59.73	34.9600 ° N	106.5740 ° W
07/27/77	22:29:15.65	35.1110 ° N	107.3930 ° W
08/25/77	19:57:24.15	35.1110 ° N	107.3930 ° W
12/06/77	19:47:57.74	34.0422 ° N	106.9640 ° W
12/07/77	23:23:23.83	34.0422 ° N	106.9640 ° W
06/08/81	16:44:59.48	34.9600 ° N	106.5800 ° W
09/16/81	12:35:39.07	33.6210 ° N	106.4770 ° W
10/07/81	16:59:59.87	33.3810 ° N	106.3670 ° W
09/21/82	22:42:14.23	34.0422 ° N	106.9640 ° W
10/04/82	20:51:40.93	34.0422 ° N	106.9640 ° W
10/18/82	18:06:40.33	33.7390 ° N	107.0100 ° W
11/16/82	00:14:22.23	33.7390 ° N	107.0100 ° W
11/18/82	00:05:22.93	33.7390 ° N	107.0100 ° W
01/09/83	23:46:45.13	33.7390 ° N	107.0100 ° W
01/26/83	23:41:27.07	33.7390 ° N	107.0100 ° W
02/06/83	23:48:24.63	33.7390 ° N	107.0100 ° W
07/21/83	18:51:20.33	34.0422 ° N	106.9640 ° W
10/26/83	18:06:00.06	33.6212 ° N	106.4747 ° W
11/28/84	19:05:00.03	33.6122 ° N	106.4848 ° W
06/27/85	18:20:00.03	33.6212 ° N	106.4747 ° W
06/28/85	21:11:51.20	33.9550 ° N	106.9628 ° W
07/03/85	17:19:29.85	33.9550 ° N	106.9628 ° W
07/09/85	18:02:48.58	33.9550 ° N	106.9628 ° W
07/17/85	17:36:48.38	33.9550 ° N	106.9628 ° W
07/25/85	20:17:28.27	33.9550 ° N	106.9628 ° W
07/29/85	19:58:27.63	33.9550 ° N	106.9628 ° W
08/09/85	16:59:09.50	34.9565 ° N	106.5778 ° W
09/21/85	18:40:00.00	34.9565 ° N	106.5778 ° W
01/16/86	18:00:00.00	34.9600 ° N	106.5803 ° W
03/26/86	23:48:16.53	34.0422 ° N	106.9640 ° W

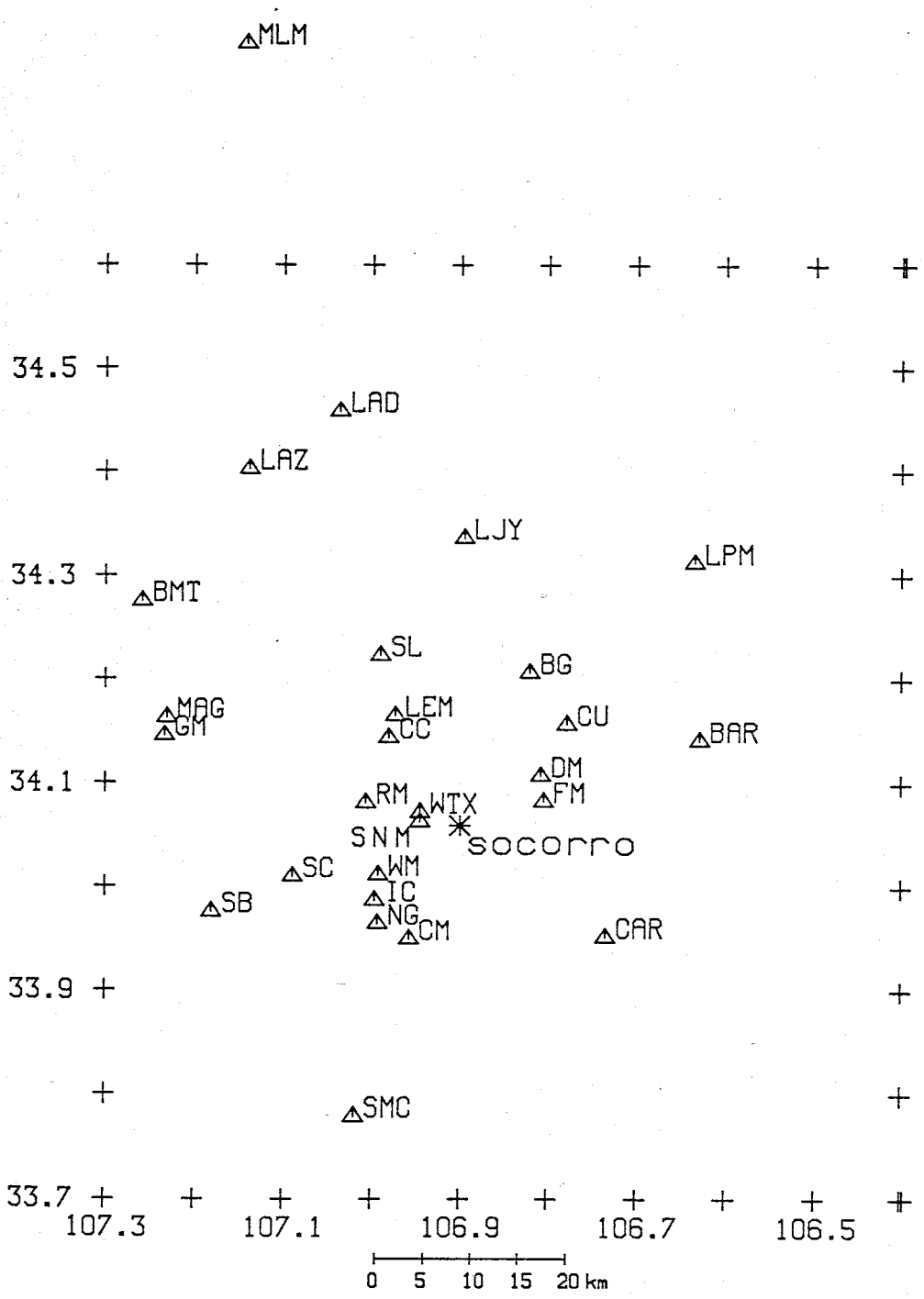

Figure 18: Stations of the Socorro seismograph networks which recorded Pg data.

Table 4

List of Events

P Phase*

Date	Time	Latitude	Longitude
10/19/82	23:13:31.83	35.4330 ° N	106.1110 ° W
01/17/83	18:58:54.63	34.6380 ° N	105.5850 ° W
11/27/84	19:06:02.82	33.6138 ° N	105.3622 ° W
12/08/84	00:37:36.94	34.9053 ° N	105.2793 ° W
01/22/85	00:03:37.47	34.1642 ° N	108.7797 ° W
06/27/85	01:47:12.12	32.9180 ° N	108.2593 ° W
07/16/85	06:18:05.88	35.1158 ° N	106.4600 ° W
07/17/85	06:23:20.02	35.1627 ° N	106.5385 ° W
08/14/85	01:03:20.33	34.6583 ° N	105.5917 ° W
09/01/85	01:35:44.80	34.6583 ° N	105.5917 ° W
12/13/85	10:20:28.46	33.7577 ° N	108.8978 ° W
01/15/86	21:01:40.59	34.5068 ° N	105.4592 ° W
08/02/86	00:31:09.25	34.6743 ° N	105.5397 ° W
11/26/86	22:56:44.30	34.6583 ° N	105.5917 ° W
03/12/87	07:50:25.63	34.5897 ° N	105.8485 ° W
03/27/87	04:36:49.49	34.8205 ° N	105.5930 ° W
03/28/87	17:16:14.94	35.3655 ° N	106.6212 ° W
04/25/87	08:17:47.09	35.2013 ° N	105.8148 ° W
04/29/87	13:36:31.14	32.6377 ° N	105.9367 ° W
07/04/87	13:57:53.29	33.7282 ° N	108.8015 ° W
08/02/87	21:29:32.98	33.5062 ° N	105.4580 ° W
08/12/87	02:02:18.75	33.5417 ° N	105.3897 ° W
09/13/87	14:27:30.50	35.6528 ° N	108.2717 ° W
03/09/88	20:11:40.11	35.8293 ° N	106.8107 ° W

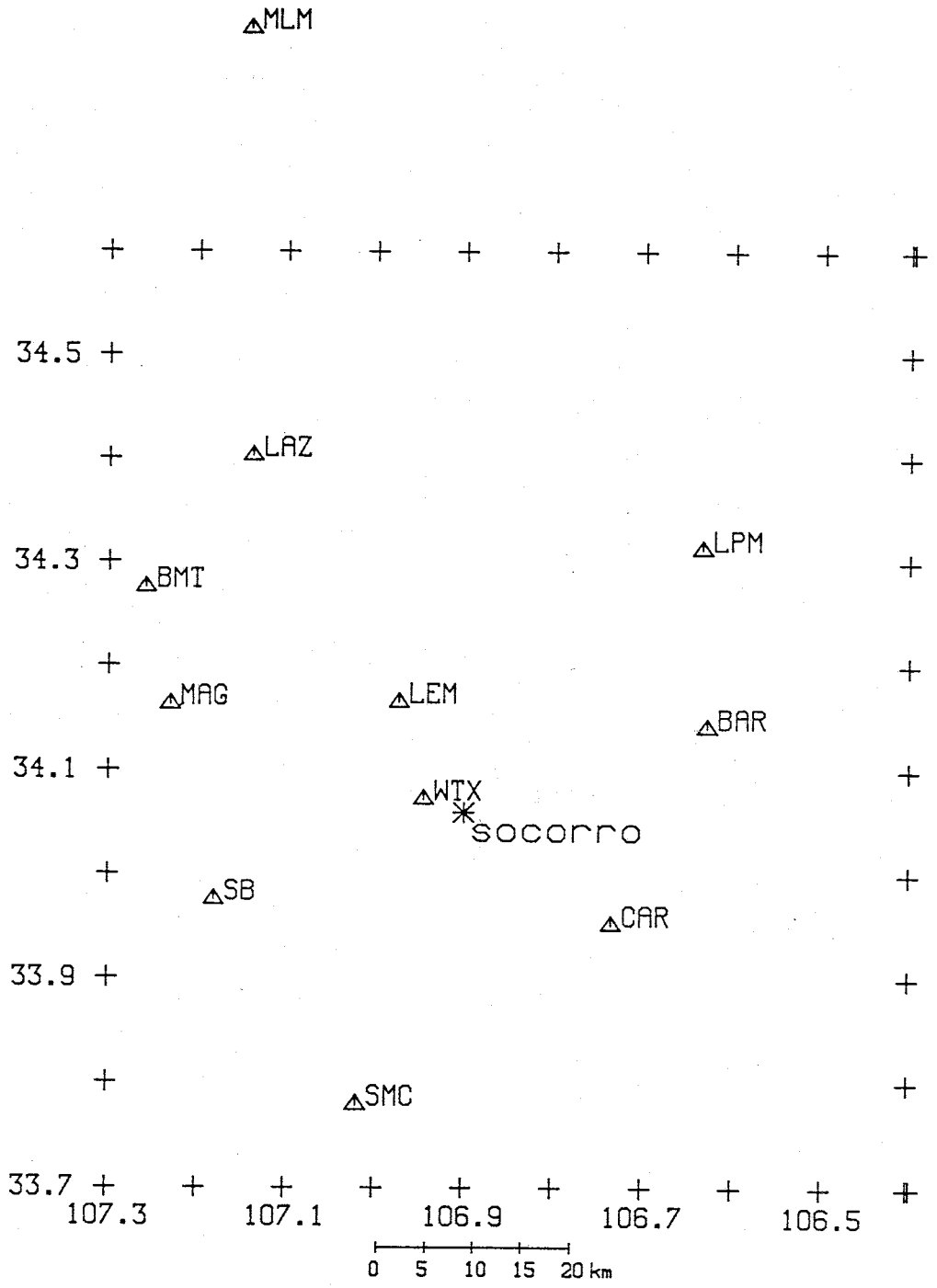

Figure 19: Stations of the Socorro seismograph networks which recorded P* data.

Table 5

List of Events

Pn Phase

Date	Time	Latitude	Longitude
12/10/67	19:30:00.10	36.6780 ° N	107.2080 ° W
12/03/75	10:12:22.80	32.8300 ° N	108.6630 ° W
01/29/76	08:04:28.46	32.9190 ° N	108.7100 ° W
01/30/76	08:45:01.55	34.5070 ° N	109.8910 ° W
02/04/76	00:04:58.10	34.6550 ° N	112.5000 ° W
02/28/76	20:53:58.50	35.9100 ° N	111.7880 ° W
06/24/76	15:27:32.00	35.6180 ° N	103.2780 ° W
07/12/76	19:25:54.10	32.8010 ° N	108.0708 ° W
08/04/76	22:31:35.44	33.0630 ° N	109.3350 ° W
08/16/76	18:39:42.66	33.0902 ° N	109.3592 ° W
08/16/76	19:33:09.24	32.8010 ° N	108.0708 ° W
08/16/76	21:03:16.66	32.6522 ° N	108.3688 ° W
08/23/76	21:54:30.36	33.0902 ° N	109.3592 ° W
02/14/77	21:10:50.14	32.8010 ° N	108.0708 ° W
02/14/77	22:29:28.36	33.0902 ° N	109.3592 ° W
02/14/77	22:50:28.31	32.6522 ° N	108.3688 ° W
04/11/77	20:14:42.25	32.6522 ° N	108.3688 ° W
04/25/77	21:57:08.51	33.0902 ° N	109.3592 ° W
05/02/77	20:14:49.93	32.6522 ° N	108.3688 ° W
05/02/77	20:31:35.67	32.8010 ° N	108.0708 ° W
06/08/77	13:09:07.40	31.0240 ° N	109.2270 ° W
07/20/77	07:40:49.49	35.6270 ° N	109.0000 ° W
06/16/78	11:46:53.20	33.0200 ° N	100.7200 ° W
03/05/79	13:00:02.70	36.3770 ° N	106.1740 ° W
05/03/81	22:54:09.37	32.2703 ° N	108.9387 ° W
05/04/81	10:55:32.17	32.2703 ° N	108.9387 ° W
05/07/81	01:38:20.57	32.2703 ° N	108.9387 ° W
05/11/81	23:28:12.87	32.2703 ° N	108.9387 ° W
10/21/82	22:31:53.82	33.0630 ° N	109.3350 ° W
10/23/82	20:14:37.06	36.5400 ° N	110.3860 ° W
11/03/82	17:54:11.57	35.1750 ° N	108.7220 ° W
11/28/82	02:36:53.19	33.5780 ° N	100.8710 ° W
01/27/83	20:48:48.49	32.8010 ° N	108.0708 ° W
02/17/83	20:50:26.21	36.7410 ° N	108.0830 ° W
04/26/83	22:34:17.63	35.6242 ° N	109.0852 ° W
06/30/83	02:12:18.53	35.9740 ° N	104.6760 ° W
09/15/83	23:25:35.24	35.0625 ° N	104.3442 ° W
09/29/83	07:44:10.45	35.0902 ° N	104.4552 ° W
04/27/84	10:05:54.41	32.7457 ° N	109.3475 ° W
01/29/85	05:37:59.96	35.4572 ° N	111.7052 ° W
06/05/85	10:36:00.00	32.5425 ° N	106.9407 ° W
07/23/85	00:44:49.17	36.6187 ° N	108.4667 ° W
08/01/85	01:44:16.57	36.6400 ° N	110.2750 ° W

Table 5 (continued)

09/06/85	05:22:46.10	32.5425 ° N	106.9407 ° W
09/30/85	20:21:29.31	32.8010 ° N	108.0708 ° W
12/15/85	07:14:52.43	35.4282 ° N	104.6263 ° W
03/27/86	22:36:35.54	36.4623 ° N	110.1250 ° W
04/03/86	20:32:10.11	32.5925 ° N	108.0565 ° W
04/17/86	21:04:29.40	32.5425 ° N	106.9407 ° W
05/14/86	15:03:03.60	37.3447 ° N	110.2662 ° W
05/22/86	16:42:44.81	35.7467 ° N	108.9645 ° W
05/24/86	00:14:31.76	32.9868 ° N	109.5155 ° W
06/12/86	03:52:16.37	33.0828 ° N	109.4802 ° W
08/27/86	17:27:48.41	32.6522 ° N	108.3688 ° W
08/27/86	18:06:58.46	35.1183 ° N	105.1773 ° W
08/27/86	18:34:45.01	33.0902 ° N	109.3592 ° W
09/08/86	19:40:05.74	35.7717 ° N	108.8332 ° W
12/23/86	03:20:36.10	30.9415 ° N	109.1538 ° W
12/27/86	21:56:04.51	33.0902 ° N	109.3592 ° W
02/01/87	19:26:55.18	35.6638 ° N	108.9638 ° W
03/19/87	12:20:49.49	35.0448 ° N	109.8357 ° W
04/01/87	20:02:15.63	33.1408 ° N	109.5612 ° W
04/21/87	17:19:21.91	32.6522 ° N	108.3688 ° W
04/21/87	21:56:08.31	33.0902 ° N	109.3592 ° W
04/29/87	13:36:31.14	32.6377 ° N	105.9367 ° W
06/01/87	21:27:31.50	32.3940 ° N	106.8682 ° W
07/04/87	13:57:53.29	33.7282 ° N	108.8015 ° W
09/10/87	14:16:23.27	32.3770 ° N	109.0467 ° W
09/13/87	14:27:30.50	35.6528 ° N	108.2717 ° W
10/02/87	07:15:12.46	37.1732 ° N	107.8692 ° W
10/02/87	10:02:50.46	37.1732 ° N	107.8692 ° W
10/02/87	20:50:19.41	37.1732 ° N	107.8692 ° W
01/31/88	09:24:36.18	29.8947 ° N	105.1845 ° W
02/14/88	07:39:52.61	36.1660 ° N	111.0183 ° W
03/18/88	23:56:39.33	36.4508 ° N	108.6888 ° W
03/26/88	18:08:10.71	32.6522 ° N	108.3688 ° W
03/26/88	18:27:33.69	32.8010 ° N	108.0708 ° W
03/26/88	21:05:48.18	36.5667 ° N	108.4322 ° W
06/11/88	08:58:35.50	30.7890 ° N	109.4160 ° W

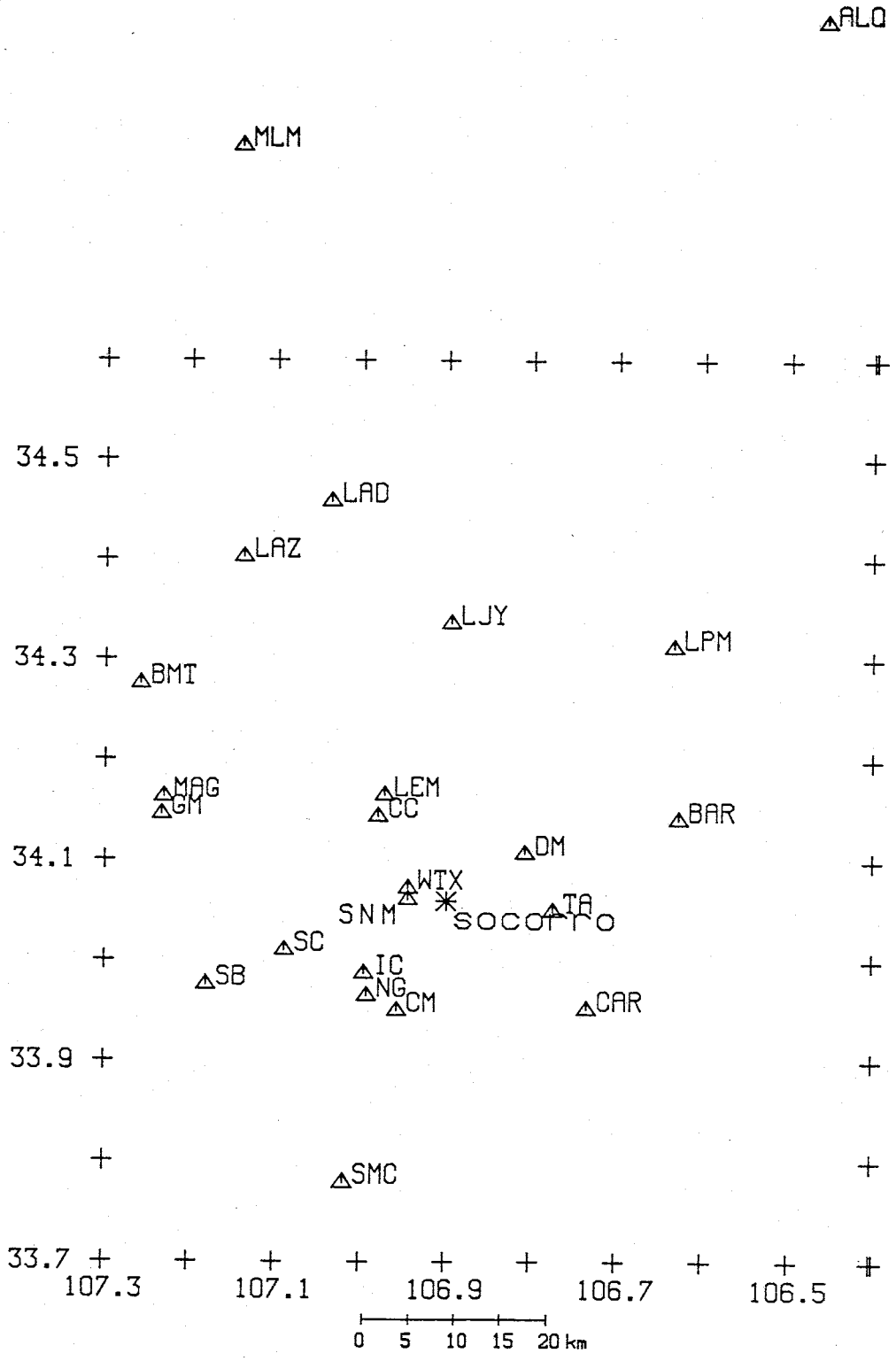

Figure 20: Stations of the Socorro seismograph networks which recorded Pn data.

ANALYSES PERFORMED

Four separate time-term analyses were performed on each data set. Unmodified analysis was done using equation (2), as well as three modified analyses:

1. anisotropy analysis based on equation (9);
2. dip analysis based on equation (13); and
3. distance analysis based on equation (11).

Unmodified Analysis

The results of the unmodified analysis consist of an average refractor velocity and time terms for each source and station, as well as standard errors for each of these parameters. Equation (2) assumes a simple velocity structure and so requires no further analysis.

Modified Analyses

In order to investigate the effects of anisotropy, dip or a lateral velocity gradient, and a vertical velocity gradient, an offset distance must be assumed for each major refractor. Using the velocity/depth model of Toppozada and Sanford (1976) (Model 1, Figure 5), and replacing the upper 2 km of upper crustal material with Phanerozoic rocks (compressional velocity = 3.4 km/s), offset distances of 1.5 km for Pg, 30 km for P*, and 40 km for Pn, were obtained. Varying the offset distance within reasonable bounds does not significantly affect the analyses (Zervas and Crosson, 1986).

Anisotropy Analysis

The results of the anisotropy analysis are in the form of time terms, a velo-

city, and the four coefficients of the sine and cosine terms of equation (9). The magnitude of the $cos(2\Phi)$ dependence is:

$$|dV|_{2\Phi}=(A^2+B^2)^{1/2}, \tag{17}$$

with a phase angle (Ω) of:

$$\Omega_{2\Phi}=\frac{\tan^{-1}\left(\frac{A}{B}\right)}{2}, \tag{18}$$

where

A is the coefficient of the $sin(2\Phi)$ term;

B is the coefficient of the $cos(2\Phi)$ term.

In the same way, the $cos(4\Phi)$ dependence is:

$$|dV|_{4\Phi}=(C^2+D^2)^{1/2}, \tag{19}$$

with a phase angle (Ω) of:

$$\Omega_{4\Phi}=\frac{\tan^{-1}\left(\frac{C}{D}\right)}{4}, \tag{20}$$

where

C is the coefficient of the $sin(2\Phi)$ term;

D is the coefficient of the $cos(2\Phi)$ term.

Dip Analysis

The results of the dip analysis are computed in a similar manner to those of the anisotropy analysis., except A is now the coefficient of the $sin(\Phi)$ term, and B is the coefficient of the $cos(\Phi)$ term of equation (13). That is,

$$A=-V_o\,\alpha cot(\Theta_c)sin(\Psi), \tag{21}$$

and

$$B=-V_o\,\alpha cot(\Theta_c)cos(\Psi), \tag{22}$$

where

alpha is the true dip angle,

Θ_c is the critical angle, and

Ψ is the azimuth of the true dip direction.

The magnitude of the $cos(\Phi)$ dependence is:

$$|dV|_{\Phi}=(A^2+B^2)^{1/2}, \tag{23}$$

with a phase angle (Ω) of:

$$\Omega_{\Phi}=\tan^{-1}\left(\frac{A}{B}\right) \tag{24}$$

Ω is the direction of maximum apparent velocity, i.e. the up-dip direction. It is standard practice to list the down-dip direction. Hence, the dip direction is equal to Ω plus 180°. As previously discussed in the Theory section, equation (14), when the shot-station azimuth and the phase (the up-dip direction) are the same, dV is a maximum and

$$|dV|=V_o \alpha cot(\Theta_c). \tag{25}$$

Assuming a Θ_c, a true dip angle can be computed using equation (14):

$$\alpha = \frac{|dV|}{V_o} tan(\Theta_c). \tag{14}$$

The critical angle for each of the three refractors was computed using Snell's Law. Thus,

$$\Theta_c=\sin^{-1}\left(\frac{V_i}{V_{i+1}}\right), \tag{26}$$

where

V_i is the velocity of the layer above the refractor of interest, and

V_{i+1} is the average dip velocity of the refractor of interest.

Distance Analysis

The results of the distance analysis yield a velocity and a distance coefficient W_1 for the linear change in velocity with distance. To compute the velocity change for a given refractor,

$$dV = W_1 \Delta_{ij}, \tag{27}$$

for any Δ_{ij} within the distance range of the data, e.g. Δ_{ij} for Pg would range from a few kilometers out to ~150 km. Generally, W_1 is positive which is indicative of an increase in velocity with depth below the refracting interface (Appendix 4).

Validity of Modified Analyses

It is important to ascertain whether or not the modified time-term analyses used are valid, i.e. provide a better explanation of the data. Following Hearn (1974) and Zervas and Crosson (1986), the F test was used to determine whether a modified equation provided a better fit to the data than the unmodified equation. The F ratio is defined as:

$$F = \frac{(SSWR_u - SSWR_m)/(DF_u - DF_m)}{SSWR_m / DF_m}, \tag{28}$$

where

SSWR is the sum of the squared weighted residuals, and

DF are the number of degrees of freedom.

The subscripts u and m refer to the unmodified and modified time-term equations, respectively. If the F ratio is larger than the value given by the F probability distribution at the 5 percent level for $DF_u - DF_m$ and DF_m degrees of freedom, there is a 95 percent probability that the modified time-term equation has significantly improved the fit. The F test was applied to the results from equations (9) and (11) for all three data sets.

TIME-TERM ANALYSES OF VELOCITY, ANISOTROPY, AND DIP

Pg

The Pg data set (Figure 21) consists of 265 high-quality readings from 43 local explosions (Table 3 and Map 1) recorded at 27 stations (Figure 18). Unmodified and modified analyses were performed on the complete Pg data set.

Unmodified Analysis

The unmodified analysis gave an average velocity of 5.95 ± 0.03 km/s (1 s.d.) for the Precambrian basement. This value falls within the range of velocities observed for the central rift, but is 0.10 to 0.15 km/s higher than typical values for the Socorro area (Table 6). Also, examining Figure 22, the fit of the data to the unmodified model decreases with increasing distance. Both of these points will be addressed in the section on distance analysis.

Modified Analyses

Anisotropy. Table 7 tabulates the computational results of the anisotropy analysis. There is no change in the refractor velocity from the unmodified analysis, and the velocity variations with respect to azimuth are very small and of the order of their uncertainties (Figure 23). Thus, these variations have little meaning. Moreover, this model shows no significant improvement in fitting the data (Table 8). Hence, no anisotropy in the basement velocity is indicated in this part of the rift. Ward (1980) also found no evidence for an azimuthal velocity distribution in the Socorro area.

Dip. The results of the dip analysis are presented in Table 7. Figure 24 shows the generally small velocity perturbations resulting from time term

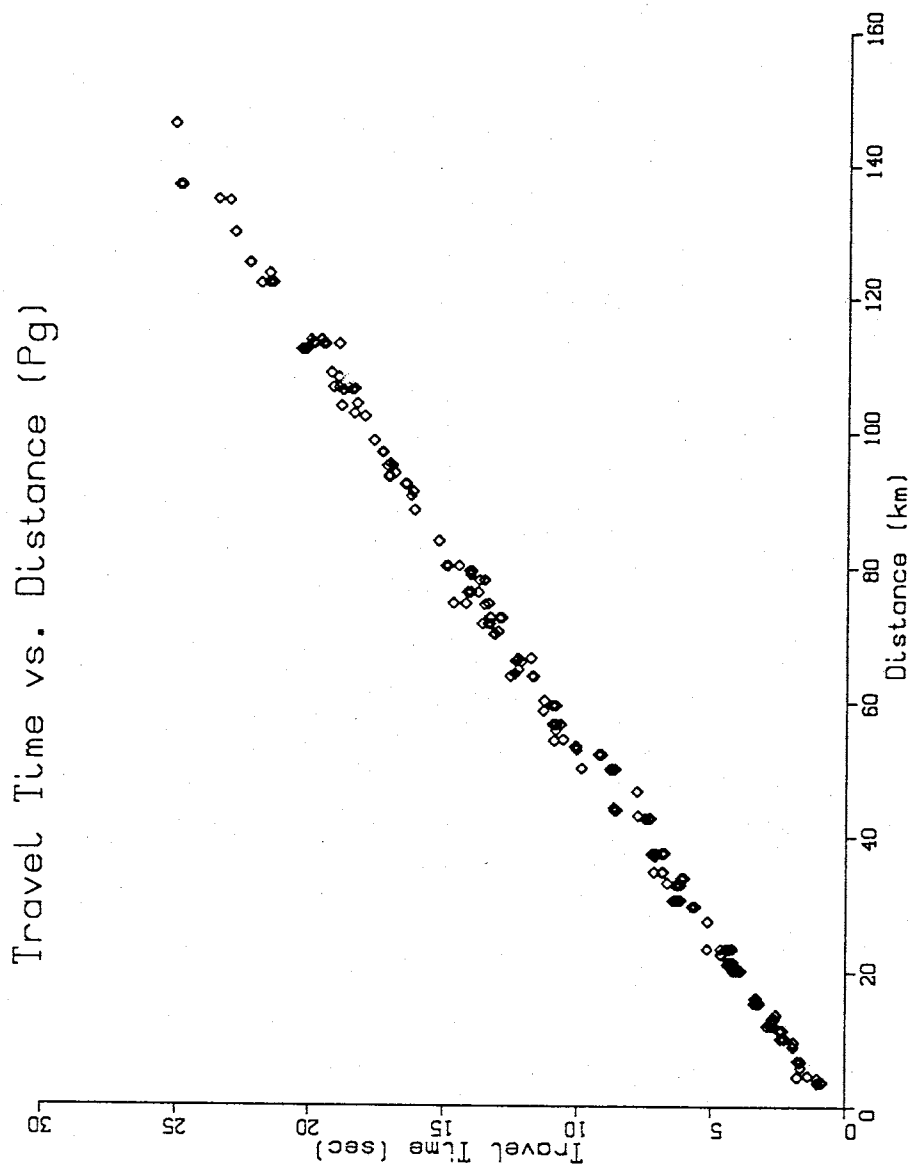

Figure 21: Travel time plot of Pg data. Data is essentially linear but shows a small increase in velocity with distance.

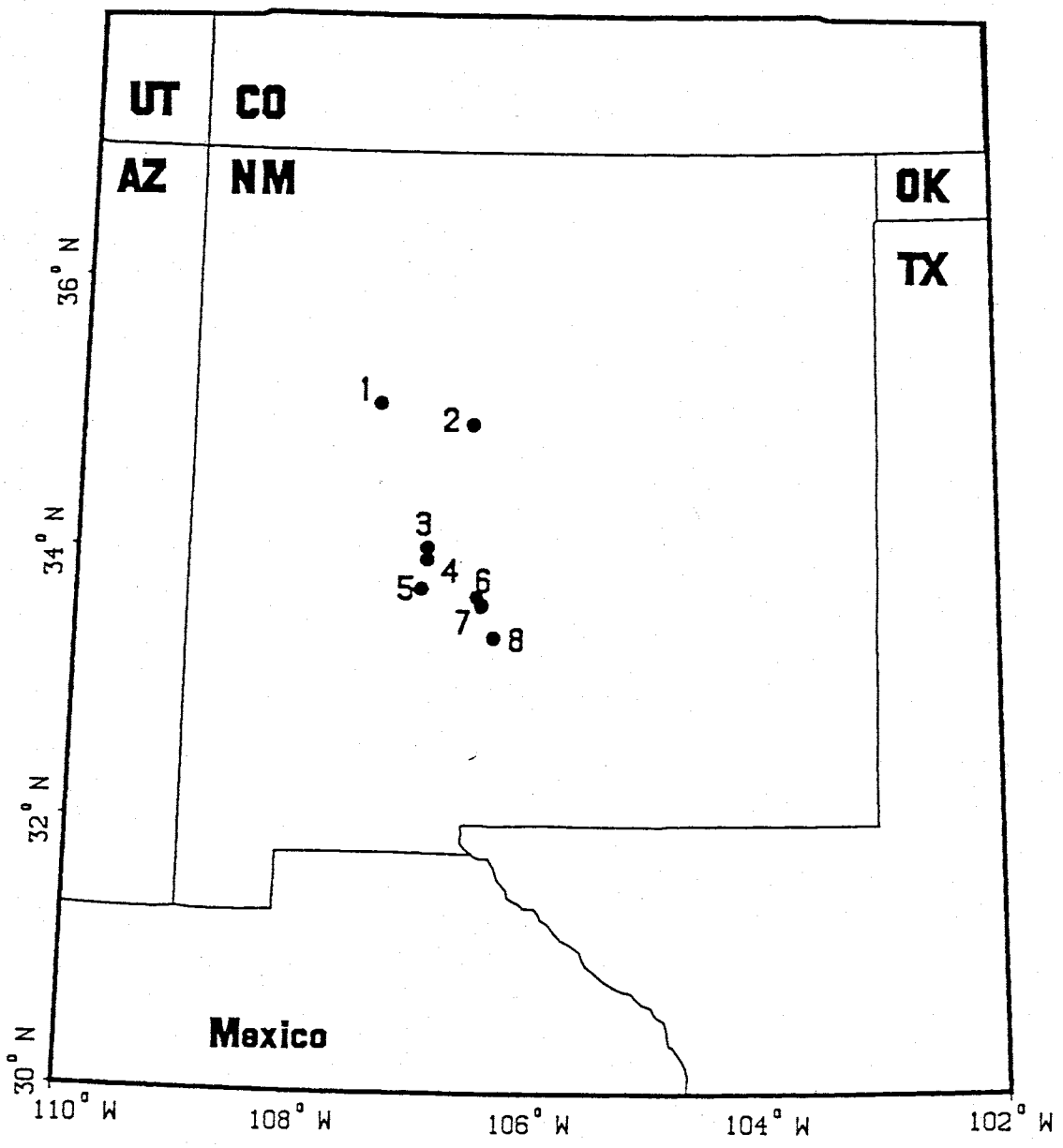

Map 1: Geographical distribution of the sources for the Pg data set. Each point represents several sources recorded by the Socorro seismic networks from the given locales: (1) Jackpile Mine, (2) Kirtland Air Force Base, (3) TERA, on the New Mexico Tech campus, (4) Red Canyon Mine, (5) San Marcial Mine, and (6), (7), and (8) White Sands Missile Range.

Table 6

Upper Crustal Velocities

State of New Mexico

Study	Region	Velocity (km/s)	Depth Range (km)
Toppozada & Sanford (1976)	RGR	5.8	0 - 19
Sanford et al. (1973)	Socorro	5.8	0 - 18
Ward (1974)	Socorro	5.9	0 - 14
Rinehart & Sanford (1974)	Socorro	5.8 6.0	0 - 10 10 - 19
Olsen et al. (1979)	Central RGR	6.0	3 - 22
Phinney (1964)	Albuquerque	6.1	0 - 20
Ankeny et al. (1986)	N Central RGR	5.9	3 - 23
Olsen et al. (1986)	N Central RGR	5.9	Basement
Cook et al. (1974)	Southern RGR	5.7 6.2	0 - 7 7 - 27
Sinno et al. (1986)	Southern RGR	5.9 6.1	0 - 9 9 - 19
Dee (1973)	Southwest NM	6.2	2 - 36
Jaksha (1982)	Southwest NM	6.0	3 - 24
Jaksha & Evans (1984)	Col. Plateau	6.1	3 - 31
Stewart & Pakiser (1964)	Great Plains	6.1	4 - 19

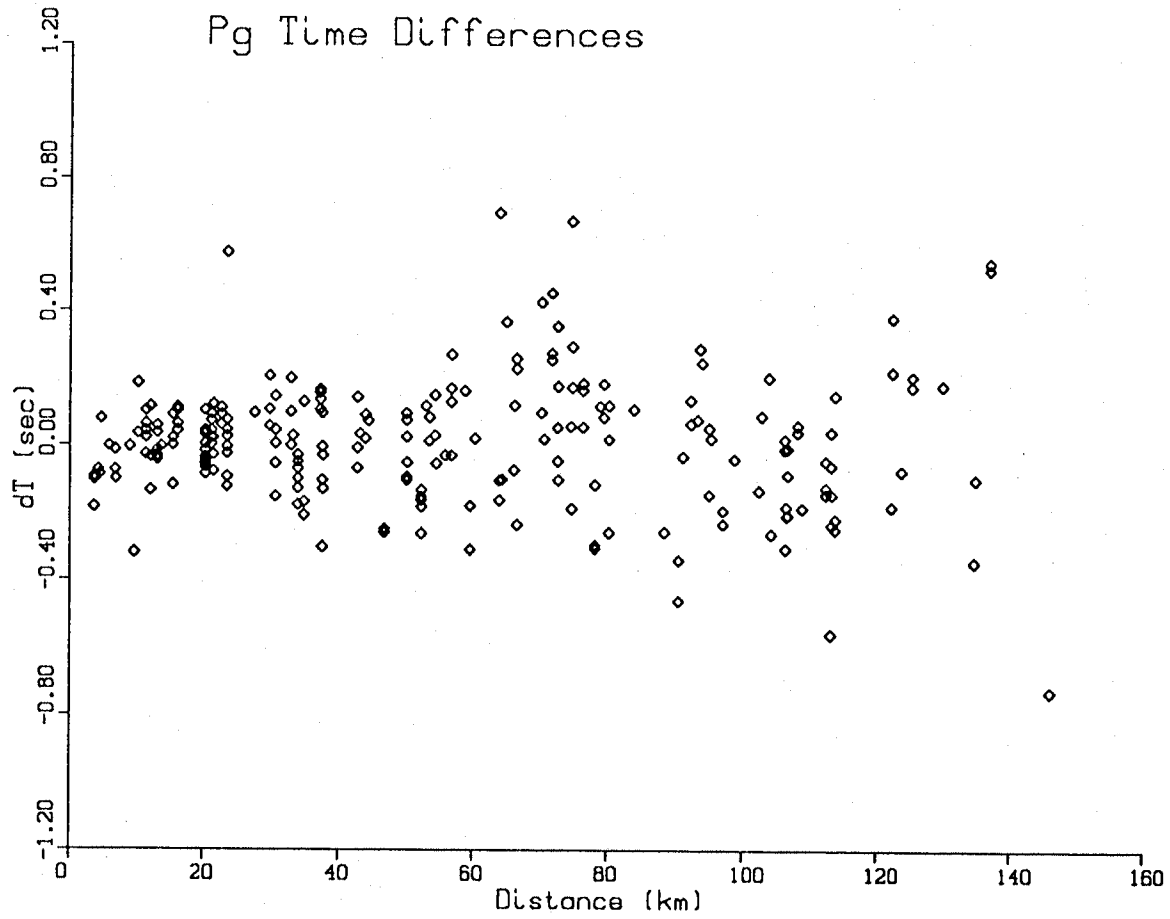

Figure 22: Travel time residuals versus distance for Pg data resulting from an unmodified time-term analysis. The fit of the model decreases with increasing distance.

Table 7

Time Term Results

Pg Refractor

Model	Velocity (km/s)	Data	Parameters	SSWR
Unmodified	5.95±0.03	269	41	7229
Anisotropy	5.95±0.03	269	45	7040
	Sin2ϕ Factor −0.01668±0.01991			
	Cos2ϕ Factor 0.02663±0.02247			
	Sin4ϕ Factor −0.01665±0.02041			
	Cos4ϕ Factor 0.00498±0.01485			
Dip	5.91±0.04	269	16	13505
	Sinϕ Factor 0.01500±0.02450			
	Cosϕ Factor 0.11920±0.03297			
Distance	5.71±0.07	269	42	6817
	Distance Factor (1/s) 0.00172±0.00047			

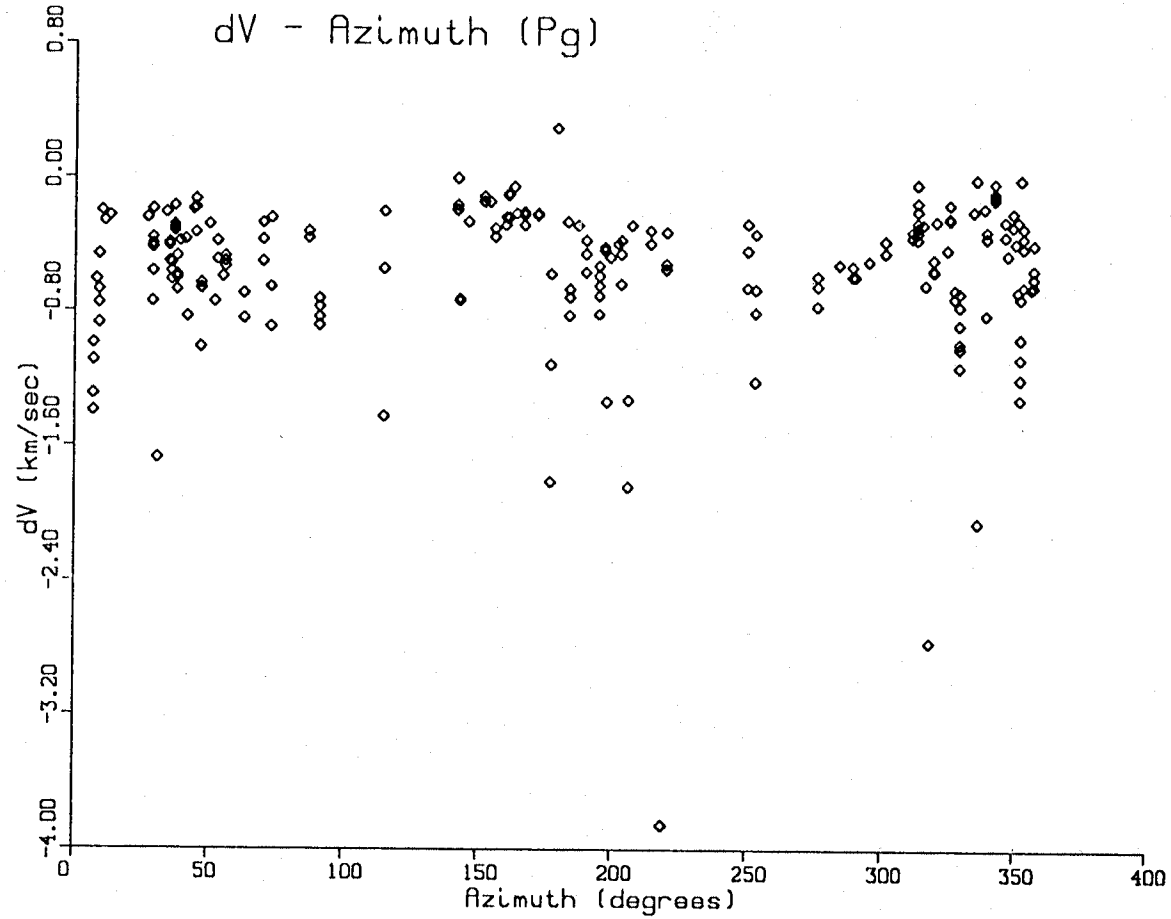

Figure 23: Velocity perturbations versus azimuth for Pg data resulting from a modified time-term analysis assuming a slightly anisotropic upper crust. Little if any anisotropy is indicated.

Table 8

Analysis of Variance Table for Modified Time Term Equations

Pg Refractor

Model	SSWR	DF	$DF_U - DF_M$	F
Unmodified	7229	228		
Azimuth Dependence	7040	224	4	1.5
Distance Dependence	6817	227	1	13.7

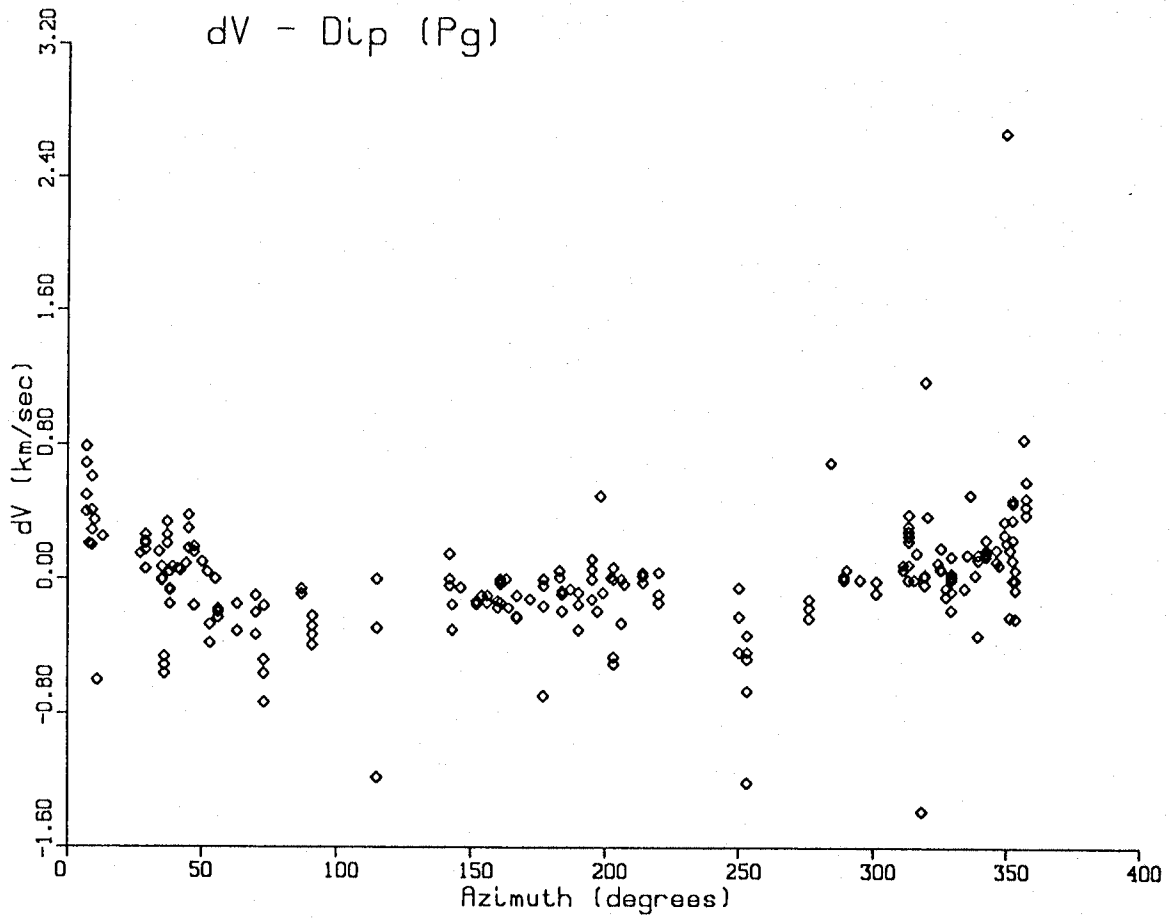

Figure 24: Velocity perturbations versus azimuth for Pg data resulting from a modified time-term analysis in which a sloping Precambrian basement is assumed. The $cos(\Phi)$ azimuth dependence indicated by these data is consistent with an average basement dip of less than 1°.

alysis in which a sloping Precambrian basement is assumed. The magnitude the $cos(\Phi)$ dependence is 0.120 ± 0.033 km/s, with a phase angle of 7.2 ± .8°. Assuming a critical angle of 36.3°, a dip angle of 0.9 ± 0.2° to the uth is indicated, but considering the the extreme complexity of the ~~of~~ refractor face, it is considered of little significance (see section of Pg Time Terms).

Distance. Table 7 displays the results of the distance analysis. This odified analysis assuming a linear increase in velocity with distance provided e best model of the Pg data (Table 8). Figure 25 indicates the generally excel- fit of the data to the distance model. This distinct dependence of the Pg locity on source distance implies a velocity gradient with depth in the Precam- an basement. The relationship between the horizontal and vertical gradients is lined in Appendix 4. Figure 26 shows the determined velocity increase with pth.

Both laboratory (e.g. Birch, 1960) and field measurements (e.g. Giese, 1963) monstrate that P wave velocity increases rapidly with increasing overburden ssure, especially in the upper part of the upper crust, as cracks and voids are osed. While the effect of increasing temperature with depth is to decrease velo- ty, the velocity increase due to pressure is the more significant effect down to ound 20 km (Smithson et al., 1981). The results of the present study are well thin this bound because the deepest Pg waves bottomed just below 10 km. nce, a increase in velocity with depth seems to exist in the Rio Grande rift sement. The 1986 PASSCAL experiment in the Basin and Range shows a ilar velocity increase in the upper crust with a velocity of 5.5 km/s at 2 km pth increasing to a velocity of just over 6.0 km/s at 10 km. From this study the Rio Grande rift, the corresponding values are a 5.7 km/s velocity at the p of the Precambrian increasing to a just under 6.0 km/s at a depth of 10 km.

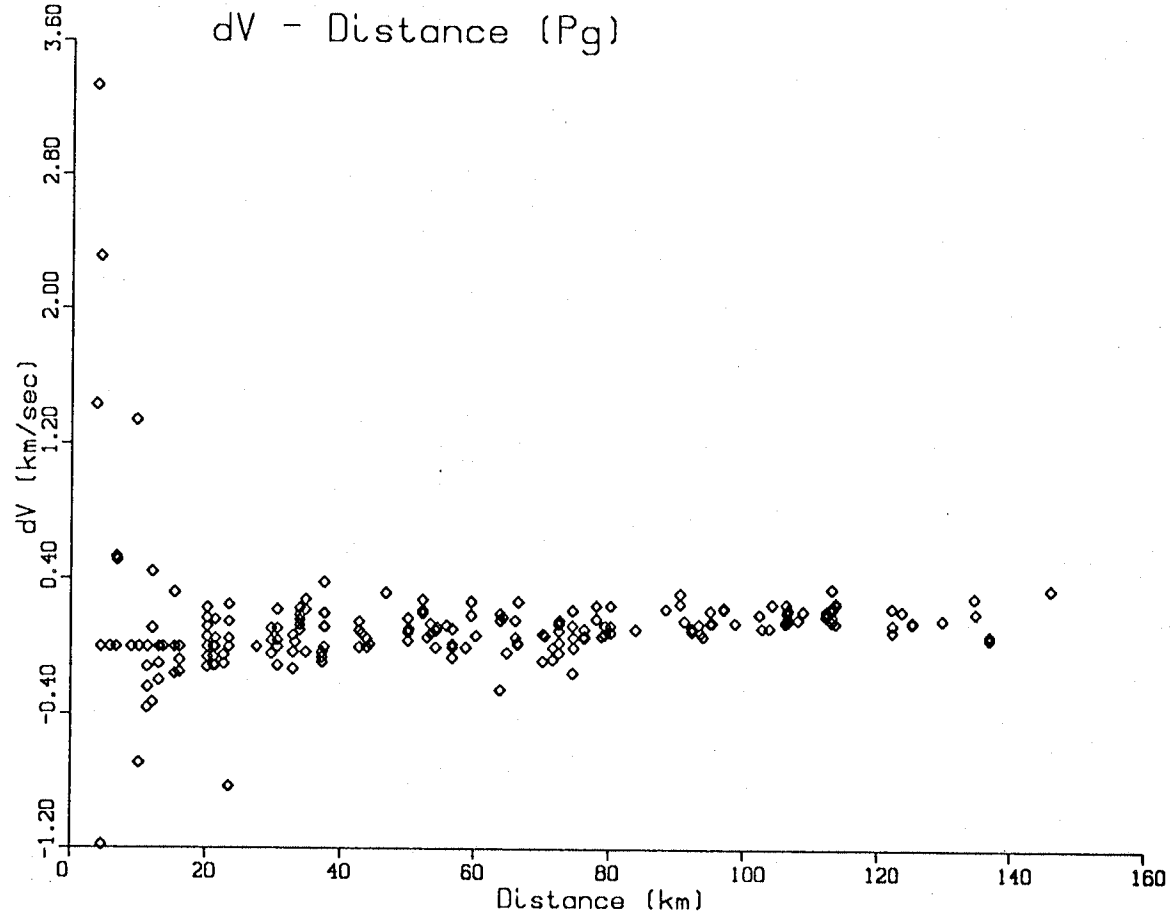

Figure 25: Velocity perturbations versus distance for Pg data resulting from a modified time-term analysis assuming a small vertical velocity gradient in the Precambrian basement (see text). Increase with distance indicates a small positive gradient in the upper part of the crust for this region. The large scatter at close distances may be the result of direct arrivals in the data set.

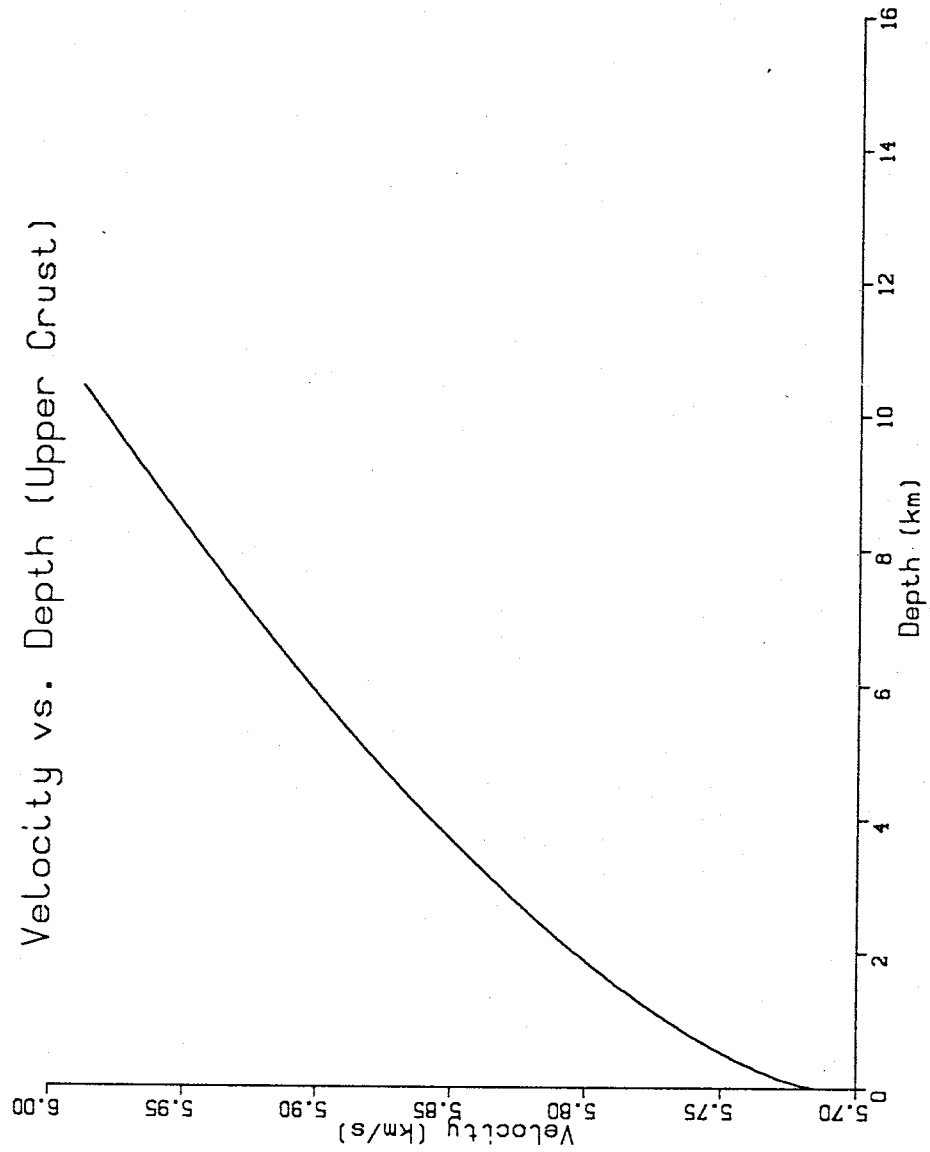

Figure 26: Velocity gradient in the upper crust as determined from a modified time-term analysis. The absence of Pg data from beyond 160 km allows determination of the basement velocity to only 10 km.

Assuming an average upper crustal velocity of approximately 6.0 km/s (Rinehart and Sanford, 1981), the velocity gradient in the upper crust must decrease dramatically below this depth.

The average velocity of the upper 10 km of the crust is 5.86 km/s. The agrees well with the 5.85 $\pm$ 0.02 km/s value Ward (1980) obtained from an inversion of microearthquake data in the Socorro area which had an average focal depth of ~8 km.

P*

The P* data set is smaller and more uncertain than either the Pg or Pn data sets. Only 72 readings (Figure 27) were obtained from 24 regional earthquakes (Map 2) recorded at 11 stations (Figure 19). Unmodified and modified analyses were run on the complete P* data set.

Unmodified

The unmodified time-term analysis yielded an average velocity of 6.40 ± 0.16 km/s for the mid-crustal refractor. Figure 28 shows that the fit of the P* data to the unmodified model is not nearly as good as was the fit of the Pg data (Figure 21). Nevertheless, this value falls within the range of mid-crustal velocities observed in the rift (Table 9), and agrees exactly with the velocity of Olsen et al. (1979) in the central rift. In accord with previous studies in the rift, the P* velocity is low with respect to the adjacent Great Plains and Colorado Plateau geologic provinces, which exhibit mid-crustal velocities of 6.7 km/s or higher (Stewart and Pakiser, 1962; Jackson et al., 1963; Roller, 1965; Jackson and Pakiser, 1965; Warren, 1969; Jaksha and Evans, 1984). The low velocity values are most likely to be the result of elevated temperatures at mid-crustal levels caused by lithospheric thinning and magmatic intrusion. Given the presence of a laterally extensive magma body at the depth of the Conrad beneath the Socorro area (Sanford, 1977; Rinehart et al., 1979), and temperature estimates on the order of 700 ° C at this level (Baldridge et al., 1984), a low P* velocity should be expected.

Modified

It should be noted that because of the sparsity and less-than-optimum quality of the data, the following modified time-term results are not considered as

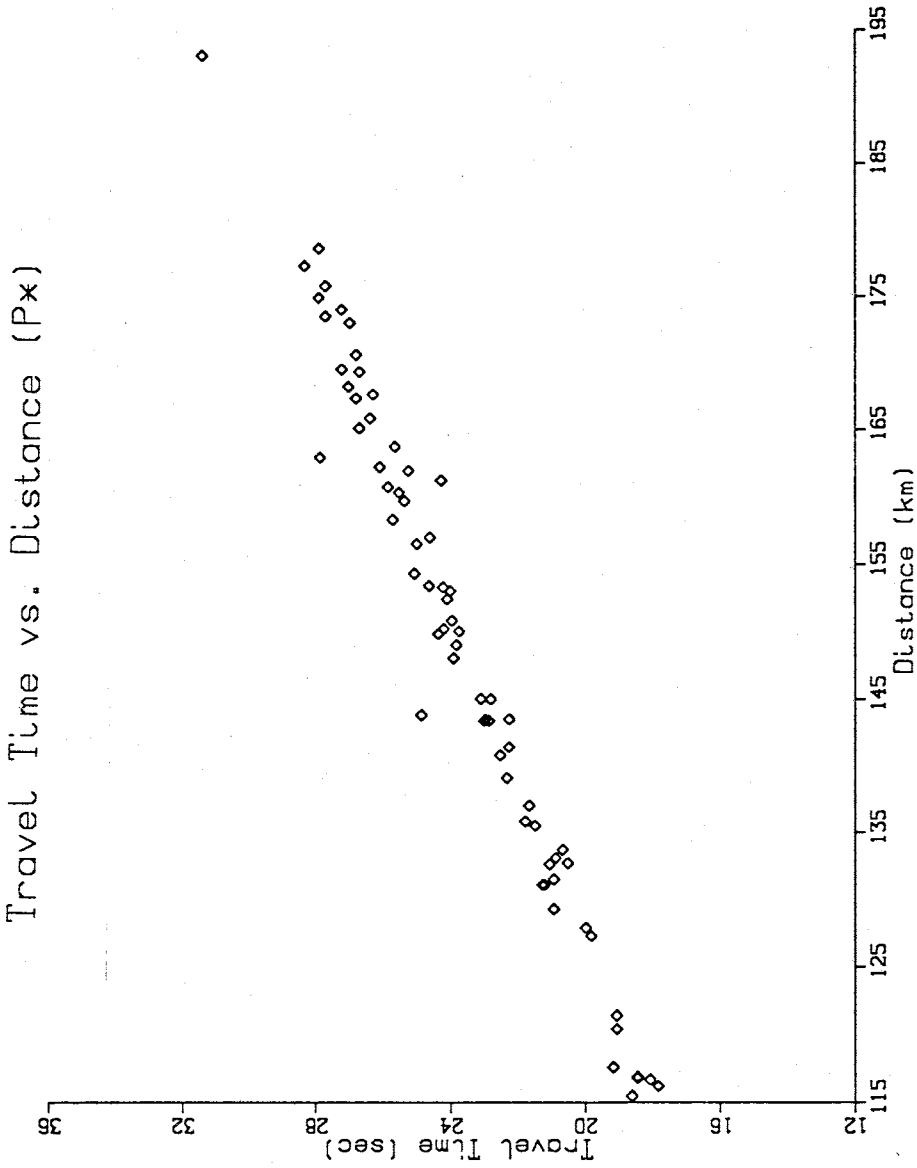

Figure 27: Travel time plot of P* data. The density and quality of the P* data is much less than that of the Pg or Pn data sets.

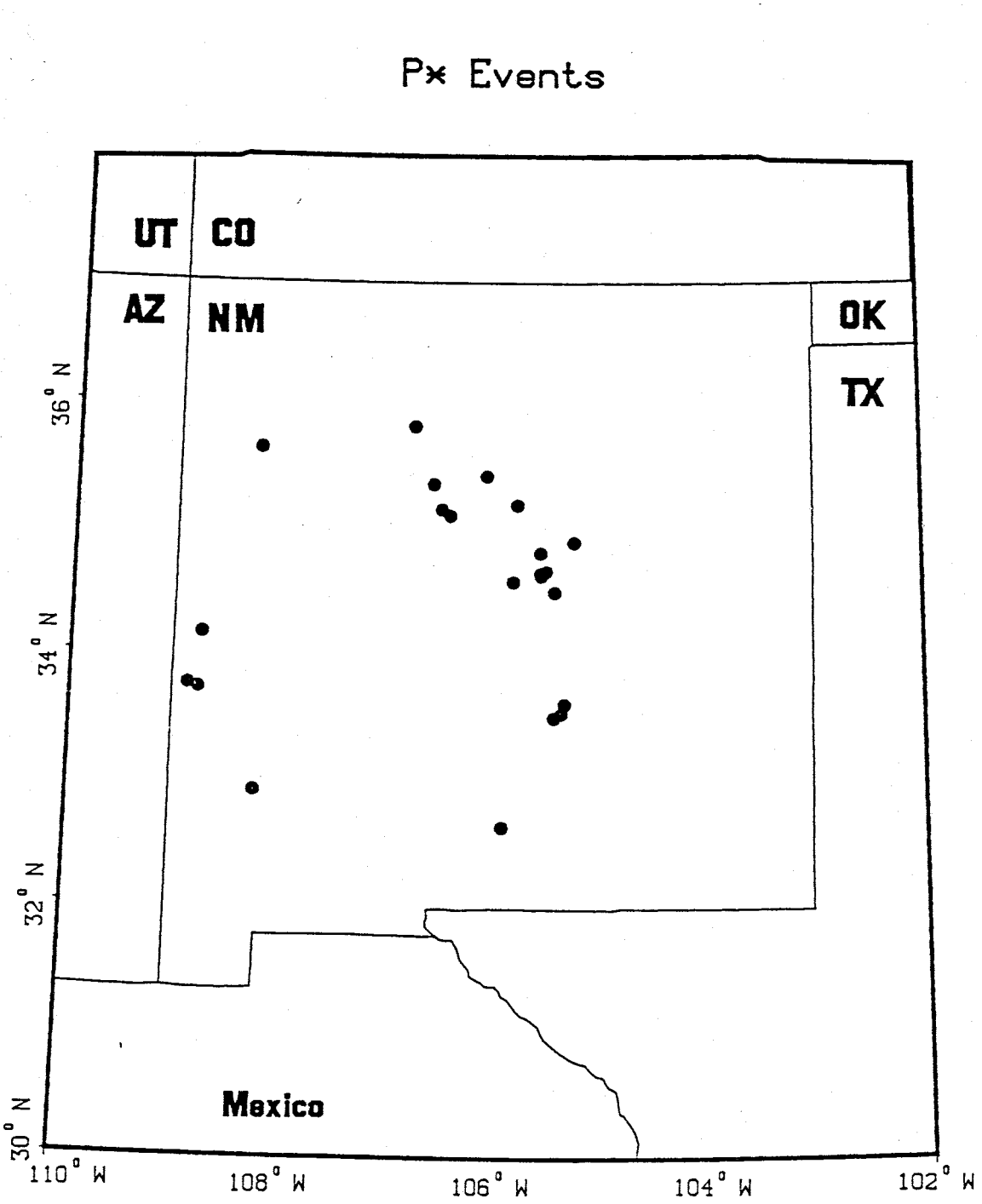

Map 2: Geographical distribution of the sources for the P* data set. Events must be within a narrow band of distances for P* to be recorded as a first arrival at the networks.

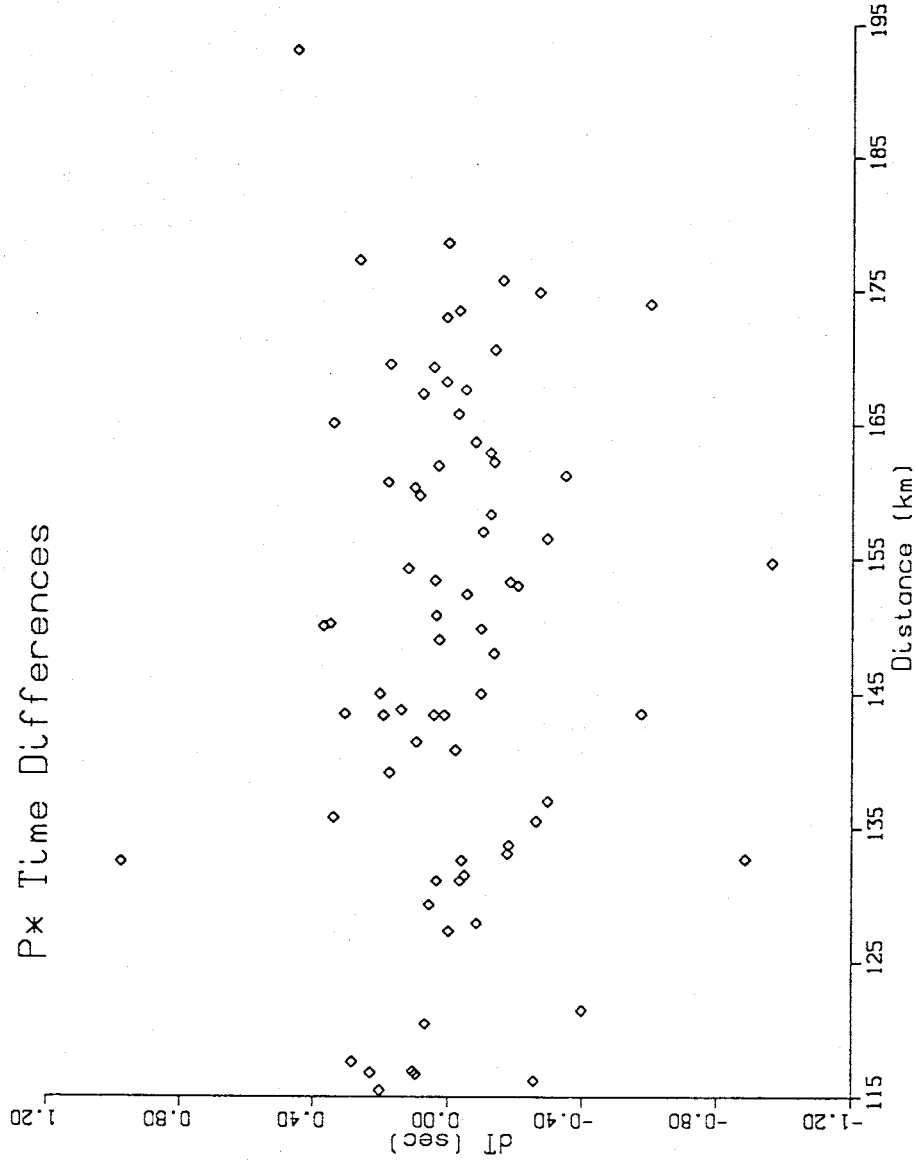

Figure 28: Travel time residuals versus distance for P* data resulting from an unmodified time-term analysis. The scatter is probably related to the uncertainty in the original data set rather than structural effects.

Table 9

Lower Crustal Velocities

State of New Mexico

Study	Region	Velocity (km/s)	Depth Range (km)
Toppozada & Sanford (1976)	RGR	6.5	19 - 40
Olsen et al. (1979)	Central RGR	6.4	22 - 34
Phinney (1964)	Albuquerque	6.7	20 - 40
Cook et al. (1974)	Southern RGR	6.2	7 - 27
		7.4	27-35
Sinno et al. (1986)	Southern RGR	6.6	19 - 30
Dee (1973)	Southwest NM	6.2	2 - 36
Jaksha (1982)	Southwest NM	6.5	24 - 30?
		7.4	30? - 33?
Jaksha & Evans (1984)	Col. Plateau	7.0	31 - 48
Stewart & Pakiser (1964)	Great Plains	6.7	19 - 31
		7.4	31 - 51

meaningful as the results for the other two refractors.

Anisotropy. The results of the anisotropy analysis are listed in Table 10. This model shows a small decrease in the average refractor velocity and a fairly large $\cos 2\phi$ dependence of 0.274 $\pm$ 0.113 km/s with a phase angle of 4.8 $\pm$ 16.1°. Figure 29 shows the velocity perturbations with respect to azimuth assuming anisotropy. Although a north-south anisotropy is consistent with rift geometry, this model does not provide any statistically significant improvement in fit to the data (Table 11).

Dip. Table 10 displays the computational results of the dip analysis. Of particular interest is the fairly large $cos(\Phi)$ dependence of 0.291 $\pm$ 0.133 km/s and phase angle of 301.3 $\pm$ 22.0°. Figure 30 shows the the velocity perturbations with respect to azimuth for the dip model. Assuming a critical angle of 67.8°, this corresponds to a dip of 6.5 $\pm$ 3.0° to the southeast. The result is not well constrained and it appears to be inconsistent with previous work in the area. The microearthquake reflection studies in the area (Sanford et al., 1973; Rinehart and Sanford, 1981) and the COCORP reflection profiles (Brown et al., 1980) both show a north-dipping refractor. COCORP lines 2 and 2a (Figure 31) indicate that the Conrad may suddenly deepen to the northeast. Dip to the northeast is ~7° on line 2a, increasing substantially at the northeastern end. This may indicate that the mid-crustal boundary is a complicated surface.

Distance. Solving for an increase in velocity with distance, the unmodified time-term method gives an unreasonably high velocity with a huge uncertainty (Table 10). Figure 32 displays the unrealistically large velocity perturbations for this model. Although this study was unable to quantify a velocity gradient below the Conrad, such an increase is not unreasonable. For instance, the 1986

Table 10

Time Term Results

P Refractor*

Model	Velocity (km/s)	Data	Parameters	SSWR
Unmodified	6.40±0.16	72	33	959
Anisotropy	6.29±0.15	72	37	761
	Sin2ϕ Factor 0.04632±0.15475			
	Cos2ϕ Factor 0.26983±0.11152			
	Sin4ϕ Factor 0.02803±0.09332			
	Cos4ϕ Factor 0.05091±0.05660			
Dip	6.32±0.15	72	25	1493
	Sinϕ Factor -0.24878±0.14402			
	Cosϕ Factor 0.15121±0.09758			
Distance	9.97±3.10	72	34	882
	Distance Factor (1/s) -0.02359±0.01955			

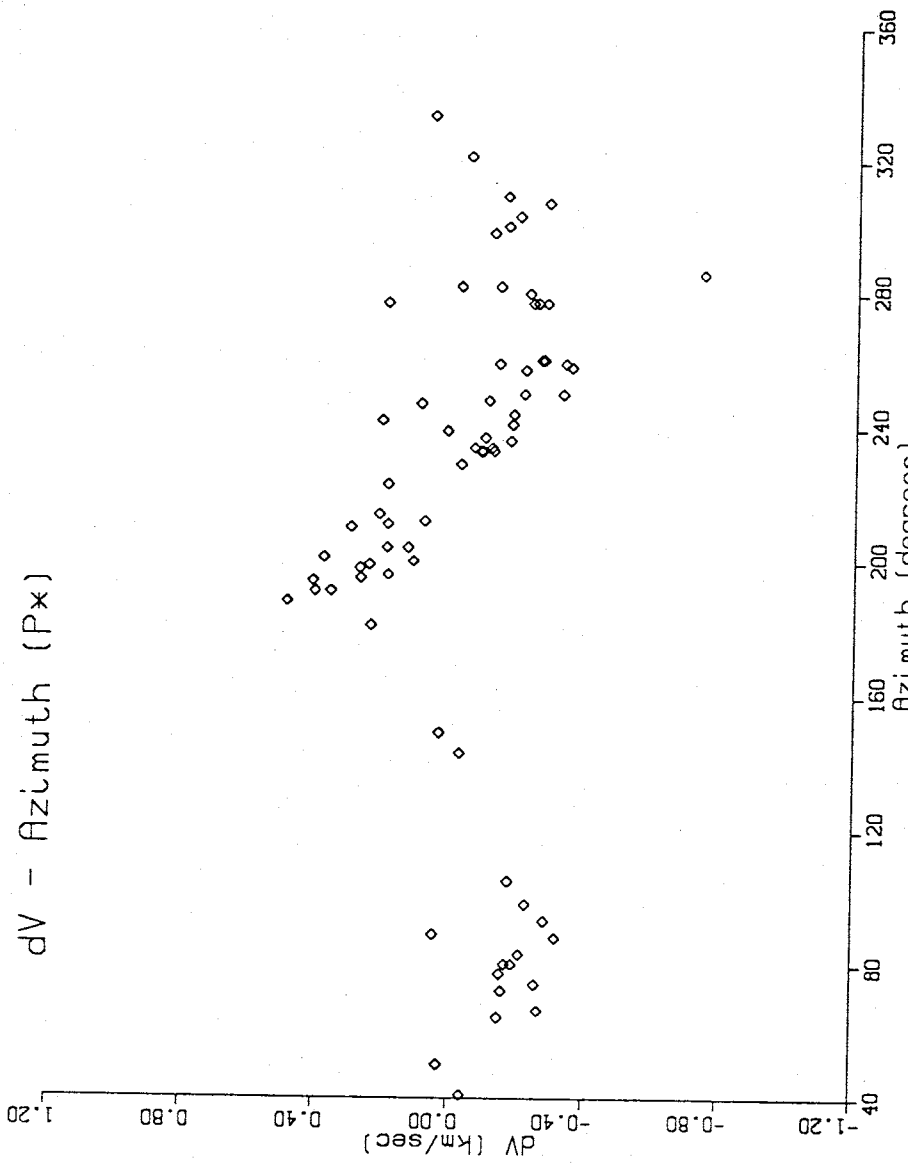

Figure 29: Velocity perturbations versus azimuth for P* data resulting from a modified time-term analysis assuming a slightly anisotropic mid-crust. The anisotropy is consistent with rift geometry but is not statistically significant.

Table 11

Analysis of Variance Table for Modified Time Term Equations

P Refractor*

Model	SSWR	DF	$DF_U - DF_M$	F
Unmodified	959	39		
Azimuth Dependence	761	35	4	2.3
Distance Dependence	882	38	1	3.3

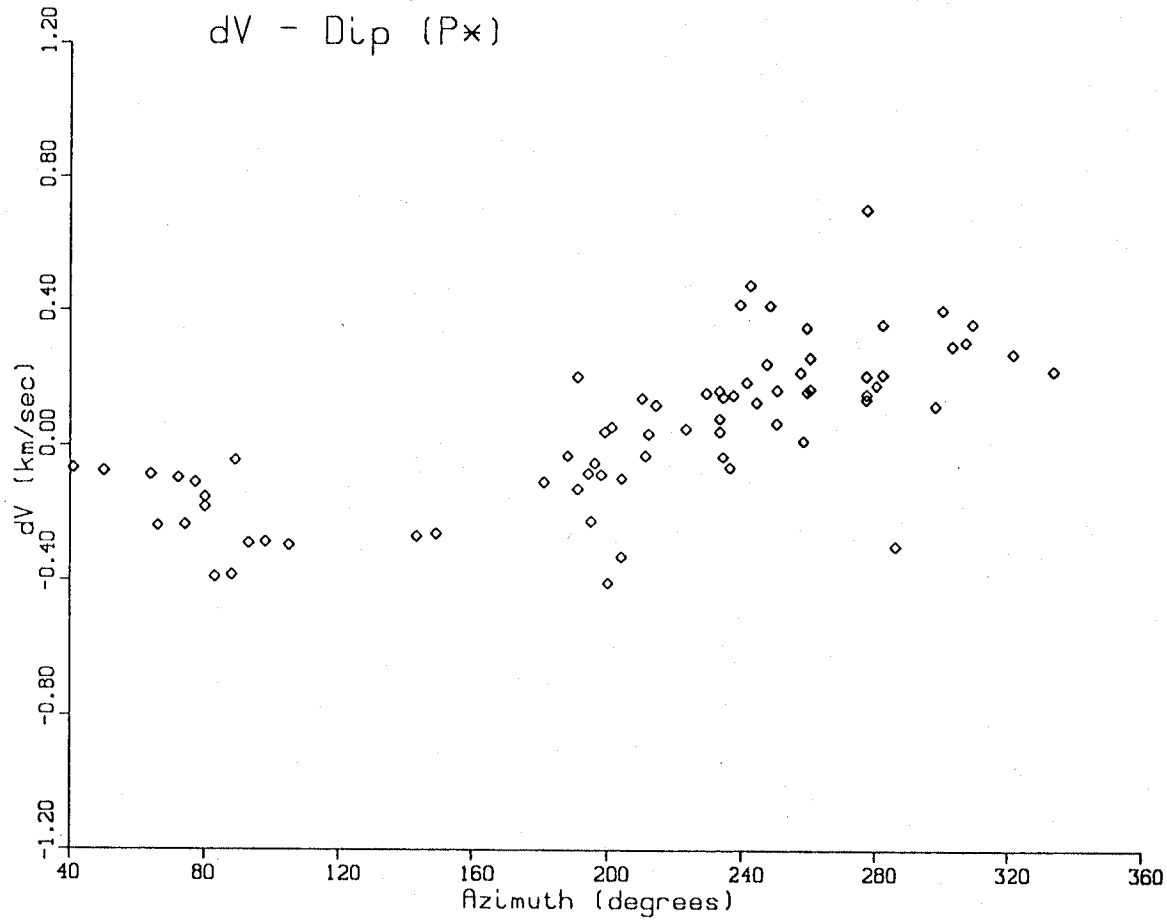

Figure 30: Velocity perturbations versus azimuth for P* data resulting from a modified time-term analysis in which a sloping mid-crustal refractor is assumed. The $cos(\Phi)$ azimuth dependence indicated by these data is large but highly uncertain (see text).

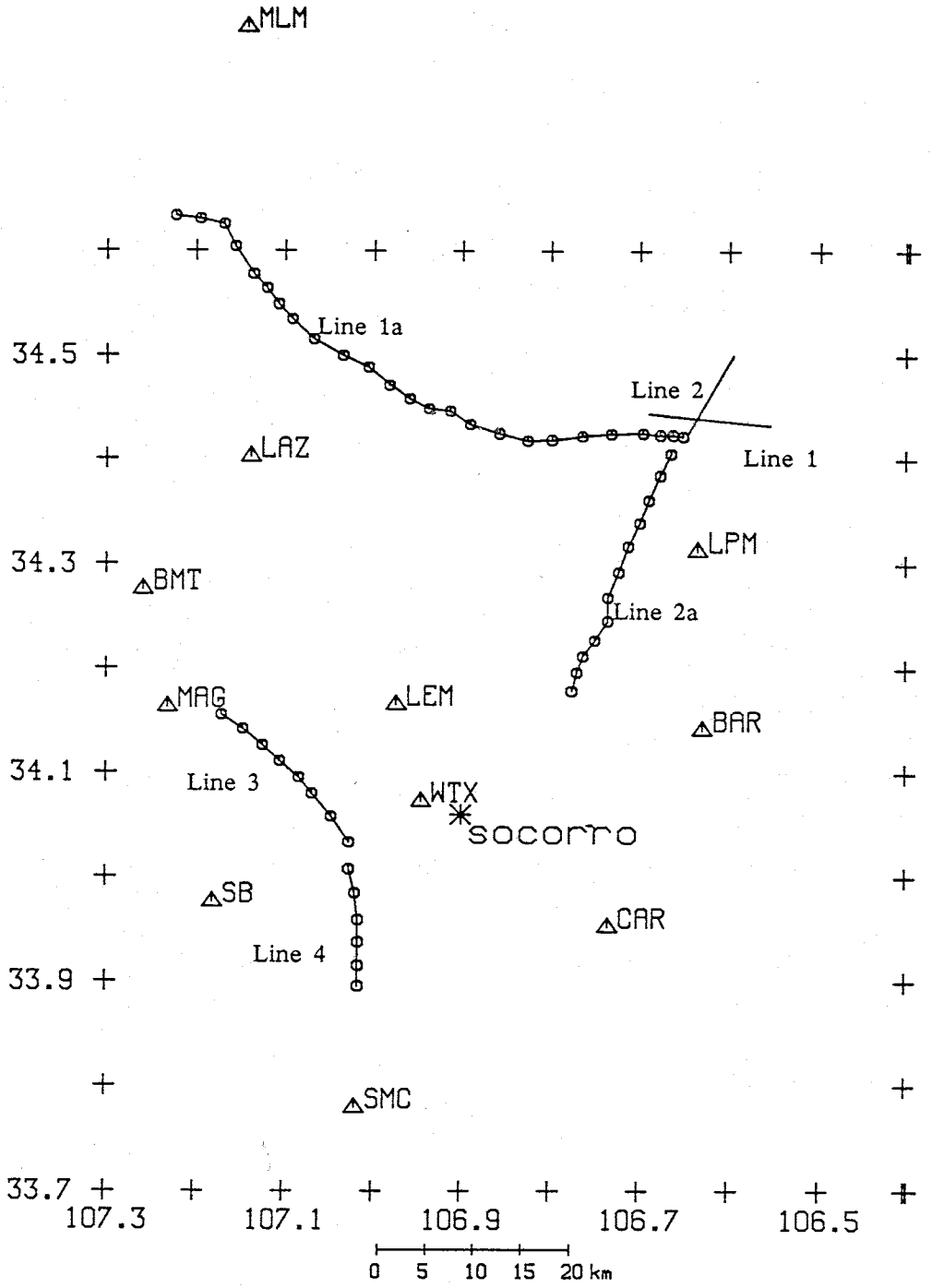

Figure 31: Locations of the COCORP lines with respect to the stations used in the time- term analyses of the P* data set.

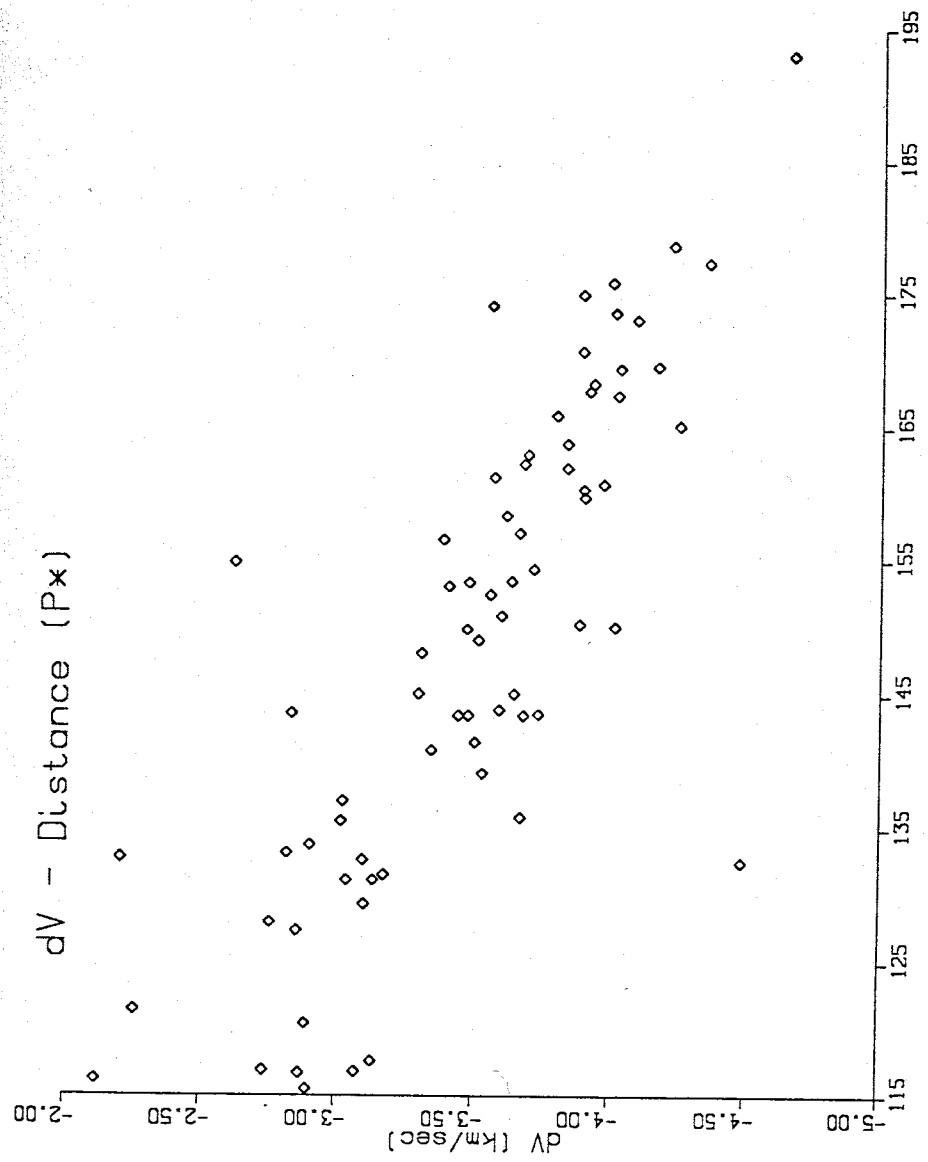

Figure 32: Velocity perturbations versus distance for P* data resulting from a modified time-term analysis assuming a small vertical velocity gradient in the lower crust. This analysis failed to provide a reasonable model.

PASSCAL study in the Basin and Range shows a velocity gradient in the lower crust with the velocity increasing from 6.3 km/s at a depth of 18 km to 7.0 km/s at 30 km.

In summary, the results of the P* analysis indicate a depressed velocity for at least the upper part of the lower crust. This reduced velocity is likely the result of high temperatures. The southeast dip on the refractor inferred by this study and the northeast dip determined by other studies indicate a non-planar refracting surface. The probable complexity of this surface is discussed in the section on P* time terms.

Pn

A data set of 402 high-quality Pn readings (Figure 33) was assembled from 79 regional earthquakes and explosions in and around New Mexico (Map 3) recorded at 23 stations (Figure 20). The data were restricted to well-recorded events with epicentral distances less than 600 km. The low seismicity of the Great Plains province resulted in the recording of few events from east of the network, and led to the somewhat skewed distribution of sources with respect to azimuth shown in Figure 9.

Unmodified

The unmodified time-term analysis yielded an average refractor velocity of 8.14 $\pm$ 0.05 km/s, and provided a good fit to the data (Figure 34). This is a very important result because some previous studies have reported low Pn velocities in the Rio Grande rift (Table 12). These low velocities, specifically a 7.6 km/s velocity in the central rift (Olsen et al., 1979) and a 7.7 km/s velocity in the southern rift (Sinno et al., 1986), have been interpreted to indicate that the asthenosphere is in direct contact with the base of the crust (Baldridge et al., 1984). While the low value in the southern rift cannot be addressed by this study, the low Pn velocity reported in the central rift by Olsen et al. (1979) relates directly to the Socorro area. The low value appears to be mostly a dip phenomenon since the Moho surface dips 4.6° to the northwest in this area (see later section).

Two other studies done in the central rift (Phinney, 1964; Murdock and Jaksha, 1981), both report normal lithosphere mantle velocities (8.0 - 8.2 km/s). The 8.14 $\pm$ 0.05 km/s velocity of this study could indicate normal lithosphere rocks or possibly mantle material with a greater than usual mafic fraction at greater than usual temperatures. A high mafic content might result from the loss

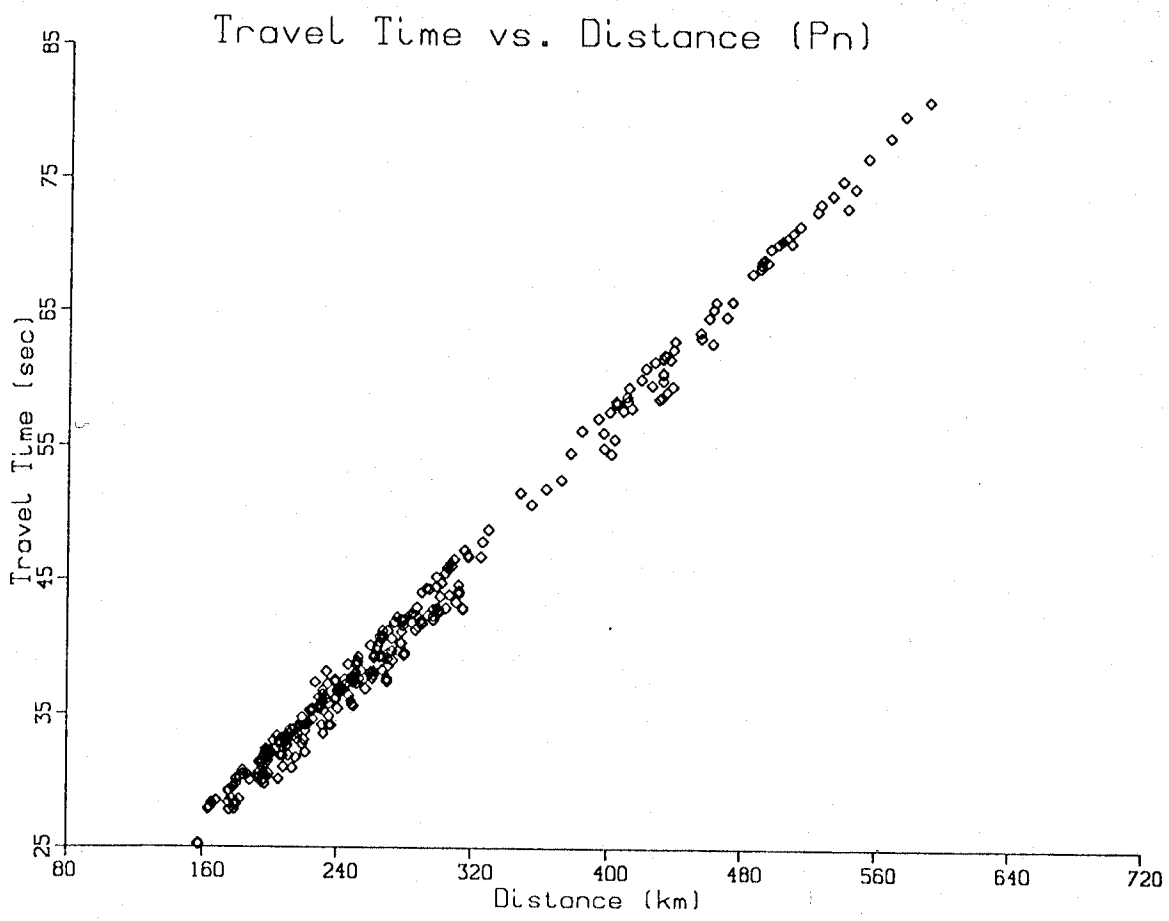

Figure 33: Travel time plot of Pn data. Data was restricted to events with epicenters less than 600 km away from the array.

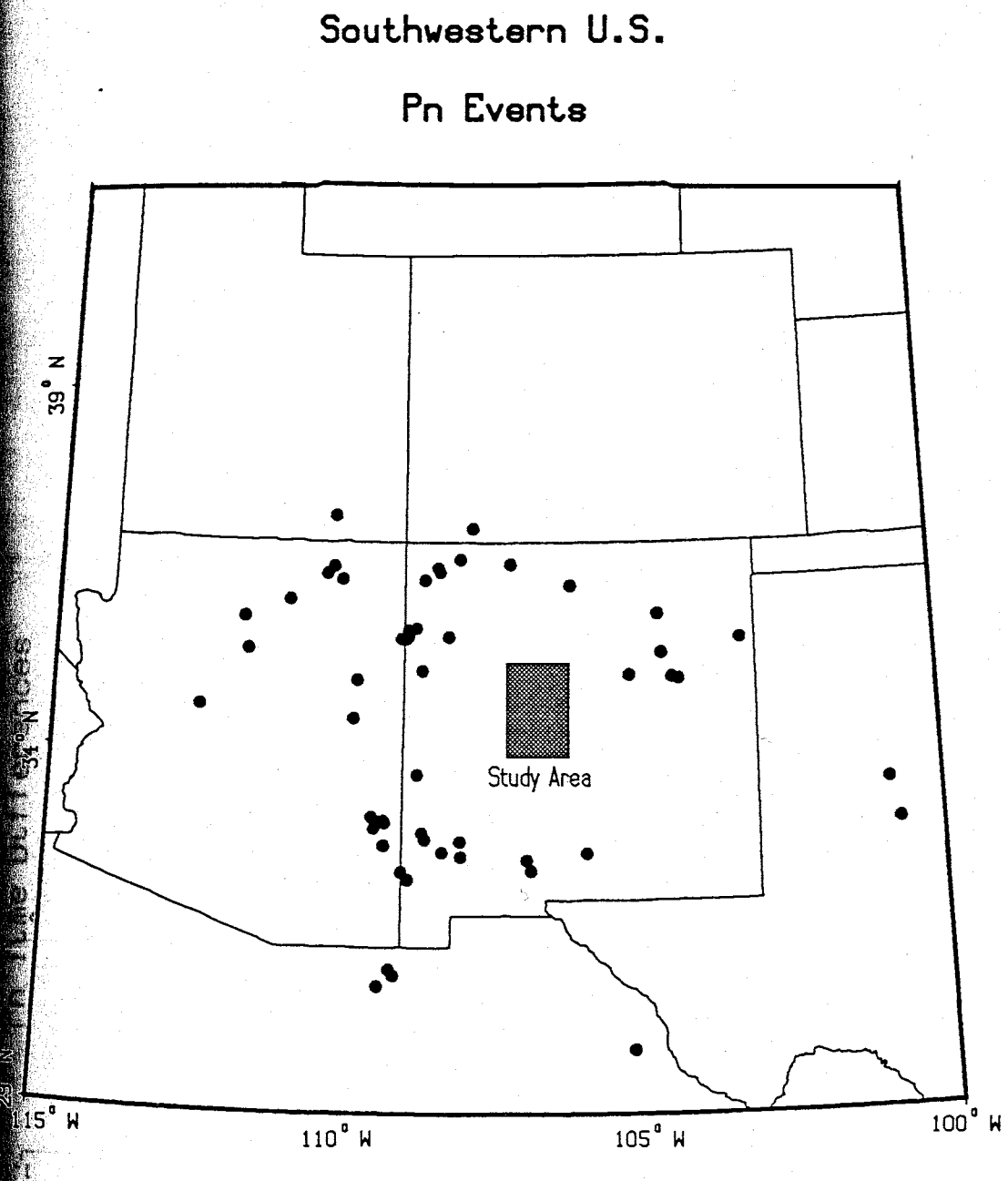

Map 3: Geographical distribution of the sources for the Pn data set. Only events occurring within 600 km of the networks were used in this study.

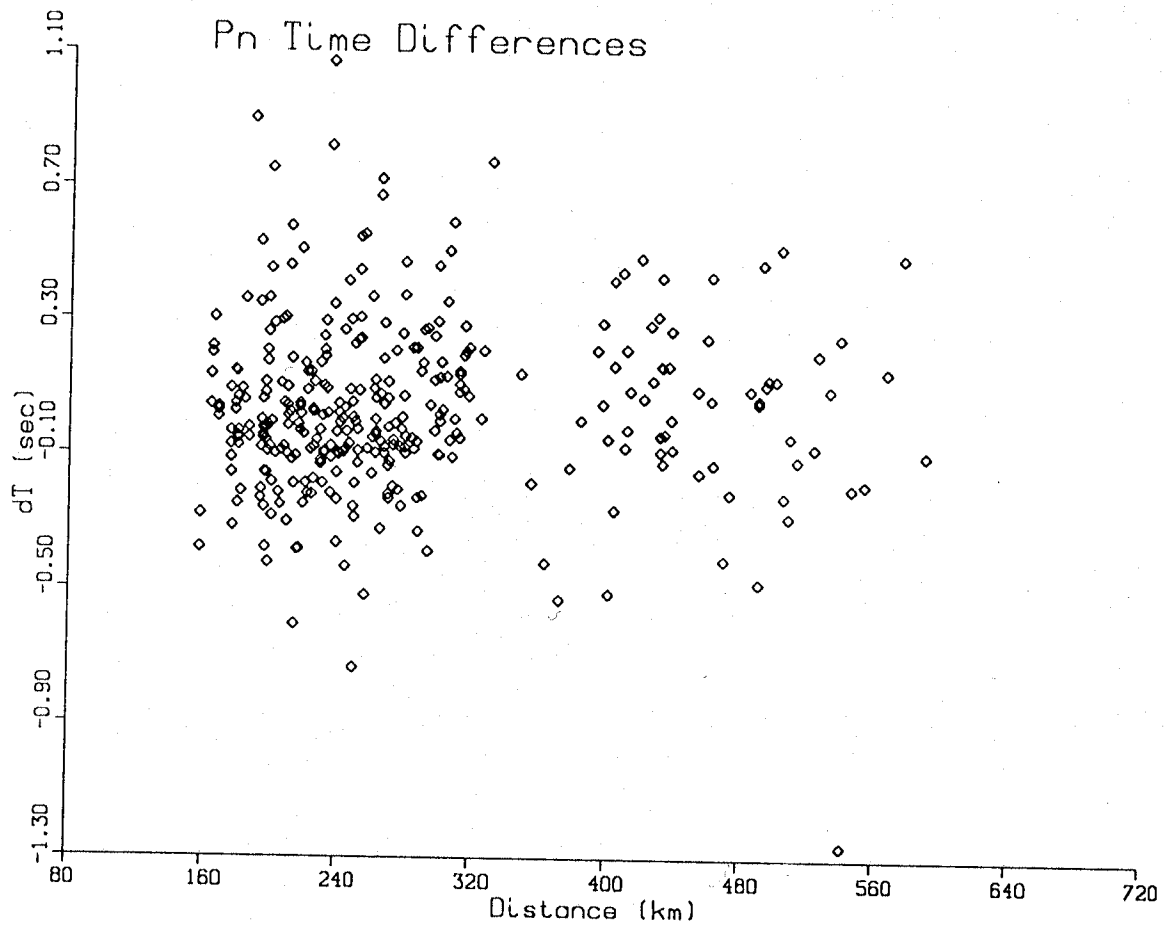

Figure 34: Travel time residuals versus distance for Pn data resulting from an unmodified time-term analysis.

Table 12

Upper Mantle Velocities

State of New Mexico

Study	Region	Velocity (km/s)	Moho Depth (km)
Toppozada & Sanford (1976)	RGR	7.9	40
Olsen et al. (1979)	Central RGR	7.6	34
Phinney (1964)	Albuquerque	8.1	40
Murdock & Jaksha	N Central RGR	8.0	37
Cook et al. (1974)	Southern RGR	8.0	35
Sinno et al. (1986)	Southern RGR	7.7	30
Dee (1973)	Southwest NM	8.1	36
Jaksha (1982)	Southwest NM	8.0	33
Jaksha & Evans (1984)	Col. Plateau	8.0	48
Stewart & Pakiser (1964)	Great Plains	8.2	50

of some of the lighter fractions of normal lithosphere rocks by intrusion into the overlying crust. This is consistent with the belief that the mid-crustal magma body at Socorro is likely to contain basalt (Sanford and Einarsson, 1982). However, a compositional change of sub-Moho mantle from iron-rich to magnesium-rich rock, would only have a small effect on the Pn velocity (B. Kudo, personal communication). Hence, the Pn velocity of 8.14 km/s observed in this study precludes the presence of an asthenospheric upwarp in direct contact with the base of the crust in the Socorro area.

Modified

Anisotropy. Table 13 lists the results of the anisotropy analysis performed on the Pn data set. Only a slight change in the refractor velocity from that of the unmodified analysis was noted, and the velocity variations with respect to azimuth were of the order of their uncertainties (Figure 35). The results do not fit the data any better than the unmodified analysis (Table 14). Considered as a whole, the upper mantle appears to have no anisotropy associated with it. Examination of the results from different areal subsets, though, indicates that the upper mantle may be fairly complex with respect to anisotropy and horizontal velocity structure (see later section).

Dip. The results of the dip analysis are listed in Table 13. While the velocity of 8.13 $\pm$ 0.05 km/s changes only marginally from the unmodified model, there is a a significant $cos(\Phi)$ dependence of 0.517 $\pm$ 0.052 km/s at a phase of 129.5 $\pm$ 5.5 $^\circ$ (Figure 36). Assuming a critical angle of 51.9 $^\circ$, this corresponds to a dip on the refractor of 4.6 $\pm$ 0.5 $^\circ$ to the northwest.

Several studies, using both refraction and time-term techniques, have indicated a north dip on the Moho in the central rift (Figure 37). Jaksha and Evans

Table 13

Time Term Results

Pn Refractor

Model	Velocity (km/s)	Data	Parameters	SSWR
Unmodified	8.14±0.05	402	76	11444
Anisotropy	8.16±0.05	402	80	11339
	Sin2ϕ Factor -0.00574±0.04316			
	Cos2ϕ Factor -0.04733±0.04237			
	Sin4ϕ Factor -0.00758±0.02232			
	Cos4ϕ Factor -0.02424±0.02018			
Dip	8.13±0.05	402	56	13435
	Sinϕ Factor 0.39906±0.05701			
	Cosϕ Factor -0.32848±0.04386			
Distance	8.38±0.13	402	77	11301
	Distance Factor (1/s) -0.00042±0.00020			

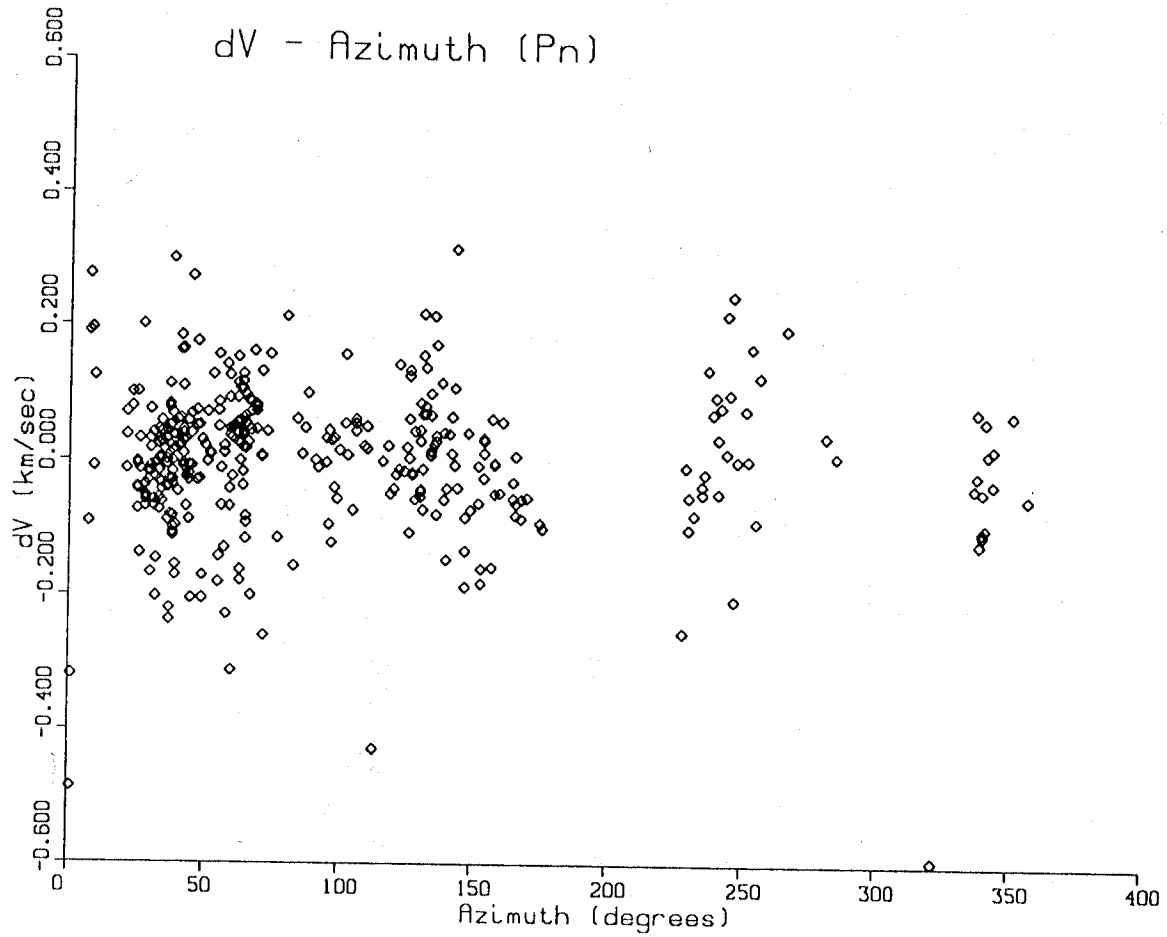

Figure 35: Velocity perturbations versus azimuth for Pn data resulting from a modified time-term analysis assuming a slightly anisotropic upper mantle. Little if any anisotropy is indicated.

Table 14

Analysis of Variance Table for Modified Time Term Equations

Pn Refractor

Model	SSWR	DF	$DF_U - DF_M$	F
Unmodified	11444	326		
Azimuth Dependence	11339	322	4	0.7
Distance Dependence	11301	325	1	4.1

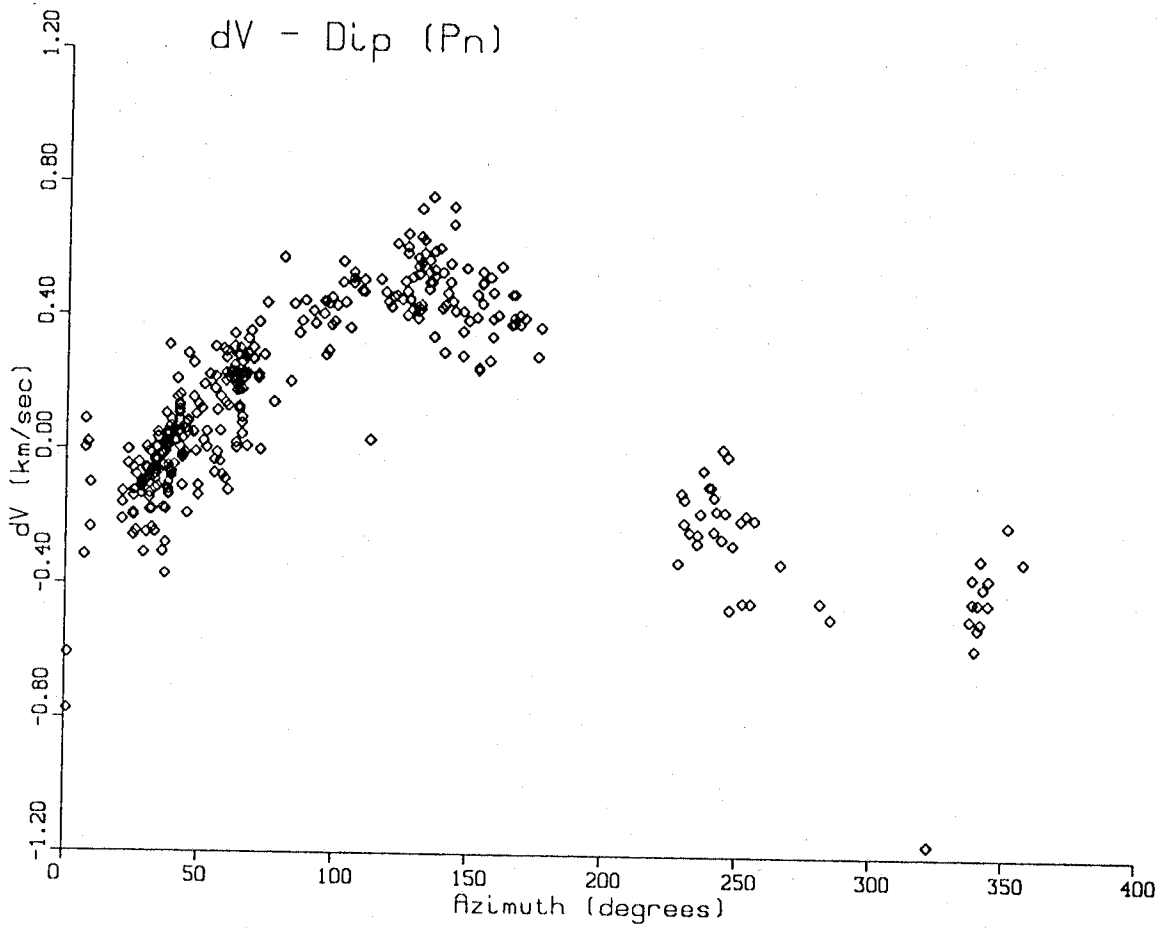

Figure 36: Velocity perturbations versus azimuth for Pn data resulting from a modified time-term analysis in which a sloping Moho interface is assumed. The $cos(\Phi)$ azimuth dependence indicated by these data is consistent with an average Moho dip of greater than 4°.

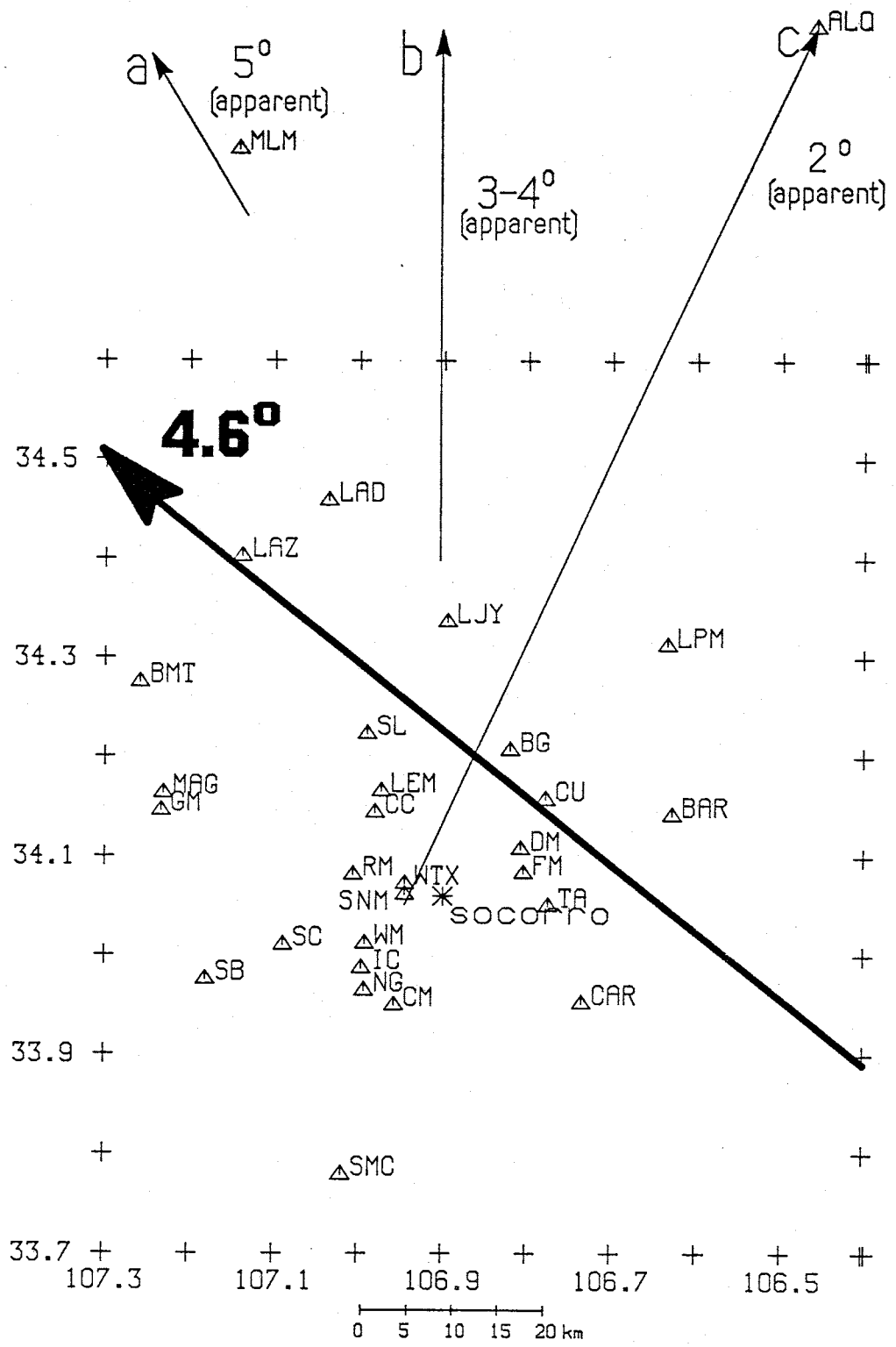

Figure 37: True dip estimate of this study along with apparent dip estimates of previous studies: a. [Jaksha and Evans, 1984], b. [Murdock and Jaksha, 1981], c. [Toppozada, 1974].

(1984) found an apparent north-northwest dip of about 5° on the Moho near station MLM. In earlier work, Toppozada (1974) found an apparent northward dip of 2° on the Moho from Socorro to Albuquerque, with possible values ranging from 1 to 3°. Examination of the time terms from their study in north central New Mexico led Murdock and Jaksha (1981) to propose 3 to 4° of apparent northward dip on the Moho. All these values concur with our results, and seem to explain the anomalously low Pn value (7.6 km/s) reported by Olsen et al. (1979). This unreversed refraction profile (Line 3, Figure 6) was shot northward, i.e. in a down-dip direction. Thus, the reported velocity would be low depending on the degree of dip. Assuming an apparent north dip of 3 to 4° yields a true Pn velocity of ~8 km/s, a normal lithosphere mantle velocity. Hence, because the fit of this model to the data is extremely good and the model agrees well with existing data, it is believed that the northwest dip of 4.6 $\pm$ 0.5° accurately represents the dip on the Moho surface.

It should be noted that such a steep dip must have a limited lateral extent since it requires an increase of ~8 km in depth per 100 km in distance perpendicular to strike. Given that the M discontinuity is near 40 km depth beneath the eastern Colorado Plateau (Roller, 1965), the observed dip in the Socorro area must flatten out rather rapidly to the northwest.

Distance. The results of looking at a velocity dependence on distance are listed in Table 13. The resulting model shows a linear decrease in velocity with distance that is statistically significant at the 95 percent confidence level (Table 14; Figure 38). While no other study in the rift has investigated such a model, there is an interesting parallel in the work of Murdock and Jaksha (1981). From time-term analysis of their full data set, with epicentral distances from 200 to 1000km, the resulting Pn velocity was 8.02 $\pm$ 0.08 km/s. However, when the

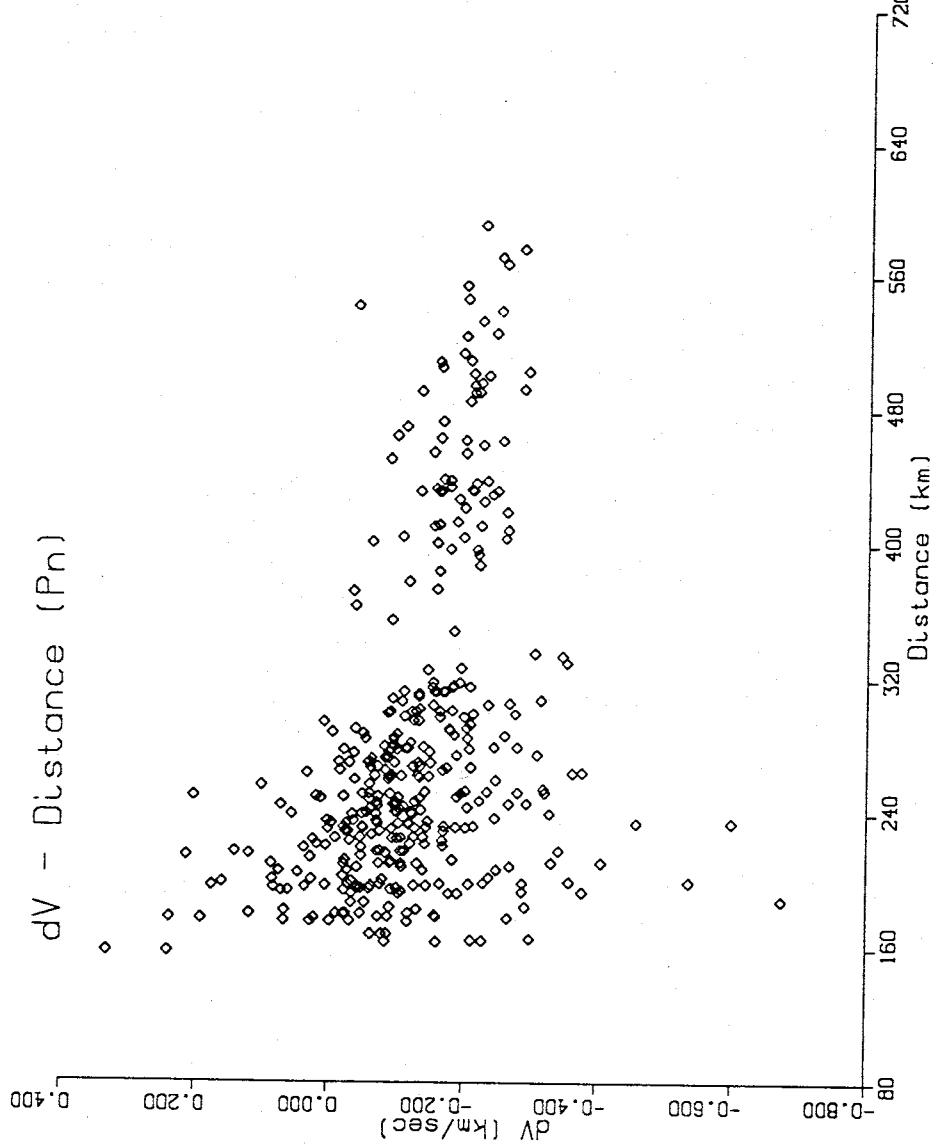

Figure 38: Velocity perturbations versus distance for Pn data resulting from modified time-term analysis assuming a small lateral increase in velocity with distance. Decrease with distance could indicate a variety of possibilities (see text).

upper limit on epicentral distance was reduced to 600 km, the average Pn velocity increased to 8.12 ± 0.09 km/s. This velocity difference between these two data sets indicates a distance dependence in the data. The distance function from this study corresponds to a Pn velocity of 8.29 km/s at a distance of 200 km grading to a velocity of 8.12 at 600 km. However, this observation cannot be the direct result of a decrease in velocity with depth, since critically refracted rays would not be propagated deeper with increasing distance in such a structure.

A velocity decrease with distance could be related to the quality of the first arrivals. The Pn phase becomes weaker and more emergent with increasing distance so the initial onset may be lost as it travels across the array of stations in the Socorro area. As a result, distant events would appear to have slightly lower average velocities than close events. However, since only high quality arrivals were used, this seems an unlikely explanation.

Attenuation, however, may be an important factor since the progressive loss of high frequencies gradually changes the velocity of propagation. Anstey (1977) states:

> A spike pulse starts with the normal velocity appropriate to an infinite bandwidth, but gradually slows to a low-frequency velocity as the high frequency components are removed and the pulse broadens.

Figure 39 attempts to illustrate this point. Thus, since attenuation can cause a decrease in velocity with distance, it might explain the observed velocity variations, at least in part.

Another possible explanation centers on the fact that the quality of Pn arrivals used in this study is generally consistent over the entire data set. To maintain this consistency, the more distant events used in this study were gen-

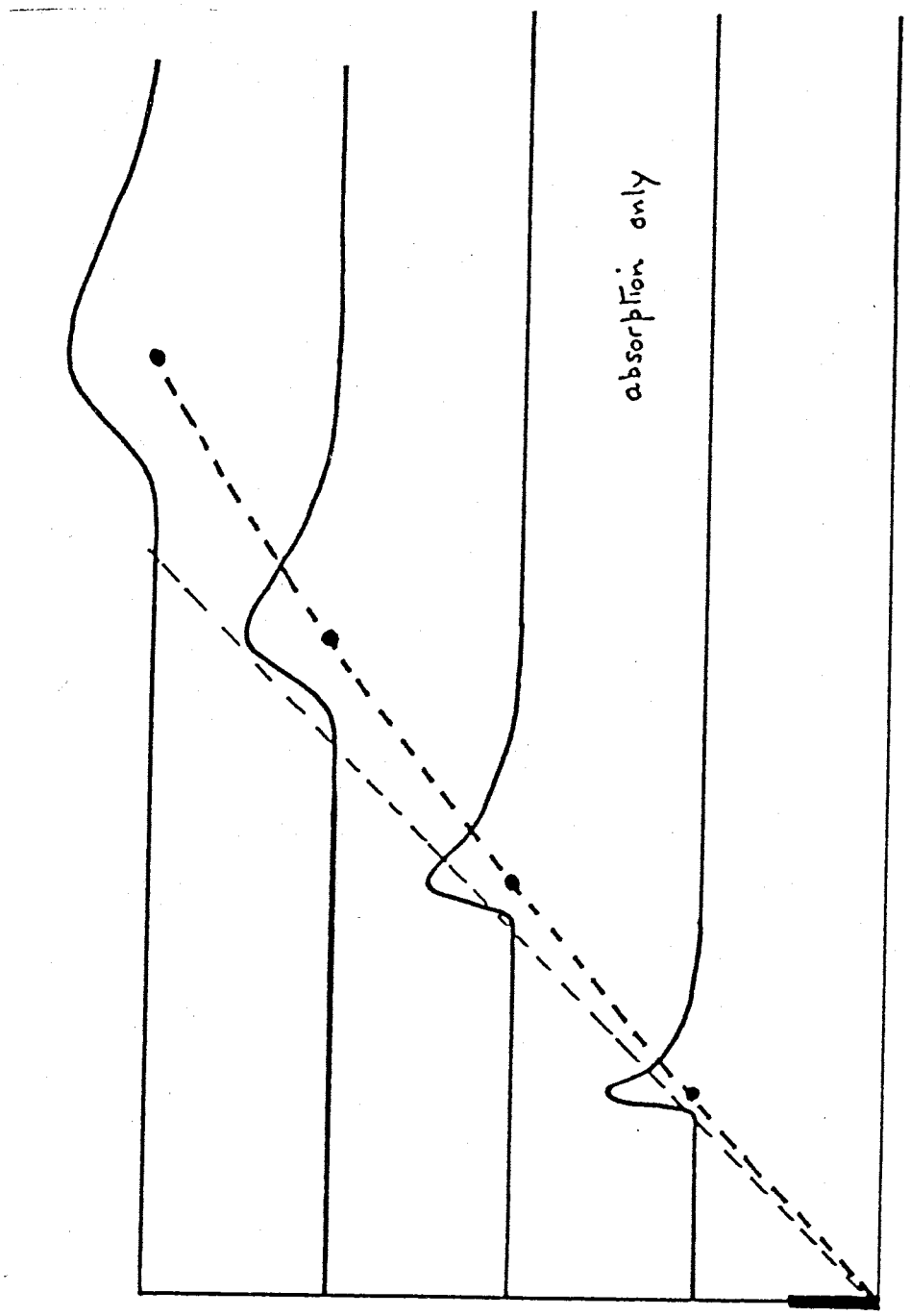

Figure 39: Progressive loss of high frequencies gradually changes the velocity of propagation of a body wave. No part of the pulse travels at a constant velocity (from Anstey, 1977).

erally of higher magnitude than were the nearer events (Figure 40). Since source spectra depend on event magnitude (Figure 41), the source spectra, i.e. the frequency content of the source wavelets, are distance dependent. Since head waves are most sensitive to the velocity structure of the order of a wavelength beneath the refractor boundary (Hill, 1971), the P-waves will sample the upper mantle differently because of different dominant wavelengths. In this way then, a decrease in velocity with depth might become evident. Archambeau et al. (1969) defined the fine structure of the upper mantle for the tectonic provinces of the United States. Their mantle models showed velocity structures that decreased with depth directly below the Moho. Therefore, one would expect that waves with longer dominant wavelengths would have slower average velocities than those with shorter dominant wavelengths. Since larger earthquakes have longer dominant wavelengths, this is consistent with the observations. Hence, a decreasing velocity with distance can be explained for this specific data set and may indicate a decrease in velocity with depth below the crust-mantle boundary.

All the possibilities presented are speculative and difficult to quantify. Furthermore, since they are not mutually exclusive, the observed velocity decrease with distance may be the result of a combination of causes. Nevertheless, they do provide working hypotheses that may be advanced in later work.

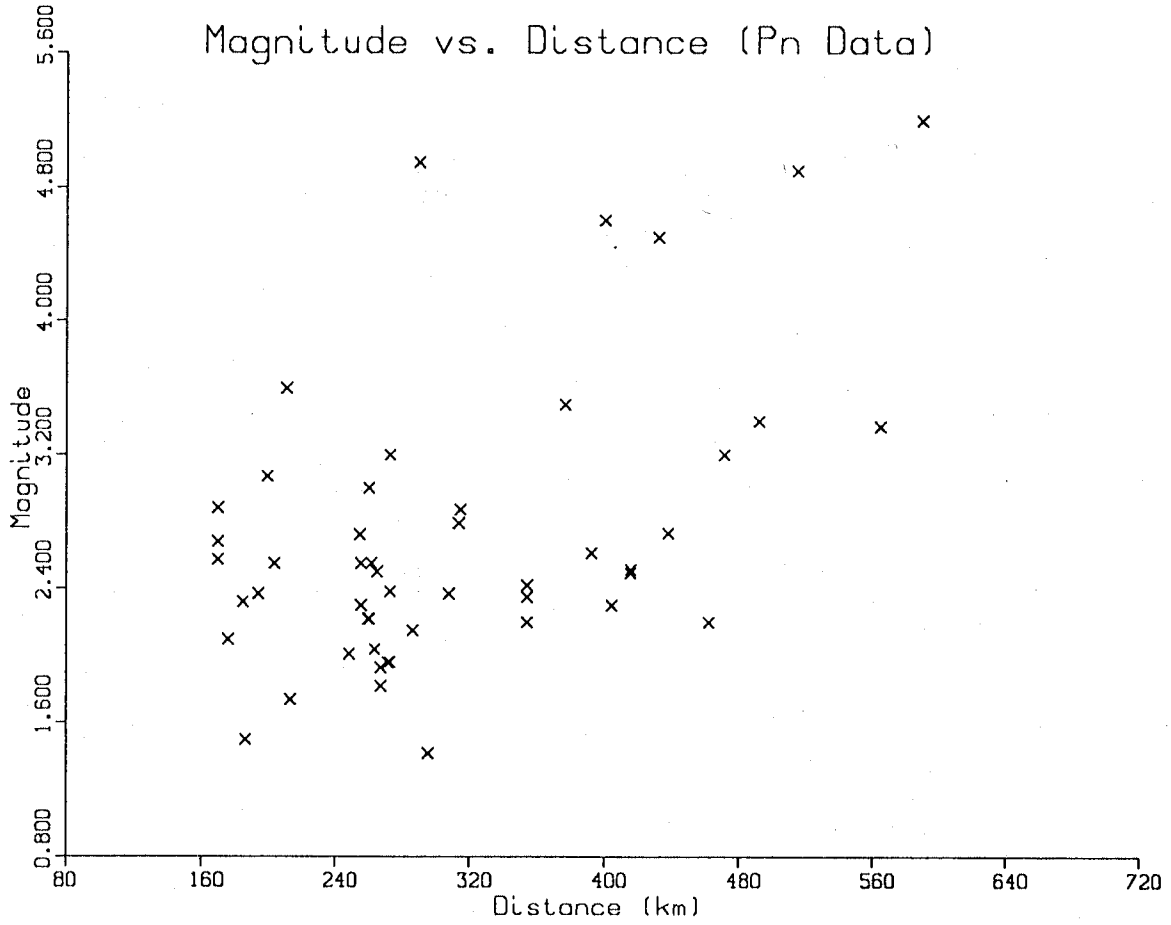

Figure 40: Magnitude versus distance plot for Pn events. Not all events are represented since many did not have determined magnitudes.

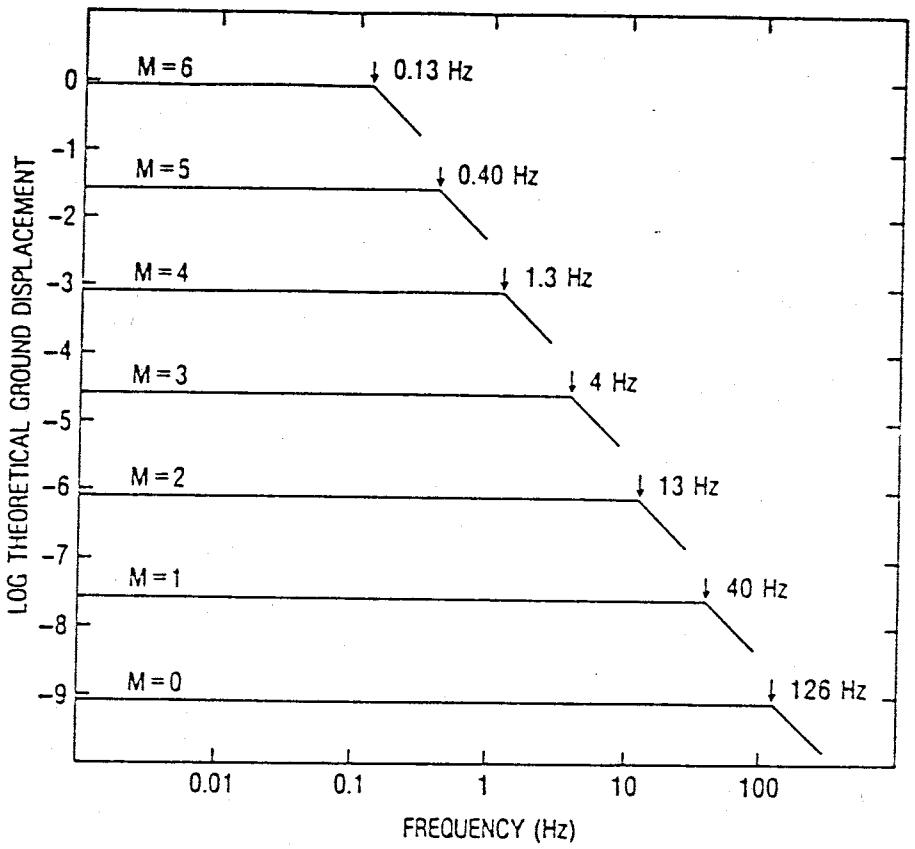

Figure 41: Theoretical spectral amplitude of ground displacement as a function of frequency for earthquakes ranging in magnitude (M) from 0 to 6. Corner frequencies are shown by arrows. Label for ordinate has been shortened (from Lee and Stewart, 1981).

Pn Areal Subsets

This section presents the results of the unmodified and modified analyses performed on a series of areal subsets of the Pn data set (Figure 42). These subsets divide the study area into regions north and south of latitude 34.13, and east and west of longitude 106.95. The demarcation was done so that each subset had approximately the same areal extent yet also contained a sufficient number of stations for reasonable analyses to be done. While the placement of the boundaries was somewhat arbitrary, minor changes in the positions of the dividing lines had no significant effect on the results.

Pn East contains 163 data recorded at 9 stations (Figure 43), Pn West contains 250 data recorded at 16 stations (Figure 44), Pn North contains 227 data recorded at 12 stations (Figure 45), and Pn South contains 218 data recorded at 13 stations (Figure 46). The four subsets are discussed as a group because their importance centers on their interrelatedness with one another and their relation to the complete Pn data set.

Unmodified

Tables 15, 16, 17, 18 present the results of the time-term analysis for each subset. Each of the unmodified analyses is within one standard deviation of the 8.14 ± 0.05 km/s velocity from the complete Pn data set. Figures 47, 48, 49, 50 show the fit of the data to each model. These analyses give no new information about the upper mantle in the Socorro area.

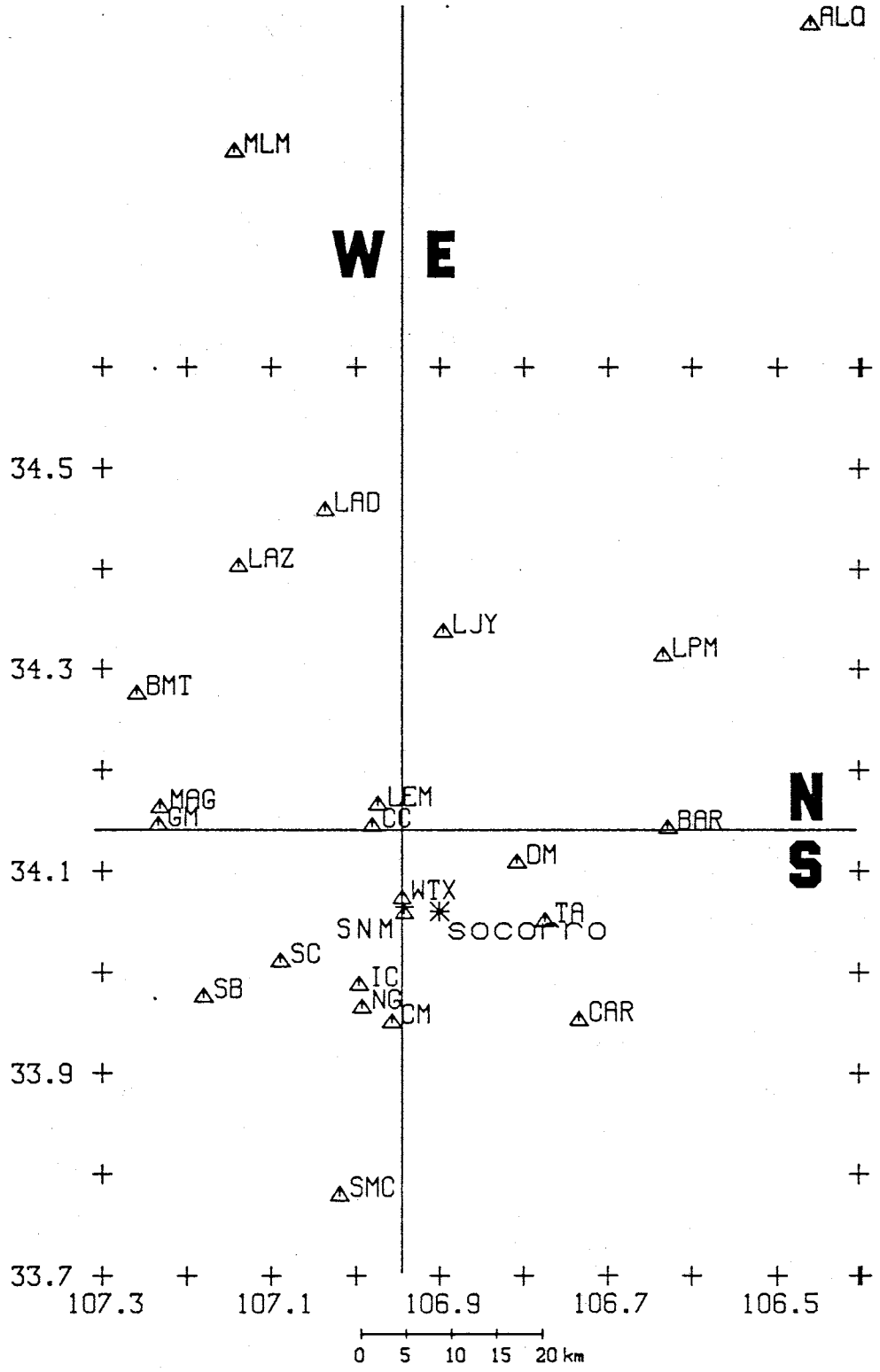

Figure 42: Division of the Pn data set into areal subsets. Pn East (E) is the area east of longitude 106.95, Pn West (W) is the area west of this longitude. Pn North (N) is the area north of latitude 34.13, Pn South (S) is the area south of this latitude.

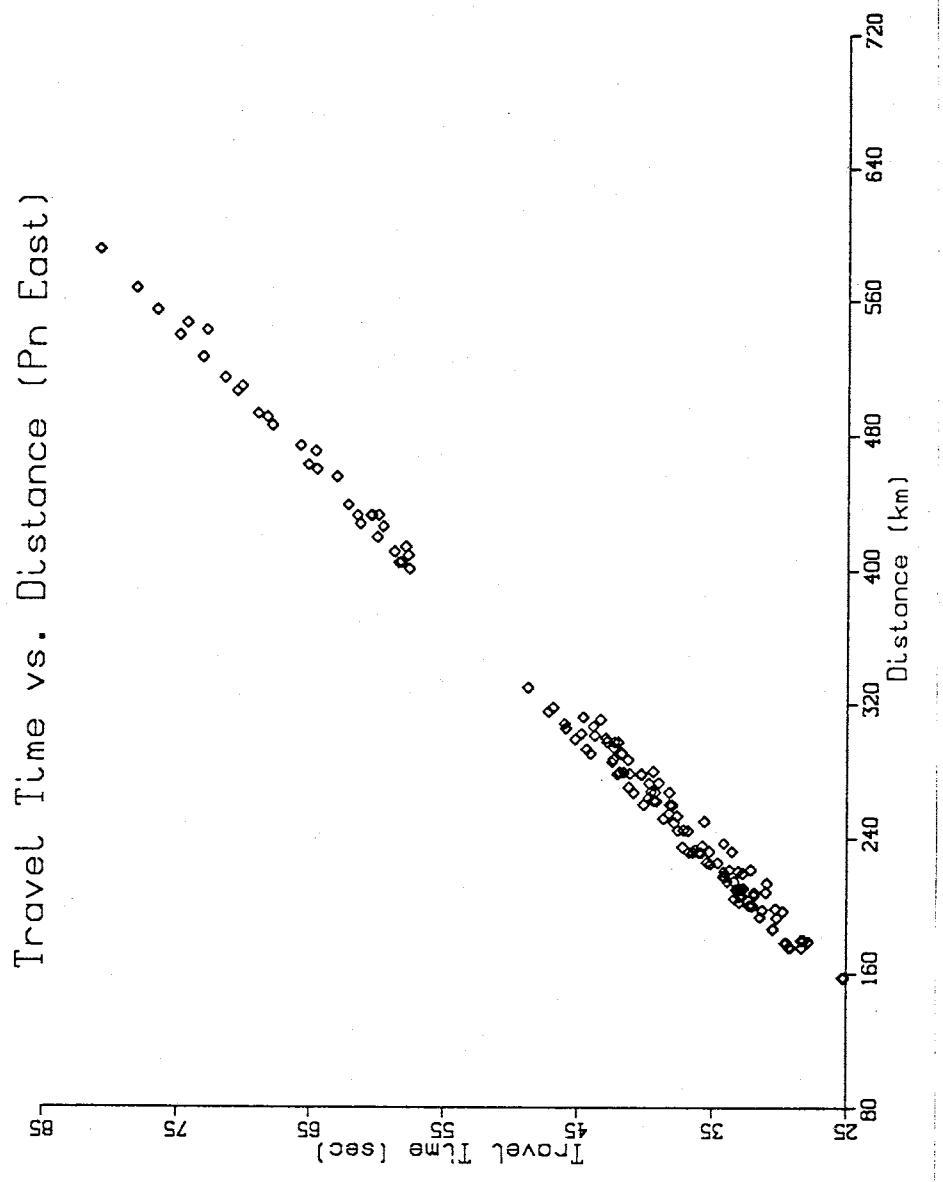

Figure 43: Travel time plot of Pn East data.

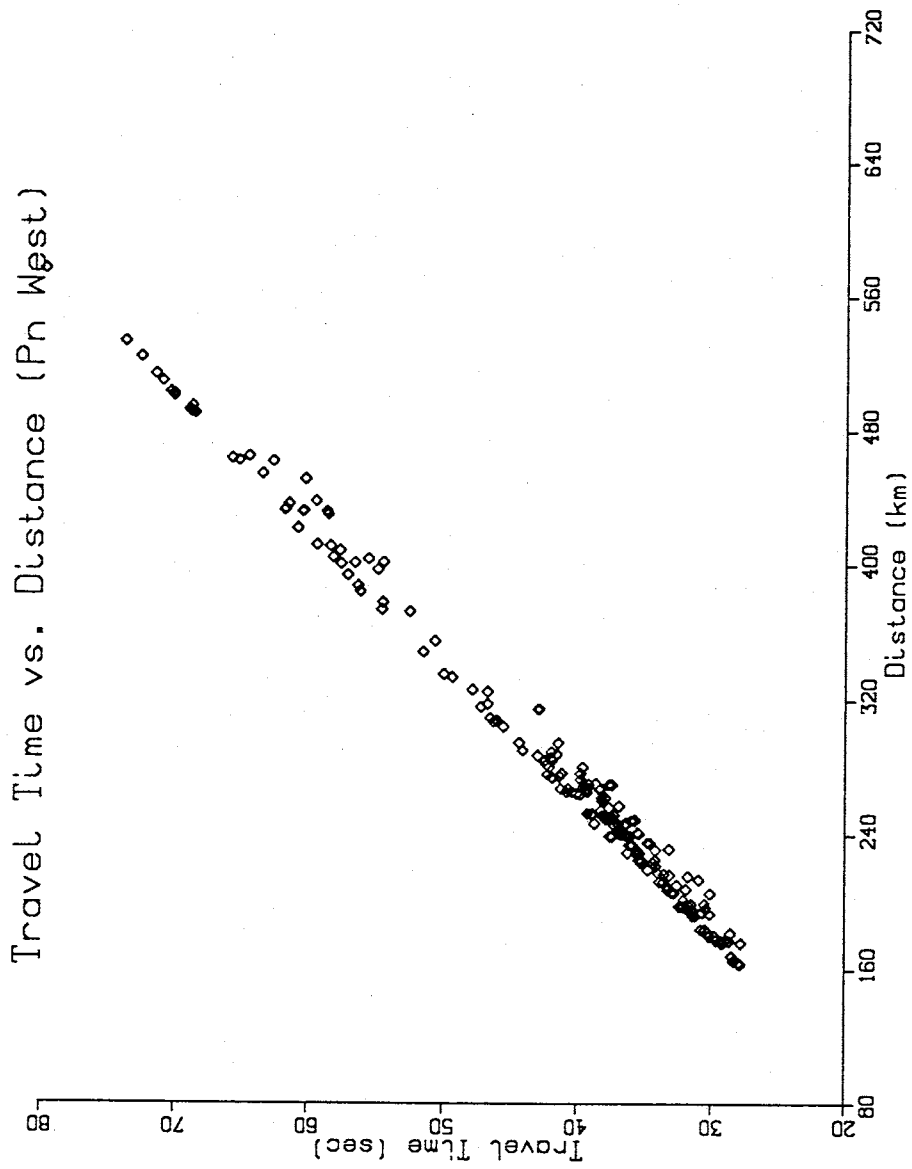

Figure 44: Travel time plot of Pn West data.

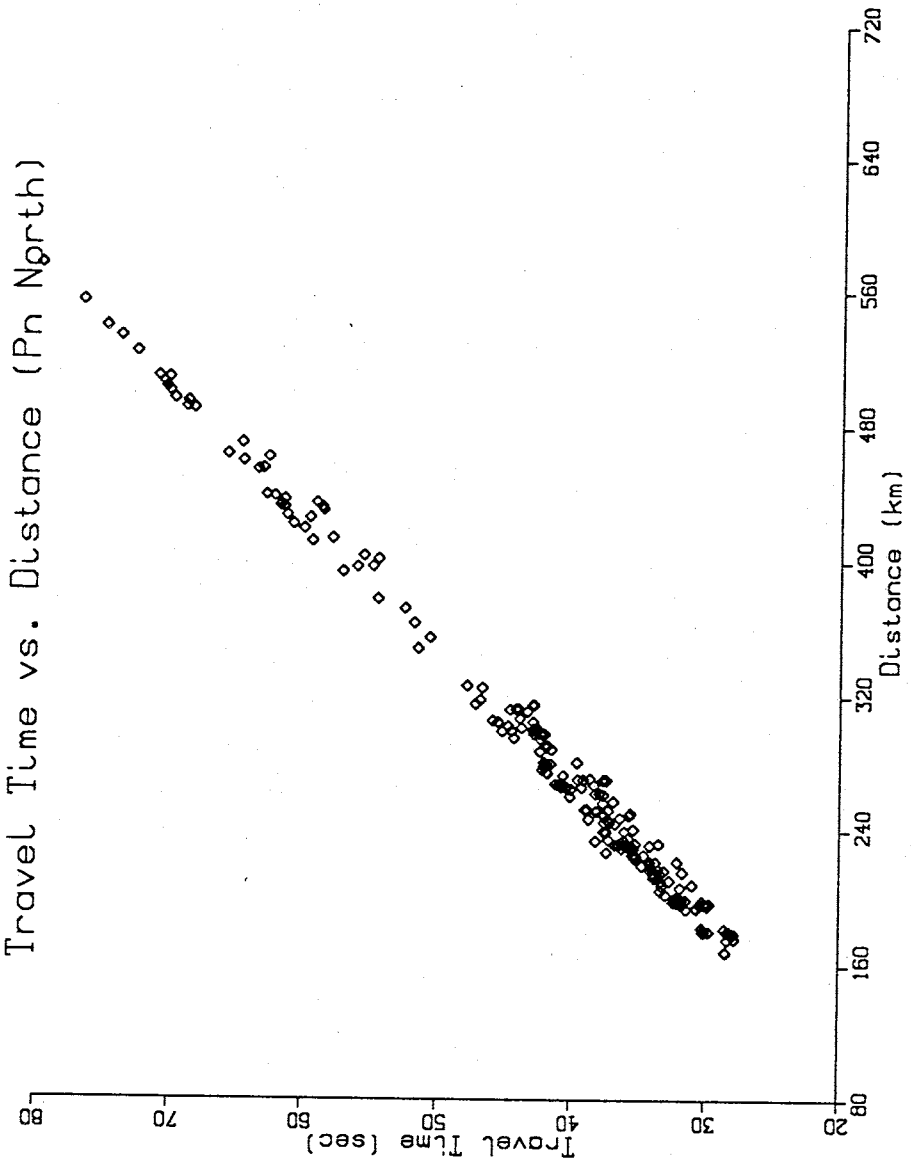

Figure 45: Travel time plot of Pn North data.

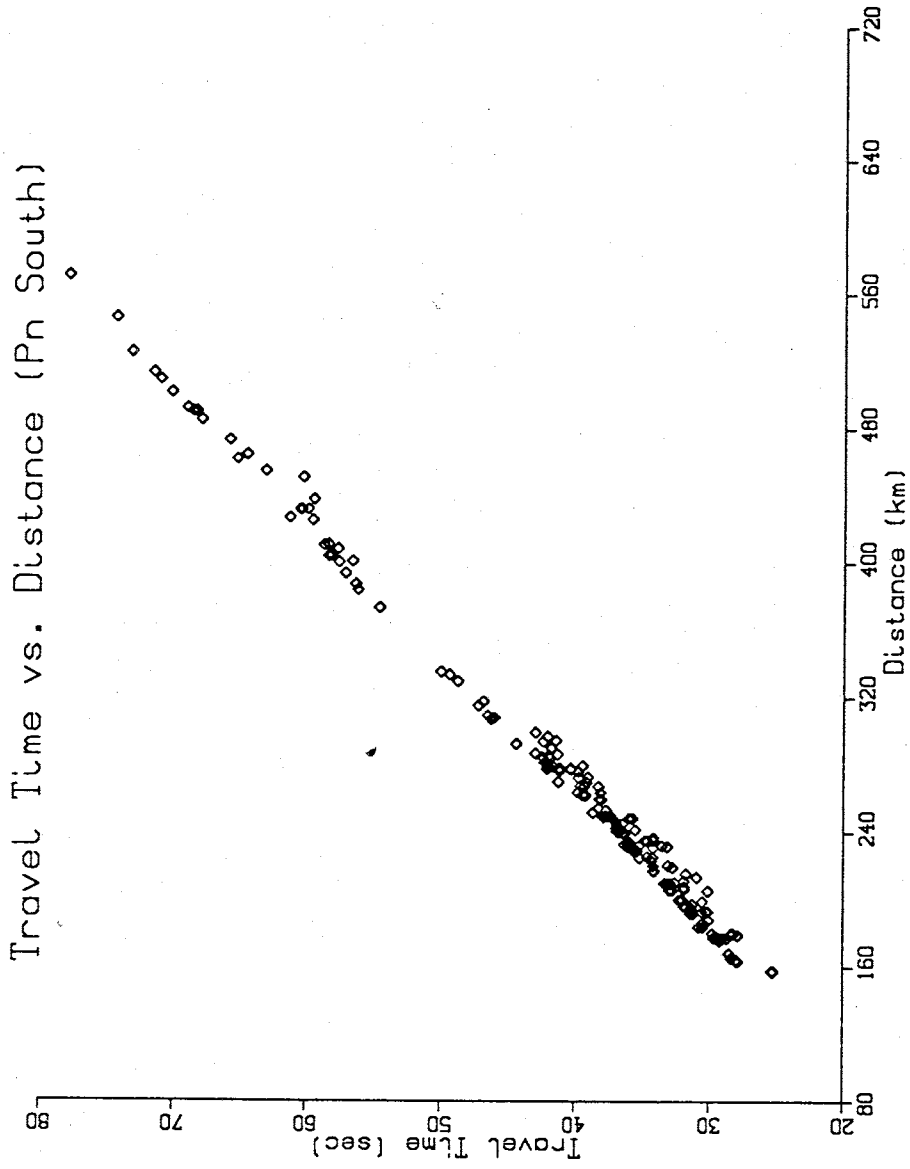

Figure 46: Travel time plot of Pn South data.

Table 15

Time Term Results

Pn East

Model	Velocity (km/s)	Data	Parameters	SSWR
Unmodified	8.11±0.08	163	46	2864
Anisotropy	7.96±0.13	163	50	2633
	Sin2ϕ Factor –0.00088±0.07250			
	Cos2ϕ Factor 0.23857±0.12223			
	Sin4ϕ Factor 0.04175±0.04852			
	Cos4ϕ Factor 0.06056±0.03880			
Dip	8.10±0.08	163	40	3675
	Sinϕ Factor 0.57936±0.15173			
	Cosϕ Factor –0.44117±0.08949			
Distance	8.09±0.24	163	47	2864
	Distance Factor (1/s) 0.00003±0.00039			

Table 16

Time Term Results

Pn West

Model	Velocity (km/s)	Data	Parameters	SSWR
Unmodified	8.06±0.07	250	57	6948
Anisotropy	8.23±0.18	250	61	6614
	Sin2ϕ Factor –0.17617±0.08515			
	Cos2ϕ Factor –0.17827±0.13876			
	Sin4ϕ Factor 0.00973±0.03577			
	Cos4ϕ Factor –0.05699±0.03389			
Dip	8.01±0.07	250	58	6867
	Sinϕ Factor 0.62504±0.13949			
	Cosϕ Factor –0.22723±0.05941			
Distance	8.30±0.17	250	58	6867
	Distance Factor (1/s) –0.00040±0.00026			

Table 17

Time Term Results

Pn North

Model	Velocity (km/s)	Data	Parameters	SSWR
Unmodified	8.19±0.07	227	59	5678
Anisotropy	8.25±0.07	227	63	5363
	Sin2ϕ Factor 0.13567±0.06274			
	Cos2ϕ Factor −0.12181±0.05453			
	Sin4ϕ Factor 0.01803±0.02945			
	Cos4ϕ Factor −0.01394±0.02943			
Dip	8.18±0.07	227	50	6879
	Sinϕ Factor 0.26481±0.07268			
	Cosϕ Factor −0.43346±0.06979			
Distance	8.58±0.21	227	60	5536
	Distance Factor (1/s) −0.00065±0.00032			

Table 18

Time Term Results

Pn South

Model	Velocity (km/s)	Data	Parameters	SSWR
Unmodified	8.15±0.10	218	51	5317
Anisotropy	8.02±0.10	218	55	5013
	Sin2ϕ Factor 0.26922±0.10809			
	Cos2ϕ Factor −0.05985±0.09405			
	Sin4ϕ Factor −0.00235±0.06301			
	Cos4ϕ Factor −0.02880±0.03588			
Dip	8.11±0.11	218	40	6279
	Sinϕ Factor 0.48256±0.10759			
	Cosϕ Factor −0.28385±0.12095			
Distance	8.66±0.26	218	52	5144
	Distance Factor (1/s) −0.00119±0.00051			

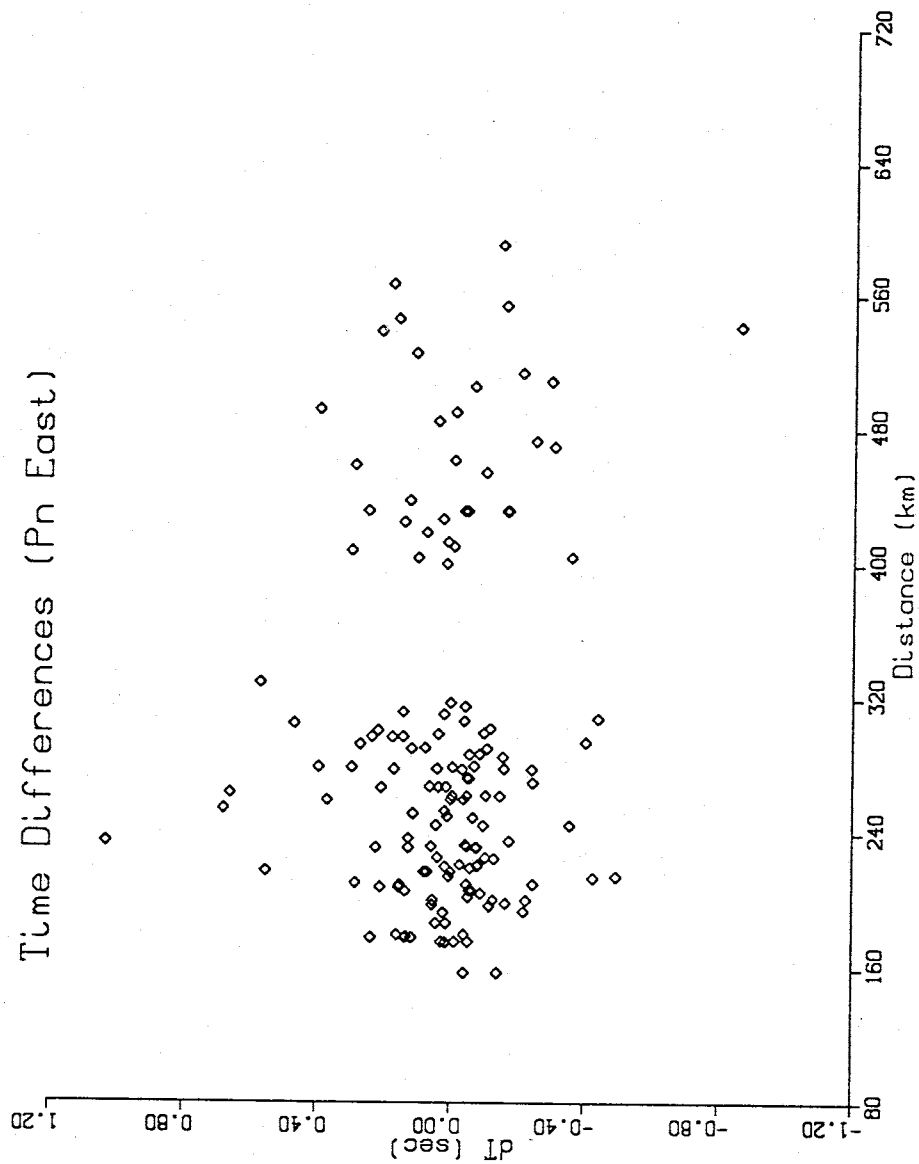

Figure 47: Travel time residuals versus distance for Pn East data resulting from unmodified time-term analysis.

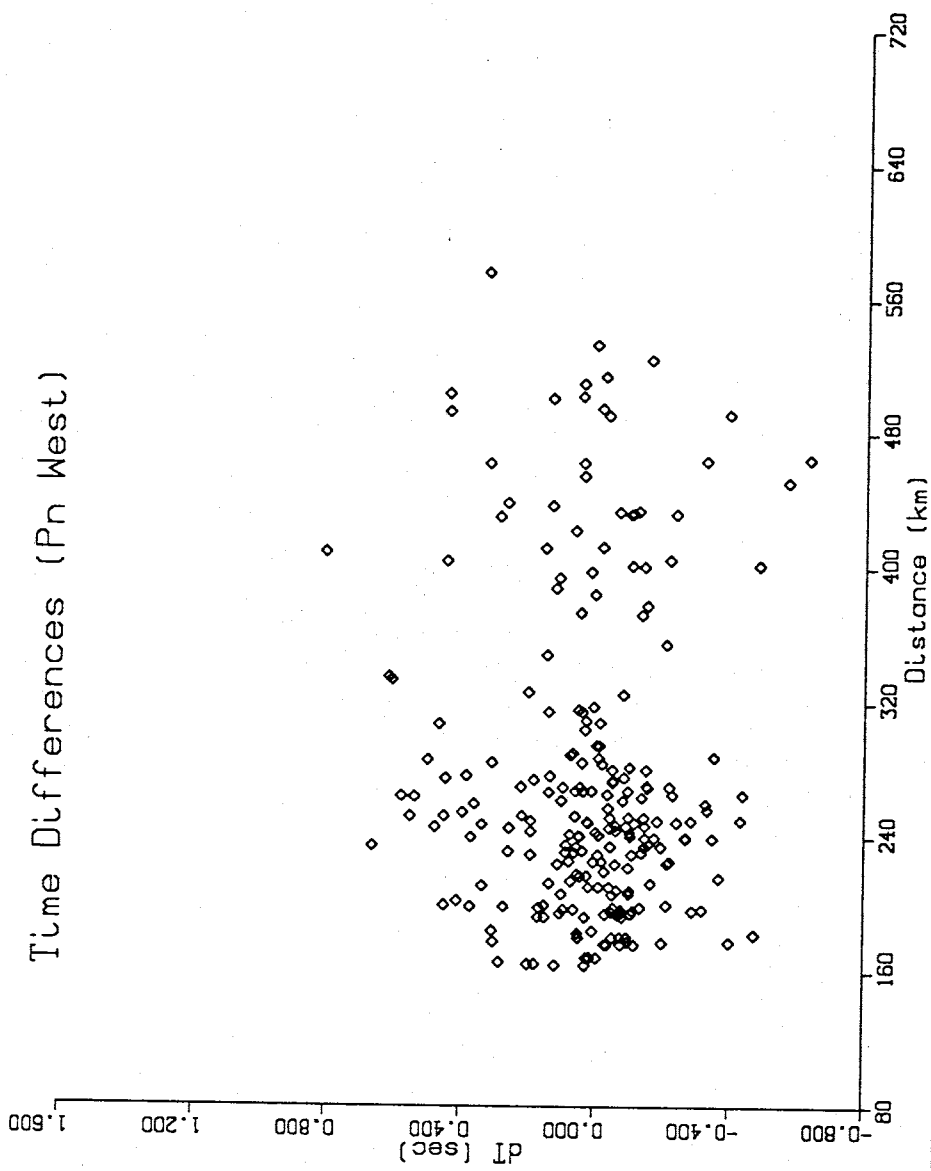

Figure 48: Travel time residuals versus distance for Pn West data resulting from unmodified time-term analysis.

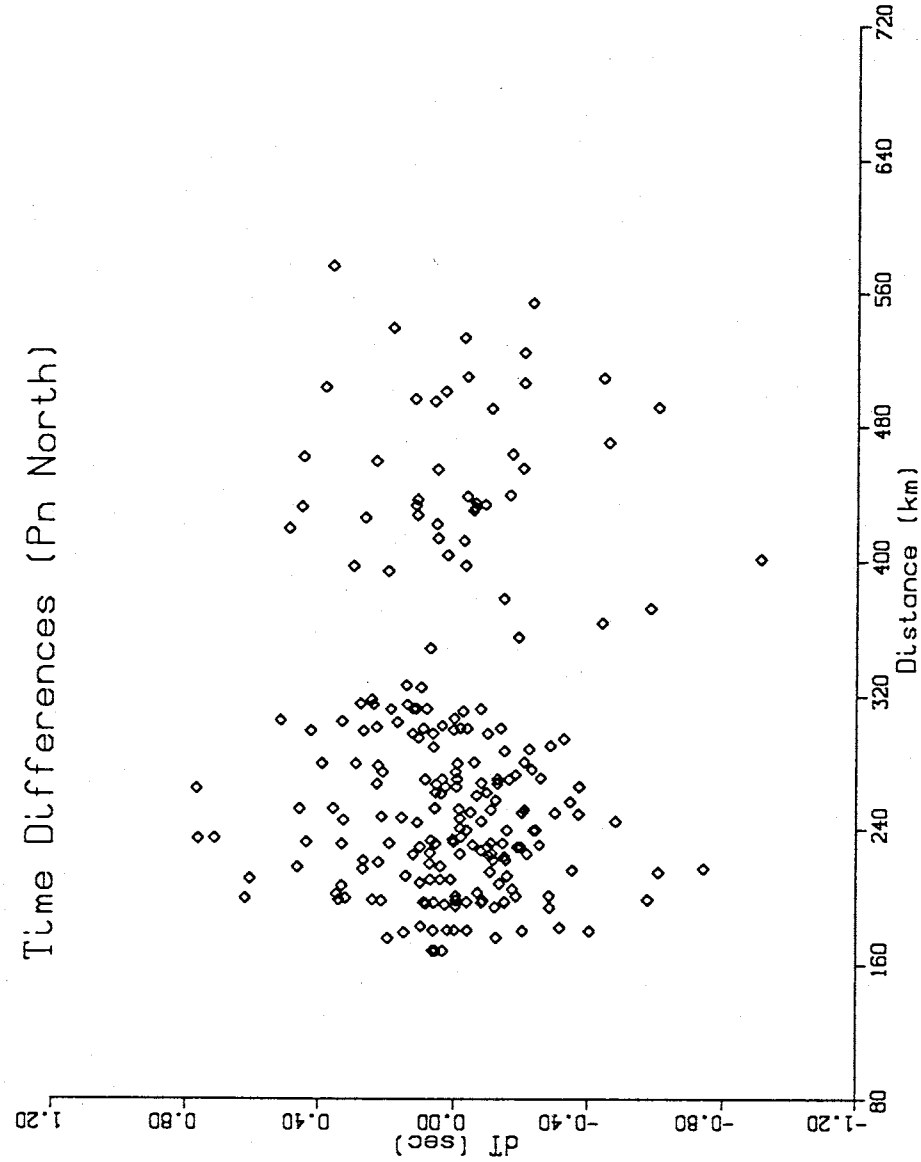

Figure 49: Travel time residuals versus distance for Pn North data resulting from unmodified time-term analysis.

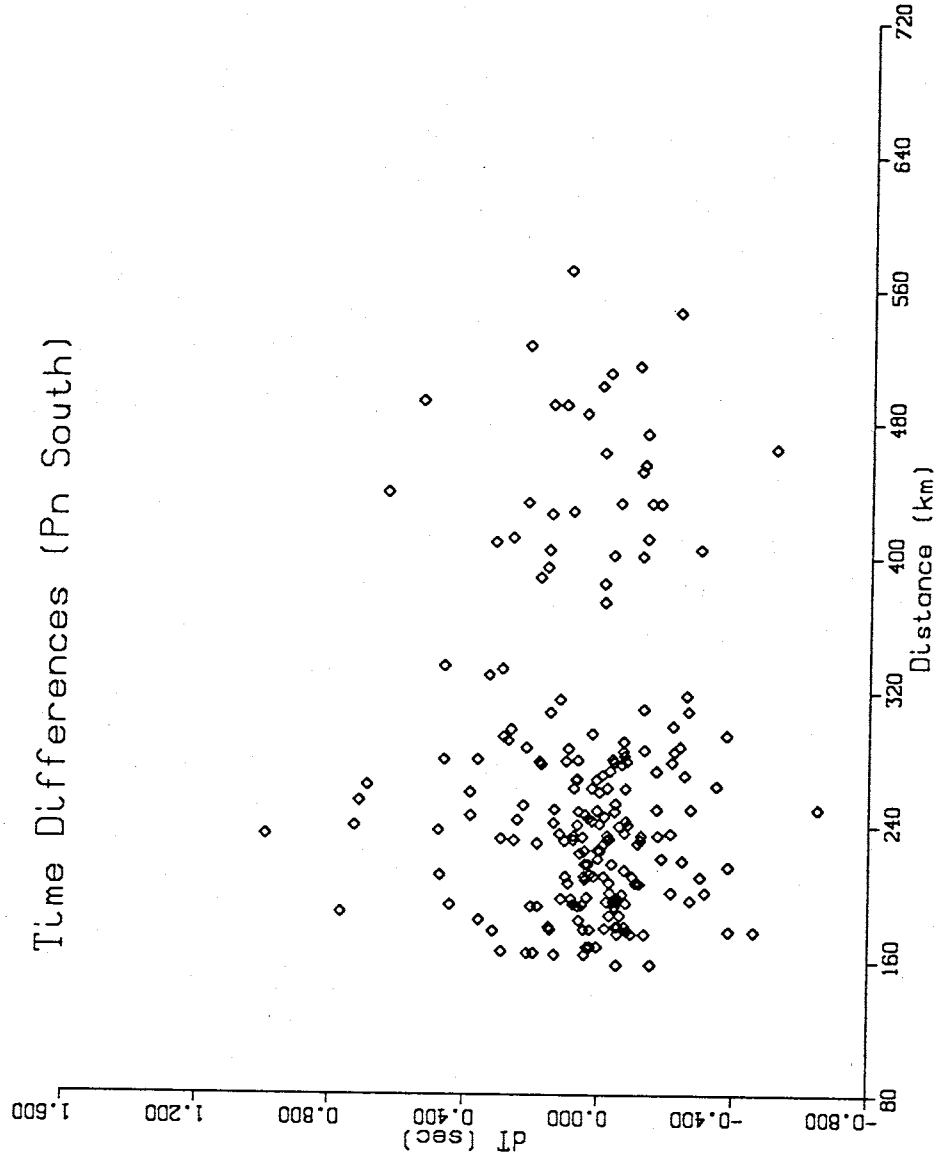

Figure 50: Travel time residuals versus distance for Pn South data resulting from unmodified time-term analysis.

Modified

Anisotropy. The anisotropy analyses of the areal subsets present some of the most interesting and confusing results from this study. The analysis of the complete Pn data set indicated that there was no anisotropy in the upper mantle. However, the subsequent subset analyses not only indicate anisotropy, but anisotropy of a fairly large magnitude. The results that follow are all significant at or close to a 95 percent confidence level (Tables 19, 20, 21, 22).

When the area is divided into East and West data subsets, the results define two anisotropies with comparable magnitudes but differing directions (Figures 51, 52). In fact, the two are almost completely out of phase (Figure 53). North and South, though, show anisotropies with slightly differing magnitudes, but nearly identical directions (Figures 54, 55). These directions lie between those of the East and West subsets. All in all, these anisotropy results present a complicated picture.

The magnitudes of the $cos(2\Phi)$ dependence of each data subset lie within one standard deviation of each other and can be considered equal. However, the phases, i.e. the directions of maximum velocity, are significantly different (Figure 56).

Considering the results of the East and West analyses, it seems logical that a north-south oriented anisotropy in half the study area would be cancelled out by an essentially east-west anisotropy in the other half, provided their magnitudes were comparable. Thus, no anisotropy should be seen when analysis of the entire area is done. This is consistent with the results of the total Pn data set. Unfortunately, the results of the North and South anisotropy analyses are not as straightforward. These results may indicate an even more complicated upper mantle structure, or may be the consequence of some sort of averaging of the

Table 19

Analysis of Variance Table for Modified Time Term Equations

Pn East

Model	SSWR	DF	$DF_U - DF_M$	F
Unmodified	2864	117		
Azimuth Dependence	2632	113	4	2.5
Distance Dependence	2864	116	1	0.0

Table 20

Analysis of Variance Table for Modified Time Term Equations

Pn West

Model	SSWR	DF	$DF_U - DF_M$	F
Unmodified .	6948	193		
Azimuth Dependence	6614	189	4	2.4
Distance Dependence	6867	192	1	2.3

Table 21

Analysis of Variance Table for Modified Time Term Equations

Pn North

Model	SSWR	DF	$DF_U - DF_M$	F
Unmodified	5678	168		
Azimuth Dependence	5363	164	4	2.4
Distance Dependence	5536	167	1	4.3

Table 22

Analysis of Variance Table for Modified Time Term Equations

Pn South

Model	SSWR	DF	$DF_U - DF_M$	F
Unmodified	5317	167		
Azimuth Dependence	5013	163	4	2.5
Distance Dependence	5144	166	1	5.6

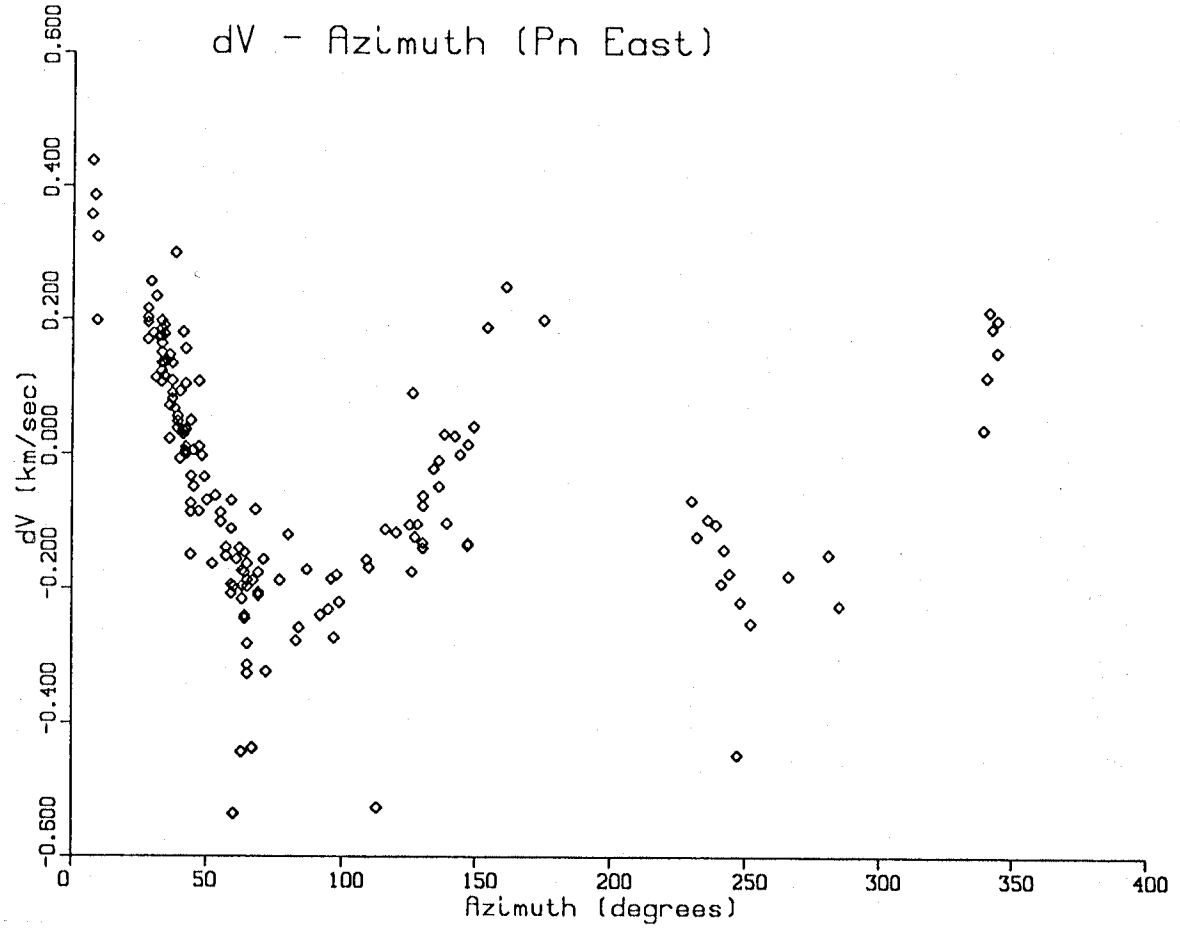

Figure 51: Velocity perturbations versus azimuth for Pn East data resulting from a modified time-term analysis assuming a slightly anisotropic upper mantle. The $cos(2\Phi)$ term effect is dominant over the $cos(4\Phi)$ terms here. The orientation is north-south.

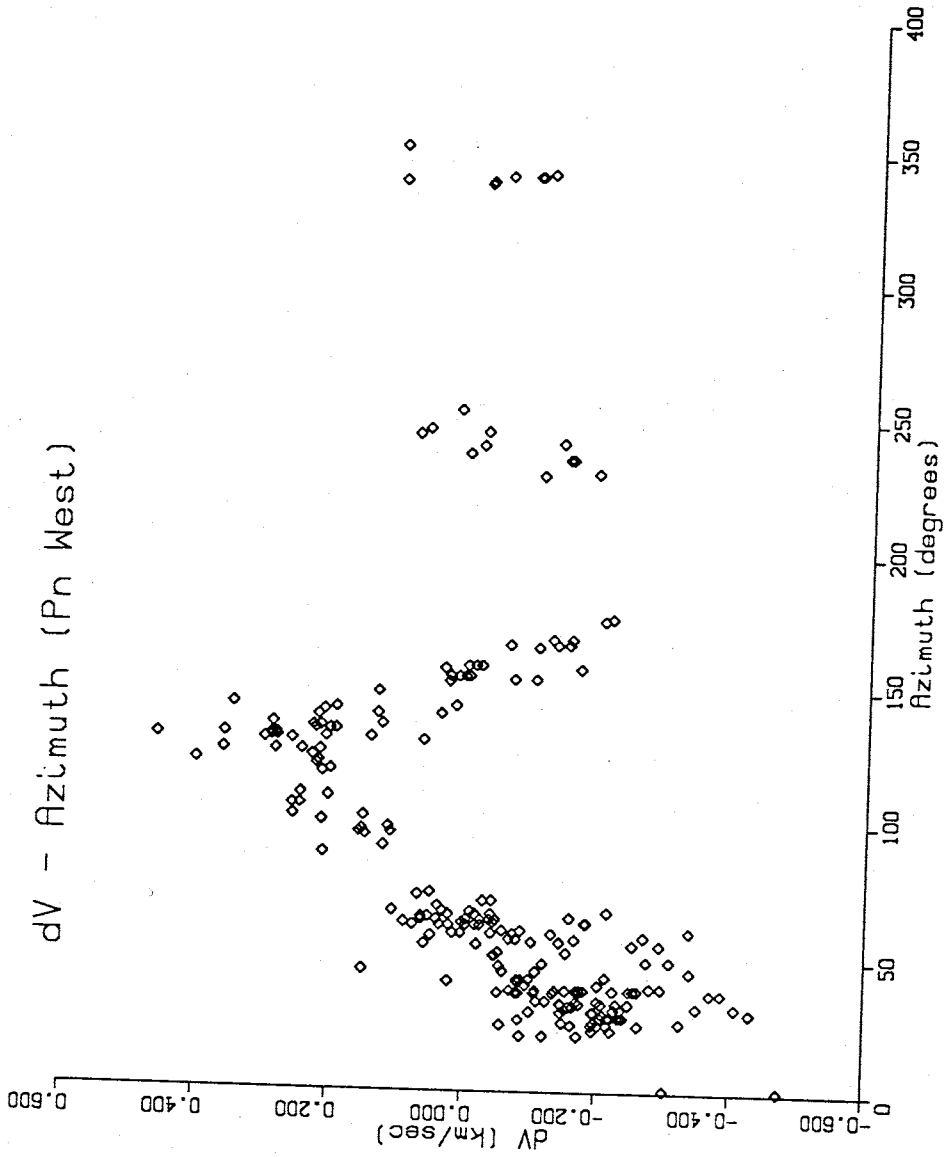

Figure 52: Velocity perturbations versus azimuth for Pn West data resulting from a modified time-term analysis assuming a slightly anisotropic upper mantle. The $cos(2\Phi)$ term effect is dominant over the $cos(4\Phi)$ terms here. The orientation is ESE-WNW.

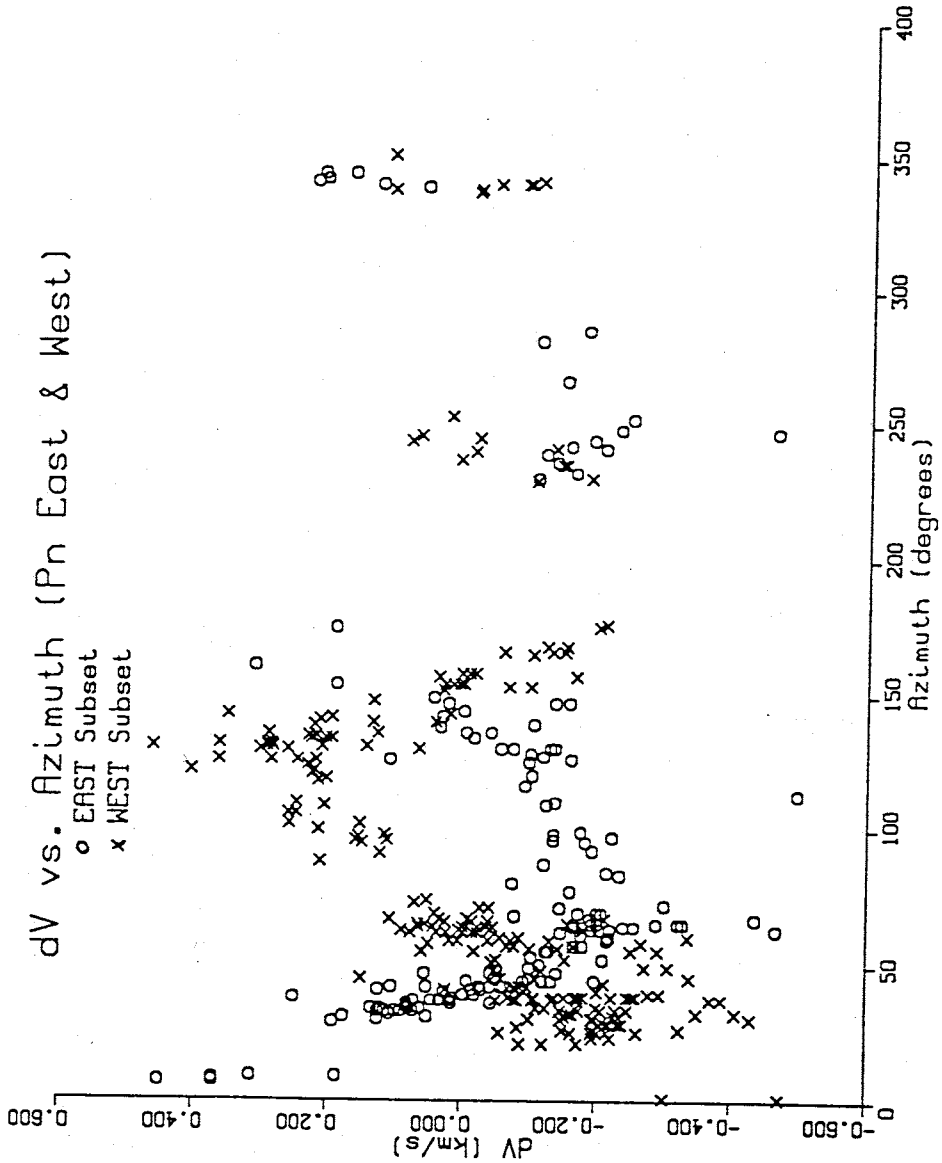

Figure 53: Velocity perturbations versus azimuth for Pn East (x's) and the Pn West (o's) from Figures 50 and 51, respectively. The two anisotropies are almost completely out of phase.

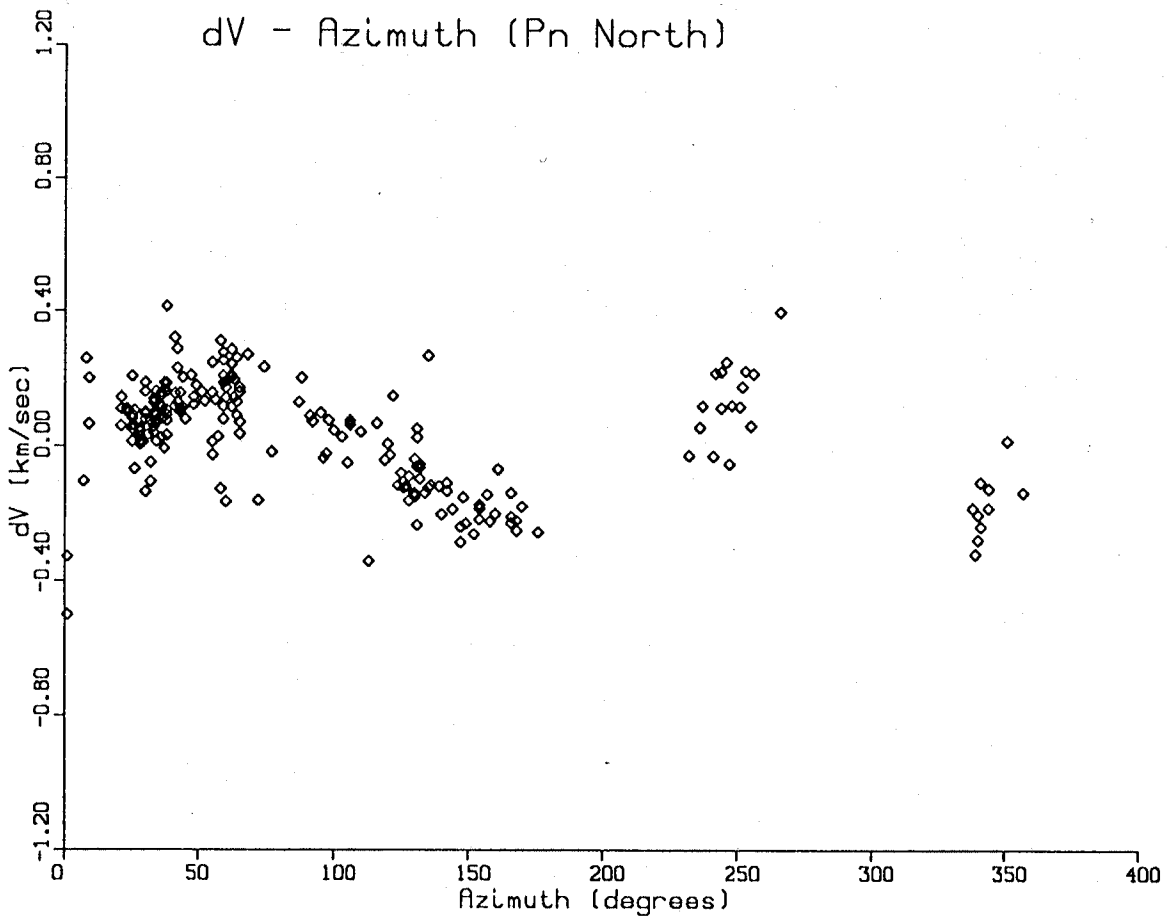

Figure 54: Velocity perturbations versus azimuth for Pn North data resulting from a modified time-term analysis assuming a slightly anisotropic upper mantle. The $cos(2\Phi)$ term effect is dominant over the $cos(4\Phi)$ terms here. The orientation is NE-SW.

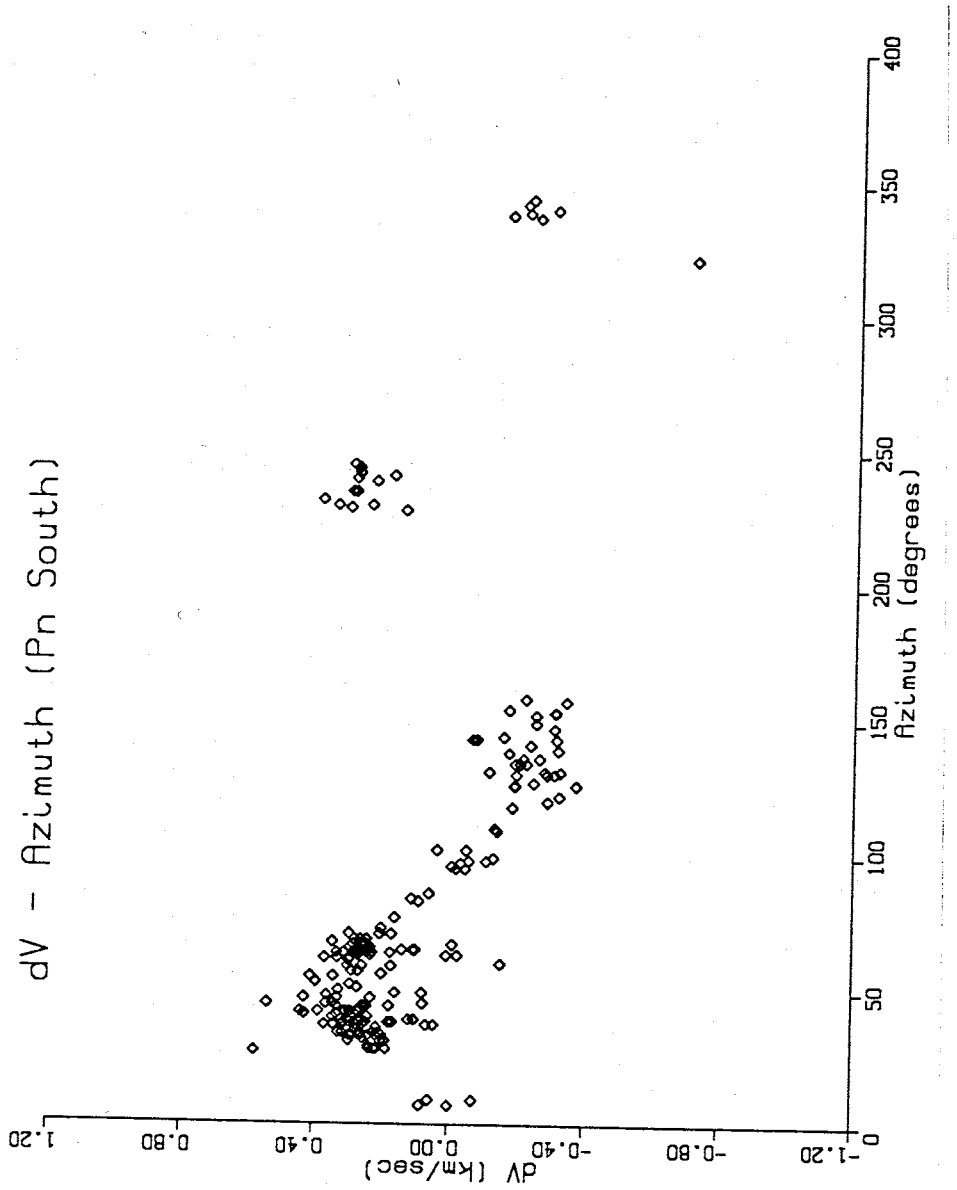

Figure 55: Velocity perturbations versus azimuth for Pn South data resulting from a modified time-term analysis assuming a slightly anisotropic upper mantle. The $cos(2\Phi)$ term effect is dominant over the $cos(4\Phi)$ terms here. The orientation is NE-SW.

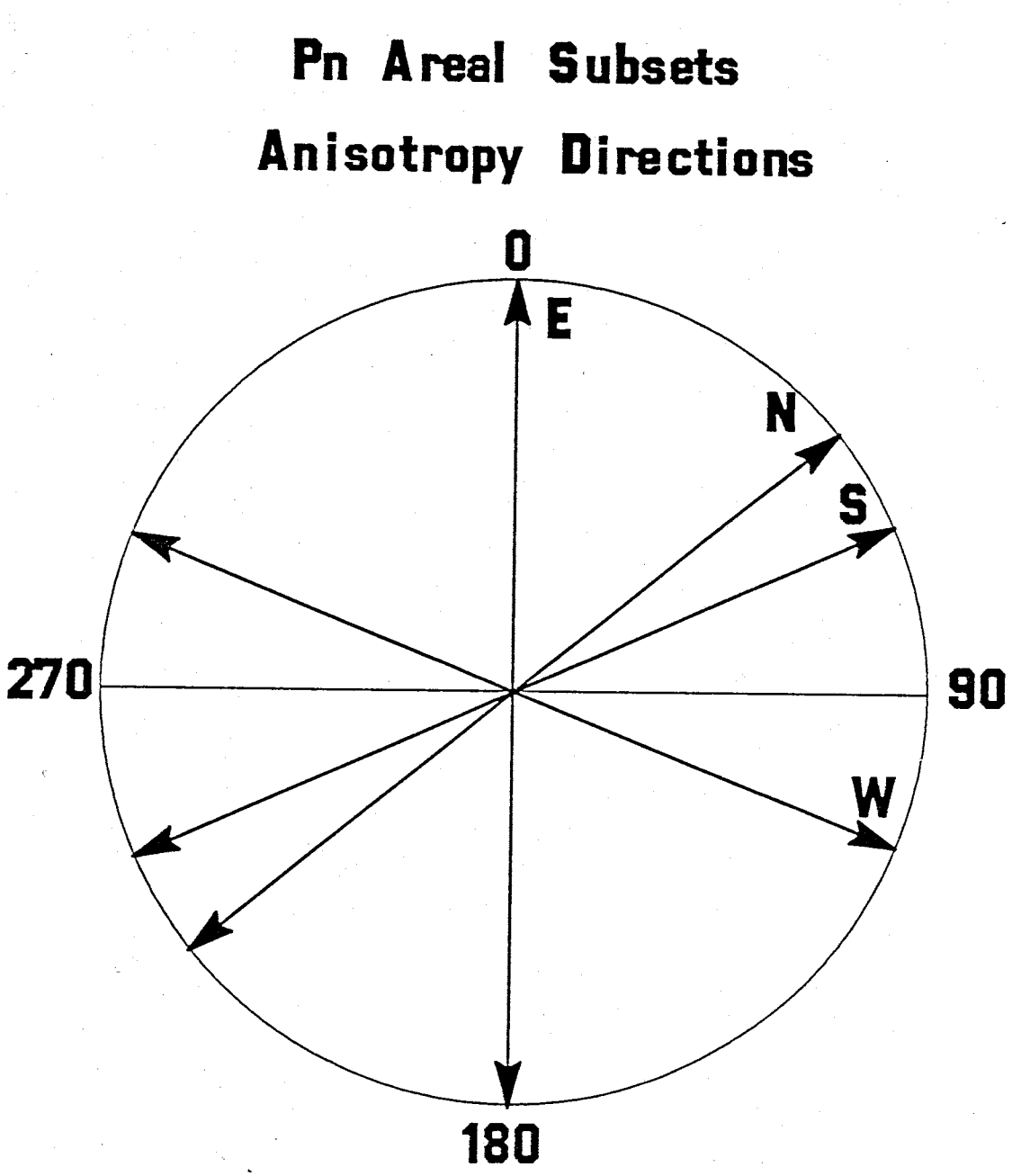

Figure 56: Phase angles of the $cos(2\Phi)$ dependence from modified time-term analysis of the Pn areal subsets assuming a slightly anisotropic upper mantle. E, W, N, S represent Pn East, Pn West, Pn North, and Pn South data subsets respectively.

two anisotropy directions. Such averaging would likely depend on the station distribution as well as the azimuthal distribution of the sources.

Assume a model which has a north-south oriented anisotropy in the eastern region of the study area and an east-west oriented anisotropy in the western region. This basically indicates that the sub-Moho materials beneath each section have experienced significantly different tectonic histories. In other words, the upper mantle rocks from two different tectonic regimes and therefore, two different locations are now in contact with one another. The most likely cause for such a juxtaposition is the large strike-slip movement during the Eocene postulated by Chapin and Cather (1981) (also Chapin, 1983), whereby the Colorado Plateau was translated approximately 100 km to the north-northeast. Figure 57 shows the approximate ~~location~~ inferred location of the Hot Springs- Montosa fault zone through the study area.

Another possibility is that is that the shear zone could be quite wide to the west and east of the Hot Springs-Montosa fault. This would account for the north-south anisotropy for the East data set. The essentially east-west anisotropy for the West data set could be indicating the regional anisotropy, i.e. the anisotropy of of the area not affected by the shear zone of the fault. This would be consistent with the east-west oriented anisotropy for western North America reported by Bamford et al. (1979).

Finally, the observed anisotropy may be related to the geometry of the array. When the Pn data set is subdivided, inter-station distances are dramatically reduced perpendicular to the dividing line, e.g. when the area is subdivided by longitude 106.95, the maximum east-west inter-station distance is reduced by half, from 58 km to 29 km. In this case, the Pn velocity in the north-south direction will be better determined than the velocity in the east-west direction.

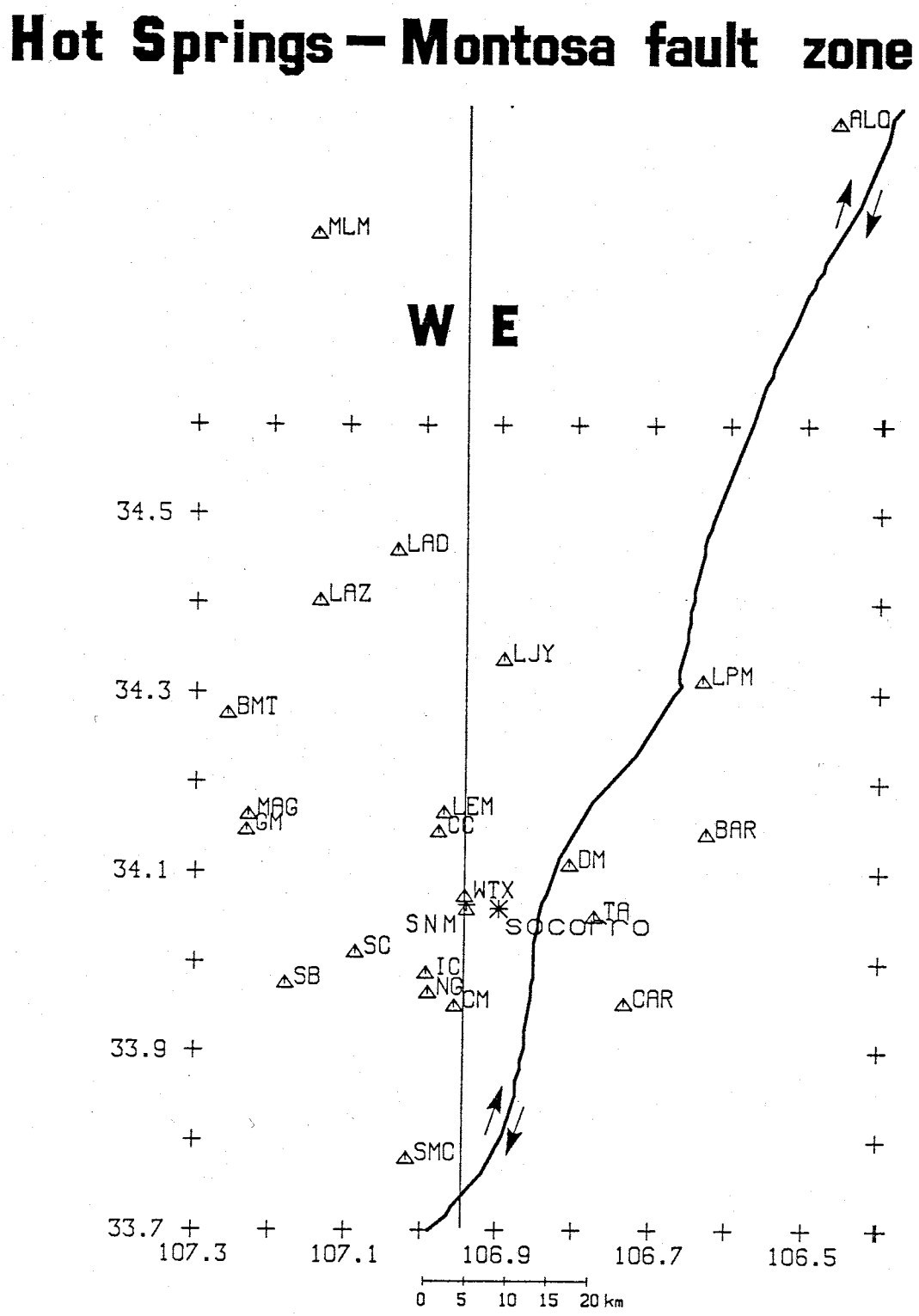

Figure 57: Inferred position of the Hot Springs-Montosa fault zone through the study area (after Chapin, 1983).

Large uncertainties in the velocity along a given azimuth could erroneously indicate anisotropy where none existed (J. Murdock, personal communication). Hence, the existence of the observed anisotropy is not certain.

In summary, the anisotropy analyses of the Pn areal subsets present a complicated picture of the upper mantle beneath the Socorro area. The exact nature of this complexity has not been determined, however it may well be the consequence of large strike-slip faulting in the Eocene. The possibility also exists that the observed anisotropy is not real but the consequence of reduced inter-station distances.

Dip. The results of the dip analyses are presented in Tables 15, 16, 17, 18. Figures 58, 59, 60, 61 plot the velocity perturbations with respect to azimuth. The magnitudes of the $cos(\Phi)$ dependence correspond to $6.6 \pm 1.2^\circ$ for East, $6.3 \pm 1.3^\circ$ for West, $4.5 \pm 0.6^\circ$ for North, and $5.1 \pm 1.0^\circ$ for south. The various dip directions are displayed in Figure 62. Structural complexities and differing data sets cause some scatter in the dip results, but on the whole, the subset results confirm the results of the full Pn data set, i.e. a relatively large dip on the Moho to the northwest.

Distance. Three of the four Pn subsets indicated a velocity decrease with increasing epicentral distance comparable to the results of the full data set, although only North and South were statistically significant (Tables 19, 20, 21, 22). Figures 63, 64, 65, 66 display the velocity perturbations with distance for each subset. No additional information about the upper mantle was forthcoming from these analyses beyond that gained from the analysis of the total data set.

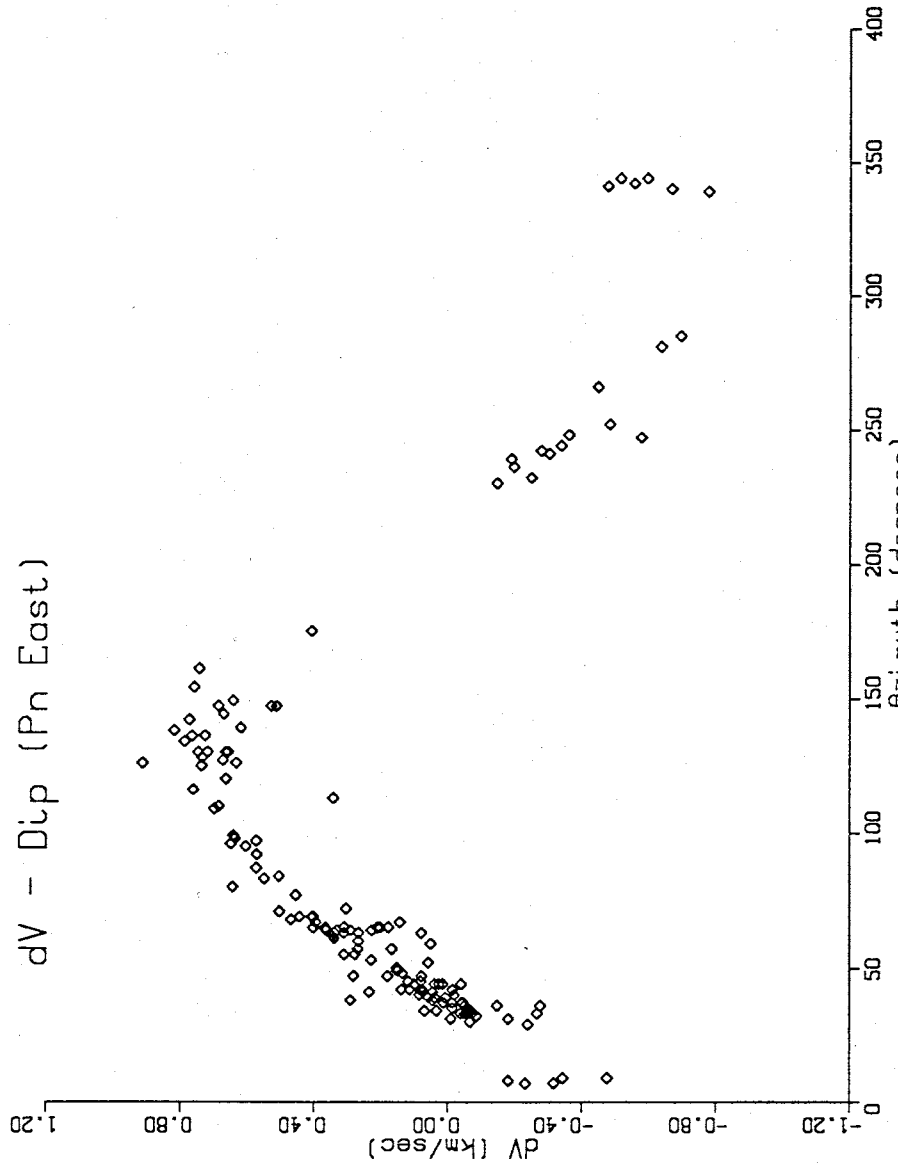

Figure 58: Velocity perturbations versus azimuth for Pn East resulting from modified time-term analysis in which a sloping Moho interface is assumed. The $cos(\Phi)$ azimuth dependence indicated by these data is consistent with an average Moho dip of greater than 6°.

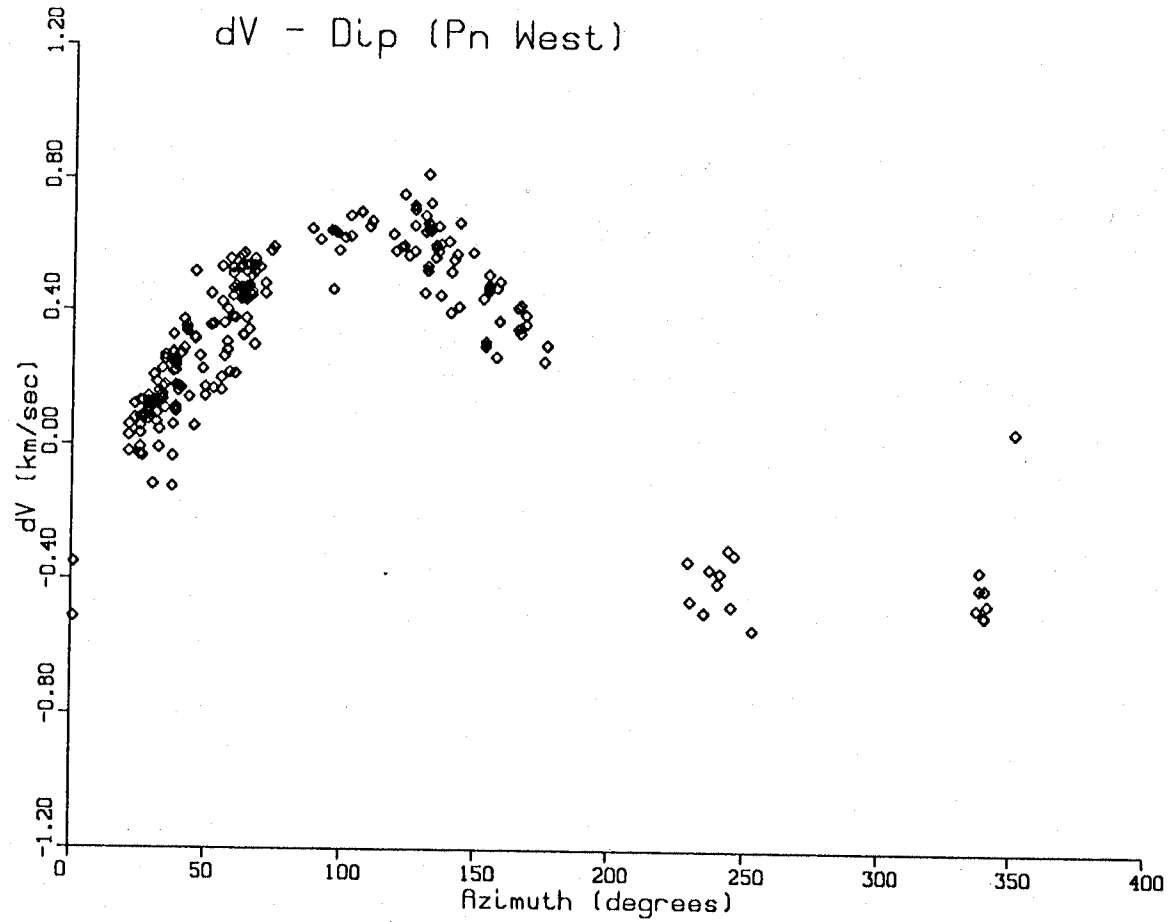

Figure 59: Velocity perturbations versus azimuth for Pn West resulting from modified time-term analysis in which a sloping Moho interface is assumed. The $cos(\Phi)$ azimuth dependence indicated by these data is consistent with an average Moho dip of greater than 6°.

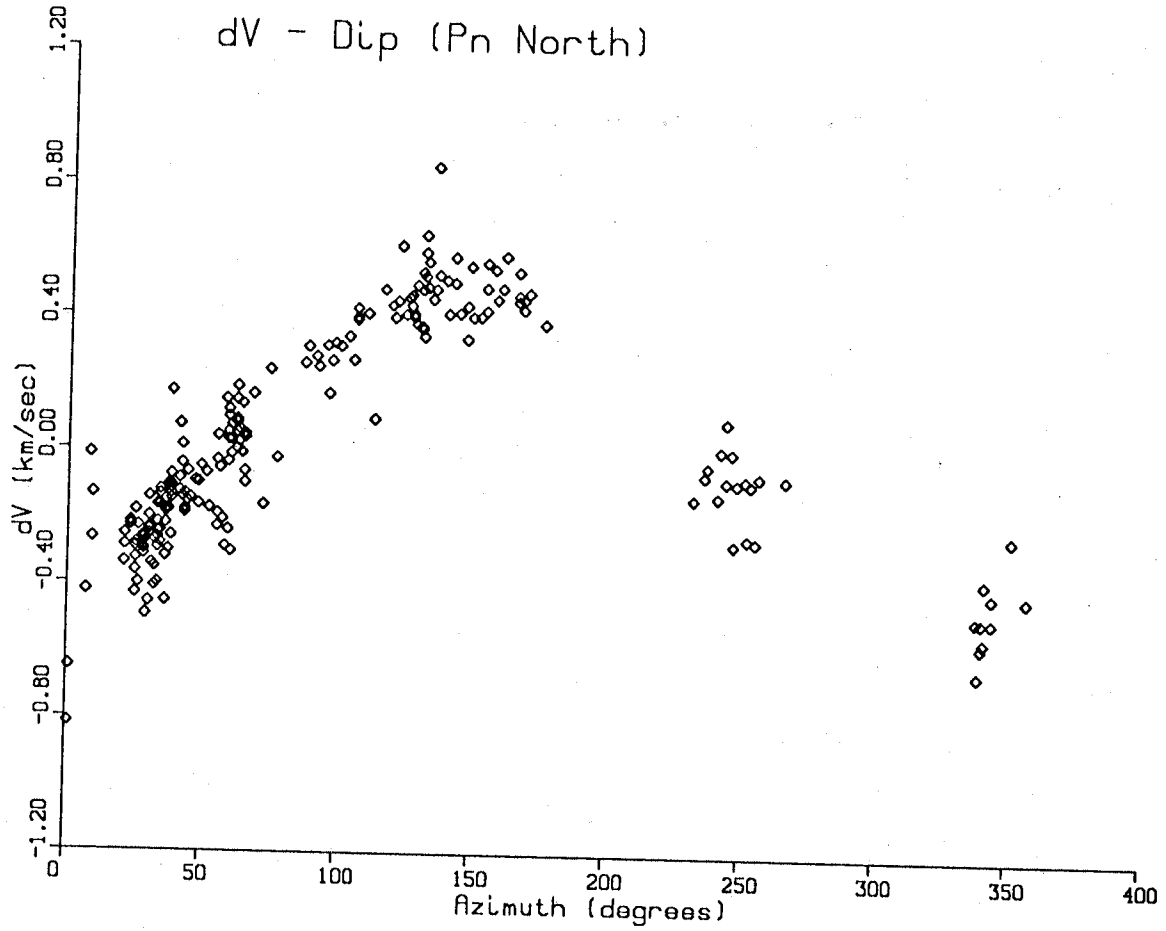

Figure 60: Velocity perturbations versus azimuth for Pn North resulting from modified time-term analysis in which a sloping Moho interface is assumed. The $cos(\Phi)$ azimuth dependence indicated by these data is consistent with an average Moho dip of greater than 4°.

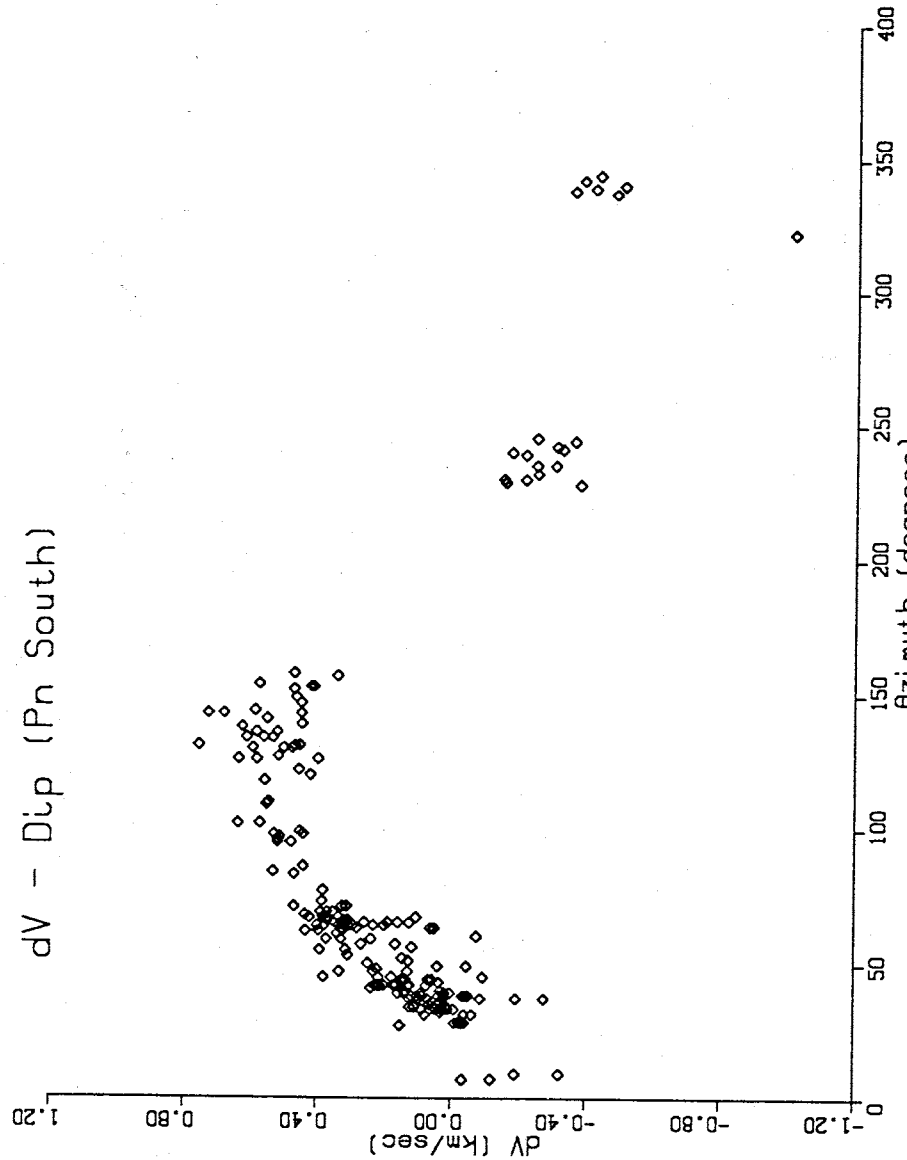

Figure 61: Velocity perturbations versus azimuth for Pn South resulting from modified time-term analysis in which a sloping Moho interface is assumed. The $cos(\Phi)$ azimuth dependence indicated by these data is consistent with an average Moho dip of greater than 6°.

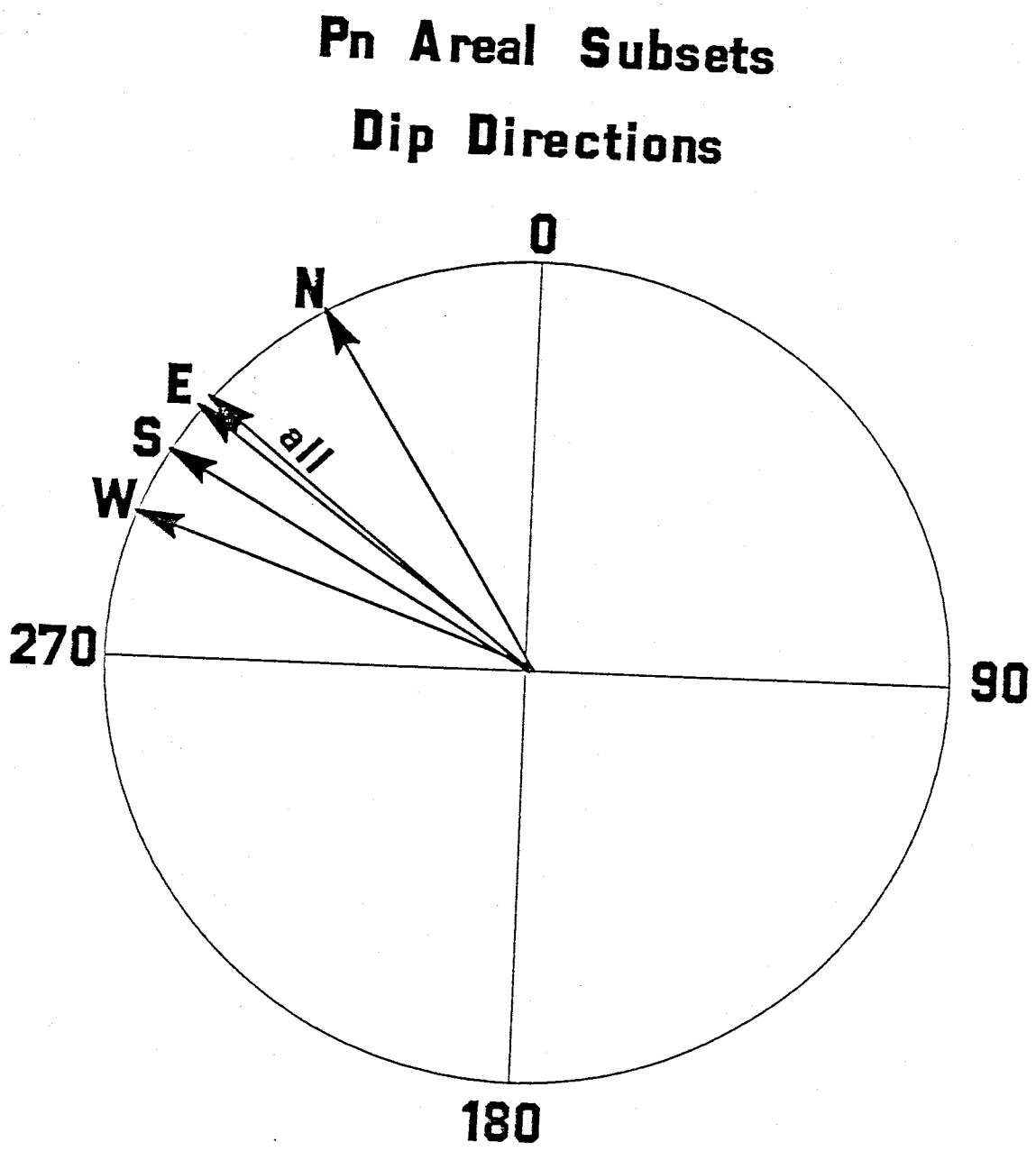

Figure 62: Phase angles of the $cos(\Phi)$ dependence from modified time-term analysis of the Pn areal subsets assuming a sloping Moho interface. E, W, N, S represent Pn East, Pn West, Pn North, and Pn South data subsets respectively.

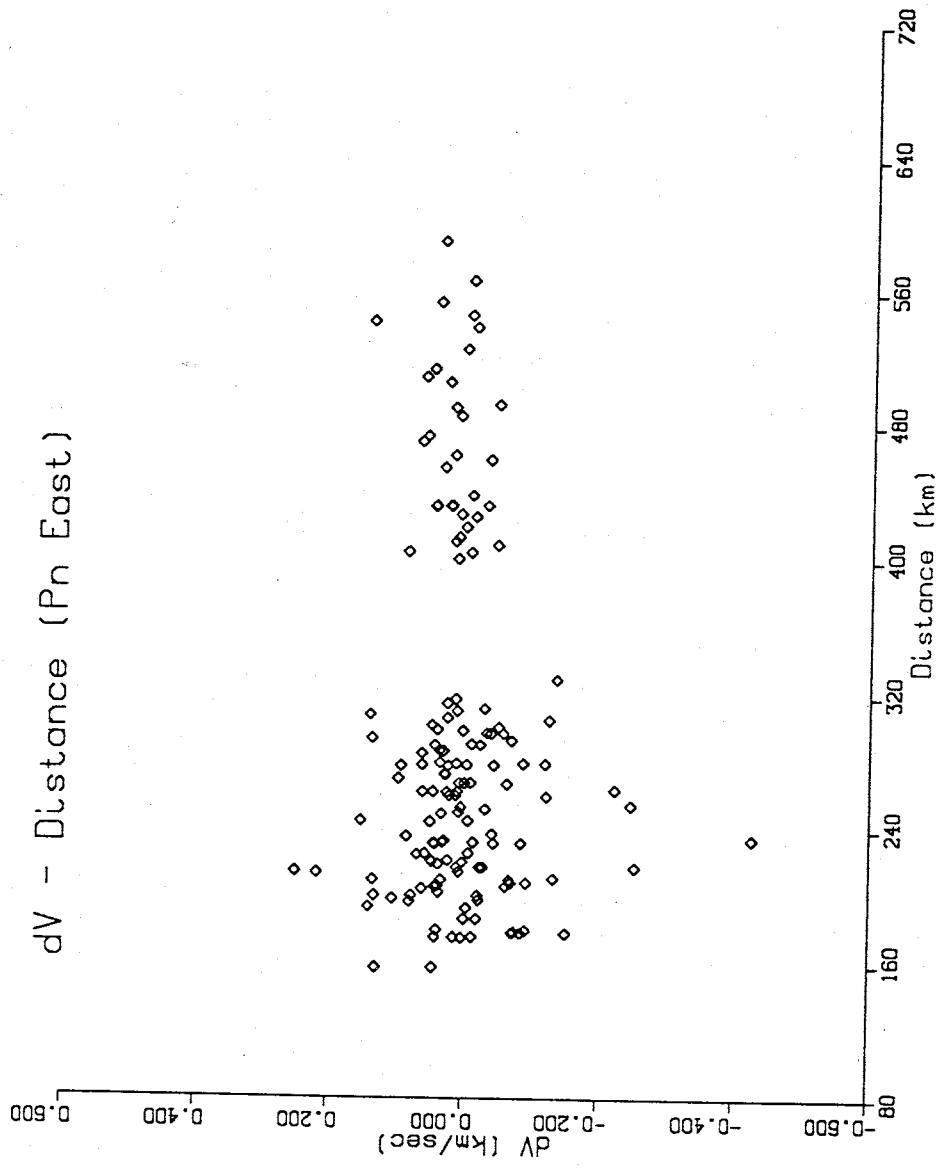

Figure 63: Velocity perturbations versus distance for Pn East resulting from modified time-term analysis assuming a small lateral increase in velocity with distance. No lateral gradient is observed.

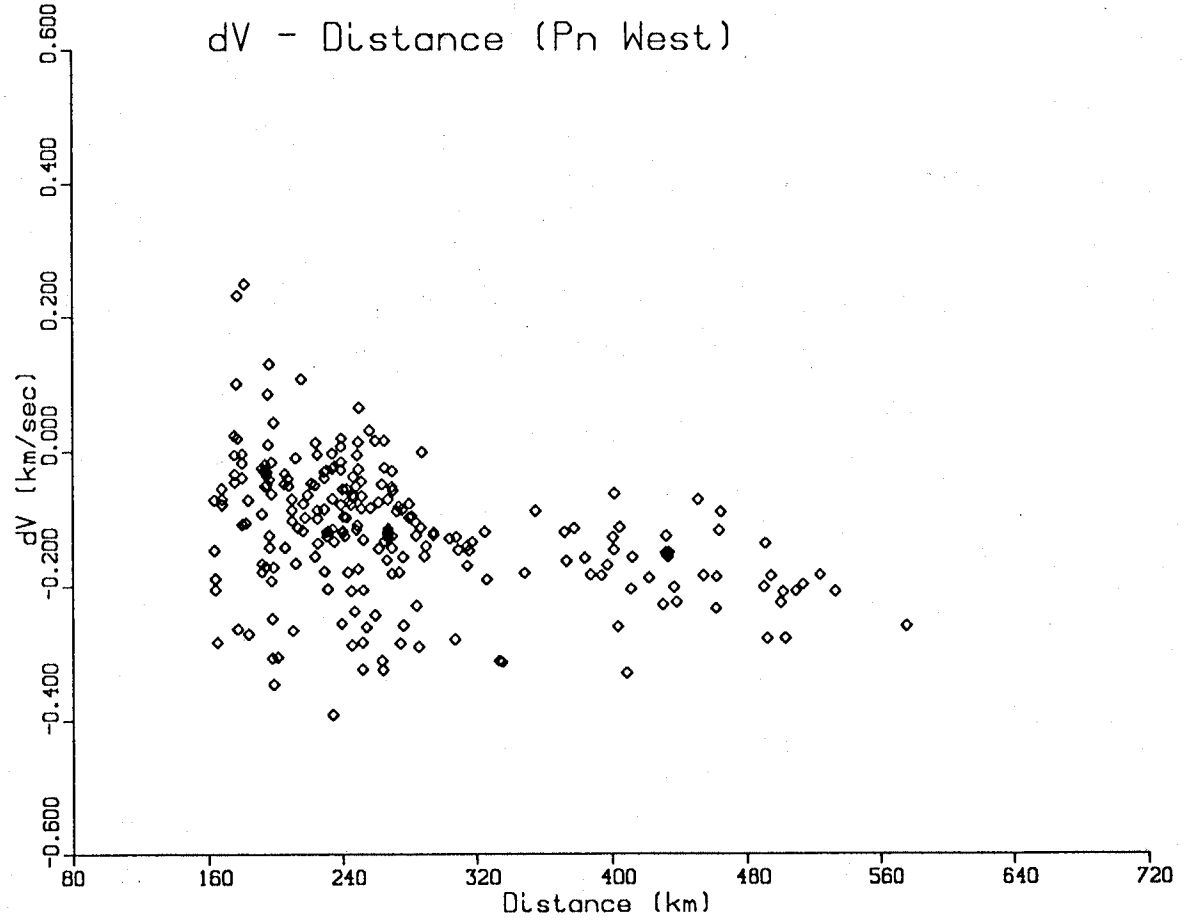

Figure 64: Velocity perturbations versus distance for Pn West resulting from modified time-term analysis assuming a small lateral increase in velocity with distance. Decrease with distance could have a variety of causes, however, it is not statistically significant.

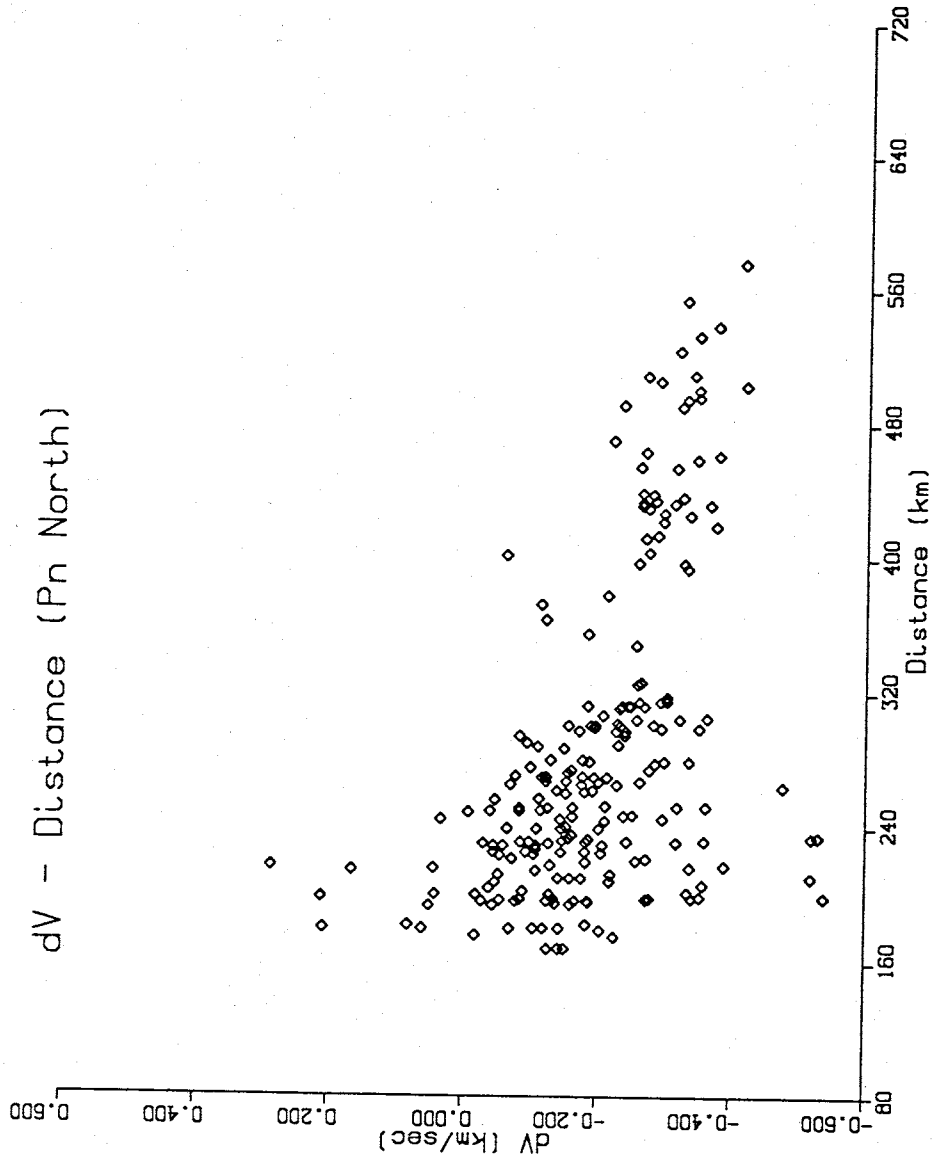

Figure 65: Velocity perturbations versus distance for Pn North resulting from modified time-term analysis assuming a small lateral increase in velocity with distance. Decrease with distance could have a variety of causes (see text).

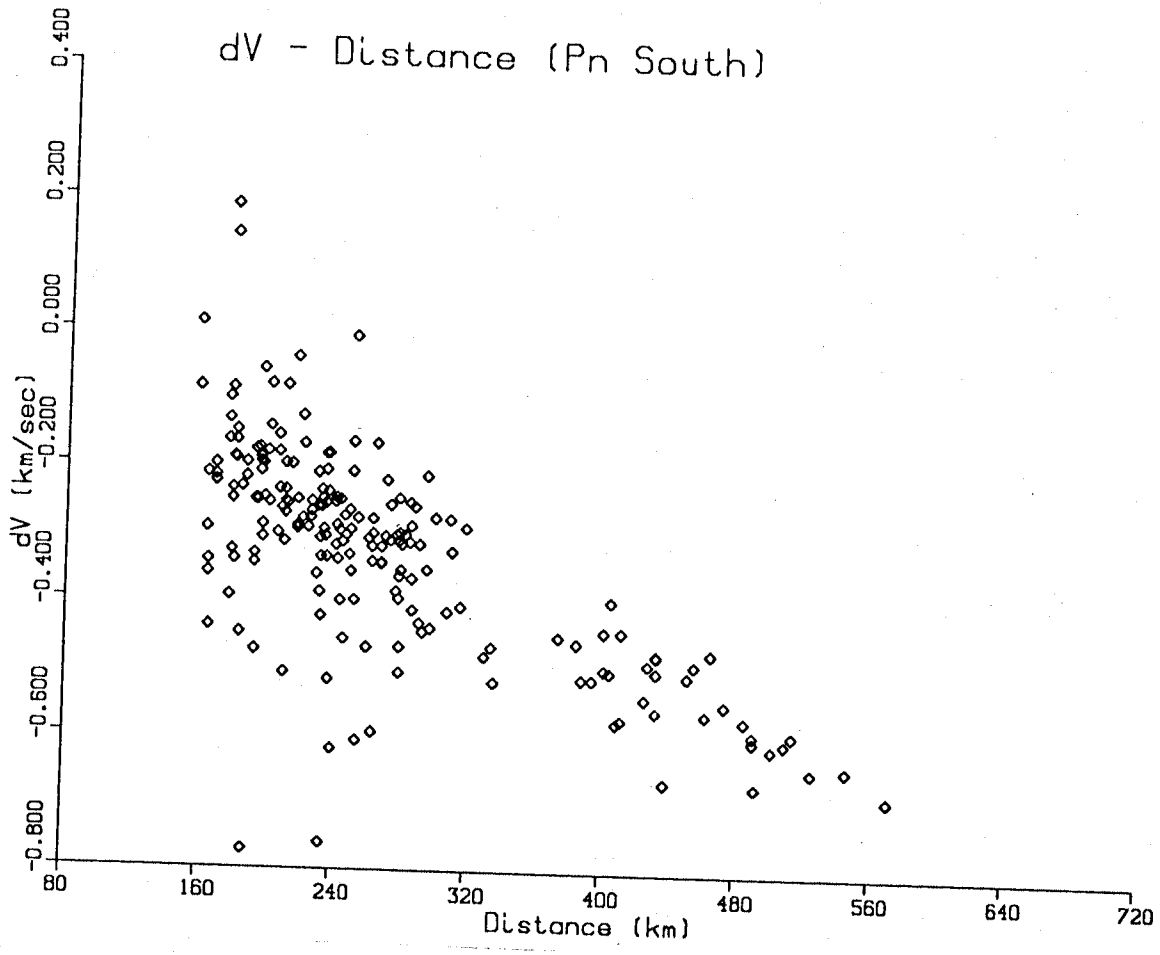

Figure 66: Velocity perturbations versus distance for Pn South resulting from modified time-term analysis assuming a small lateral increase in velocity with distance. Decrease with distance could have a variety of causes (see text).

ANALYSIS OF TIME TERMS

As discussed previously, a time term may be thought of as the difference between the time it takes a critically refracted wave to pass through the layers above the refracting interface and the time for the head wave to travel the offset distance (the horizontal distance between the point of critical refraction and the source or receiver) at the sub-interface velocity. Therefore, a time term is directly related to the thickness of the layers overlying the refractor. Knowledge of the overburden and refractor velocities allows conversion of the time term to a depth. The depth equation (Berry and West, 1966) is

$$H = \sum_{j=1}^{n} d_j = \sum_{j=1}^{n} \left\{ \left[a_j - \sum_{i=1}^{j-1} d_i \; / \; K_{j+1,i} \right] K_{j+1,j} \right\}, \tag{29}$$

where

$$K_{j,i} = \frac{V_i V_j}{\sqrt{V_j^2 - V_i^2}}, \tag{30}$$

and

a_j = the time term for the jth refractor,

V_j = the velocity of the jth refractor,

d_j = the depth to the jth refractor,

H = the total depth to the refractor of interest.

It is important to remember that the velocity structure above a refractor is usually fairly complex, especially in a tectonically active region. When a simple velocity structure is assumed for a tectonically complicated region, depth errors will occur. Furthermore, unlike near-vertical reflections, head waves do not sample the crust directly beneath the recording stations. Rather, they refract upward at the critical angle to the station from points that can be a considerable

distance away, especially when refracting from deeper layers. The time term for a given station then, is actually an average of the travel times for a cone of refracted waves travelling through the overlying layers. For Pn, the base of this cone is on the order of 80 km in diameter. Hence, depth estimates from time terms not only depend on the velocity structure chosen and the topography of the refracting surface, but can also depend on the azimuthal distribution of sources. Consequently, the depth estimates from this study may not always agree precisely with those made by others within the region.

Given a sufficient station density, a general idea of a refractor's surface may be obtained. Highly accurate modeling of the subsurface, however, is really not possible without a dense array of stations and good velocity information. Station distribution is also a factor. To enhance signal quality, the majority of the New Mexico Tech seismic network is placed on competent rock, since alluvial fill is highly attenuative. Hence, most of the station sites in this study are associated with structural highs, few with structural lows. The effect of this type of skewed distribution can be illustrated if one compares a surface developed from station elevation data (Figures 67, 68) with an outline of the actual surface topography (Figure 3). Many major features, both highs and lows, are missed, and extended features are often replaced by isolated structures.

In this study, surfaces were developed for each of the three refractors. As might be expected, the Pg refractor, i.e. the Precambrian basement beneath the network, is the best constrained. Excellent data, short offset distances, and good geologic control permit a much more involved analysis and discussion than is practical for the deeper layers. The P* refractor surface is the most uncertain because the standard errors on the P* time terms are often as large as the relative differences between stations. However, use of the results from other studies in the region has resulted in a reasonable model of the mid-crustal surface. The

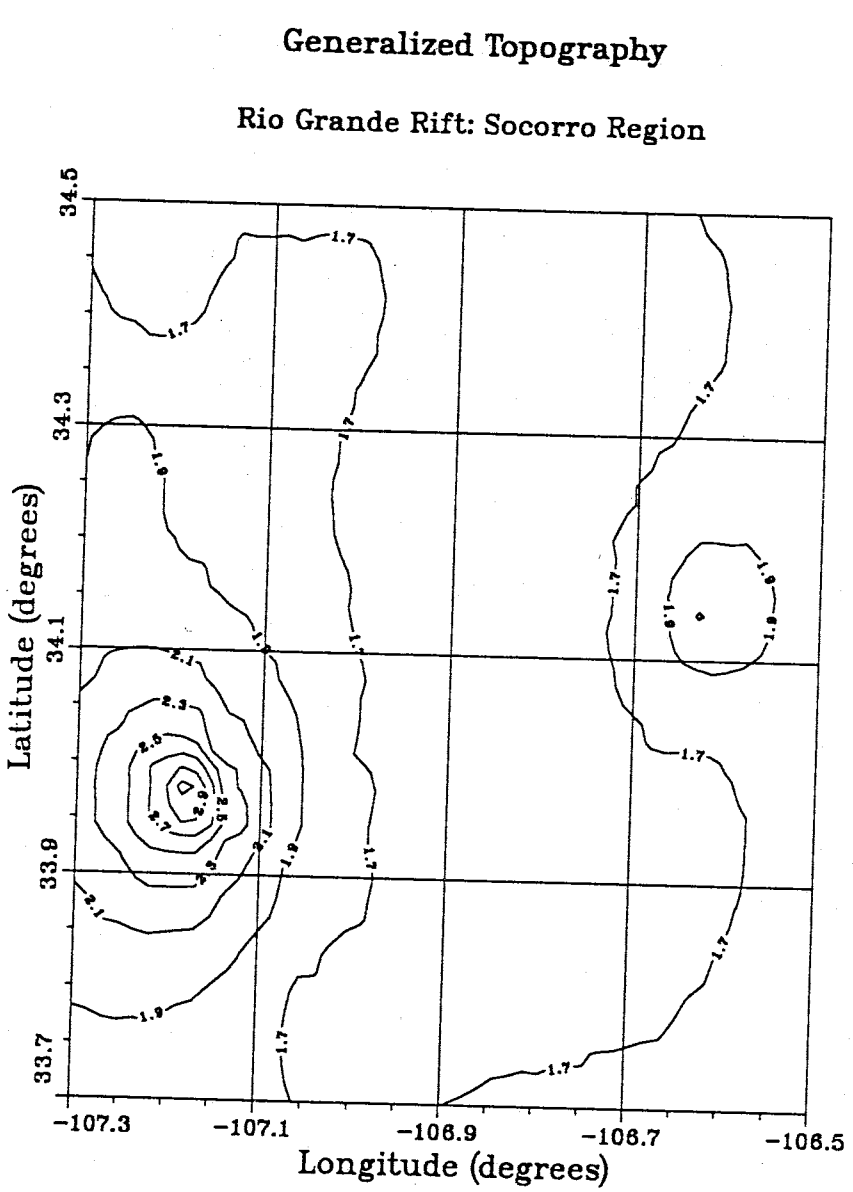

Figure 67: Contour plot of general surface topography from kriging of elevation data at 52 station sites.

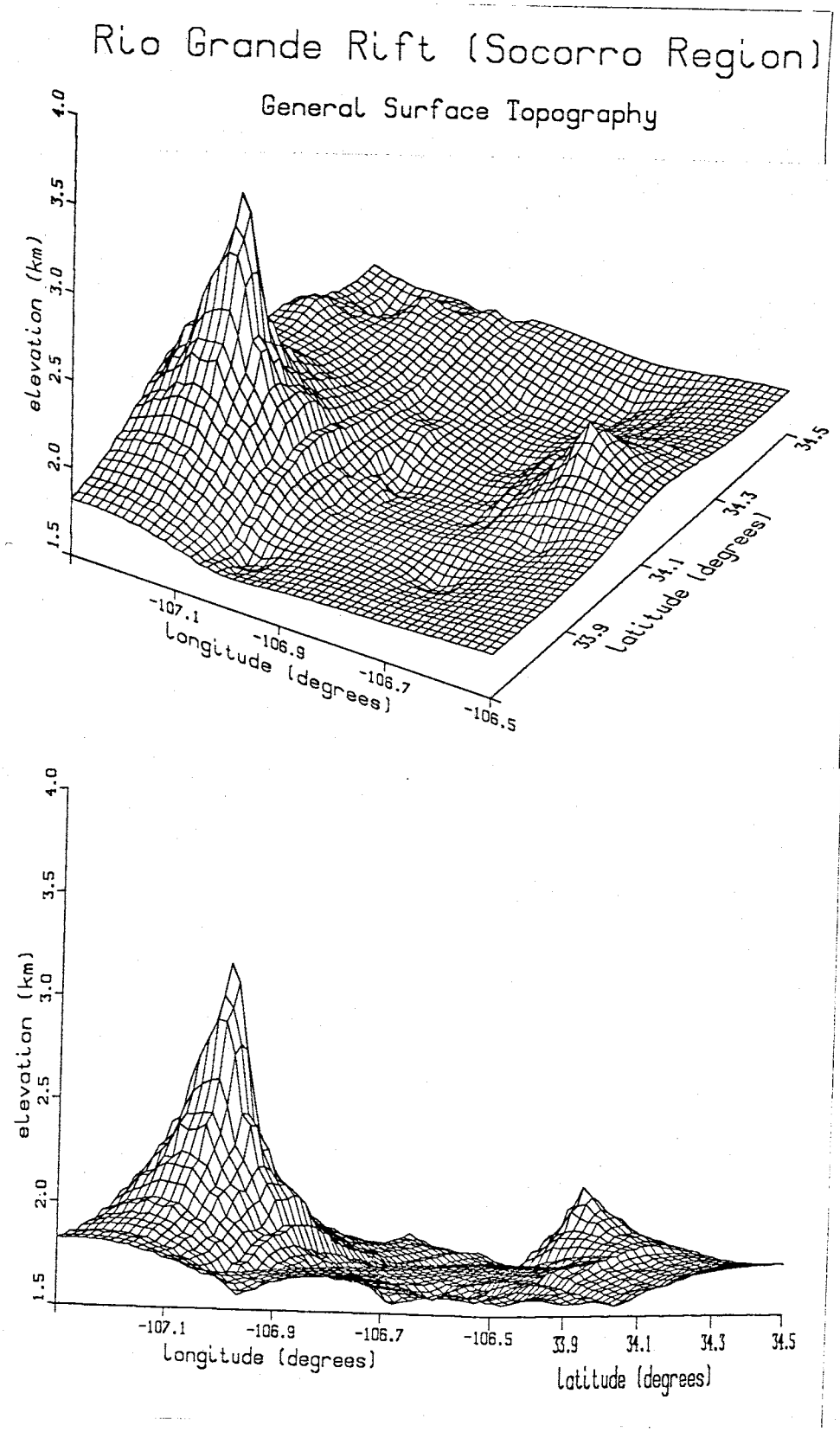

Figure 68: Three-dimensional representation of general surface topography from kriging of elevation data at 52 station sites. Two perspectives are presented.

Pn refractor model is obtained by using an average crustal velocity of 6.2 km/s (Toppozada and Sanford, 1976), overlain by a Phanerozoic section with an average velocity of 3.4 km/s. Initially, it was hoped a more accurate rendition of the thickness of the crust could be obtained by "peeling off" each progressively deeper layer. However, the limited number of stations at which P* was recorded and the fairly large uncertainties on the depth to the Conrad made this unfeasible. As a result, only the effect of the Phanerozoic layer was removed. Nevertheless, the procedure of removing the overburden effects, which are often very large, and then using an average velocity for the crust seems to provide good results.

Pg Time Terms

As mentioned previously, geologic constraint allows greater interpretation of the Pg time terms than those of the other data sets. However, this interpretation is complicated since the study area has been folded and faulted, uplifted and eroded, undergone extensions and compressions, rifting and volcanism. Furthermore, stratigraphic and structural changes are abrupt and drastic. The extreme complexity of the area has led to conflicting interpretations and models. As a result, the following discussion is necessarily "broad stroke", yet it is specific enough to explain the observed variations in the time terms.

The velocity model obtained from the modified distance analysis provided the best fit to the Pg data. Therefore, it is appropriate that time-term results from that analysis be used to define the Precambrian surface. The Pg time terms along with their standard errors from the distance analysis are listed in Table 23. Their geographic distribution is shown in Figure 69. Using an overburden velocity of 3.40 $\pm$ 0.10 km/s and a refractor velocity of 5.71 $\pm$ 0.07 km/s, depths to basement were computed for each station using equation (29) (see Table 24; Figure 70). Three stations, LAD, LEM, and LPM, have slightly negative time terms. Although a negative time term converts to a negative depth to basement, it actually indicates that the velocity beneath the station is higher than the average refractor velocity. LAD, LEM, and LPM are all on competent Precambrian blocks (Table 25), which may not be as highly fractured as basement rock in general in the region. As such, these blocks would be expected to have higher velocities than the more highly fractured basement rock. A velocity of ~6.00 km/s would explain the negative values at LAD and LPM, while only a slightly higher velocity than the average is required for LEM.

Stations WTX and CC are also on the Precambrian. The time-term results

Table 23

Pg Time Terms

New Mexico Tech Seismic Network

Station	Time Term (sec)
BAR	0.28 ± 0.08
BG	0.43 ± 0.09
BMT	0.22 ± 0.09
CAR	0.35 ± 0.07
CC	0.15 ± 0.07
CM	0.24 ± 0.10
CU	0.40 ± 0.13
DM	0.26 ± 0.09
FM	0.43 ± 0.09
GM	0.12 ± 0.10
IC	0.32 ± 0.09
LAD	-.12 ± 0.09
LAZ	0.14 ± 0.09
LEM	-.04 ± 0.08
LJY	0.70 ± 0.22
LPM	-.16 ± 0.08
MAG	0.04 ± 0.11
MLM	0.53 ± 0.15
NG	0.16 ± 0.17
RM	0.41 ± 0.17
SB	0.34 ± 0.07
SC	0.48 ± 0.09

Table 23 (continued)	
SL	0.24 ± 0.10
SMC	0.32 ± 0.07
SNM	0.28 ± 0.11
WM	0.17 ± 0.13
WTX	0.06 ± 0.06

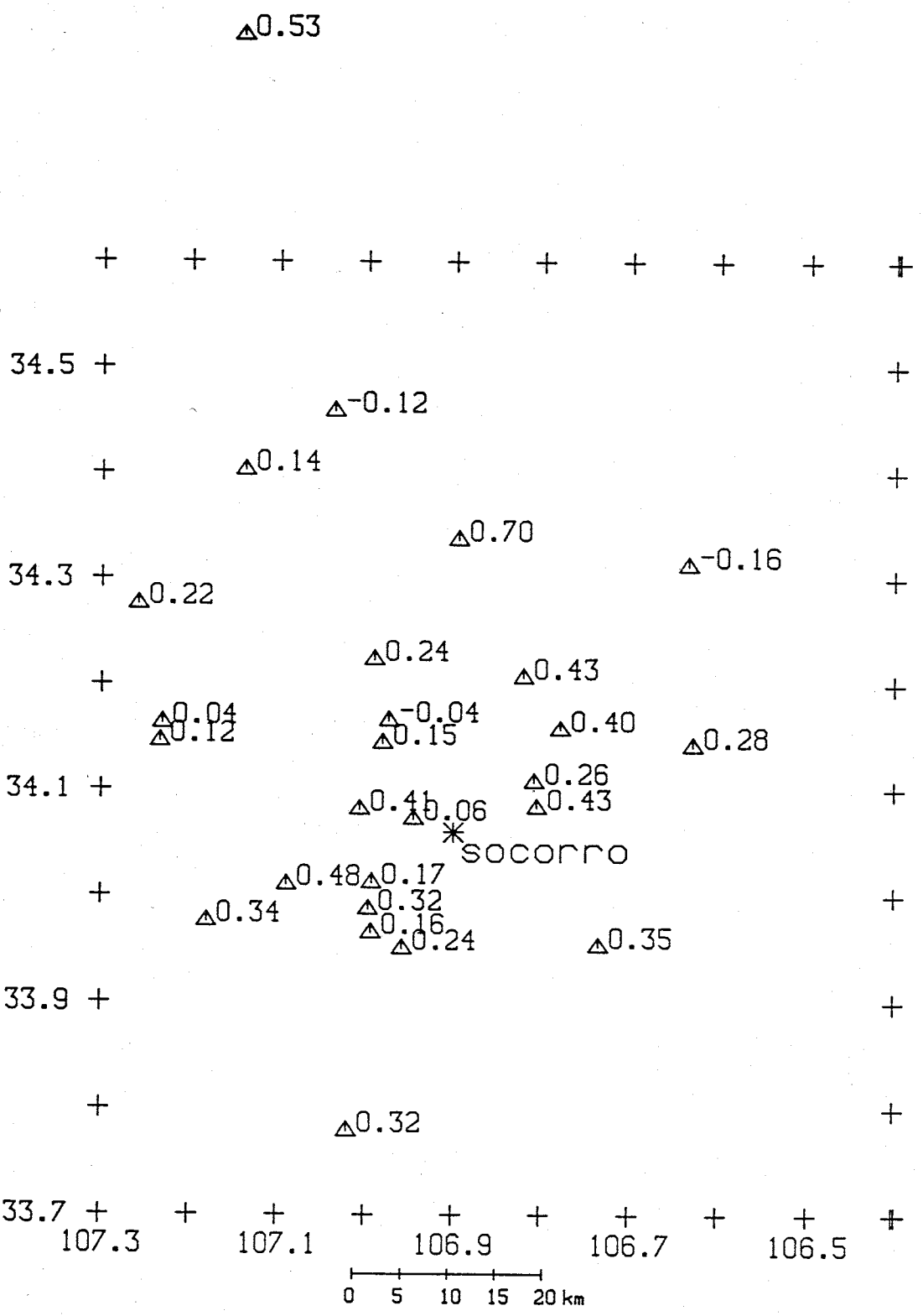

Figure 69: Geographical distribution of Pg time terms from modified time-term analysis assuming a small vertical velocity gradient in the Precambrian basement.

Table 24

Depth to Precambrian Basement

New Mexico Tech Seismic Network

Station	Depth (km)
BAR	1.185 ± 0.272
BG	1.819 ± 0.306
BMT	0.931 ± 0.306
CAR	1.481 ± 0.238
CC	0.635 ± 0.238
CM	1.015 ± 0.340
CU	1.692 ± 0.442
DM	1.100 ± 0.306
FM	1.819 ± 0.306
GM	0.508 ± 0.340
IC	1.354 ± 0.306
LAD	-.508 ± 0.306
LAZ	0.592 ± 0.306
LEM	-.169 ± 0.272
LJY	2.962 ± 0.748
LPM	-.677 ± 0.272
MAG	0.169 ± 0.374
MLM	2.242 ± 0.510
NG	0.677 ± 0.578
RM	1.735 ± 0.578
SB	1.439 ± 0.238
SC	2.031 ± 0.306

Table 24 (continued)	
SL	1.015 ± 0.340
SMC	1.354 ± 0.238
SNM	1.185 ± 0.374
WM	0.719 ± 0.442
WTX	0.254 ± 0.204

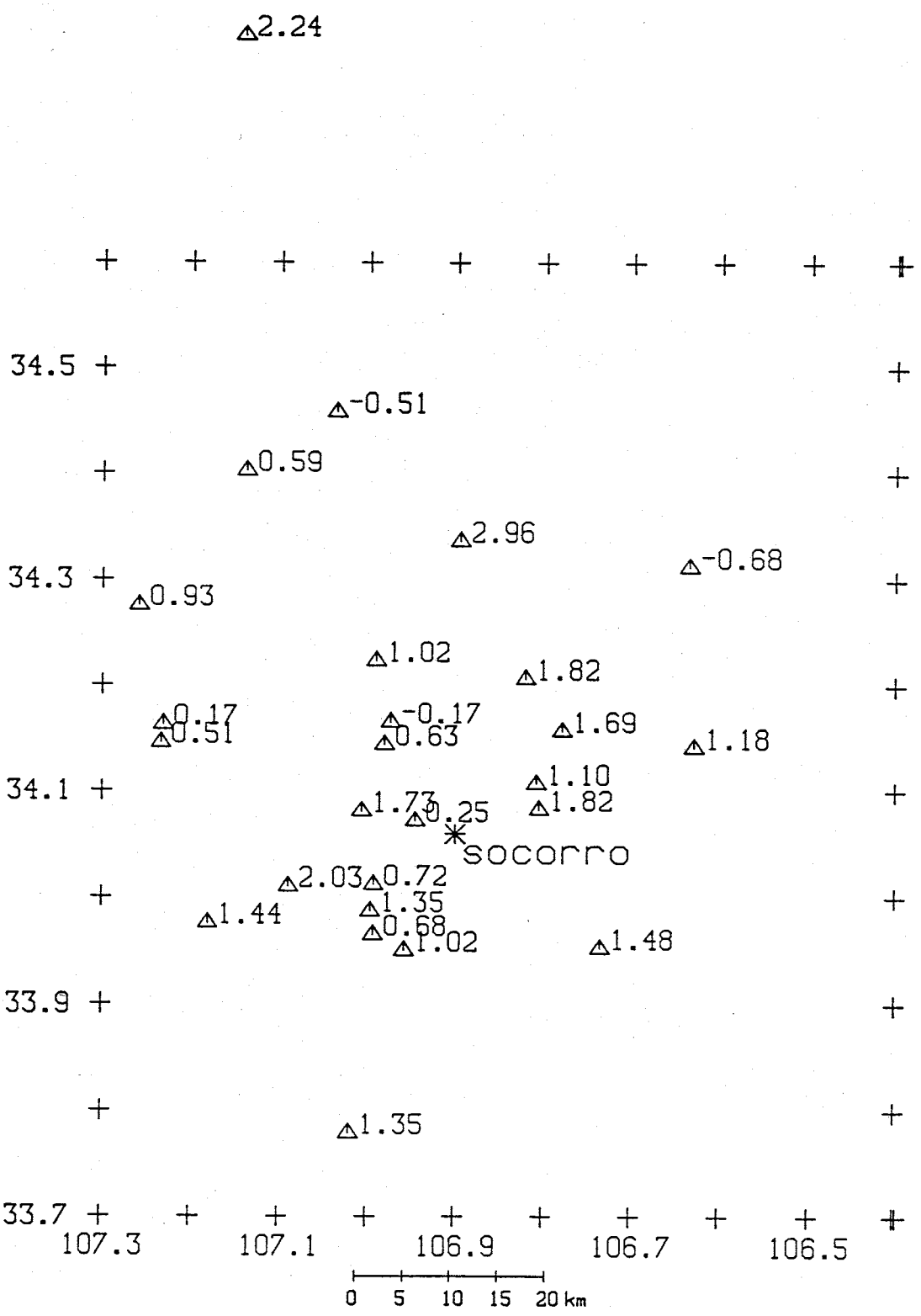

Figure 70: Computed depths to the Precambrian basement plotted at their respective station locations. Negative values indicate the station lies directly upon basement rock which has a slightly higher Pg velocity than the average.

Table 25

Near Surface Geology

New Mexico Tech Seismic Network

Station	Near Surface Geology
BAR	Permian limestone (San Andres Limestone)
BG	Tertiary ash flow tuffs
BMT	Tertiary ash flow tuffs
CAR	Permian limestone
CC	Precambrian granite
CM	Tertiary ash flow tuffs (Socorro Cauldron moat deposits)
CU	Permian sandstones & limestones (Glorieta & San Andres)
DM	Pennsylvanian limestone (Madera Formation)
FM	Precambrian overlying Pennsylvanian (sliver of Precambrian Tajo pluton)
GM	Tertiary monzonite intrusion
IC	Tertiary basaltic & rhyolitic lavas (center of Socorro Cauldron)
LAD	Precambrian metasediments & metavolcanics
LAZ	Pennsylvanian limestone
LEM	Precambrian metasediments & metavolcanics

Table 25 (continued)	
LJY	Quaternary terrace deposits
LPM	Precambrian granite
MAG	Tertiary ash flow tuffs
MLM	Quaternary extrusive basalt (upper flow of Mesa Lucero)
NG	Tertiary intrusive
RM	Tertiary red & green playa claystones
SB	Tertiary ash flow tuffs
SC	Tertiary ash flow tuffs (Socorro Cauldron)
SL	Tertiary fanglomerates, mudstones & sandstones (Popotosa Formation)
SMC	Tertiary volcanics
SNM	Tertiary moat deposits (Socorro Cauldron)
TA	Permian interbedded ss., shales, & limestones (Torres, Cañas, Joyita Members)
WM	Tertiary moat deposits
WTX	Precambrian granite

show that Precambrian basement is 254 m beneath WTX, and 635 m beneath CC. Both station sites are geologically complex with extensive fracturing and faulting. As a result, the velocity beneath these stations is probably slower than the average basement velocity which would result in the computation of a positive depth to basement. The larger depth value of 635 m at CC most likely indicates that the refracted ray paths to the station are not all within Precambrian rock. Since fairly thick sedimentary sections surround this location, energy traveling to the station along rays from certain azimuths would be delayed. The time term at CC is likely a composite average of slightly positive time terms for those ray paths traveling strictly in Precambrian rock, and somewhat more positive time terms for those ray paths traveling partially through slower sedimentary strata on the way to the station.

Plutonic Precambrian rocks compose the northeastern end of the Magdalena Mountains west of Socorro. Just north of the Magdalena pluton are stations GM, on a Tertiary monzonite intrusion, and MAG, on a Tertiary ash-flow tuff. GM and MAG show depths to basement of ~500 m and ~170 m respectively. Given the large exposed sections of Precambrian rock surrounding these locales, these depths are considered appropriate. To the north of these stations in the Bear Mountains lies BMT, showing a much thicker Phanerozoic section, ~930m, than is observed at GM or MAG. A thick Paleozoic section (Pennsylvanian or perhaps Permian) underlies the Tertiary volcanics on which the station is situated (C. T. Smith, personal communication). Realizing this and utilizing the stratigraphic column of Brown (1972) for the southern Bear Mountains, it is possible for only the lower section of the Datil volcanic group to be present beneath BMT.

The next group of stations are all in the eastern part of the study area, where there is much better stratigraphic control than elsewhere in the region

(Figure 71). Station FM is emplaced near the Gonzales fluorite prospect on a sliver of the Precambrian Tajo pluton, yet the time term for this station indicates a depth to basement of greater than 1.8 km. This agrees well with the hypothesis that these Precambrian slivers are allochthonous and rootless, and overlie a fairly thick section of Paleozoic strata (C. T. Smith, personal communication). Inasmuch as the Pennsylvanian section in this area is only ~640 m thick, the 1.8 km thickness delineated by the time term suggests a repeated section along low angle faults. An alternate interpretation postulates that the FM lies in a north-south right lateral shear zone which bends to the northeast or is joined by a second northeast trending shear zone (R. Chamberlin, personal communication). The large time term would have to be caused by low velocity material within deeply penetrating fault zones. In addition, work by Carpenter (1984) indicates that the material below FM has a very low Q value. Low Q is consistent with a thick sedimentary section although extremely faulted basement rock is not ruled out.

Stations DM, on Pennsylvanian limestone, and CU, on Permian strata, are just north of FM. The time terms for both stations show evidence of thickened sections, but to a lesser degree than seen at FM. DM is on a section that is at least 470 m thicker than is indicated from its position in the geologic column, while the section beneath CU is at least 455 m thicker. Given the uncertainty in the calculated depth, the degree of thickening beneath these stations is not certain. Nevertheless, assuming FM lies above a greatly thickened section, some thickening would be expected at nearby stations.

Outside of this confined area of possibly repeated section (Figure 72), normal thicknesses are observed beneath the remainder of the eastern stations. BAR, lying on Permian limestone, CAR, located on Cretaceous sandstones and shales, and BG, situated on Tertiary ash flows, each has a calculated elevation

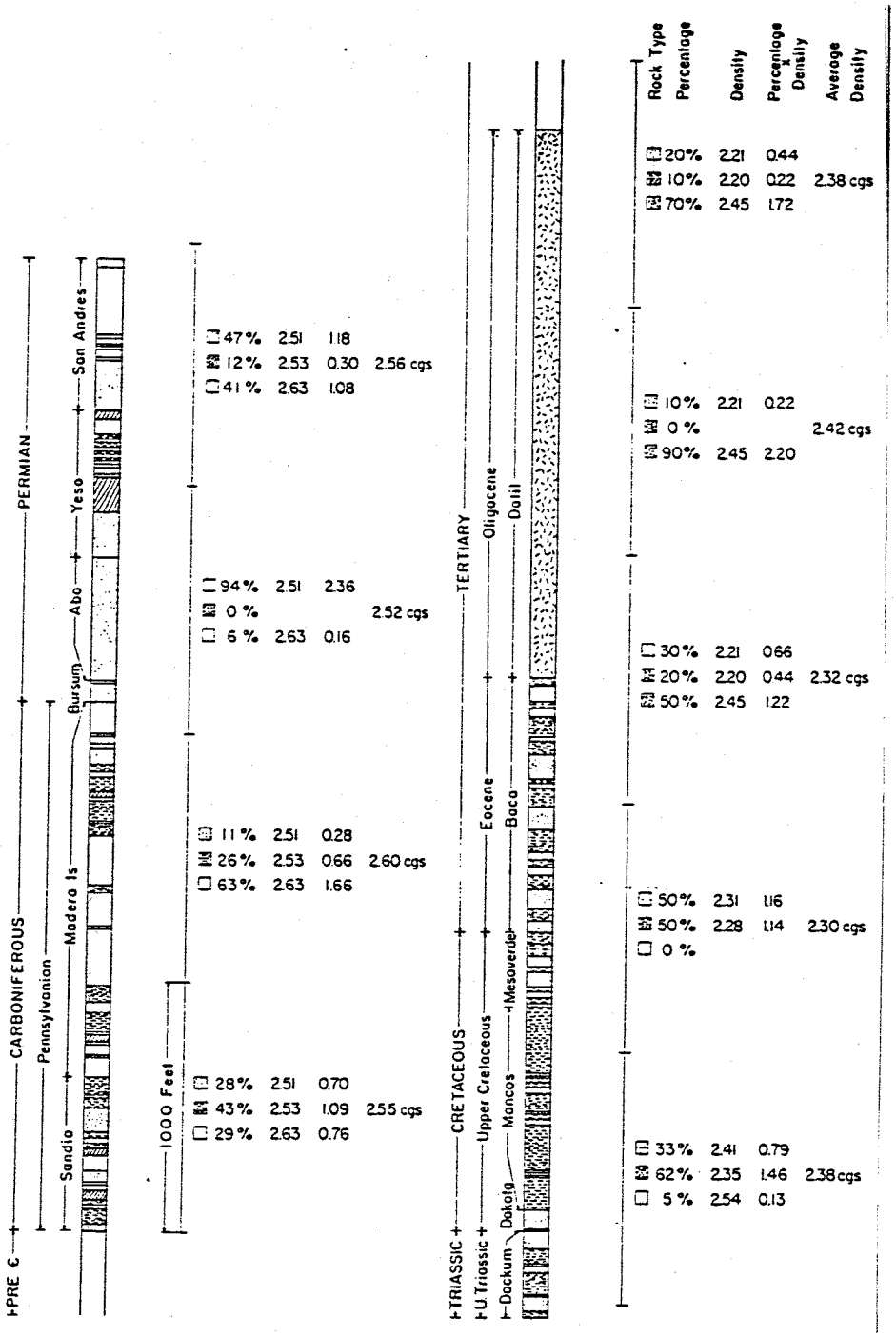

Figure 71: Geologic column used in depth-to-basement comparisons for the eastern part of the study area (from Sanford, 1968).

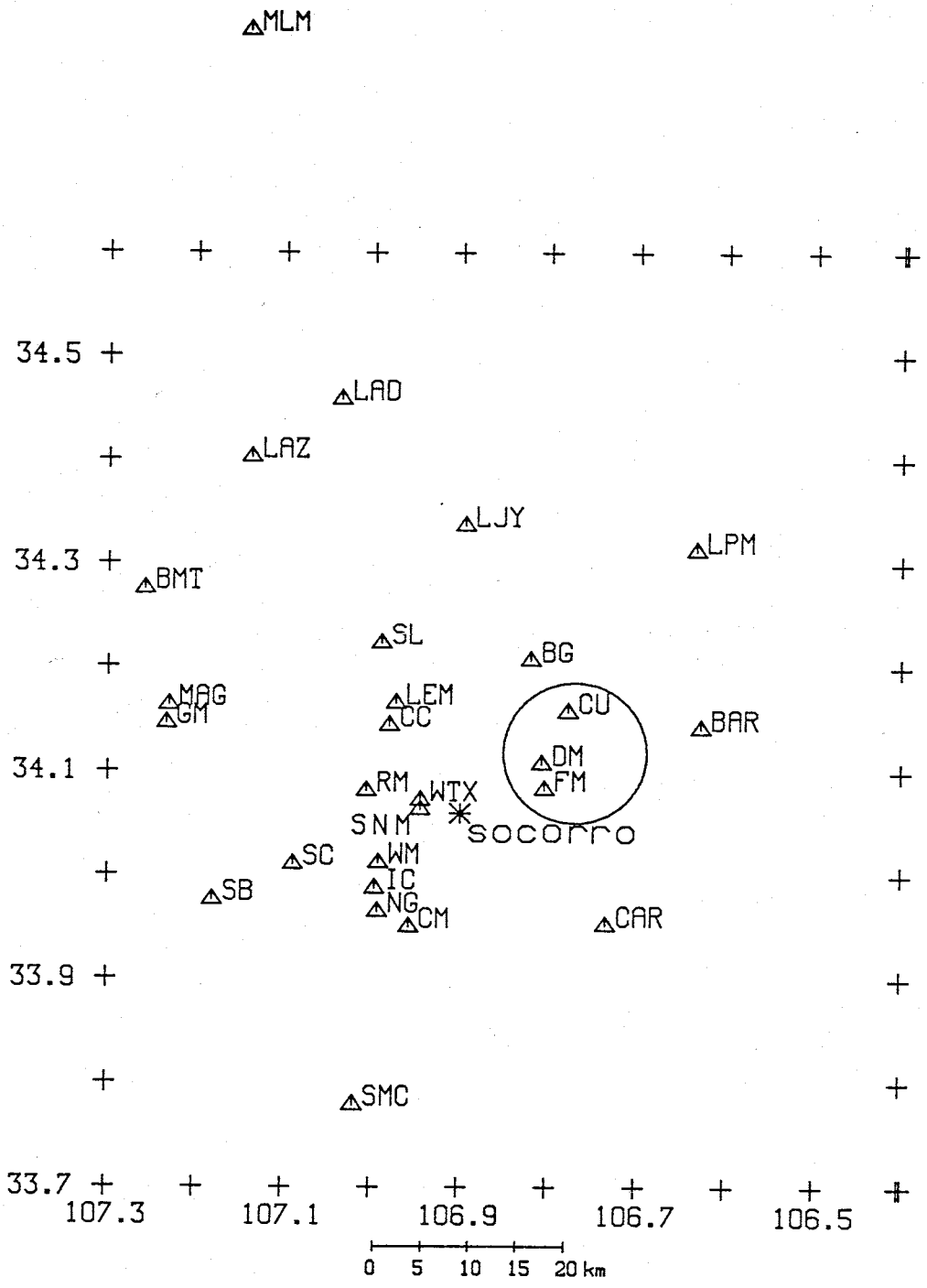

Figure 72: Location of area showing thickened Phanerozoic section. Outside this area normal thicknesses are observed.

above the Precambrian surface representative of its true stratigraphic position.

Eight of the stations in this study, CM, IC, NG, RM, SB, SC, SNM, and WM, lie within or on the boundaries of a series of overlapping cauldrons west and southwest of Socorro. Three of these Oligocene cauldrons, named Socorro, Magdalena, and Sawmill, have been delineated by Osburn and Chapin (1983) (Figure 73), and there is evidence for the existence of several others (Deal and Rhodes, 1976; R. Chamberlin, personal communication). The entire cauldron area is assumed to be underlain by an extensive Tertiary pluton. Accordingly, the depths to basement computed are not to the top of the Precambrian, but rather to the top of this pluton.

Situated toward the center of the Socorro caldera, stations IC, NG, and WM lie in close proximity to one another yet show dramatic differences in depth to basement. NG and WM are 677 m and 719 m above the basement respectively, while IC is 1354 m above basement rock. NG and WM are on moat deposits and are associated with a structural high, while IC, on a thick ash-flow tuff sequence above an inferred resurgent dome (Chapin et al., 1978), is associated with a structural low (R. Chamberlin, personal communication). The ~800 m difference in the basement depth is the simple consequence of NG and WM being on the cauldron rim, while IC is in the caldera itself.

Moving outward from the caldera complex, CM, RM, and SNM (Figure 73) each lie above a thick sequence of Socorro cauldron moat deposits. At RM, near the northern boundary of the Socorro caldera, a thick section of the Popotosa Formation overlies these moat deposits. Accordingly, this station shows the basement to be deeper beneath the surface that at either CM or SNM.

The last two caldera stations are SC and SB. Located near the entrance of South Canyon in the Magdalena Mountains, SC shows the thickest section of

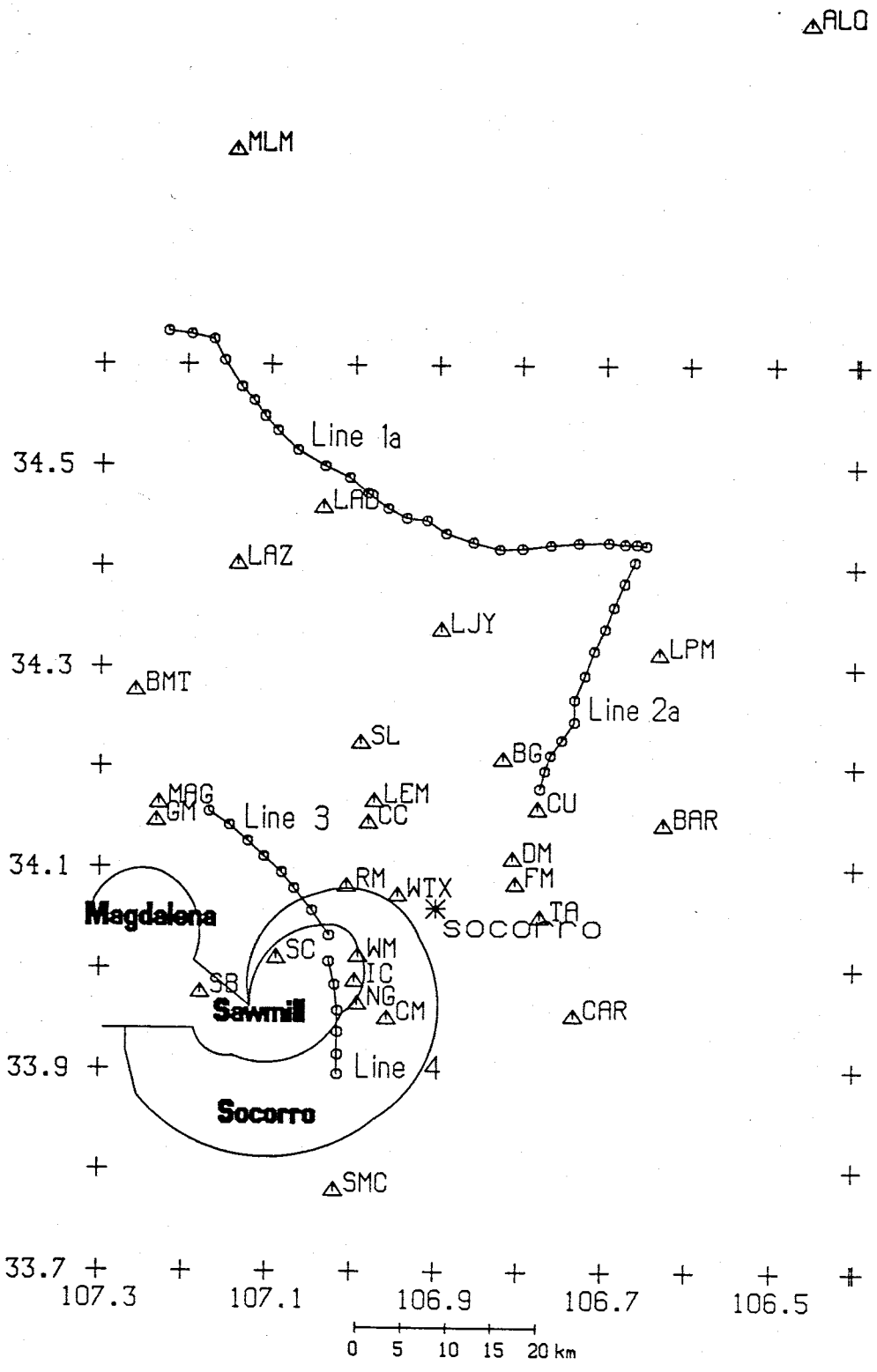

Figure 73: Location of cauldron structures as delineated by Osburn and Chapin (1983) with respect to network station locations.

cauldron ash-flow tuff deposits, over 2 km of Tertiary volcanics. However, lying near the center of both the Sawmill and Socorro cauldrons, this station should have a greater thickness of volcanics beneath it than the other caldera stations. The time term for SB, the most elevated station (over 3 km above sea level), indicates ~1.4 km of volcanic rocks. The thicknesses beneath SC and SB fall within the range of total thickness of Tertiary volcanics as defined by Chapin et al. (1978). Furthermore, the depth of basement beneath South Baldy agrees well with that predicted from the cross-sections of Bowring (1980).

The final three stations used in the Pg study were LAZ, LJY, and MLM. LAZ, on the west side of the Ladron Mountains, is situated just west of the north-south trending Ladron fault. Moving westward from the fault, the Paleozoic thickens to over a kilometer (Chamberlin et al., 1982; Kelley and Woods, 1946). Given the proximity of LAZ to the fault and the depth estimates in the cross-sections of Kelley and Wood (1946), the ~0.6 km depth to the Precambrian basement is quite realistic. Station LJY is located near the axis of the Albuquerque Basin, and overlies a very thick Tertiary sedimentary section. The ~3 km overburden thickness may be an overestimate since unconsolidated sedimentary material generally has a velocity less than 3.4 km/s. The most northerly station is MLM, located on top of Mesa Lucero very near Lucero crater. The thickness of the Phanerozoic, ~2.2 km, is very close to the estimated depth to the Precambrian by Kelley and Wood (1946), whose cross-section passes within a few hundred meters of the station site (Figure 74).

Although decidedly rough, the depth estimates computed from the time-term results appear to be in reasonable agreement with the known geology of the Socorro region. Furthermore, in certain cases, they allow discrimination between conflicting geologic models, or at the very least, give greater credence to a specific interpretation.

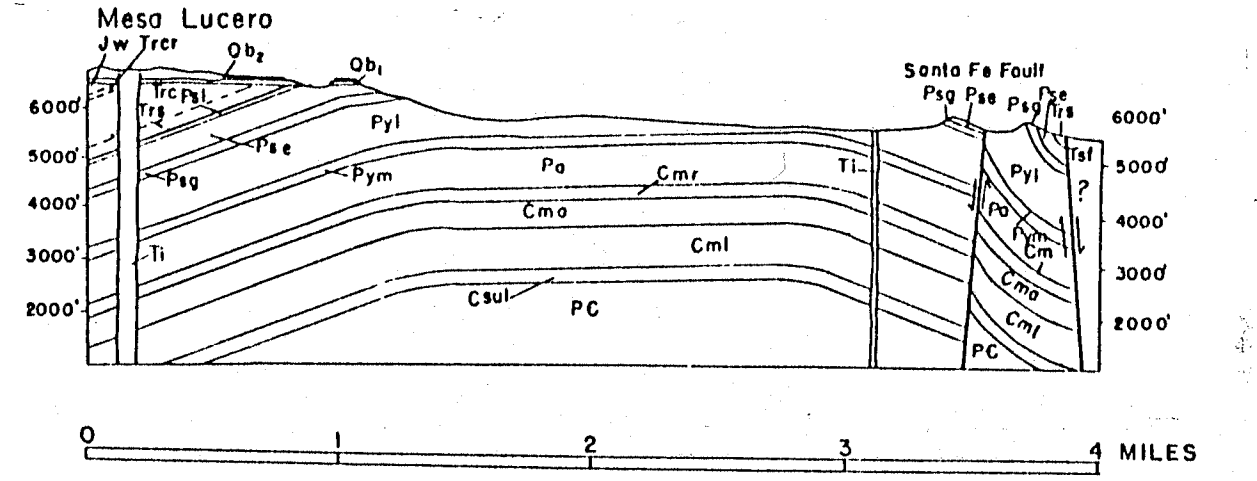

Figure 74: East-west profile of Mesa Lucero area (from Kelley and Wood, 1946). Station MLM is located near the far western edge of profile.

Figures 75 and 76 show the basement surface developed from the 26 time term depth estimates. This surface is topographically very rough and complicated, which is consistent with the complex surface geology of the area.

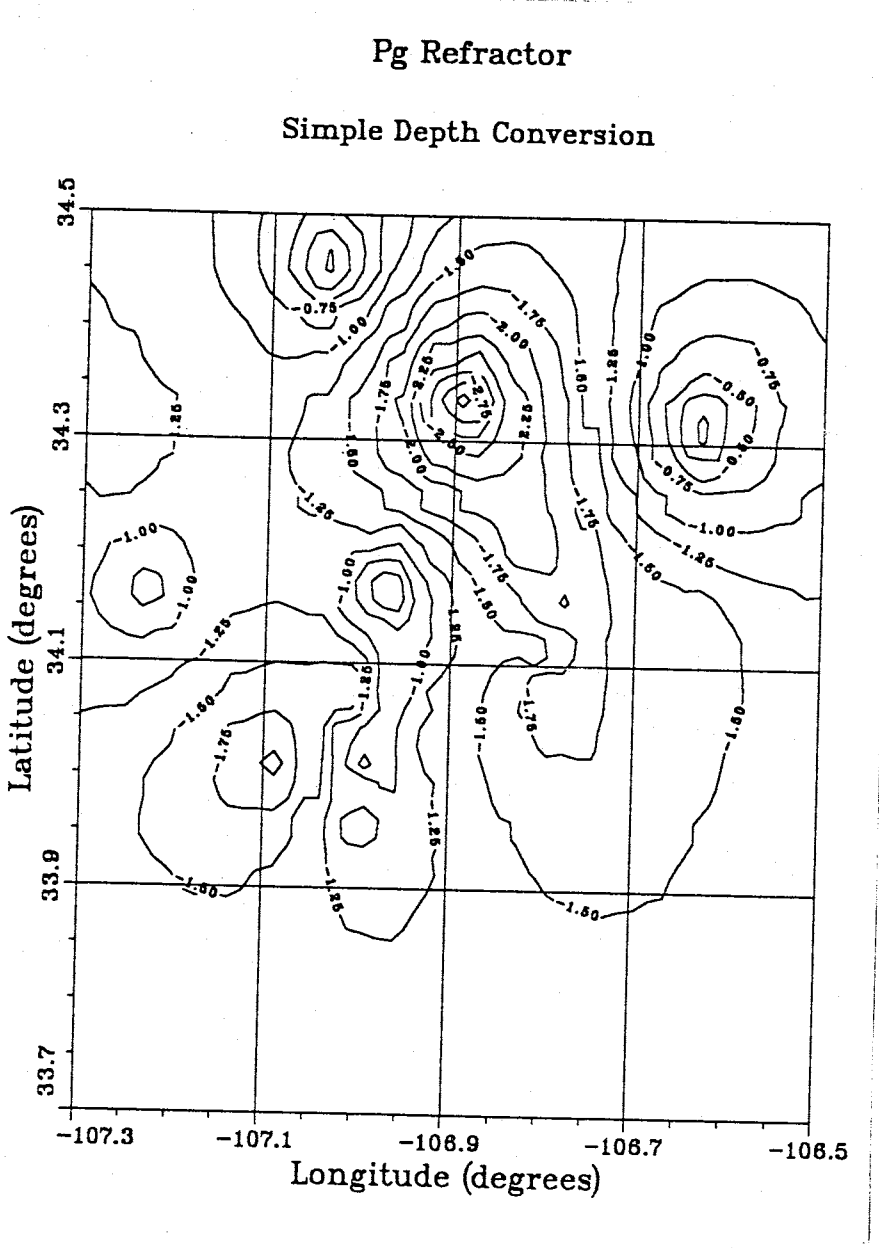

Figure 75: Contour plot of Precambrian surface from kriging of 26 depth-to-basement data. Datum is the topographic surface.

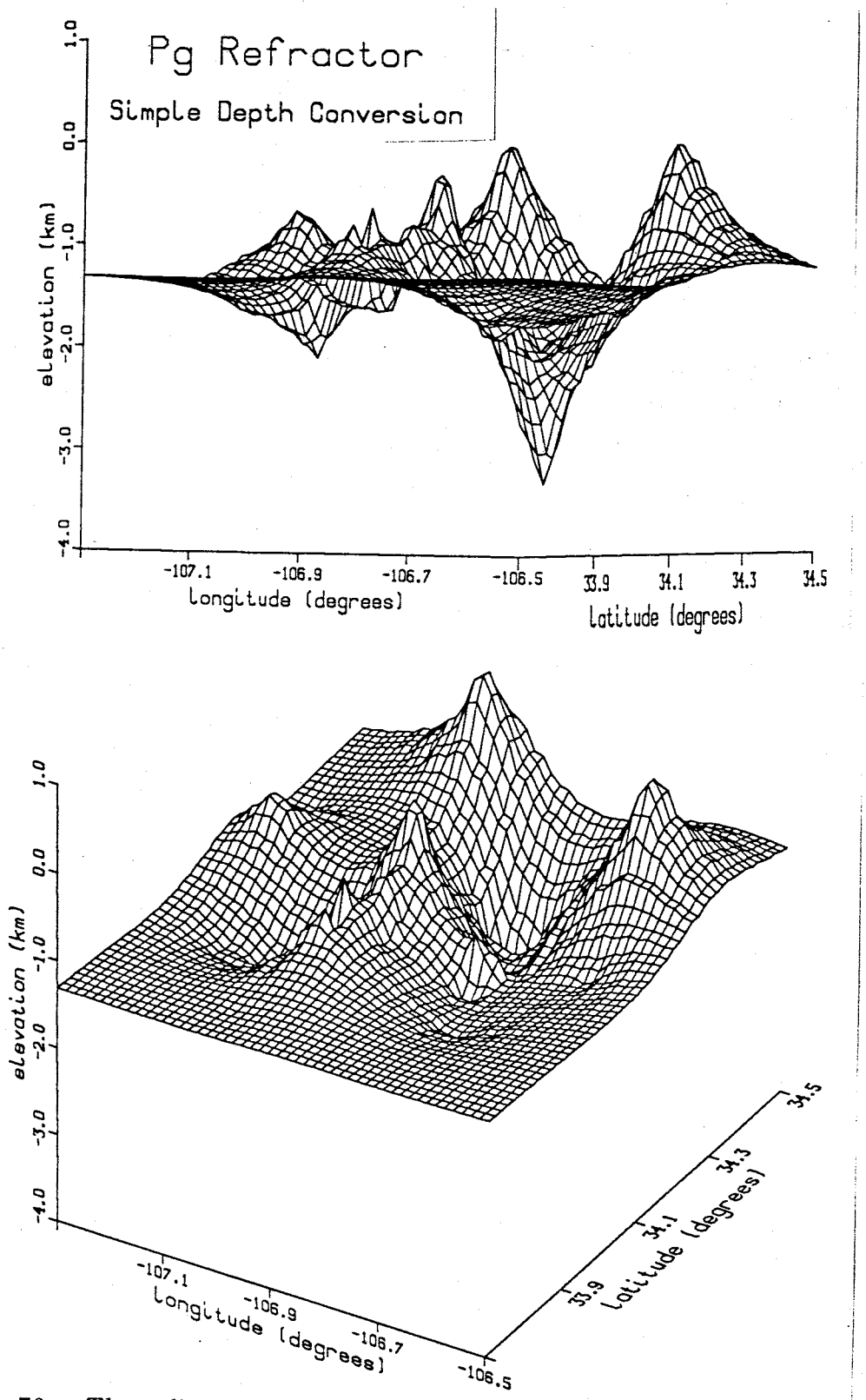

Figure 76: Three-dimensional representation of Precambrian refractor surface from kriging of 26 depth-to-basement data. Two perspectives are presented. Datum is the topographic surface.

P* Time Terms

Because the P* time terms are relative, a strictly independent estimate of the upper crustal thickness cannot be made. However, by utilizing some of the results of previous studies in the region, absolute time terms may be approximated for each station and depth estimates made.

From Rinehart and Sanford (1981), the average depth to the mid-crustal discontinuity beneath Socorro is 19.2 ± 0.6 km. The depth estimates from the Pg time terms allow computation of an average thickness of the Phanerozoic beneath the array. Using the values for all stations and setting any negative time terms to zero, the average thickness of the overburden is found to be 1.1 km. Therefore, the average thickness of the upper crust is 18.1 km in the Socorro area.

Using

$$P^*tt = \left[\frac{z_1}{V_1}\right]\cos(i_1) + \left[\frac{z_2}{V_2}\right]\cos(i_2), \tag{31}$$

and assuming a velocity structure of:

$V_1 = 3.40$ km/s

$V_2 = 5.95$ km/s

$V_3 = 6.40$ km/s,

an average theoretical P* time term of 1.39 seconds is obtained. Subtracting the average relative time term (0.20 s) from each individual P* time term and adding the theoretical average value yields a series of time terms whose average value equals the average theoretical value. Thus, some reasonable approximation of the absolute time term may be realized for each station. A list of these is given in Table 26 and their geographical distribution is shown in Figure 77.

Table 26

P* Time Terms

New Mexico Tech Seismic Network

Station	Time Term (sec)
BAR	1.25 ± 0.19
BMT	1.27 ± 0.42
CAR	1.75 ± 0.12
LAZ	1.24 ± 0.12
LEM	1.70 ± 0.21
LPM	1.13 ± 0.23
MAG	1.26 ± 0.14
MLM	1.55 ± 0.18
SB	1.30 ± 0.17
SMC	1.52 ± 0.12
WTX	1.35 ± 0.57

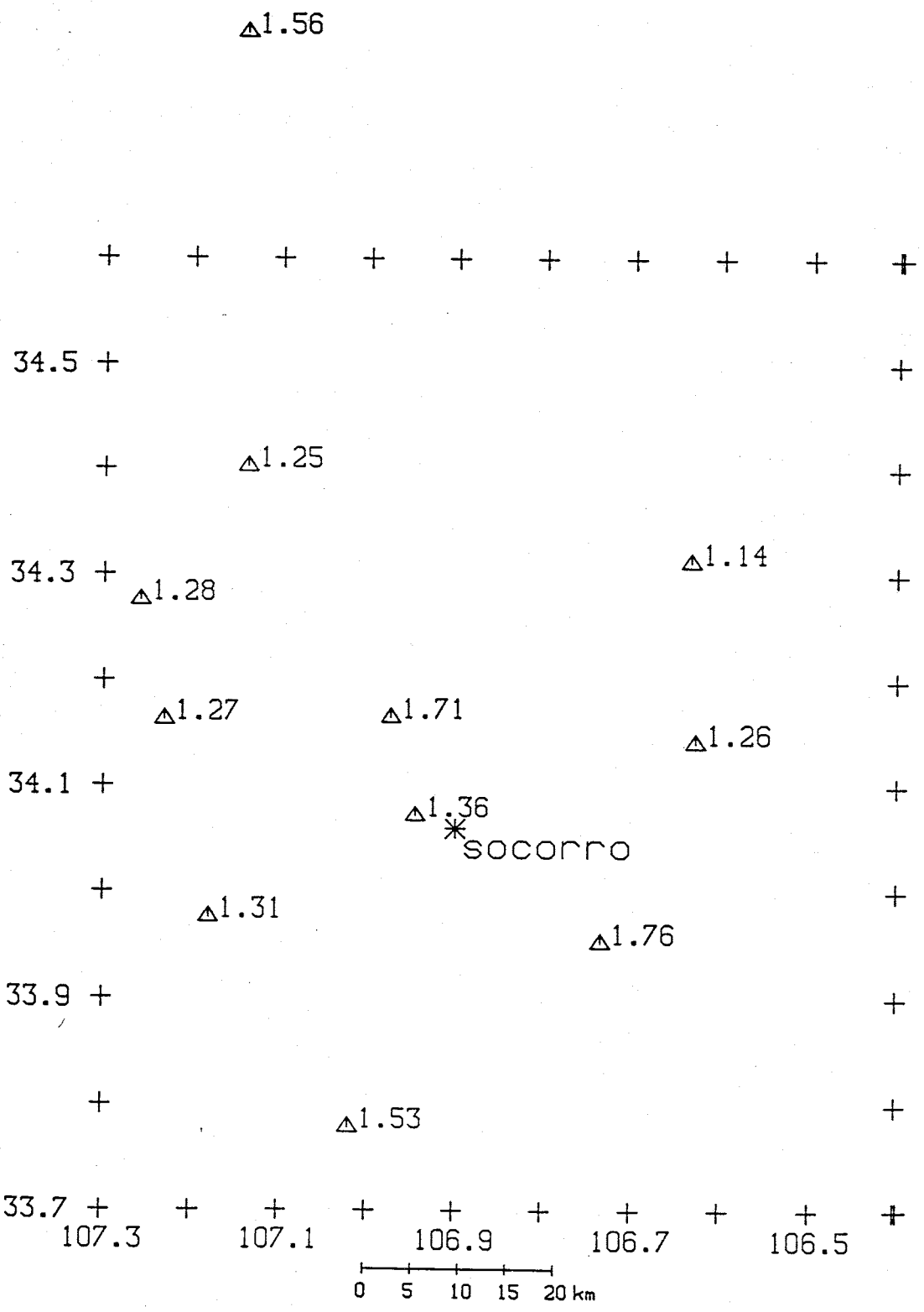

Figure 77: P* time terms from unmodified time-term analysis plotted at their respective station locations.

Using the same velocity structure as given above, depth estimates to the Conrad discontinuity were made from the P* time terms (Table 27; Figure 78). Because of the sparsity and generally less-than-optimum quality of the data, the P* time terms have larger standard errors associated with them than do the time terms of the other refractors. As a result, the uncertainties in the computed depths are often on the order of the depth variations between stations (Table 27).

Comparing the time terms of the various stations though, the time term at LEM appears abnormally large, especially considering the station is located on Precambrian basement. Using strict depth conversion, the estimated depth to the mid-crustal refractor, nearly 30 km, is unreasonable. While the standard error of the LEM time term is ~12 percent, the calculated depth does not overlap the average depth of 19.2 $\pm$ 0.6 km at three standard deviations, and fails to do so by several kilometers. It appears that the unexpectedly large LEM time terms merits additional analysis.

Analysis of the Pg arrivals for LEM indicates that this station is on Precambrian rock of slightly higher than average velocity. Hence, in order to explain the LEM time term, the head waves from the mid-crustal refractor must pass through anomalously low velocity upper crustal material on the way to the station. How slow this velocity would need to be can be computed.

Since LEM is sitting on Precambrian basement, equation (31) can be written:

$$P^{*}tt = \left[\frac{z_2}{V_2}\right]\cos(i_2) = \left[\frac{z_2}{V_2}\right]\left\{1-\left[\frac{V_2}{V_3}\right]^2\right\}^{\frac{1}{2}}. \qquad (32)$$

Table 27

Depth to Mid-Crustal Discontinuity

New Mexico Tech Seismic Network

Station	Depth (km)
BAR	16.682 ± 1.131
BMT	17.757 ± 2.499
CAR	23.881 ± 0.714
LAZ	18.275 ± 0.714
LEM	27.962 ± 1.250
LPM	20.258 ± 1.369
MAG	19.852 ± 0.833
MLM	18.395 ± 1.071
SB	16.738 ± 1.012
SMC	20.542 ± 0.714
WTX	21.055 ± 3.392

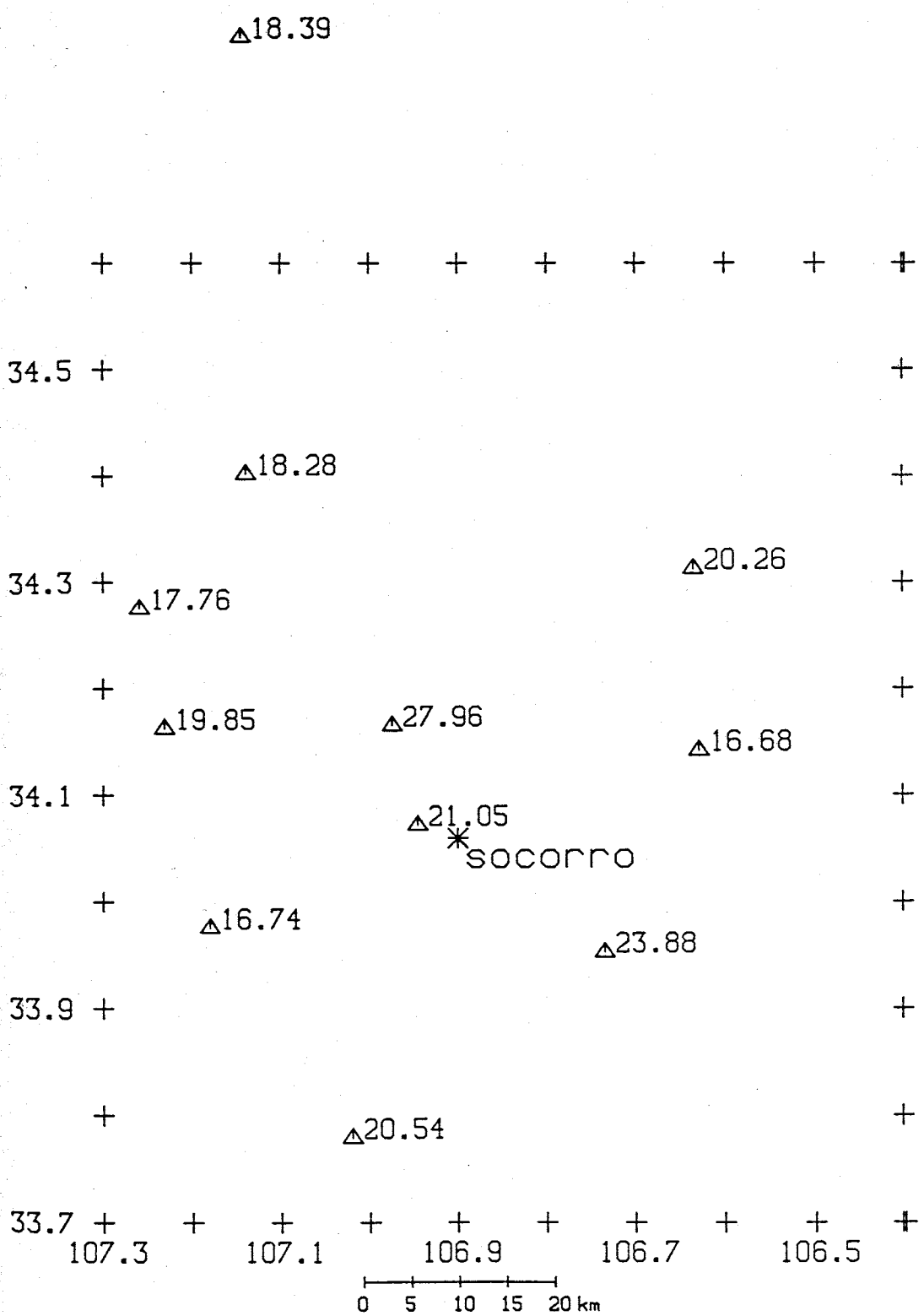

Figure 78: Computed depths to the mid-crustal discontinuity plotted at their respective station locations. The 27.96 km value for station LEM in the center of the figure is due to a highly anomalous time term and does not represent a true depth to the Conrad (see text).

This equation can be solved for the velocity of the upper crust yielding

$$V_2 = \left\{ \frac{(z_2)^2}{(P^*tt)^2 + \left[\frac{z_2}{V_3}\right]^2} \right\}^{\frac{1}{2}}. \qquad (33)$$

Assuming an average depth to the Conrad of 18.1 km and using the LEM time term of 1.70 s, V_2 is 5.49 km/s, an extremely low average value for the upper crust. Subtracting one standard deviation (0.21 s), the P* time term for LEM becomes 1.49 s, and yields a V_2 velocity of 5.66 km/s. Again, this value is low, however, all of the raypaths into LEM pass through areas of low P wave velocity ($<$ 5.7 km/s) as defined by Ward (1980) (Figure 79). In fact, the four arrivals with the highest quality weightings pass through or very close to the 5.45 km/s block, the slowest block in the area. Although the values of Ward (1980) are applicable only to the upper 10 km of the crust, they do indicate an area of significantly reduced velocity with respect to the areas surrounding it.

A third possibility is that only a section of the travel paths to the station is anomalously low in velocity. None of the arrivals into LEM come from the west, and a majority of raypaths pass very near station LJY, which is located near the maximum of the surface uplift as delineated by Larsen et al. (1986) and within the minimum velocity block of Ward (1980). This section of the Socorro region has the highest level of seismicity in the form of earthquake swarms, with some events showing shallow focal depths ($<$ 5 km) and anomalous focal mechanisms (Jarpe, 1984). It is thought that this seismicity may be related to the movement of magma in the upper crust. As such, the large time term at LEM could be caused by the passage of the P* head wave through an area of pure melt.

The minimum travel path through an area of pure melt necessary to explain the LEM time term can be estimated. Assuming an average V_2 velocity of 5.66

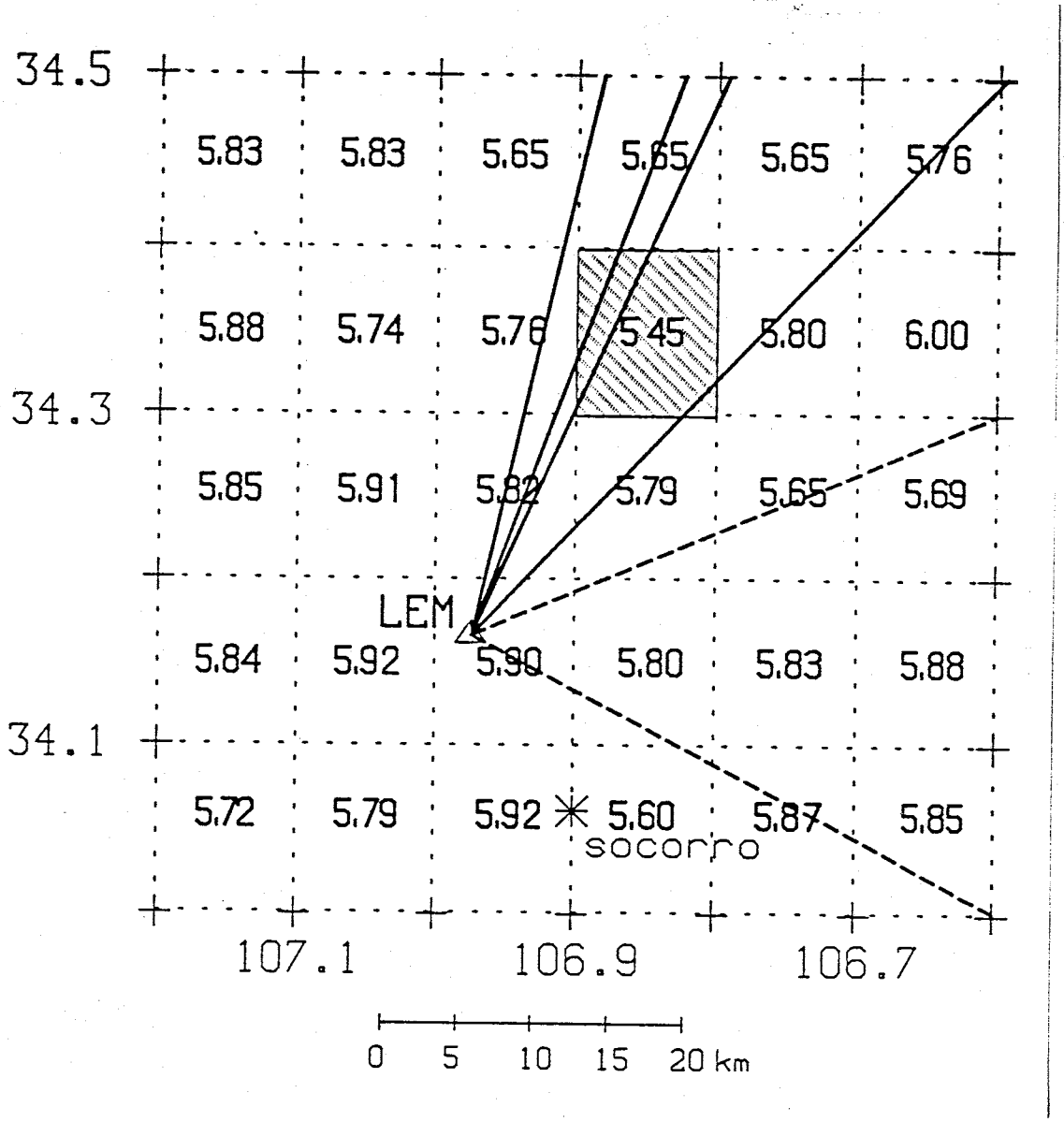

Figure 79: Raypaths into station LEM for the P* data set overlying the block velocities computed by Ward (1980). Notice all the raypaths pass through areas of low velocity (<5.7 km/s) with most travelling through the lowest velocity block in the region (highlighted). Solid lines indicate high quality arrivals; dashed lines are of lower quality.

km/s in this area, and an upper crustal velocity of 5.95 km/s, and a sub-Conrad velocity of 6.4 km/s, the refracted ray travels ~40 km from the point of critical refraction to the surface. Assuming the velocity through a pure melt is approximately one-half the normal P-wave velocity (A. Sanford, personal communication), the travel time through the upper layer may be written:

$$\frac{L}{5.66} = \frac{(L-x)}{5.95} + \frac{x}{(5.95/2)}, \tag{34}$$

where

L = path length through the upper crust

x = path length through pure melt.

Rewriting this equation,

$$x = L\left[\frac{5.95}{5.66} - 1\right], \tag{35}$$

or

$$x = 2.0\ km.$$

That is, given the model, the ray to the station would have to pass through 2 km of total melt to lower the average velocity from 5.95 km/s to 5.66 km/s. This is considered unlikely, although not impossible. If the average crustal velocity in this area were 5.8 km/s though, less than half this value is needed. A low average velocity could be caused by high crustal temperatures, possibly the result of magma intrusion.

Assuming that the LEM time term is a reasonable number, the rays to the station must pass through low velocity crustal material. Whether or not the region has a low crustal velocity overall, or there are magma intrusions present in the upper crust, or some combination thereof, cannot be determined. However, further study of this highly anomalous area seems to be in order.

Returning to the P* time terms as a group, a surface was developed from the P* depth estimates (Figures 80, 81). This modelled surface though, is not considered reliable since it is based on only ten data, several of which have large uncertainties associated with them. Moreover, this surface is dominated by the anomalously large value at LEM. Another surface was estimated without the LEM datum, but obviously also suffers from a lack of data (Figures 82, 83). In order to achieve a reasonable approximation to the refractor topography, other data must be acquired.

Figure 31 shows the positions of the COCORP reflection lines within the Socorro area. Using the COCORP sections processed by Cornell University in June 1988, the best picks to the base of the Phanerozoic and the top of the Conrad were made for lines 1a, 2a, and 3. Using these times, the thickness of the Phanerozoic and the upper crust were estimated.. These values were then added to increase the size and coverage of the refraction data set. Similarly, the depth data of Rinehart and Sanford (1981) from the inversion of microearthquake S-wave reflections was added. Thus, the data set from which the Conrad surface was to be estimated, was increased from nine to thirty-seven total data.

Figures 84 and 85 show the kriged surface from this larger data set, which differs noticeably from that obtained using only the time term data. This new surface dips to the northeast as well as to the southeast. The northern dip was previously noted (Sanford et al., 1973; Rinehart and Sanford, 1981), but not the southeast dip. This southeastern slope may explain the nearly total absence of reflected phases from the mid-crustal magma body at stations BAR and CAR (A. Sanford and J. Ake, personal communication). In addition, the large upper crustal thickness at CAR falls very close to a large gravity low (Figure 86). Since CAR shows no Phanerozoic anomalies, the gravity low must be more deeply seated, and is probably related to a thickening of the upper crust in this

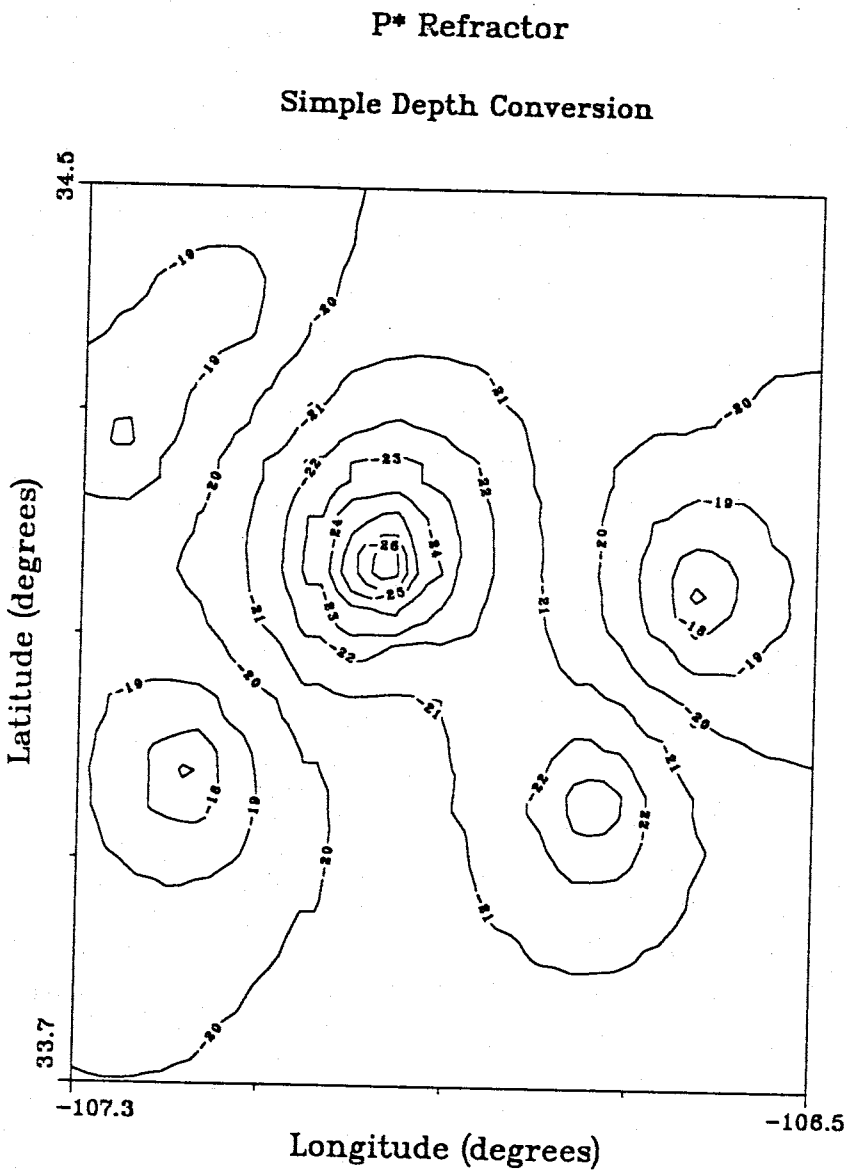

Figure 80: Contour plot of mid-crustal refractor surface from kriging of 10 mid-crustal depth data. The anomalous LEM value is included in the data set. Datum is the topographic surface.

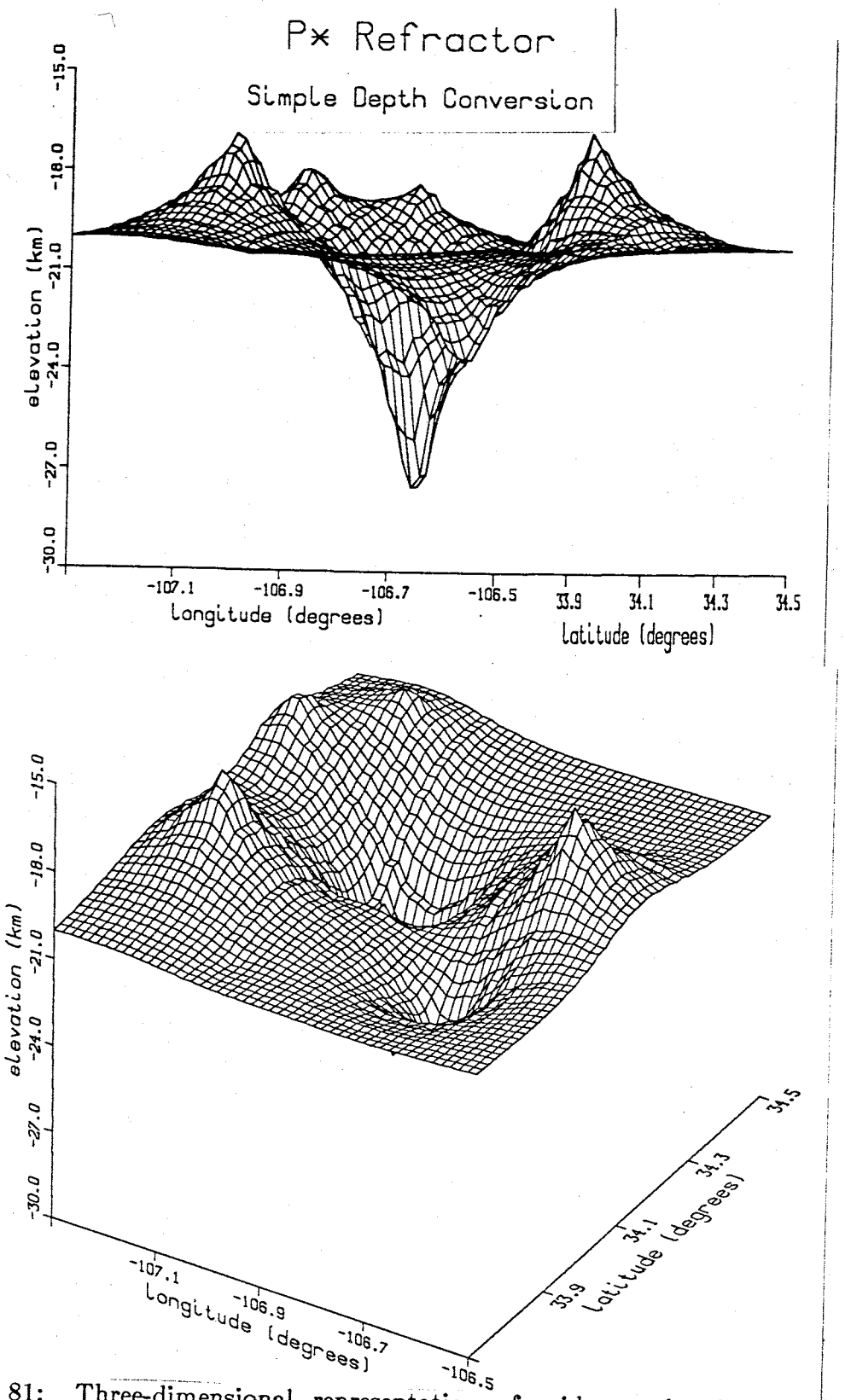

Figure 81: Three-dimensional representation of mid-crustal refractor surface from kriging of 10 mid-crustal depth data, including the anomalous LEM value. Two perspectives are presented. Datum is the topographic surface.

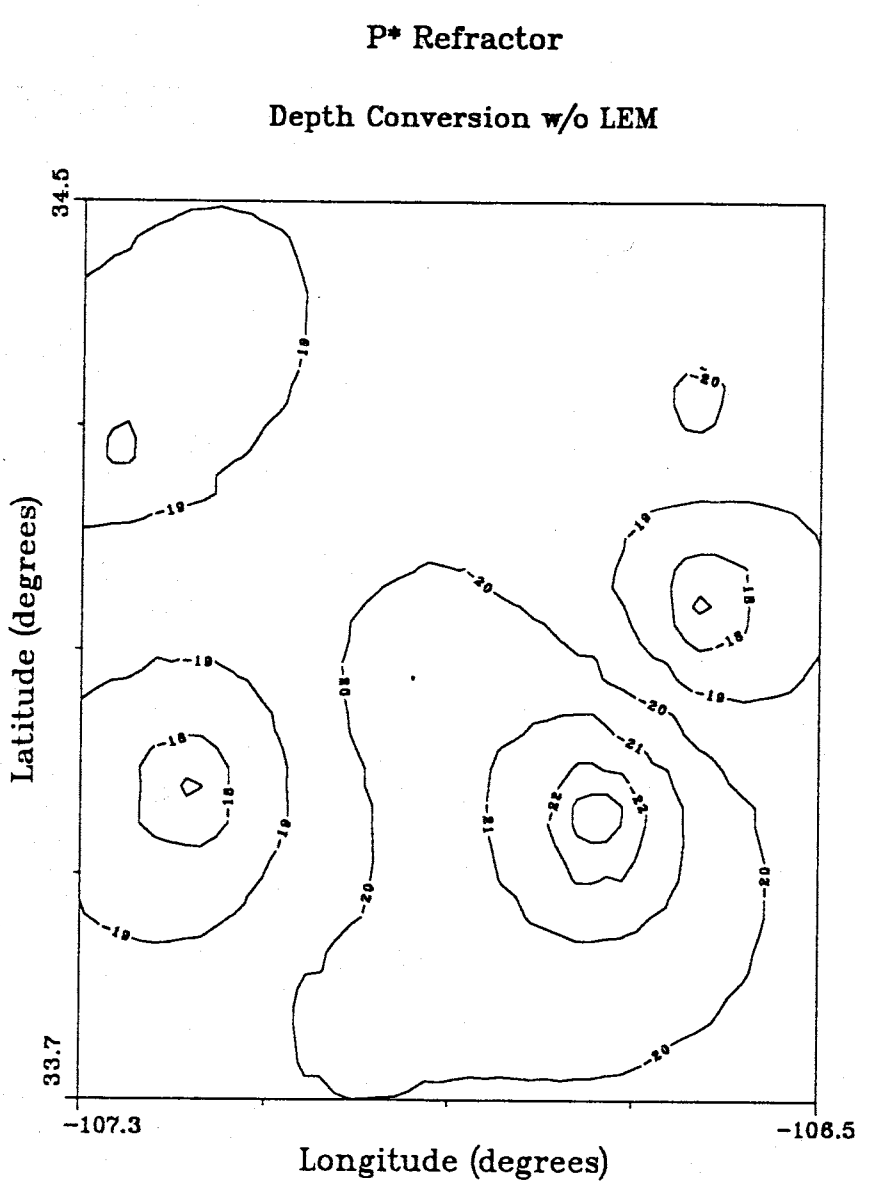

Figure 82: Contour plot of mid-crustal refractor surface from kriging of 9 mid-crustal depth data. The anomalous LEM value was excluded from the data set. Datum is the topographic surface.

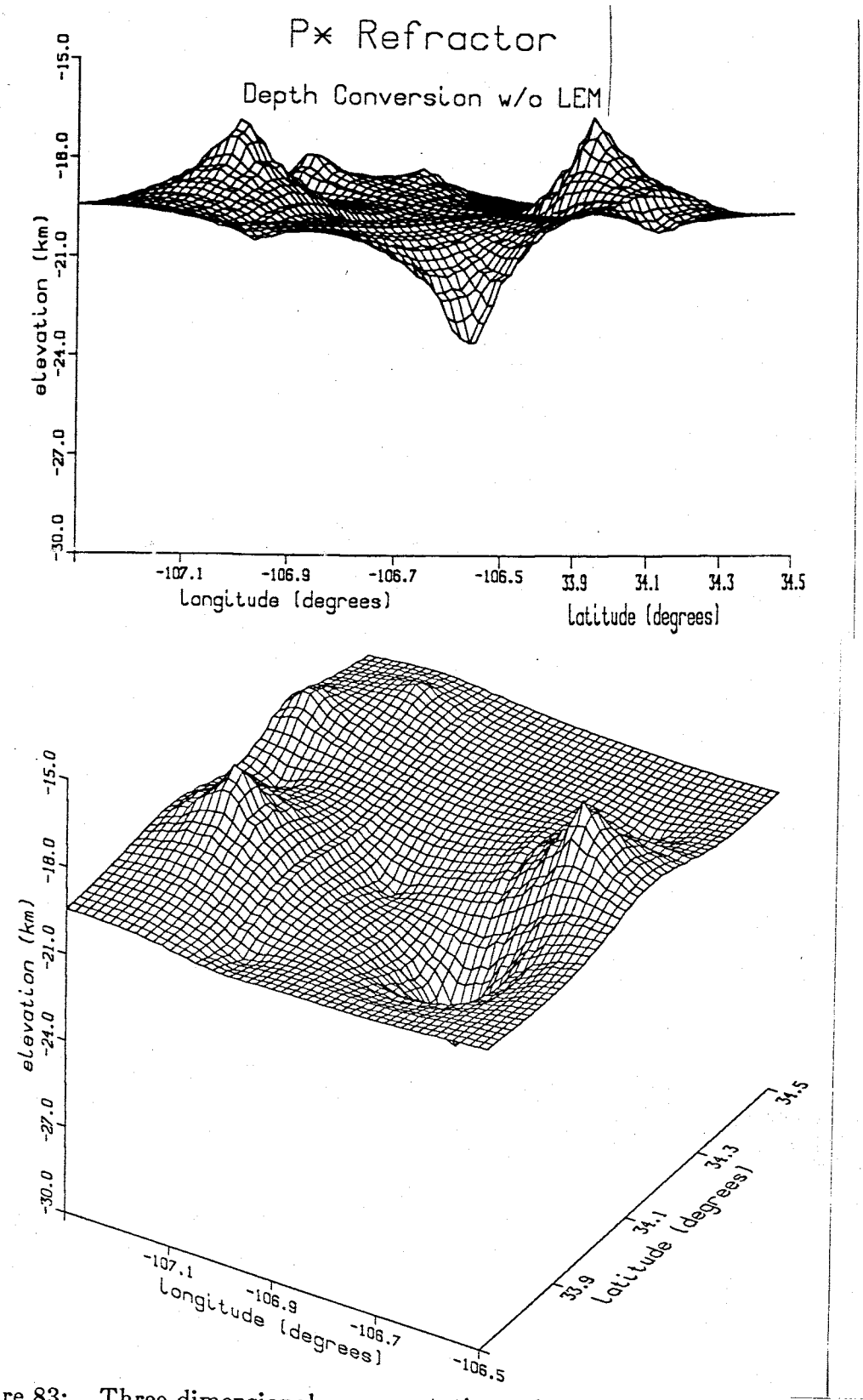

Figure 83: Three-dimensional representation of mid-crustal refractor surface from kriging of 9 mid-crustal depth data. The anomalous LEM value was excluded from the data set. Two perspectives are presented. Datum is the topographic surface.

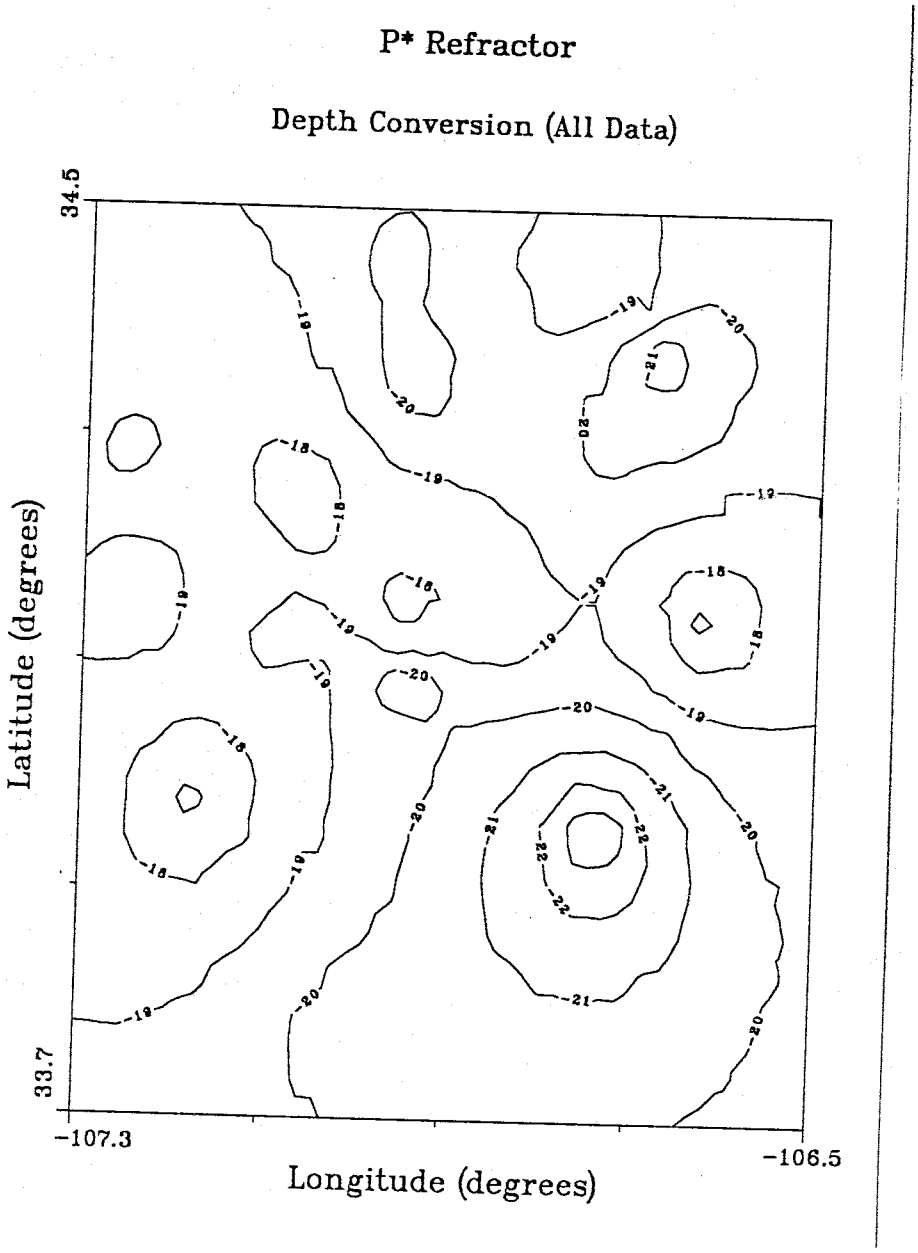

Figure 84: Contour plot of mid-crustal refractor surface from kriging of 9 time-term depth data and 28 additional depth data from COCORP profiles and Rinehart and Sanford (1981). The anomalous LEM value was excluded from the data set. Datum is the topographic surface.

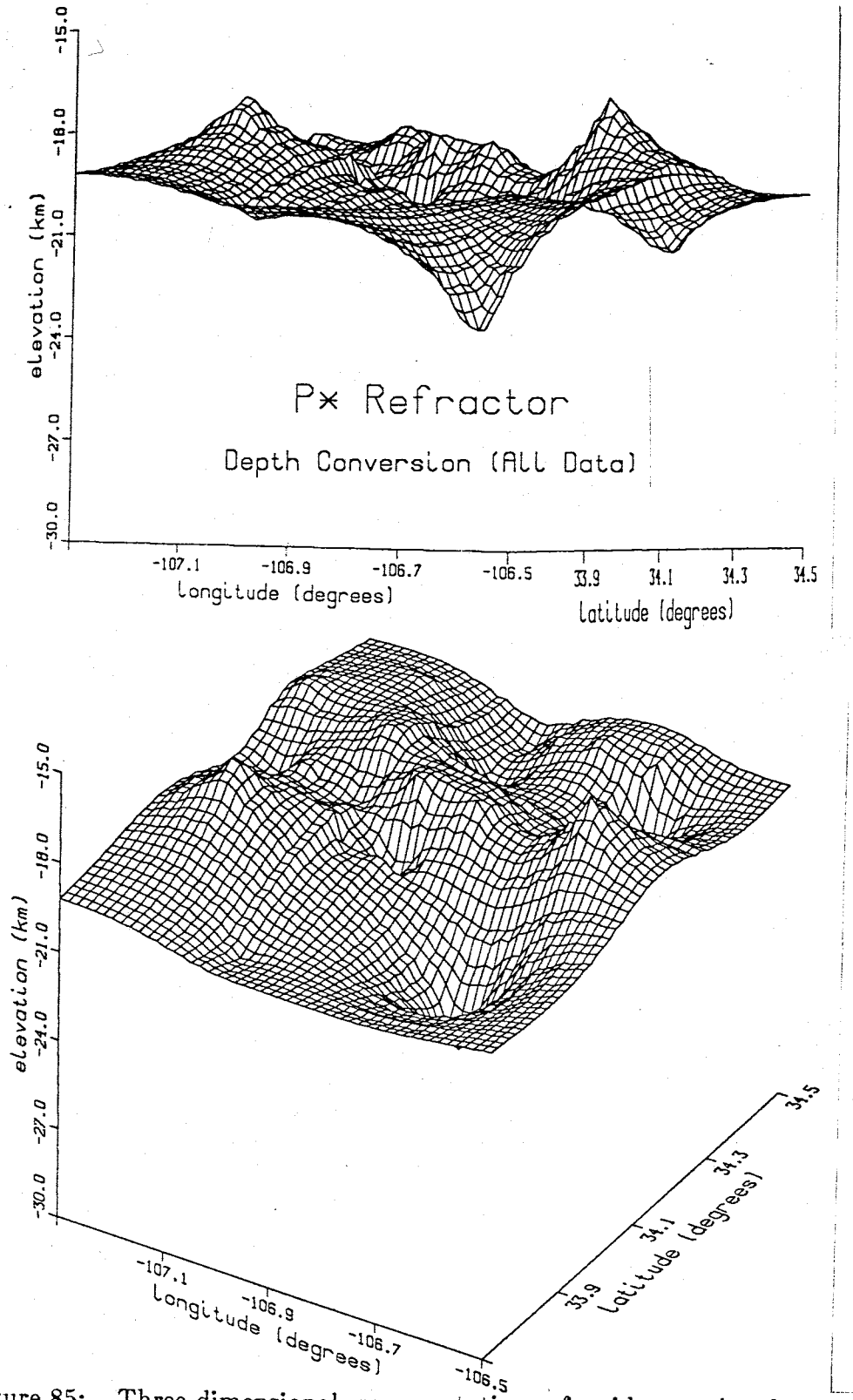

Figure 85: Three-dimensional representation of mid-crustal refractor surface from kriging of 9 mid-crustal depth data and 28 additional depth data from COCORP profiles and Rinehart and Sanford (1981). The anomalous LEM value was excluded from the data set. Two perspectives are presented. Datum is the topographic surface.

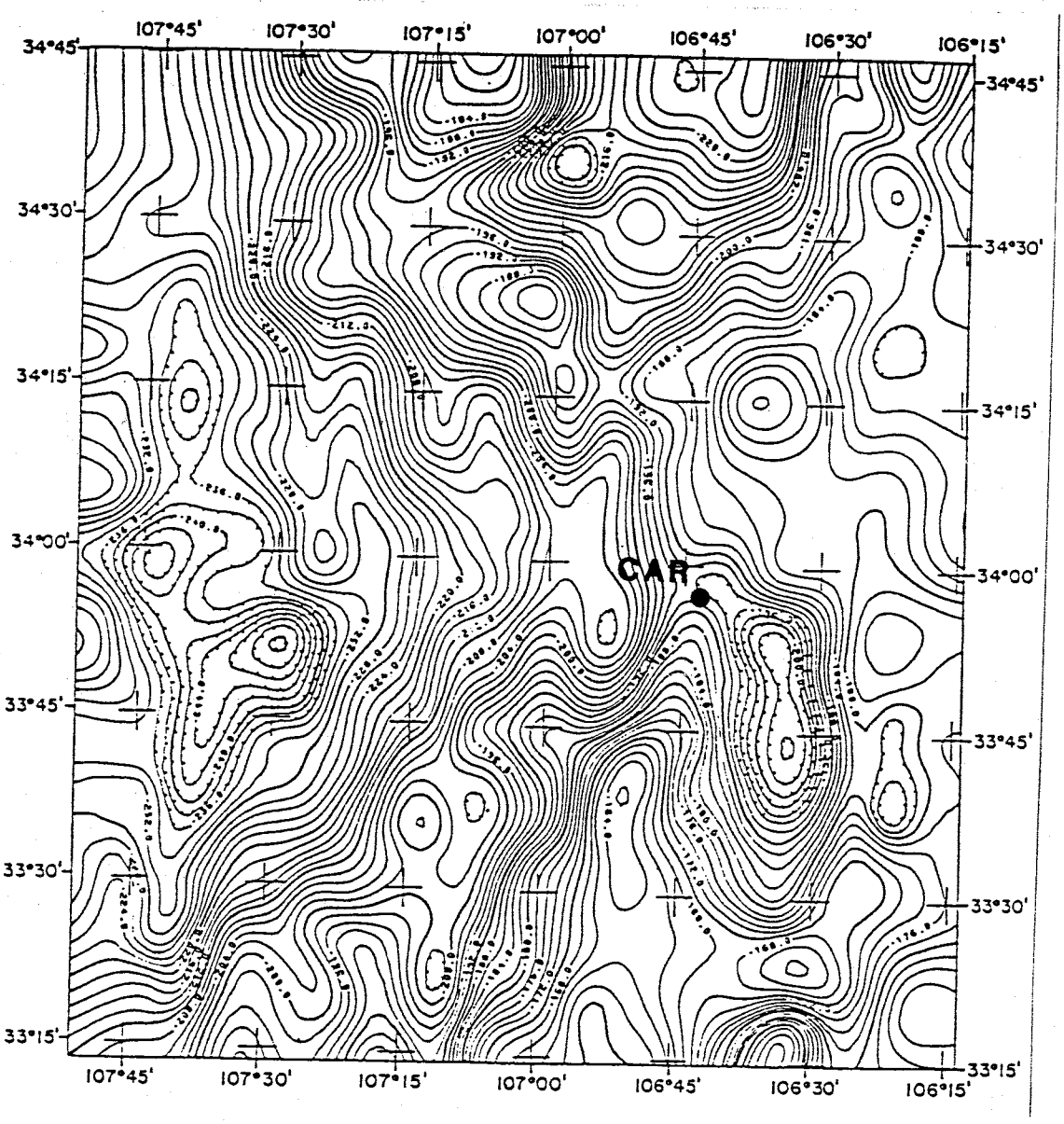

Figure 86: Gravity map of Socorro county (from Cordell, 1983). Station CAR is located northwest of a large gravity low.

area.

The question may arise whether the southeast dip so evident in the kriged surface is not the result of an anomalous value at station CAR. In order to test this hypothesis, a new surface was kriged removing the CAR datum from the data set. Figures 87 and 88 show the results. While the direction of the dip changes to the south and is decreased somewhat, the general trend of the surface remains the same. Thus, the southeast dip indicated is not the result of an anomalous point, but appears to be real.

In summary, while of themselves the refraction results are not conclusive, combined with the results of other geophysical studies, a working model of the mid-crustal layer has been developed. This model agrees with existing knowledge by displaying a dip to the northeast in the northern half of the area, and proposes additional complexity by introducing a southeasterly dip in the southwest quadrant of the area.

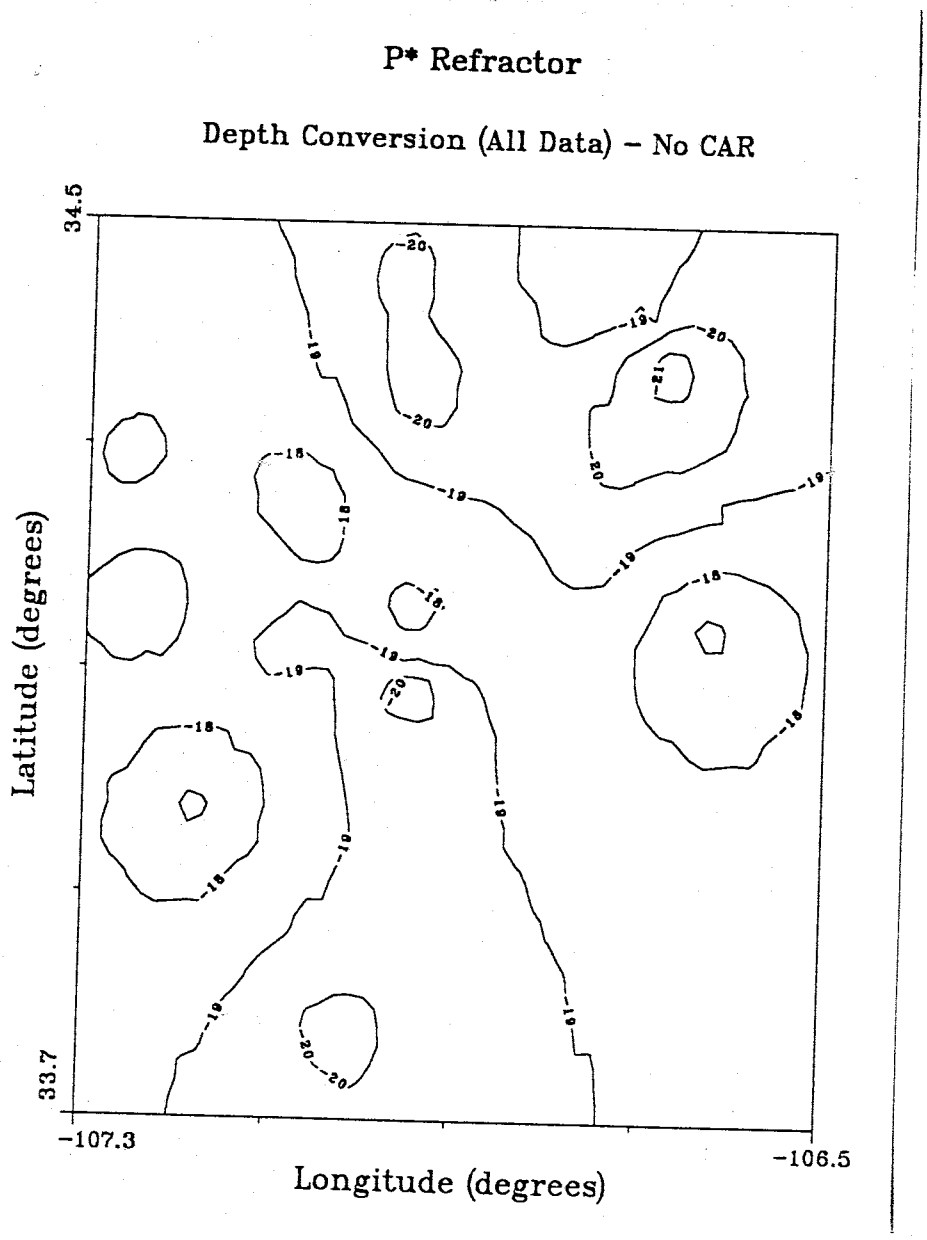

Figure 87: Contour plot of mid-crustal refractor surface from kriging of 8 time-term depth data and 28 additional depth data from COCORP profiles and Rinehart and Sanford (1981). The LEM and CAR value were excluded from the data set. Although the direction and degree of dip change somewhat in the southern part of the region, the overall surface is not affected. Hence, CAR is not an anomalous point. Datum is the topographic surface.

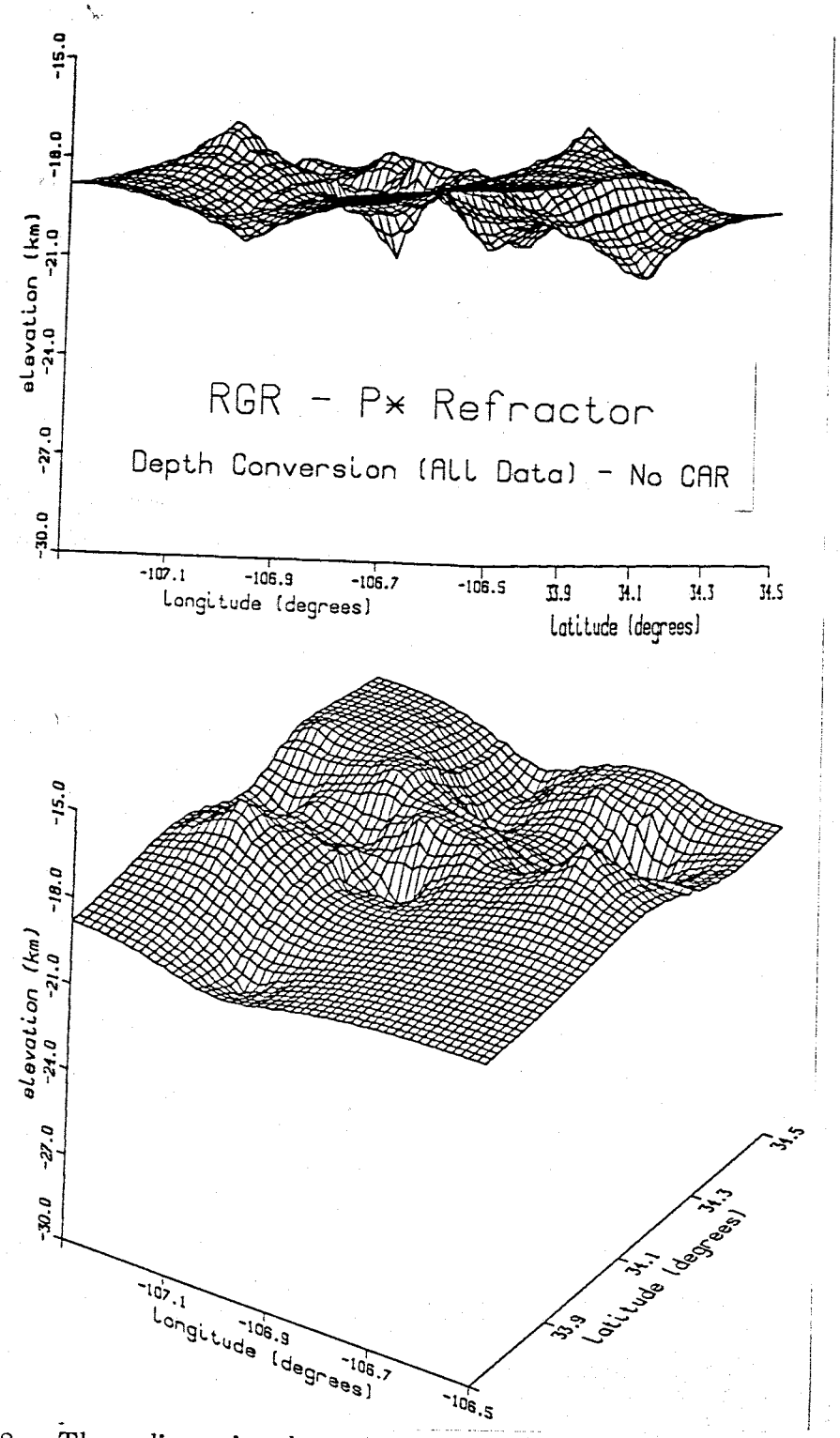

Figure 88: Three-dimensional representation of mid-crustal refractor surface from kriging of 8 time-term depth data and 28 additional depth data from COCORP profiles and Rinehart and Sanford (1981). The LEM and CAR values were excluded from the data set. Although the direction and degree of dip change somewhat in the southern part of the region, the overall surface is not affected. Hence, CAR is not an anomalous point. Datum is the topographic surface.

Pn Time Terms

As was the case with the P* time terms, the Pn time terms are relative and independent depth estimates cannot be made. However, the overlap of five stations of this study with those from the work done by Murdock and Jaksha (1981) allows absolute time terms to be approximated (Table 28).

First, the average of the five relative time terms of this study (0.14) was subtracted from the average of the five absolute time terms (3.77) from the study of Murdock and Jaksha (1981). Then, this difference was added to all of the relative time terms, converting them to absolute time terms. The absolute time terms from this work all fall within one standard deviation of their counterparts in results of Murdock and Jaksha (1981). The absolute time-term values for all the Pn stations are listed in Table 29 (Figure 89).

These time terms were depth converted using a velocity structure of:

$V_1 = 3.40$ km/s

$V_2 = 6.20$ km/s

$V_3 = 8.14$ km/s,

the V_1 velocity being the average crustal velocity of Phanerozoic rocks, the V_2 the average of upper and lower crustal velocities obtained by Toppozada and Sanford (1976). The estimated crustal thicknesses are listed in Table 30 and their distribution shown in Figure 90. Adjacent stations show similar depths to the Moho and these values are consistent and credible. Furthermore, the overall variation in the depths is quite smooth and define a northwest dipping Moho. Thus, the estimates of crustal thickness are all in good agreement with one another and seem appropriate for the area. The estimates of crustal thickness from this study have an advantage over many others in that the effects of the highly variable Phanerozoic are well quantified by the Pg time terms, and

Table 28

Pn Time Term Conversion

Relative to Absolute

Station	Relative Time Term *(This Study)*	Absolute Time Term *(Murdock & Jaksha)*	Absolute Time Term *(This Study)*
ALQ	0.24±0.09	3.75±0.23	3.87±0.09
LAD	0.04±0.14	3.98±0.23	3.67±0.14
LPM	–0.06±0.07	3.42±0.24	3.57±0.07
MLM	0.51±0.08	3.94±0.22	4.14±0.08
WTX	0.00±0.06	3.77±0.29	3.63±0.06

Table 29

Pn Time Terms

Station	Time Term (sec)
ALQ (USGS)	3.87 ± 0.09
BAR	3.58 ± 0.06
BMT	3.91 ± 0.08
CAR	3.45 ± 0.06
CC	3.59 ± 0.07
CM	3.47 ± 0.07
DM	3.50 ± 0.07
GM	3.70 ± 0.07
IC	3.64 ± 0.11
LAD	3.67 ± 0.14
LAZ	3.82 ± 0.06
LEM	3.67 ± 0.07
LJY	4.15 ± 0.14
LPM	3.57 ± 0.07
MAG	3.71 ± 0.07
MLM	4.14 ± 0.08
NG	3.62 ± 0.09
SB	3.87 ± 0.07
SC	3.67 ± 0.07
SMC	3.60 ± 0.06
SNM	3.88 ± 0.18
TA	3.39 ± 0.15
WTX	3.63 ± 0.06

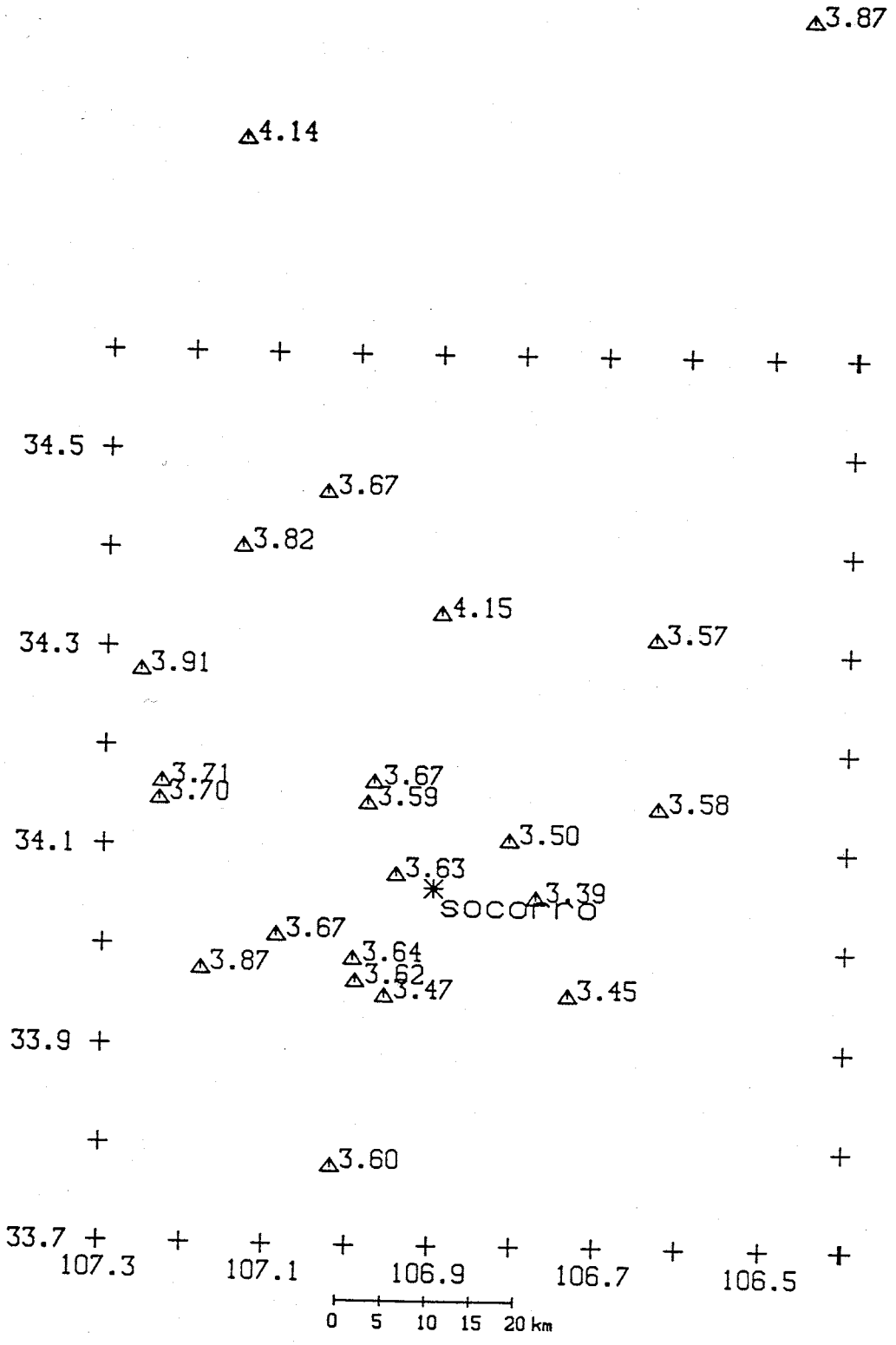

Figure 89: Pn time terms from unmodified time-term analysis plotted at their respective station locations.

Table 30

Depth to M Discontinuity

Station	Depth (km)
ALQ	37.030 ± 0.558
BAR	32.482 ± 0.372
BMT	36.020 ± 0.496
CAR	30.795 ± 0.372
CC	33.401 ± 0.434
CM	31.683 ± 0.434
DM	31.844 ± 0.434
GM	34.643 ± 0.434
IC	32.803 ± 0.682
LAD	35.876 ± 0.868
LAZ	35.665 ± 0.372
LEM	35.369 ± 0.434
LJY	35.278 ± 0.868
LPM	35.172 ± 0.434
MAG	35.246 ± 0.434
MLM	36.258 ± 0.496
NG	33.625 ± 0.558
SB	34.877 ± 0.434
SC	32.078 ± 0.434
SMC	32.421 ± 0.372
SNM	35.353 ± 1.116
TA	31.171 ± 0.930
WTX	34.354 ± 0.372

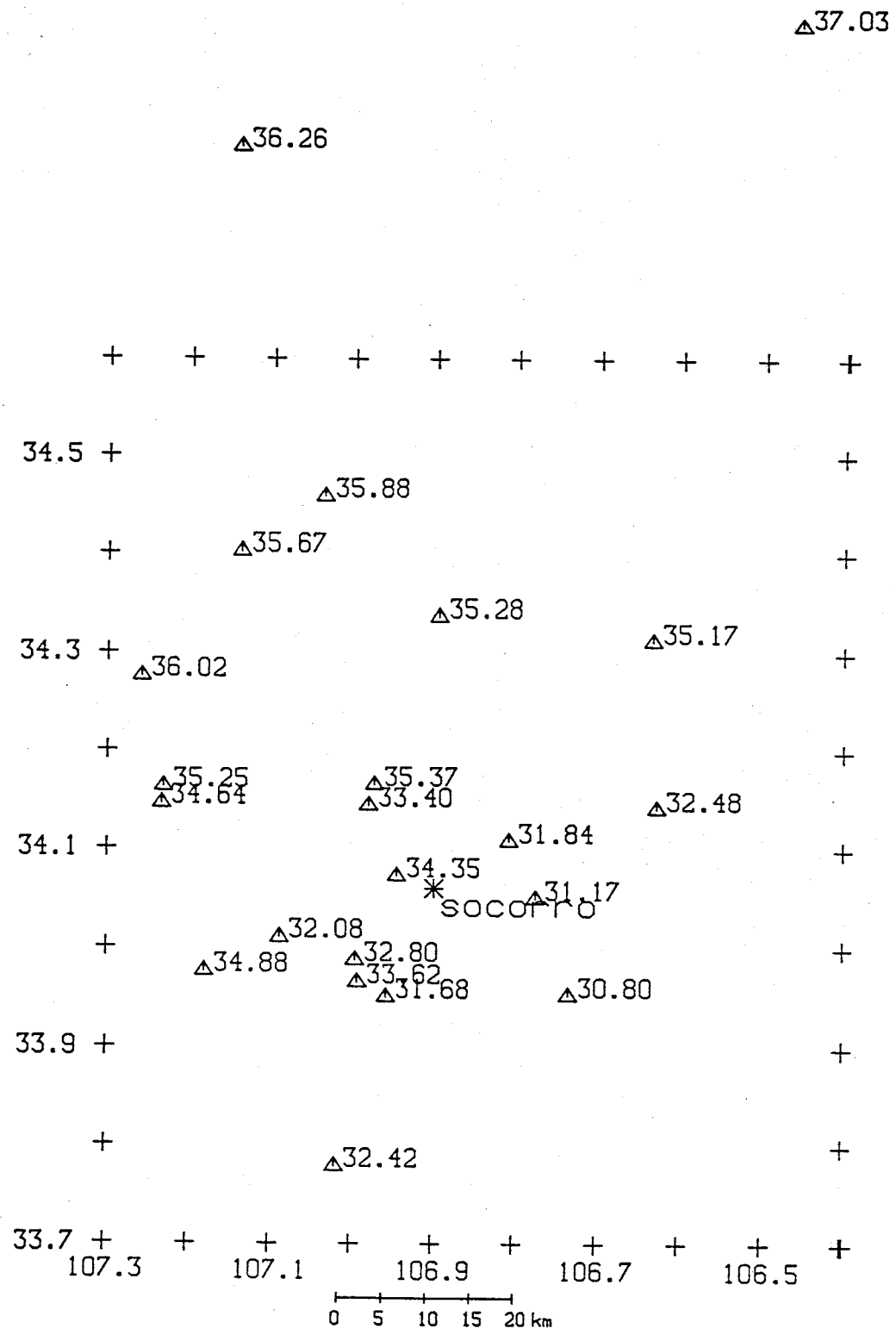

Figure 90: Computed depths to the Moho discontinuity plotted at their respective station locations. The depths show a general increase to the northwest.

therefore can be compensated for. Two stations though, TA and ALQ, did not have Pg time terms and so were assigned values of 0.20 and 0.00 respectively. TA is situated on approximately 900 meters of Permian and Pennsylvanian strata, and was assigned a time term appropriate to this thickness. ALQ, lying on Precambrian basement rock, has no intervening Phanerozoic, so a zero time term was assigned. The resulting depth estimates for these stations appear quite appropriate.

The crustal thicknesses estimated in this work are comparable to previously reported values for the central Rio Grande rift. The estimates at LAD, LAZ, and LPM are virtually identical to those from the COCORP profiles made by Brown et al. (1980). Also, estimates at three other station locations, ALQ, MLM, and WTX, are in good agreement with one another, although there are slight discrepancies between studies (Figures 91, 92, 93). These discrepancies are the result of differing assumptions concerning the average crustal velocity beneath each station, unaccommodated Phanerozoic effects, and the likely influence of non-rift structures in some of the studies. Nevertheless, the relative differences between these studies are minor.

The final comparison is with the generalized model of the Rio Grande rift proposed by Olsen et al. (1979). Their model proposed an average crustal thickness of 33.7 km, which may be appropriate to the area east and south of Socorro, but is several kilometers thinner than indicated at points to the north. Accordingly, its application as a general rift model does not seem appropriate.

As is evident from the modelled surface (Figures 94, 95), the crust-mantle boundary in this area seems fairly simple. The refracting layer shows a consistent dip to the northwest with little other complexity. Crustal effects appear to be small. First, if crustal effects were large, a much more disturbed model

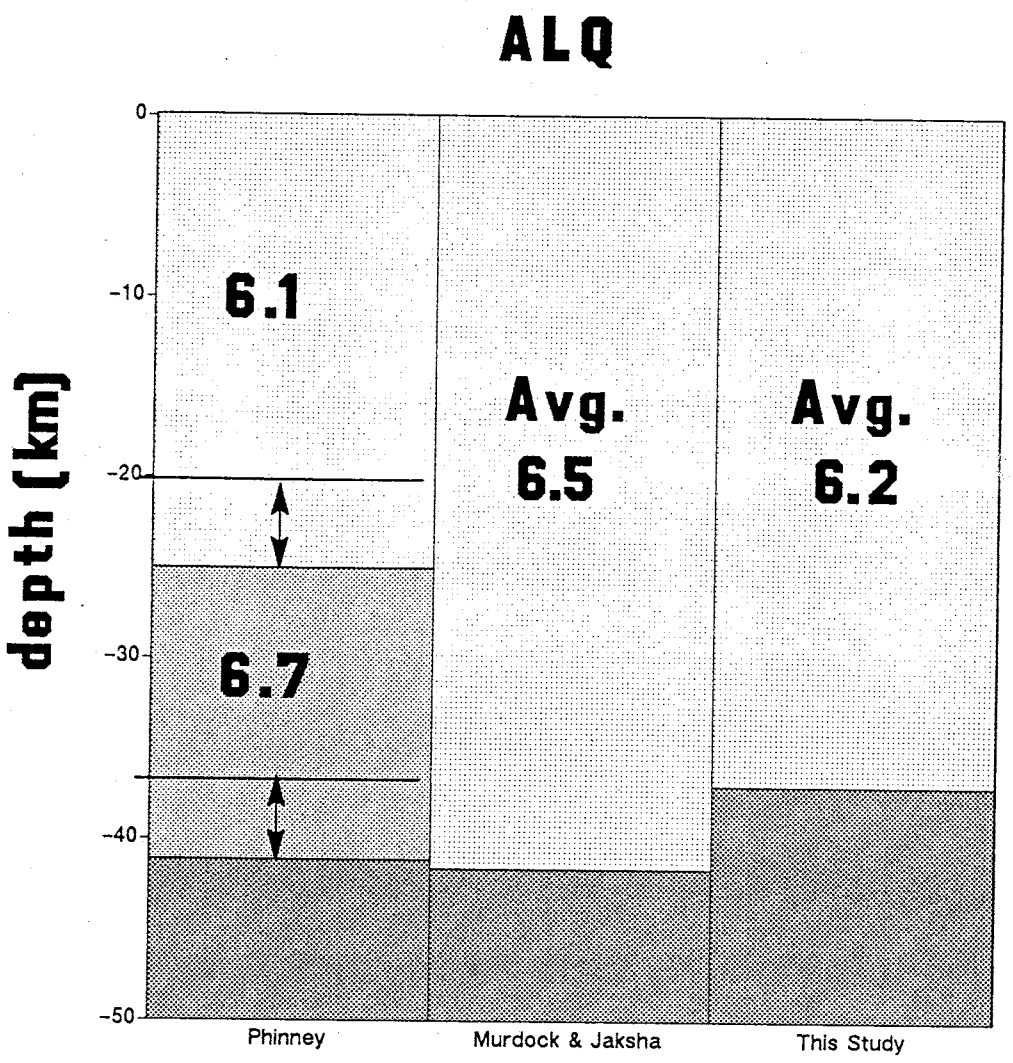

Figure 91: Crustal models at station ALQ.

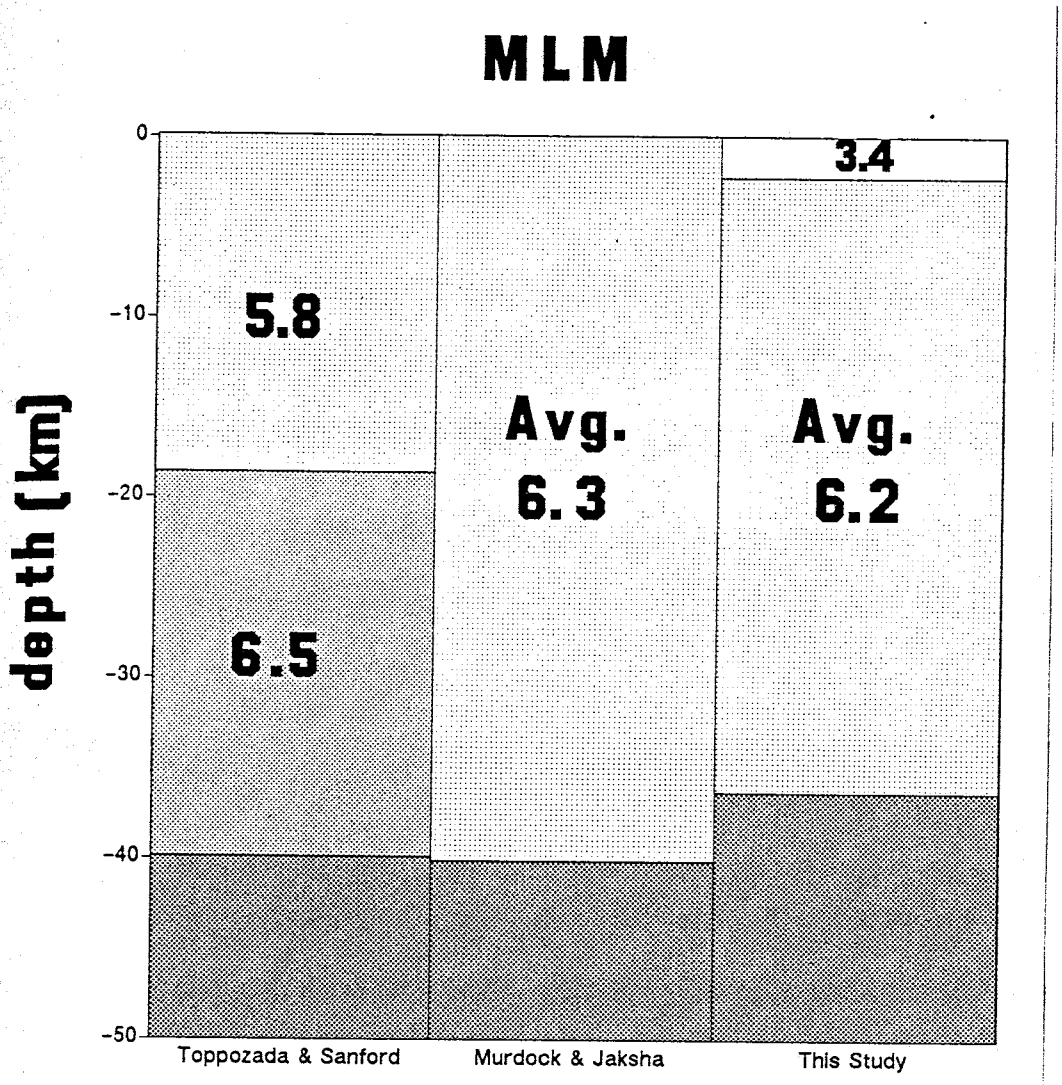

Figure 92: Crustal models at station MLM.

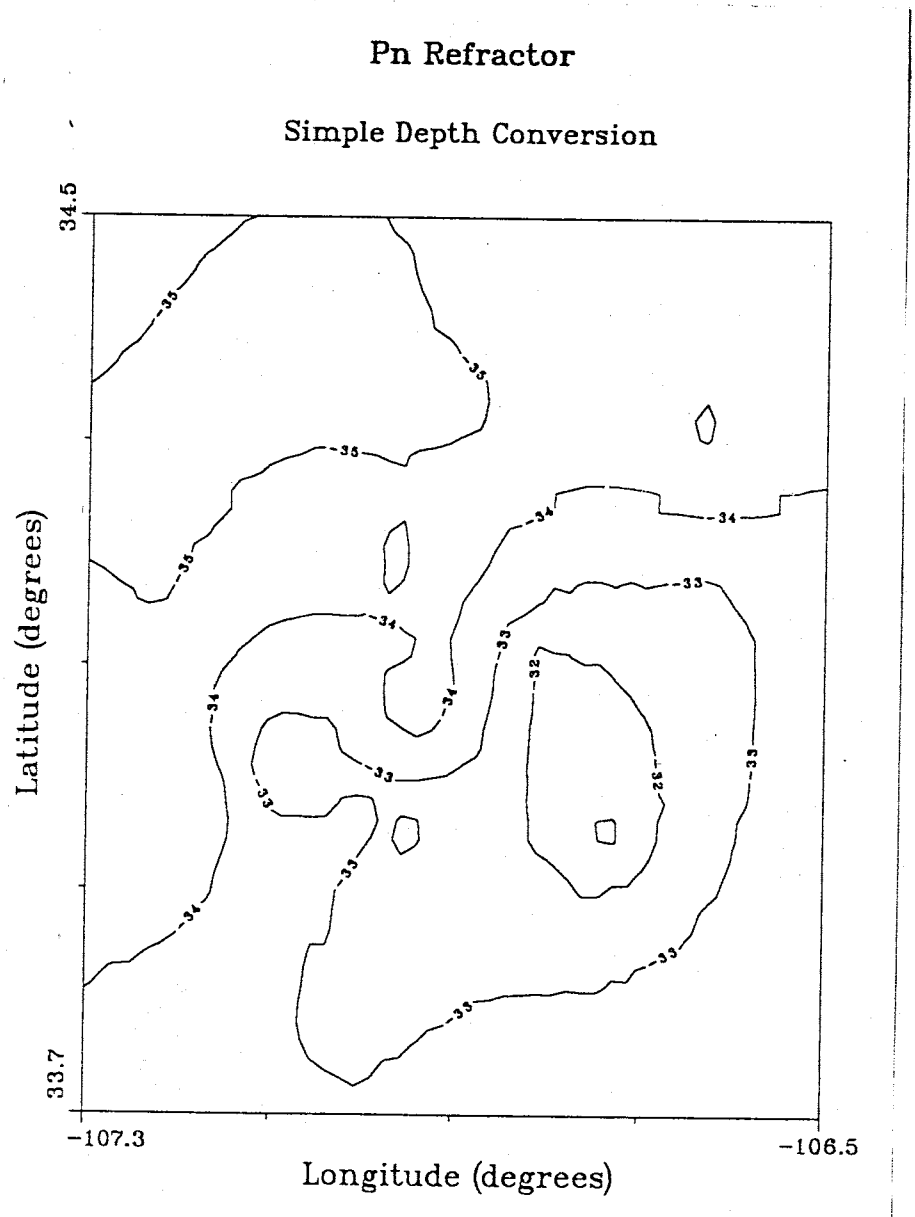

Figure 94: Contour plot of the crust-mantle boundary from kriging of 21 Moho depth data. Datum is the topographic surface.

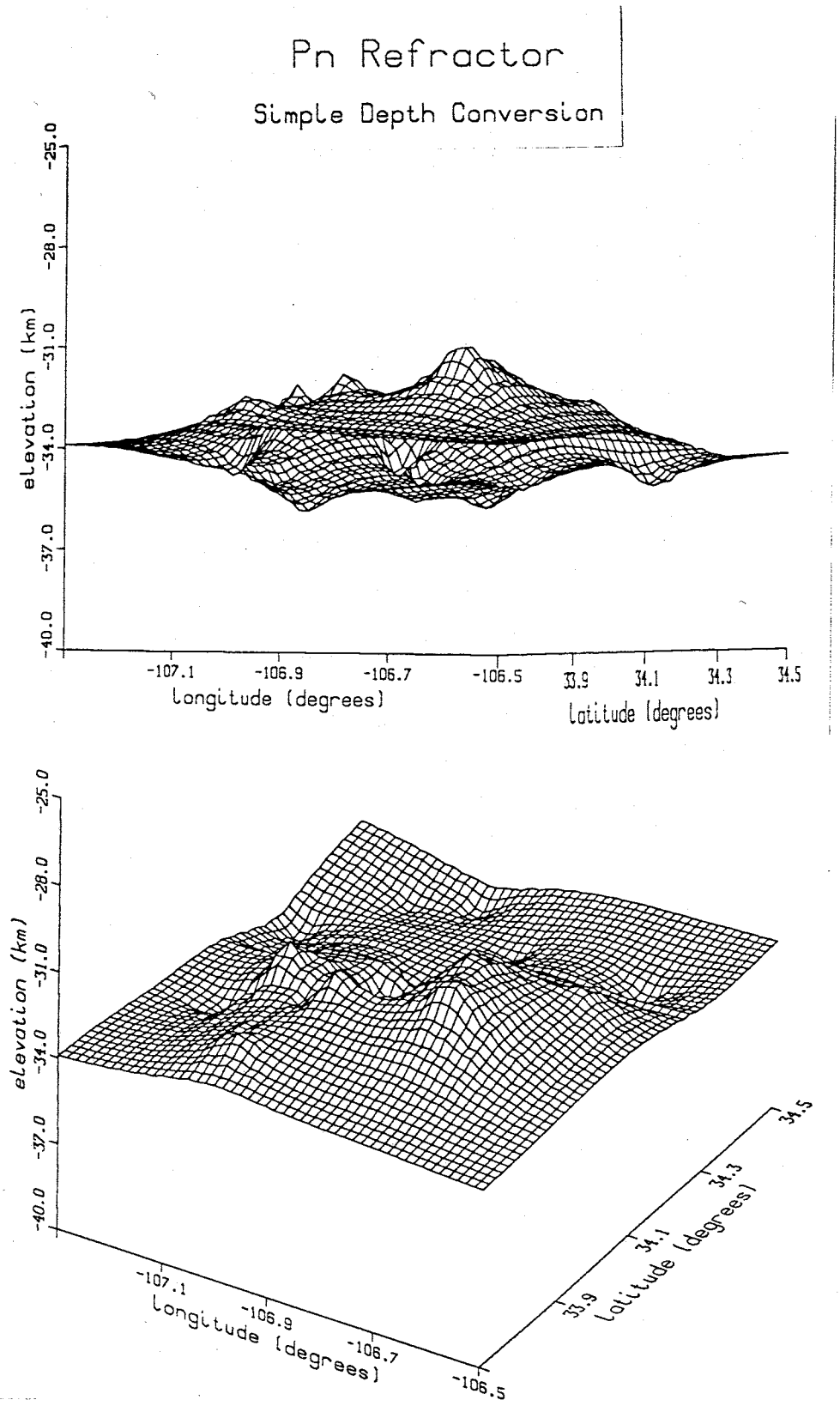

Figure 95: Three-dimensional representation of the crust-mantle boundary from kriging of 21 Moho depth data. Two perspectives are given. Datum is the topographic surface.

would result. Second, because of the large cone of refracted waves, small lateral changes in velocities and thicknesses will be averaged out. Third, where this averaging is a minimum, near the surface, complexities in the Phanerozoic are accommodated by using the Pg time terms. Furthermore, these time terms also adjust for slight differences in the upper refractor velocity immediately beneath the station. Fourth, because of the velocity gradient in the upper crust, the velocity difference across the Conrad should not be very large. As a result, even though the mid-crustal refractor shows some complicated topography, the relative travel time differences between waves passing through different thicknesses of upper crust will be small. In fact, a change of 5 km in the topography of the mid-crustal refractor will affect the total travel time by about one percent. Hence, the topography on the P* refractor should have little effect on the Pn time terms. Lastly, comparing the configuration of the P* and Pn refractors (Figures 85 and 95), there is no evidence of any similarity in configuration which would be evident if the mid-crustal refractor position were influencing the Pn time terms in any significant way.

CRUSTAL CROSS SECTIONS

Now that each of the three major refracting interfaces has been examined in detail, cross sections through the study area can be constructed (Figures 96, 97, 98, 99). These cross sections show the interrelations among the layers along several azimuths.

Comparing the various profiles, several observations can be made. First, the Conrad and Mohorovičić discontinuities are generally not parallel in this area. Second, the Moho is essentially planar and clearly dips to the northwest. Third, the Conrad is non-planar, showing dip in several directions, noticeably to the northeast and the southeast. The southeast dip is particularly interesting since the Mohorovičić discontinuity is shallowing in this direction. This results in thinning of the lower crust from ~17 km thick near LAZ to the northwest down to ~7 km thick at CAR in the southeast. Thinning of the lower crust is also evident at SMC where the lower crust is only 12 km thick. This thinning trend is consistent with observations in the southern Rio Grande rift where the upper crust is a fairly constant 20 km thick while the lower crustal thickness is less than 10 km (Sinno et al., 1986). It appears that crustal thinning in the rift takes place at the expense of the lower crust with the thickness of the upper crust remaining essentially uniform and constant.

From the surface contour plots and the cross sections, it appears that the complexity of the three refractors decreases with increasing depth. This is due in part to the fact that the cone of refracted waves arriving at a given station increases in size with increasing depth. The offset distances, i.e. the radii of the cones of refracted arrivals, are 1.5 km for Pg, 30 km for P*, and 40 km for Pn. Therefore, greater and greater averaging of the surface occurs with each progres-

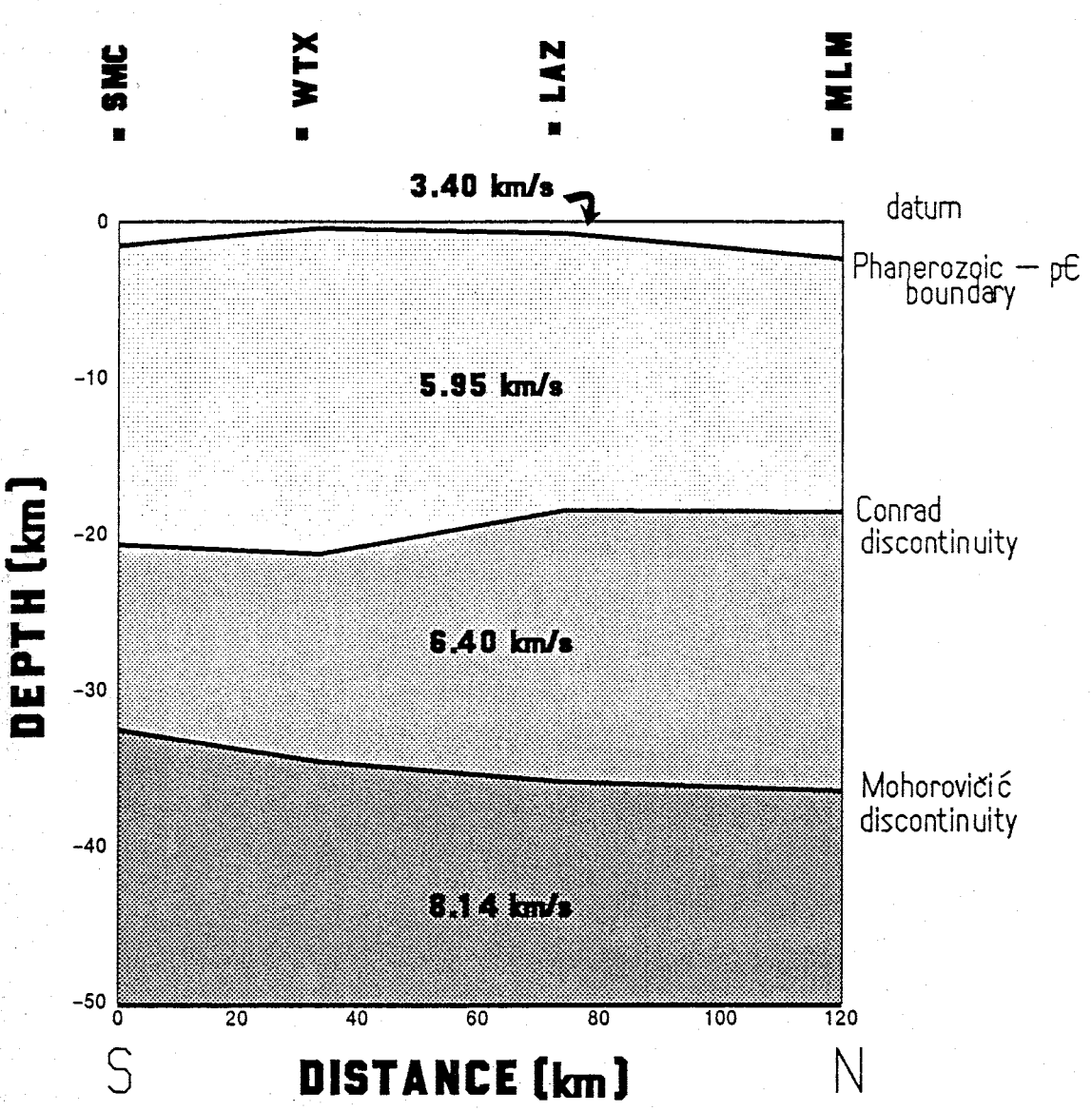

Figure 96: Derived crustal model along N-S profile through the study area. The profile was constructed by extrapolating between the crustal models at each of the stations shown above. The northward component of the dip on the Moho is clearly evident.

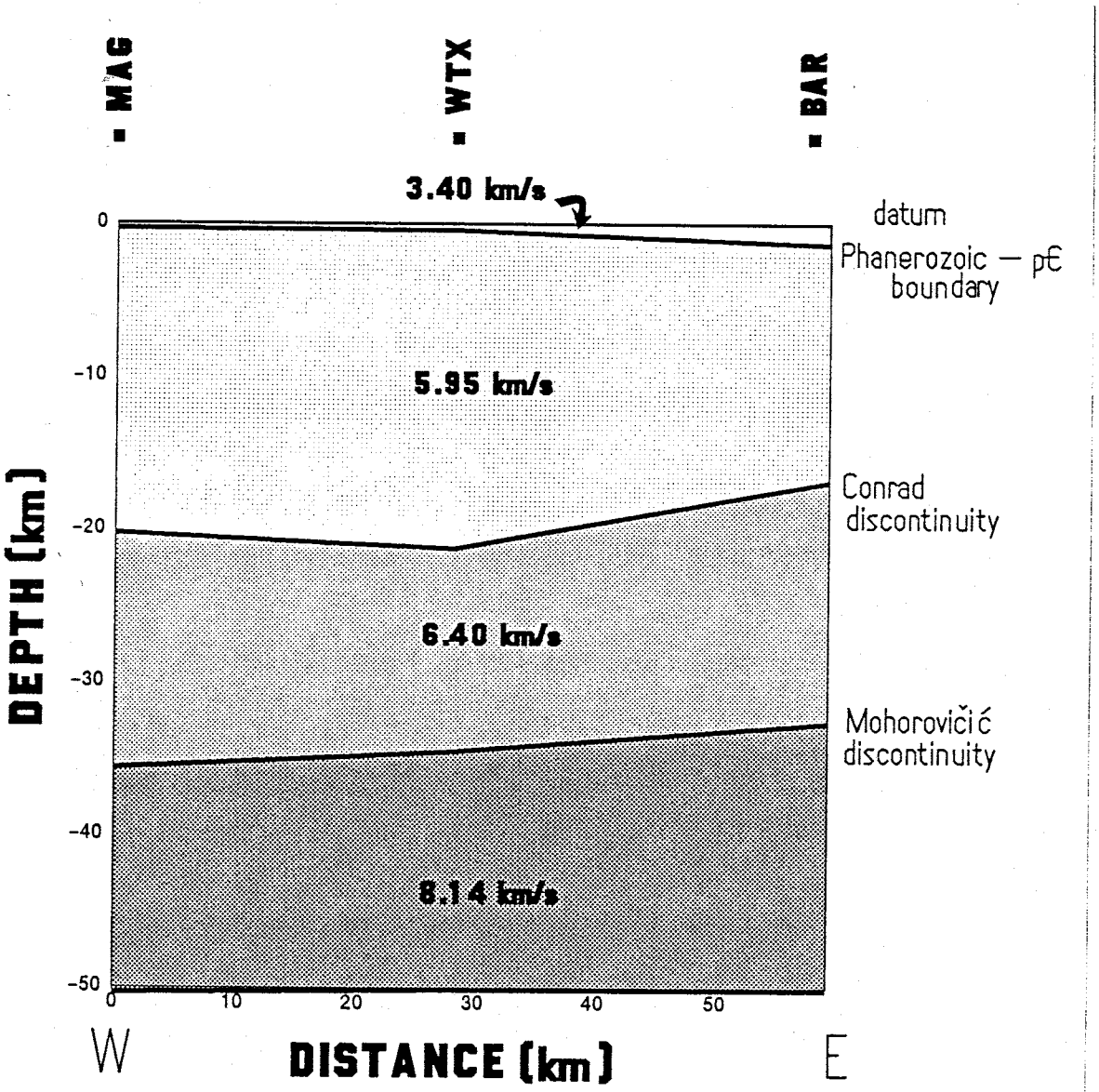

Figure 97: Derived crustal model along E-W profile through the study area. Profile was constructed by extrapolating between the crustal models at each of the stations shown above. The westward component of the dip on the Moho is clearly evident.

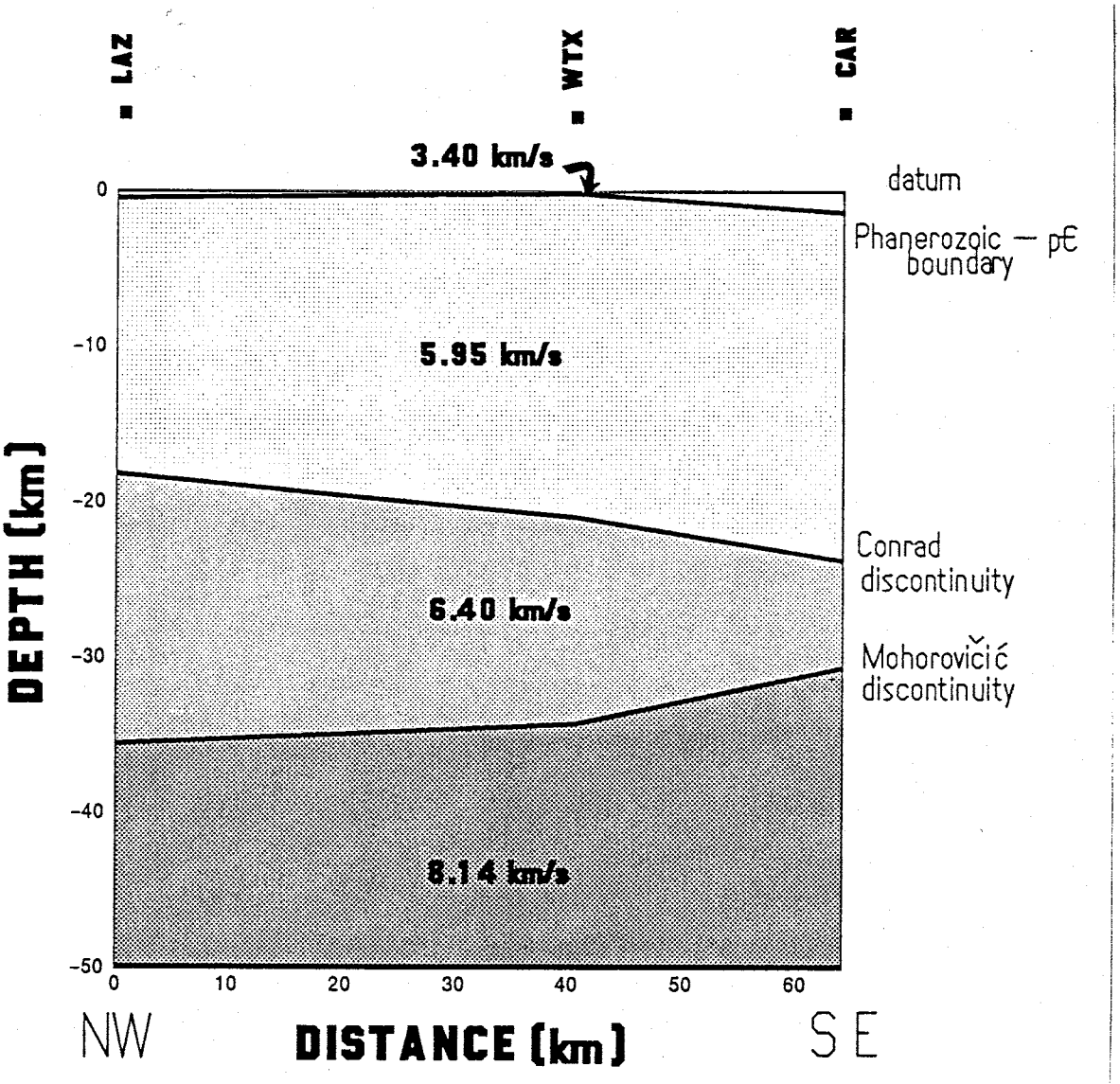

Figure 98: Derived crustal model along NW-SE profile through the study area. Profile was constructed by extrapolating between the crustal models at each of the stations shown above. The profile is along the direction of maximum dip on the Moho.

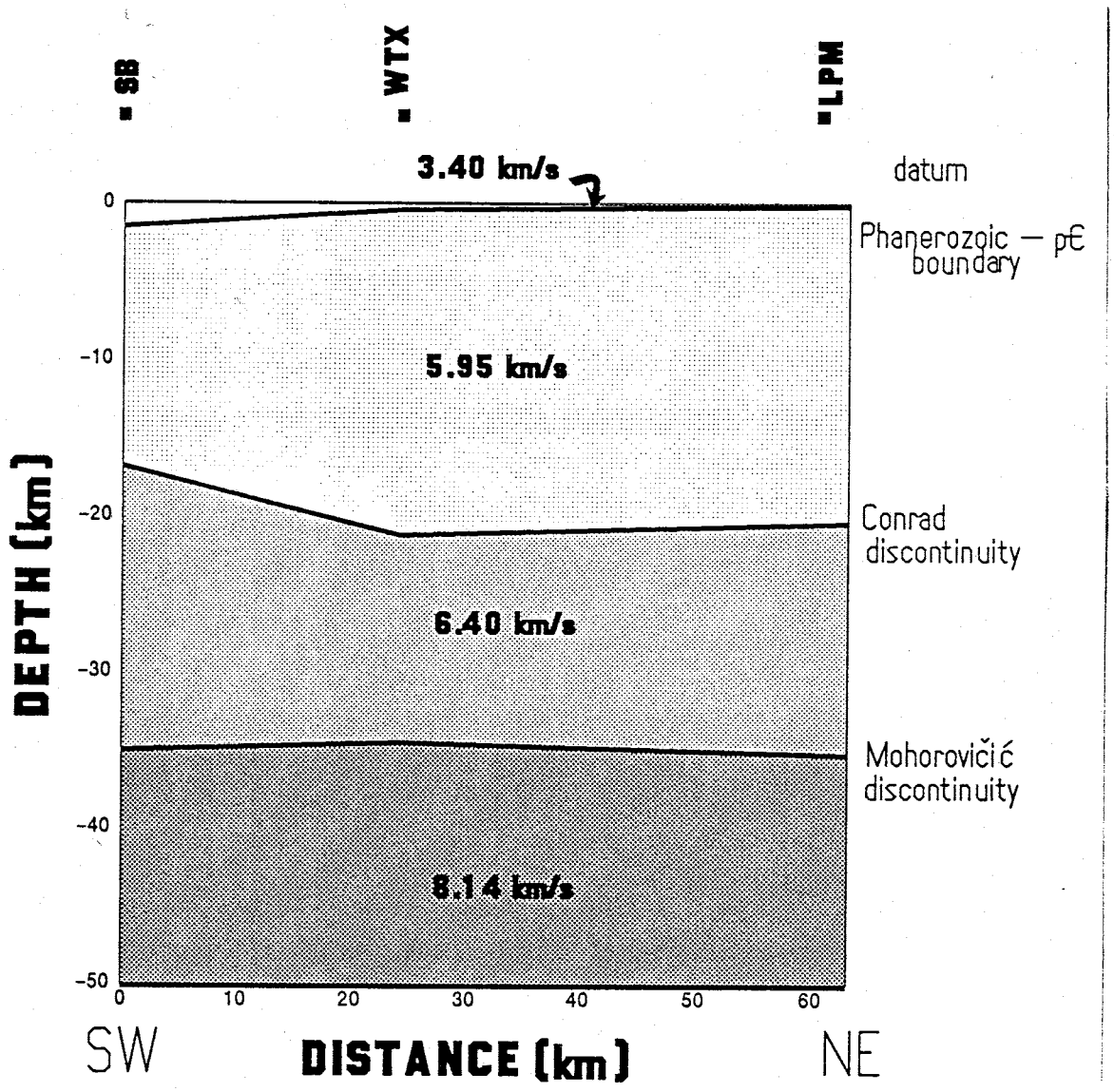

Figure 99: Derived crustal model along SW-NE profile through the study area. Profile was constructed by extrapolating between the crustal models at each of the stations shown above. The profile is along strike and shows no dip on the Moho.

sively deeper layer, i.e. the high frequency changes in the topography of the deeper layers cannot be delineated by this method. A second possibility relates to the tectonism in the region. When there is doming, the outer layers undergo much greater deformation than do the internal layers. Perhaps then, the apparent decrease in complexity with depth is evidence for the supposition that each of the three refractors has experienced differing degrees of deformation.

All in all, the cross sections indicate highly variable crustal structure with dramatic changes in thickness over short lateral distances. Considering the degree of tectonic disruption that this part of the rift has undergone, these changes are not surprising.

SUMMARY AND CONCLUSIONS

Time-term analysis provides a powerful technique for investigating the structure of the earth's crust and upper mantle. In this study, both unmodified and modified analyses were used to determine the velocity and general topography of the Phanerozoic-Precambrian boundary, the Conrad discontinuity, and the Mohorovičić discontinuity, as well as delineate the presence of anisotropy, dip, and/or a lateral or vertical velocity gradient. Furthermore, except for the dip modelling, the statistical significance of each model was determined.

Phanerozoic-Precambrian Boundary

The best-fitting model to the Pg data indicates that the velocity increases with depth from 5.7 km/s at the top of the Precambrian basement to just under 6.0 km/s at a depth of 10 km. Based on previous work, the velocity gradient should diminish dramatically below this depth. This increase in velocity results from the closing of cracks and voids by the increase in pressure with depth.

The Phanerozoic section overlying the Precambrian basement varies in thickness from 0 to 3 km, and shows evidence of thickening in the eastern part of the study area. Because of the large-scale tectonic forces that have been active in the region, the topography on the Precambrian basement is highly variable and extremely complicated. This variability and complexity are mirrored in the time terms and related depth estimates, which are consistent with known local and regional geology.

Mid-Crustal Discontinuity

The P-wave velocity below the mid-crustal discontinuity is 6.40 $\pm$ 0.16 km/s. This velocity is low with respect to P* velocities reported in the surrounding geologic provinces. Elevated temperatures due to lithospheric thinning

and magmatic intrusion are the most likely cause of this low velocity value.

Combining the data from this study with data obtained from the COCORP profiles and other sources, a fairly complex mid-crustal refractor surface was modelled. The model delineates a surface which dips both to the southeast as well as the northeast. The northeast dip is consistent with previous work. The southeast dip has not been observed before but could explain the absence of reflected phases from the mid-crustal magma body at stations in the eastern part of the study area.

An extremely large time term at station LEM is consistent with the low velocity values reported in the immediate area of the station. These low velocities and the large time term are possibly due to the presence of magma in the upper crust near the station.

Crust-Mantle Boundary

The upper mantle in the Socorro area has a Pn velocity of 8.14 $\pm$ 0.05 km/s. Since this velocity is typical of normal lithospheric mantle rocks, an asthenospheric upwarp in direct contact with the base of the crust is precluded in this area.

The Pn velocity decreases with increasing epicentral distance. This distance dependence could be the result of a number of factors including:

1. attenuation of the initial phase,
2. dispersion,
3. changes in source spectra, and/or
4. a negative velocity gradient in the upper mantle.

The specific cause or causes of the observed phenomenon cannot be ascertained from this study.

Analysis of the areal subsets of the Pn data set indicate a complex velocity structure with respect to anisotropy. Differing anisotropy directions in the eastern and western parts of the study area are indicative of mantle rocks that have different tectonic histories. Large-scale strike-slip motion in the Eocene could have brought dissimilar mantle rocks in contact with one another.

The crust-mantle boundary in the central rift has an average northwest dip of ~4.6°. This value agrees with previous apparent dip estimates, and seems to explain the anomalously low Pn velocity (7.6 km/s) of Olsen et al. (1979) since their unreversed refraction profile was shot northward, i.e. in a down-dip direction.

The model of the Moho surface in this area is fairly simple, showing a consistent dip to the northwest and little other complexity. The model is uncomplicated because crustal effects are small and any high frequency changes in the refracting surface could not be delineated by the time-term method.

Crustal Cross Sections

Two observations were elicited from the crustal cross sections through the study area. First, crustal thinning in the rift takes place at the expense of the lower crust with the thickness of the upper crust remaining uniform and constant. Second, refractor complexity decreases with increasing depth, possibly the result of doming and/or increased averaging of the surface with increasing depth.

Overall, the crustal structure of the central rift is highly variable and evidences the degree of tectonic disruption in the region.

Further Work

Many questions have been raised by this investigation. Further work should focus on:

1. defining the P wave velocity variation with depth for the entire upper crust,
2. acquisition of more P* data to better quantify the velocity structure at the mid-crust,
3. delineating the cause of the observed decrease in the Pn velocity with distance, and
4. definitively determining the presence and character of upper mantle anisotropy in the central Rio Grande rift.

REFERENCES

Anstey, N. A., *Seismic Interpretation: The Physical Aspects* , 625 pp., International Human Resource Development Corporation, Boston, 1977.

Archambeau, C. B., E. A. Flinn, and D. G. Lambert, Fine structure of the upper mantle, *J. Geophys. Res., 74* , 5825-5865, 1969.

Baldridge, W. S., Petrology and petrogenesis of Plio-Pleistocene basaltic rocks from the central Rio Grande rift, New Mexico, and their relation to rift structure, in *Rio Grande Rift: Tectonics and Magmatism* , edited by R. E. Riecker, pp. 323-353, AGU, Washington, D.C., 1979.

Baldridge, W. S., K. H. Olsen, and J. F. Callender, Rio Grande rift: Problems and perspectives, *N. M. Geol. Soc. Field Conf. Guideb., 35* , 1-12, 1984.

Bamford, D., Applications of simulated data studies to crustal refraction studies, *Bull. Geol. Soc. Am., 61* , 1013-1031, 1971.

Bamford, D., Refraction data in western Germany - A time-term interpretation, *Z. Geophys., 39* , 907-927, 1973.

Bamford, D., M. Jentsch, and C. Prodehl, *Pn* velocity anisotropy studies in northern Britain and the eastern and western United States, *Geophys. J. R. Astron. Soc., 57* , 397-429, 1979.

Berry, M. J., and G. F. West, An interpretation of the first-arrival data of the Lake Superior experiment by the time-term method, *Bull. Seismol. Soc. Am., 56* , 141-171, 1966a.

Berry, M. J., and G. F. West, A time-term interpretation of the first-arrival data of the 1963 Lake Superior experiment, *The Earth Beneath the Continents, Geophys. Monogr. Ser.* , vol. 10, edited by J. S. Steinhart and T. J. Smith, pp. 160-180, AGU, Washington, D. C., 1966b.

Birch, F., The velocity of compressional waves in rocks to 10 kilobars, part 1, *J. Geophys. Res., 65* , 1083-1102, 1960.

Bowring, S. A., The geology of the west-central Magdalena Mountains, Socorro County, New Mexico, *M. S. Thesis* , 127 pp., N. M. Inst. of Mining and Technol., Socorro, 1980.

Brown, D. M., Geology of the southern Bear Mountains, Socorro County, New Mexico, *M. S. Thesis* , 110 pp., N. M. Inst. of Mining and Technol., Socorro, 1972.

Brown, L. D., C. E. Chapin, A. R. Sanford, S. Kaufman, and J. E. Oliver, Deep structure of the Rio Grande rift from seismic reflection profiling, *J. Geophys. Res., 85* , 4773-4800, 1980.

Carpenter, P. J., Apparent *Q* for upper-crustal rocks in the Rio Grande rift of central New Mexico from the analysis of microearthquake spectra, *Ph. D. Thesis* , 150 pp., New Mexico Inst. of Mining and Technol., Socorro, 1984.

Carpenter, P. J., and A. R. Sanford, Apparent *Q* for upper crustal rocks of the central Rio Grande rift, *J. Geophys. Res., 90* , 8661-8674, 1985.

Catchings, R., C. Jarchow, S. Holbrook, H. Benz, and others, The 1986 PASSCAL Basin and Range lithospheric seismic experiment, *EOS Trans. AGU, 69,* 593, 596-598, 1988.

Cather, S. M., Laramide Sierra uplift: Evidence for major rift uplift in central and southern New Mexico, *N. M. Geol. Soc. Field Conf. Guideb., 34* , 99-101, 1983.

Chamberlin. R. M., Cenozoic domino-style crustal extension in the Lemitar Mountains, New Mexico: A summary, *N. M. Geol. Soc. Field Conf. Guideb., 34* , 111-118, 1983.

Chamberlin, R. M., Logsdon, M. J., Eveleth, R. W., and others, Preliminary evaluation of the Sierra Ladrones Wilderness Study Area, Socorro County, New Mexico, *N. M. Bur. Mines and Miner. Resour. Open File Rep., 169* , 168 pp., 1982.

Chapin, C. E., The Rio Grande rift, part I: Modifications and additions, *N. M. Geol. Soc. Field Conf. Guideb., 22* , 191-201, 1971.

Chapin, C. E., An overview of Laramide wrench faulting in the Southern Rocky Mountains with emphasis on petroleum exploration, in *Rocky Mountain Foreland Symposium - 1983* , edited by J. D. Lowell, pp. 169-180, Rocky Mountain Assoc. of Geol., Denver, 1983.

Chapin, C. E., and W. R. Seager, Evolution of the Rio Grande rift in the Socorro and Las Cruces areas, *N. M. Geol. Soc. Field Conf. Guideb., 26* , 297-321, 1975

Chapin, C. E., R. M. Chamberlin, G. R. Osburn, D. W. White, and A. R. Sanford, Exploration framework of the Socorro Geothermal Area, New Mexico, in *Field Guide to Selected Cauldrons and Mining Districts of the Datil-Mogollon Volcanic Field, N. M. Geol. Soc. Spec. Publ., 7* , 114-129, 1978.

Condie, K. C., and A. J. Budding, Geology and geochemistry of Precambrian rocks, central and south-central New Mexico, *N. M. Bur. Mines and Miner. Resour. Memoir, 35* , 58 pp., 1979.

Cook, F. A., D. B. McCullar, E. R. Decker, and S. B. Smithson, Crustal structure and evolution of the Southern Rio Grande rift, in *Rio Grande Rift: Tectonics and Magmatism* , edited by R. E. Riecker, pp. 195-208, AGU, Washington, D.C., 1979.

Cordell, L., Regional geophysical setting of the Rio Grande rift, *Geol. Soc. Am. Bull., 89* , 1073-1090, 1978.

Deal, E. G., and R. C. Rhodes, Volcano-tectonic structures in the San Mateo Mountains, Socorro County, New Mexico, in *Cenozoic Volcanism in Southwest New Mexico, N. M. Geol. Soc. Spec. Publ., 5* , 151 pp., 1976.

Draper, N., and H. Smith, *Applied Regression Analysis* , 407 pp., John Wiley, New York, 1966.

Giese, P., Die geschwindigkeitsverteilung im obersten Bereich des kristallins, abgeleitet aus refraktionsbeobachtungen auf dem profil Bohmischbruck - Eschenlohe, *Z. Geophys., 29* , 197-214, 1963.

Hearn, T. M., *Pn* travel times in southern California, *J. Geophys. Res., 89* 1843-1855, 1984.

Hill, D. P., Velocity gradients and anelasticity from crustal body wave amplitudes, *J. Geophys. Res., 76* , 3309-3325, 1971.

Jackson, W. H., and L. C. Pakiser, Seismic study of crustal structure in the Southern Rocky Mountains, *U. S. Geol. Surv. Prof. Paper, 525D* , D85-D92, 1965.

Jackson, W. H., S. W. Stewart, and L. C. Pakiser, Crustal structure in eastern Colorado from seismic refraction measurements, *J. Geophys. Res., 68* , 5767-5776, 1963.

Jaksha, L. H., Reconnaissance seismic refraction-reflection surveys in southwestern New Mexico, *Bull. Geol. Soc. Am., 93* , 1030-1037, 1982.

Jaksha, L. H., and D. H. Evans, Reconnaissance seismic refraction-reflection surveys in southwestern New Mexico, *Bull. Seis. Soc. Am., 74* , 1263-1274, 1984.

Johnston, J. A., Microearthquake frequency attenuation of *S* phases in the Rio Grande rift near Socorro, New Mexico, *Geophys. Open File Rep., 24* , 84 pp., N. M. Inst. of Mining and Technol., Socorro, 1978.

Jordan, J., R. Black, and C. C. Bates, Patterns of maximum amplitudes of *Pn* and *P* waves over regional and continental areas, *Bull. Seis. Soc. Am., 55* , 693-720, 1965.

Kelley, V. C., and A. M. Kudo, Volcanoes and related basalts of Albuquerque basin, New Mexico, *N. M. Bur. Mines and Miner. Resour. Circ., 126* , 30 pp., 1978.

Kelley, V. C., and G. H. Wood, Lucero Uplift, Valencia, Socorro, and Bernalillo Counties, New Mexico, *U. S. Geol. Surv. Oil and Gas Invest. Prelim. Map, 47* , 1946.

King, K. M., Investigation of the seismogenic zone in the vicinity of Socorro, New Mexico, from an analysis of focal depth distributions, M. S. Indep. Study, 124 pp., N. M. Inst. of Mining and Technol., Socorro, 1986.

Larsen, S., R. Reilinger, and L. Brown, Evidence of ongoing crustal deformation related to magmatic activity near Socorro, New Mexico, *J. Geophys. Res., 91* , 6283-6292, 1986.

Lee, W. H., and S. W. Stewart, Principles and Applications of Microearthquake Networks, Academic Press, New York, 1981.

Machette, M. N., and R. G. McGimsey, Quaternary and Pliocene faults in the Socorro and western part of the Fort Sumner 1^o x 2^o quadrangles, New Mexico, *U. S. Geol. Surv. Misc. Field Studies Map, MF-1465-A* , 1982.

McCollom, R. L., and R. S. Crosson, An array study of upper mantle velocity in Washington state, *Bull. Seismol. Soc. Am., 65* , 467-482, 1975.

Morris, G. B., R. W. Raitt, and G. G. Shor, Jr., Velocity anisotropy and delay-time maps of the mantle near Hawaii, *J. Geophys. Res., 74* , 4300-4316, 1969.

Murdock, J. N., and L. H. Jaksha, The P wave velocity of the uppermost mantle of the Rio Grande rift region of north central New Mexico, *J. Geophys. Res., 86* , 7055-7063, 1981.

Murdock, J. N., and J. A. Steppe, Crustal parameters estimated from P waves of earthquakes recorded at a small array, *Pure Appl. Geophys., 118* , 1179-1190, 1980.

O'Brien, P. N., Lake Superior crustal structure - A reinterpretation of the 1963 seismic experiment, *J. Geophys. Res., 73* , 2669-2689, 1968.

Olsen, K. H., G. R. Keller, and J. N. Stewart, Crustal structure along the Rio Grande rift from seismic refraction profiles, in *Rio Grande Rift: Tectonics and Magmatism* , edited by R. E. Riecker, pp. 127-143, AGU, Washington, D. C., 1979.

Osburn, G. R., and C. E. Chapin, Ash-flow tuffs and cauldrons in the northeast Mogollon-Datil Volcanic Field, *N. M. Geol. Soc. Field Conf. Guideb., 34* , 197-204, 1983.

Phinney, R. A., Structure of the earth's crust from spectral behavior of long-period body waves, *J. Geophys. Res., 69* , 2997-3017, 1964.

Raitt, R. W., G. G. Shor, Jr., T. J. G. Francis, and G B. Morris, Anisotropy of the Pacific upper mantle, *J. Geophys. Res., 74* , 3095-3109, 1969.

Reilinger, R. E., J. E. Oliver, L. D. Brown, A. R. Sanford, and E. I. Balazs, New measurements of crustal doming over the Socorro magma body, *Geology, 8* , 291-295, 1980.

Reiter, L., An investigation into the time term method in refraction seismology, *Bull. Seis. Soc. Am., 60* , 1-13, 1970.

Reiter, M., and R. Smith, Subsurface temperature data in the Socorro Peak, KGRA, New Mexico, *Geotherm. Energy Mag., 5* , 37-41, 1977.

Riecker, R. E. (ed.), *Rio Grande Rift: Tectonics and Magmatism* , AGU, Washington, D. C., 1979.

Rinehart, E. J., and A. R. Sanford, Upper crustal structure of the Rio Grande rift near Socorro, New Mexico, from inversion of microearthquake S-wave reflections, *Bull. Seismol. Soc. Am., 71* , 437-450, 1981.

Rinehart, E. J., A. R. Sanford, and R. M. Ward, Geographic extent and shape of an extensive magma body at mid-crustal depths in the Rio Grande rift near Socorro, New Mexico, in *Rio Grande Rift: Tectonics and Magmatism* , edited by R. E. Riecker, pp. 237-251, AGU, Washington, D. C., 1979.

Roller, J. C., Crustal structure in the eastern Colorado Plateau province from sesimic refraction measurements, *Bull. Seis. Soc. Am., 55* , 107-119, 1965.

Sanford, A. R., Gravity Survey in central Socorro County, New Mexico, *N. M. Bur. Mines and Miner. Resour. Circ., 91* , 14 pp., 1968.

Sanford, A. R., Temperature gradient, heat-flow measurements in the vicinity of Socorro, New Mexico, *Geophys. Open File Rep., 15* , 19 pp., N. M. Inst. of Mining and Technol., Socorro, 1978.

Sanford, A. R., and P. Einarsson, Magma chambers in rifts, in *Continental and Oceanic Rifts, Geodynamics Ser.* , volume 8, edited by G. Palmason, pp. 147-168, AGU, Washington, D. C., 1982.

Sanford, A. R., and C. R. Holmes, Microearthquakes near Socorro, New Mexico, *J. Geophys. Res., 67* , 4449-4459, 1962.

Sanford, A. R., and J. W. Schlue, Seismic exploration for shallow magma bodies in the vicinity of Socorro, New Mexico, New Mexico Energy Research and Development Program, *Final Report, EMD 77-2312* , 17 pp., 1980.

Sanford, A. R., O. S. Alptekin, and T. R. Toppozada, Use of reflection phases on microearthquake seismograms to map an unusual discontinuity beneath the Rio Grande rift, *Bull. Seis. Soc. Am., 63* , 2021-2034, 1973.

Sanford, A. R., A. J. Budding, J. P. Hoffman, O. S. Alptekin, C. A. Rush, and T. R. Toppozada, Seismicity of the Rio Grande rift in New Mexico, *Circ. N. M. Bur. Mines and Miner. Resour., 120* , 19pp., 1972.

Sanford, A. R., R. P. Mott, P. J. Shuleski, E. J. Rinehart, F. J. Caravella, R. M. Ward, and T. C. Wallace, Geophysical evidence for a magma body in the vicinity of Socorro, New Mexico, *The Earth's Crust: Its Nature and Physical Properties, Geophys. Monogr. Ser.* , volume 20, edited by J. G. Heacock, pp. 385-404, AGU, Washington, D. C., 1977.

Sanford, A. R., K. H. Olsen, and L. H. Jaksha, Seismicity of the Rio Grande rift, in *Rio Grande Rift: Tectonics and Magmatism* , edited by R. E. Riecker, pp. 87-106, AGU, Washington, D. C., 1979.

Sanford, A. R., P. J. Carpenter, and E. J. Rinehart, Characteristics of a microearthquake swarm in the Rio Grande rift near Socorro, New Mexico (abstract), *Earthquake Notes, 54* , p. 98, 1983.

Scheidegger, A. E., and P. L. Willmore, The use of a least squares method for the interpretation of data from seismic surveys, *Geophysics, 22* , 9-22, 1957.

Shuleski, P. J., Seismic fault motion and SV screening by shallow magma bodies in the vicinity of Socorro, New Mexico, *Geophys. Open File Rep., 8* , 94 pp., N. M. Inst. of Mining and Technol., Socorro, 1976.

Sinno, Y. A., P. H. Daggett, G. R. Keller, P. Morgan, and S. H. Harder, Crustal structure of the southernm Rio Grande rift determined from seismic refraction profiling, *J. Geophys. Res., 91* , 6143-6156, 1986.

Smith, T. J., J. S. Steinhart, and L. T. Aldrich, Lake Superior crustal structure, *J. Geophys. Res., 71* , 1141-1172, 1966.

Smithson, S. B., R. A. Johnson, and Y. K. Wong, Mean crustal velocity: A critical parameter for interpreting crustal structure and crustal growth, *Earth Planet. Sci. Lett., 53* , 323-332, 1981.

Toppozada, T. R., Seismic investigation of crustal structure and upper mantle velocity in the state of New Mexico and vicinity, *Ph. D. Thesis* , 152 pp., New Mexico Inst. of Mining and Technol., Socorro, 1974.

Toppozada, T. R., and A. R. Sanford, Crustal structure in central New Mexico interpreted from the GASBUGGY explosion, *Bull. Seismol. Soc. Am.*, *66* , 877-886, 1976.

Ward, R. M., Determination of three-dimensional velocity anomalies within the upper crust in the vicinity of Socorro, New Mexico, using P- arrival times from local microearthquakes, *Ph.D. Thesis* , 136 pp., N. M. Inst. of Mining and Technol., Socorro, 1980.

Warren, D. H., A seismic refraction survey of crustal structure in central Arizona, *Geol. Soc. Am. Bull.*, *80* , 257-282, 1969.

Whitcombe, D. N., and P. K. Maguire, The response of the time-term method to simulated crustal structures, *Bull. Seis. Soc. Am.*, *69* , 1455-1473, 1979.

Whitcombe, D. N., and D. E. Rogers, The effects of refractor topography and overburden anisotropy on time-term solutions of refractor anisotropy, *Geophys. J. R. Astron. Soc.*, *67* , 449-464, 1981.

Willmore, P. L., and A. M. Bancroft, The time-term approach to refraction seismology, *Geophys. J. R. Astron. Soc.*, *3* , 419-432, 1960.

Wolberg, J. R., *Prediction Analysis* , 291 pp., D. Van Nostrand, New York, 1967.

Zervas, C. E., and R. S. Crosson, *Pn* observation and interpretation in Washington, *Bull. Seismol. Soc. Am.*, *76* , 521-546, 1986.

APPENDIX I: Pg Data

```
A 7507231651 51.26 34N02.53 106W57.84
     CC       53.66      0       11.40      352.00
     SC       53.91      0       12.10      253.00
     FM       54.45      0       15.40       73.00
     XYZ       0.00      4        0.00        0.00
A 7508121659 59.80 33N22.73 106W21.90
     CM       75.05      0       83.90       41.00
     WTX      76.71      0       93.90       35.00
     SC       77.16      0       97.00       44.00
     CC       77.84      0      102.30       34.00
     XYZ       0.00      4        0.00        0.00
A 7604201856 12.81 34N02.53 106W57.84
     WTX      13.68      0        3.70       27.00
     CC       15.19      0       11.40      352.00
     DM       16.18      0       16.10       63.00
     SL       16.87      0       20.20      353.00
     BG       17.48      0       22.60       36.00
     CU       17.11      0       21.40       53.00
     XYZ       0.00      4        0.00        0.00
A 7604211916 43.96 34N02.53 106W57.84
     WTX      44.83      0        3.70       27.00
     CC       46.29      0       11.40      352.00
     DM       47.32      0       16.10       63.00
     SL       47.86      0       20.20      353.00
     BG       48.61      0       22.60       36.00
     CU       48.31      0       21.40       53.00
     XYZ       0.00      4        0.00        0.00
A 7604221945 27.82 34N02.53 106W57.84
     WTX      28.69      0        3.70       27.00
     DM       31.12      0       16.10       63.00
     CC       30.28      0       11.40      352.00
     SL       31.73      0       20.20      353.00
     XYZ       0.00      4        0.00        0.00
A 7610061400 00.50 33N40.74 106W31.26
     LPM      13.50      0       70.50        8.00
     LAD      18.20      0       98.70       29.00
     DM       11.07      0       54.40       29.00
     IC       11.35      0       55.80       52.00
     WTX      11.80      0       58.70       42.00
     SC       12.87      0       64.20       55.00
     XYZ       0.00      4        0.00        0.00
A 7702142331 43.80 35N06.66 107W23.58
     CC       63.85      0      113.70      161.00
     WTX      65.41      0      122.20      160.00
     IC       66.70      0      129.70      164.00
     DM       65.40      0      123.60      154.00
     SC       66.15      0      125.20      167.00
     LPM      63.40      0      113.10      142.00
     XYZ       0.00      4        0.00        0.00
A 7702221847 54.25 34N02.53 106W57.84
     WTX      55.12      0        3.70       27.00
     IC       55.89      0        6.80      206.00
     CM       56.50      0       10.20      177.00
     CC       56.67      0       11.40      352.00
     SC       57.00      0       12.10      253.00
     XYZ       0.00      4        0.00        0.00
A 7702231848 58.70 34N02.53 106W57.84
     IC       60.40      0        6.80      206.00
     CM       61.10      0       10.20      177.00
     CC       61.10      0       11.40      352.00
     SC       61.60      0       12.10      253.00
     XYZ       0.00      4        0.00        0.00
A 7705102348 25.06 34N02.53 106W57.84
     WTX      25.93      0        3.70       27.00
     WM       26.09      0        4.30      219.00
     RM       26.70      0        5.90      318.00
     NG       26.99      0        9.00      198.00
     FM       28.46      0       15.40       73.00
     XYZ       0.00      4        0.00        0.00
A 7705112043 26.29 34N02.53 106W57.84
     WTX      27.16      0        3.70       27.00
     FM       29.62      0       15.40       73.00
     GM       31.45      0       27.50      295.00
     XYZ       0.00      4        0.00        0.00
A 7705141950 28.55 34N02.53 106W57.84
     WTX      29.42      0        3.70       27.00
     FM       31.86      0       15.40       73.00
     XYZ       0.00      4        0.00        0.00
A 7705192249 51.48 34N02.53 106W57.84
     WTX      52.34      0        3.70       27.00
     DM       54.80      0       16.10       63.00
     FM       54.79      0       15.40       73.00
     XYZ       0.00      4        0.00        0.00
A 7706021959 59.73 34N57.60 106W34.44
     LAD      72.90      0       70.10      143.00
     LPM      73.05      0       72.60      177.00
     DM       77.13      0       97.00      167.00
     WTX      78.06      0      104.20      161.00
     GM       79.01      0      108.80      146.00
     XYZ       0.00      4        0.00        0.00
A 7707272229 15.65 35N06.66 107W23.58
     CC       35.33      0      113.70      161.00
     GM       34.67      0      108.10      172.00
     BG       35.55      0      113.20      152.00
     LPM      34.65      0      113.10      142.00
     LAD      29.75      0       79.40      156.00
     XYZ       0.00      4        0.00        0.00
A 7708251957 24.15 35N06.66 107W23.58
     CC       43.80      0      113.70      161.00
     GM       43.15      0      108.10      172.00
     BG       44.14      0      113.20      152.00
     SC       46.47      0      125.20      167.00
     CM       47.26      0      134.50      163.00
     LPM      43.65      0      113.10      142.00
     LAD      38.15      0       79.40      156.00
     WTX      45.60      0      122.20      160.00
     XYZ       0.00      4        0.00        0.00
A 7712061947 57.74 34N02.53 106W57.84
     CC       60.14      0       11.40      352.00
     BG       62.36      0       22.60       36.00
     SL       61.70      0       20.20      353.00
     LAD      65.55      0       46.70      352.00
```

```
     LPM      65.05     0       42.70      45.00
     XYZ       0.00     4        0.00       0.00
A 7712072323 23.83 34N02.53 106W57.84
     CC       26.23     0       11.40     352.00
     BG       28.48     0       22.60      36.00
     SL       27.75     0       20.20     353.00
     LAD      31.65     0       46.70     352.00
     XYZ       0.00     4        0.00       0.00
A 8106081644 59.48 34N57.60 106W34.80
     LAD      72.60     0       70.10     143.00
     LPM      72.80     0       72.60     177.00
     XYZ       0.00     4        0.00       0.00
A 8109161235 39.07 33N37.26 106W28.62
     LPM      52.60     0       78.10      10.00
     LAD      57.50     0      106.40      29.00
     SNM      51.20     1       66.00      41.00
     CC       52.60     0       74.50      39.00
     GM       55.30     0       91.10      50.00
     XYZ       0.00     4        0.00       0.00
A 8110071659 59.87 33N22.86 106W22.02
     SNM      77.00     0       93.30      35.00
     WTX      77.00     0       93.60      35.00
     LPM      78.40     0      106.30      13.00
     LAD      83.40     0      134.70      27.00
     XYZ       0.00     4        0.00       0.00
A 8209212242 14.23 34N02.53 106W57.84
     WTX      15.10     0        3.70      27.00
     SB       18.60     0       21.40     250.00
     CAR      19.40     2       23.40     115.00
     BAR      20.60     0       32.90      70.00
     XYZ       0.00     4        0.00       0.00
A 8210042051 40.93 34N02.53 106W57.84
     WTX      41.80     0        3.70      27.00
     SB       45.20     0       21.40     250.00
     CAR      45.60     0       23.40     115.00
     SMC      46.60     0       29.70     190.00
     BAR      47.20     0       32.90      70.00
     BMT      47.70     0       37.60     313.00
     LPM      48.30     0       42.70      45.00
     XYZ       0.00     4        0.00       0.00
A 8210181806 40.33 33N44.34 107W00.60
     SMC      42.10     0        4.50     349.00
     WTX      47.50     0       37.50       9.00
     BAR      51.30     0       56.70      38.00
     BMT      52.00     0       63.80     339.00
     LPM      53.60     0       72.50      29.00
     XYZ       0.00     4        0.00       0.00
A 8211160014 22.23 33N44.34 107W00.60
     SMC      24.00     0        4.50     349.00
     SB       28.40     0       30.60     329.00
     WTX      29.30     0       37.50       9.00
     BAR      32.90     0       56.70      38.00
     LPM      35.20     0       72.50      29.00
     XYZ       0.00     4        0.00       0.00
A 8211180005 22.93 33N44.34 107W00.60
     SMC      24.70     0        4.50     349.00
     BAR      33.60     0       56.70      38.00
     CAR      30.10     0       34.80      47.00
     WTX      30.10     0       37.50       9.00
     BMT      34.60     0       63.80     339.00
     SB       29.40     0       30.60     329.00
     XYZ       0.00     4        0.00       0.00
A 8301092346 45.13 33N44.34 107W00.60
     SMC      46.90     0        4.50     349.00
     SB       51.40     0       30.60     329.00
     CAR      52.00     0       34.80      47.00
     WTX      52.00     0       37.50       9.00
     BAR      56.00     0       56.70      38.00
     BMT      57.66     0       63.80     339.00
     LAZ      59.36     0       74.60     351.00
     XYZ       0.00     4        0.00       0.00
A 8301262341 27.07 33N44.34 107W00.60
     SMC      28.84     0        4.50     349.00
     SB       33.40     0       30.60     329.00
     CAR      33.90     0       34.80      47.00
     WTX      34.34     0       37.50       9.00
     BAR      37.90     0       56.70      38.00
     BMT      38.80     0       63.80     339.00
     XYZ       0.00     4        0.00       0.00
A 8302062348 24.63 33N44.34 107W00.60
     SMC      26.40     0        4.50     349.00
     SB       31.00     0       30.60     329.00
     CAR      31.50     0       34.80      47.00
     LPM      37.50     0       72.50      29.00
     LAZ      38.00     0       74.60     351.00
     BMT      36.30     0       63.80     339.00
     WTX      31.70     0       37.50       9.00
     XYZ       0.00     4        0.00       0.00
A 8307211851 20.33 34N02.53 106W57.84
     SNM      21.35     0        3.60      31.00
     WTX      21.20     0        3.70      27.00
     SMC      25.95     0       29.70     190.00
     BAR      26.50     0       32.90      70.00
     BMT      27.20     0       37.60     313.00
     LPM      27.85     0       42.70      45.00
     XYZ       0.00     4        0.00       0.00
A 8310261806 00.06 33N37.27 106W28.48
     CAR       8.70     0       43.90     327.00
     SMC      10.20     0       53.40     289.00
     BAR      10.90     0       59.50     346.00
     SNM      12.40     0       66.10     319.00
     WTX      12.30     0       66.40     319.00
     SB       14.10     0       76.30     301.00
     LPM      13.60     0       78.10     349.00
     MAG      16.60     0       92.30     311.00
     BMT      18.50     0      102.70     315.00
     LAZ      18.90     0      106.20     325.00
     ZPG1     12.31     0       64.80     316.00
     XYZ       0.00     4        0.00       0.00
A 8411281905 00.03 33N36.73 106W29.09
     CAR       8.70     0       44.30     329.00
     ZPG9      9.90     0       50.10     284.00
```

```
      SMC      10.10     1       52.90      290.00
      BAR      11.30     0       60.20      347.00
      WTX      11.80     1       66.50      320.00
      LPM      14.10     1       78.90      350.00
      LAZ      18.70     1      106.50      325.00
      XYZ       0.00     4        0.00        0.00
A 8506271820 00.03 33N37.27 106W28.48
      CAR       8.60     0       43.90      327.00
      SMC      10.10     1       53.40      289.00
      BAR      11.00     1       59.50      346.00
      WTX      12.30     1       66.40      319.00
      LEM      13.80     1       76.30      324.00
      SB       14.20     1       76.30      301.00
      LPM      13.75     0       78.10      349.00
      LJY      16.20     1       88.40      334.00
      MAG      16.50     1       92.30      311.00
      LAZ      18.90     0      106.20      325.00
      MLM      25.20     1      146.00      335.00
      XYZ       0.00     4        0.00        0.00
A 8506282111 51.20 33N57.30 106W57.77
      LEM      55.50     0       23.40      357.00
      WTX      53.90     0       13.10        7.00
      BAR      58.35     0       37.20       56.00
      LAZ      60.40     0       52.20      342.00
      SMC      55.20     0       20.20      195.00
      MAG      57.30     1       33.90      313.00
      CAR      55.60     0       21.10       91.00
      SB       55.40     0       20.20      276.00
      LPM      60.00     1       50.00       37.00
      XYZ       0.00     4        0.00        0.00
A 8507031719 29.85 33N57.30 106W57.77
      LEM      34.20     0       23.40      357.00
      WTX      32.50     1       13.10        7.00
      BAR      37.00     0       37.20       56.00
      LAZ      39.10     1       52.20      342.00
      SMC      33.90     0       20.20      195.00
      MAG      36.00     1       33.90      313.00
      CAR      34.20     0       21.10       91.00
      SB       34.00     0       20.20      276.00
      LPM      38.60     2       50.00       37.00
      XYZ       0.00     4        0.00        0.00
A 8507091802 48.58 33N57.30 106W57.77
      LEM      52.90     0       23.40      357.00
      WTX      51.30     0       13.10        7.00
      BAR      55.70     0       37.20       56.00
      LAZ      57.80     2       52.20      342.00
      SMC      52.60     0       20.20      195.00
      MAG      54.60     2       33.90      313.00
      CAR      53.00     0       21.10       91.00
      SB       52.70     0       20.20      276.00
      LPM      57.40     1       50.00       37.00
      XYZ       0.00     4        0.00        0.00
A 8507171736 48.38 33N57.30 106W57.77
      WM       49.75     0        4.70      319.00
      IC       50.13     0        6.90      336.00
      LEM      52.75     0       23.40      357.00
      BAR      55.50     0       37.20       56.00
      LAZ      57.50     1       52.20      342.00
      SMC      52.40     0       20.20      195.00
      MAG      54.45     1       33.90      313.00
      CAR      52.75     0       21.10       91.00
      SB       52.50     0       20.20      276.00
      LPM      57.00     1       50.00       37.00
      XYZ       0.00     4        0.00        0.00
A 8507252017 28.27 33N57.30 106W57.77
      LEM      32.50     0       23.40      357.00
      WTX      30.90     2       13.10        7.00
      BAR      35.45     0       37.20       56.00
      LAZ      37.50     1       52.20      342.00
      SMC      32.40     0       20.20      195.00
      MAG      34.40     1       33.90      313.00
      CAR      32.60     0       21.10       91.00
      SB       32.40     0       20.20      276.00
      LPM      36.90     1       50.00       37.00
      XYZ       0.00     4        0.00        0.00
A 8507291958 27.63 33N57.30 106W57.77
      LEM      31.95     0       23.40      357.00
      WTX      30.25     0       13.10        7.00
      BAR      34.80     0       37.20       56.00
      SMC      31.70     0       20.20      195.00
      MAG      33.80     0       33.90      313.00
      CAR      32.00     0       21.10       91.00
      SB       31.75     0       20.20      276.00
      LPM      36.25     1       50.00       37.00
      XYZ       0.00     4        0.00        0.00
A 8508091659 09.50 34N57.39 106W34.67
      MLM      20.40     1       54.20      253.00
      LPM      23.10     0       71.60      184.00
      LJY      24.20     2       74.70      203.00
      LAZ      24.50     0       80.20      220.00
      BAR      25.80     0       90.50      183.00
      LEM      26.70     1       95.00      203.00
      MAG      28.70     2      106.60      214.00
      CAR      29.80     0      112.30      187.00
      SMC      34.50     1      136.80      197.00
      XYZ       0.00     4        0.00        0.00
A 8509211840 00.00 34N57.39 106W34.67
      MLM      10.90     1       54.20      253.00
      LPM      13.40     0       71.60      184.00
      LJY      14.70     1       74.70      203.00
      LAZ      14.90     1       80.20      220.00
      BAR      16.30     0       90.50      183.00
      LEM      17.00     1       95.00      203.00
      WTX      18.90     2      103.80      199.00
      MAG      19.00     1      106.60      214.00
      CAR      20.40     1      112.30      187.00
      SB       21.90     1      122.10      207.00
      SMC      25.00     1      136.80      197.00
      XYZ       0.00     4        0.00        0.00
A 8601161800 00.00 34N57.60 106W34.82
      MLM      10.90     0       54.20      253.00
      LPM      13.30     0       71.60      184.00
```

```
      LJY       14.70      2        74.70       203.00
      LAZ       14.50      0        80.20       220.00
      BAR       16.30      0        90.50       183.00
      LEM       17.10      2        95.30       202.00
      MAG       19.00      2       106.60       214.00
      CAR       20.20      2       112.30       187.00
      SMC       24.90      1       136.80       197.00
      XYZ        0.00      4         0.00         0.00
A 8603262348 16.53 34N02.53 106W57.84
      WTX       17.40      0         3.70        27.00
      ZPG11     18.44      0         9.70       179.00
      LEM       19.10      0        13.70       356.00
      SB        20.70      0        21.40       250.00
      CAR       21.00      1        23.40       115.00
      SMC       22.30      2        29.70       190.00
      BAR       22.80      2        32.90        70.00
      LJY       23.20      2        33.20        11.00
      LAZ       24.30      2        43.10       338.00
      XYZ        0.00      4         0.00         0.00
```

APPENDIX II: P* Data

A	8210192313	31.83	35N25.98	106W06.66	
	BAR	55.80	1	150.80	198.00
	LPM	52.70	2	133.10	201.00
	XYZ	0.00	4	0.00	0.00
A	8301171858	54.63	34N38.28	105W35.10	
	SMC	82.50	1	162.90	234.00
	LAZ	79.50	1	143.80	260.00
	XYZ	0.00	4	0.00	0.00
A	8411271906	2.82	33N36.83	105W21.73	
	CAR	23.80	2	132.50	286.00
	SMC	25.10	2	154.70	277.00
	XYZ	0.00	4	0.00	0.00
A	8412080037	36.94	34N54.32	105W16.76	
	LPM	57.60	1	133.70	248.00
	BAR	59.20	2	141.40	241.00
	CAR	62.80	1	160.70	236.00
	XYZ	0.00	4	0.00	0.00
A	8501220003	37.47	34N09.85	108W46.78	
	SB	61.30	2	149.00	98.00
	LAZ	61.70	2	153.30	80.00
	SMC	64.50	2	168.20	105.00
	WTX	64.70	2	169.50	93.00
	XYZ	0.00	4	0.00	0.00
A	8506270147	12.12	32N55.08	108W15.56	
	SMC	36.50	1	149.80	50.00
	SB	37.20	1	154.30	41.00
	XYZ	0.00	4	0.00	0.00
A	8507160618	5.88	35N06.95	106W27.60	
	LEM	24.50	1	115.50	204.00
	MAG	25.70	1	127.30	214.00
	CAR	26.80	1	131.50	191.00
	SMC	30.50	1	157.00	199.00
	XYZ	0.00	4	0.00	0.00
A	8507170623	20.02	35N09.76	106W32.31	
	LEM	39.20	1	117.60	200.00
	MAG	40.00	1	127.90	210.00
	CAR	41.50	1	135.50	188.00
	SMC	45.40	1	159.70	196.00
	XYZ	0.00	4	0.00	0.00
A	8508140103	20.33	34N39.50	105W35.50	
	CAR	41.60	0	131.10	233.00
	MLM	43.30	1	143.40	277.00
	LAZ	43.30	1	143.50	259.00
	XYZ	0.00	4	0.00	0.00
A	8509010135	44.80	34N39.50	105W35.50	
	CAR	66.00	0	131.10	233.00
	LAZ	67.90	1	145.00	277.00
	SMC	71.20	1	165.80	233.00
	XYZ	0.00	4	0.00	0.00
A	8512131020	28.46	33N45.46	108W53.87	
	MAG	54.00	0	160.30	74.00
	SMC	55.70	1	174.00	89.00
	LAZ	56.80	1	177.30	66.00
	XYZ	0.00	4	0.00	0.00
A	8601152101	40.59	34N30.41	105W27.55	
	CAR	61.10	2	132.70	242.00
	MAG	66.90	2	167.60	257.00
	SB	67.30	0	169.30	250.00
	XYZ	0.00	4	0.00	0.00
A	8608020031	9.25	34N40.46	105W32.38	
	BAR	27.10	1	116.20	239.00
	LEM	31.50	2	143.50	247.00
	LAZ	33.00	1	150.00	258.00
	XYZ	0.00	4	0.00	0.00
A	8611262256	44.30	34N39.50	105W35.50	
	MLM	67.30	1	143.40	277.00
	LAZ	67.10	0	145.00	259.00
	XYZ	0.00	4	0.00	0.00
A	8703120750	25.63	34N35.38	105W50.91	
	LAZ	44.70	1	120.40	260.00
	MLM	44.70	1	121.40	282.00
	MAG	47.40	1	135.80	250.00
	XYZ	0.00	4	0.00	0.00
A	8703270436	49.49	34N49.23	105W35.58	
	MAG	76.30	0	167.30	244.00
	SB	77.20	2	173.50	237.00
	SMC	77.40	1	174.90	229.00
	XYZ	0.00	4	0.00	0.00
A	8703281716	14.94	35N21.93	106W37.27	
	LPM	33.40	1	116.80	181.00
	LAZ	33.40	1	116.90	204.00
	LEM	36.60	1	137.00	194.00
	XYZ	0.00	4	0.00	0.00
A	8704250817	47.09	35N12.08	105W48.89	
	BAR	69.40	1	139.10	212.00
	LAZ	71.30	3	150.20	234.00
	LEM	72.10	2	156.50	223.00
	CAR	73.20	1	162.20	211.00
	XYZ	0.00	4	0.00	0.00
A	8704291336	31.14	32N38.26	105W56.20	
	SMC	56.40	0	161.90	321.00
	CAR	56.80	1	163.70	333.00
	XYZ	0.00	4	0.00	0.00
A	8707041357	53.29	33N43.69	108W48.09	
	SB	77.40	0	152.40	80.00
	MAG	77.30	0	153.00	72.00
	SMC	80.00	0	165.10	88.00
	LAZ	80.10	0	170.60	64.00
	WTX	81.00	2	175.80	77.00
	CAR	84.70	1	193.00	83.00
	XYZ	0.00	4	0.00	0.00
A	8708022129	32.98	33N30.37	105W27.48	
	BAR	53.90	0	129.30	303.00
	LPM	55.50	1	140.80	309.00
	SMC	56.90	1	148.00	282.00
	LEM	58.70	2	158.30	298.00
	XYZ	0.00	4	0.00	0.00
A	8708120202	18.75	33N32.50	105W23.38	
	BAR	39.80	0	132.60	300.00
	LPM	41.60	2	143.40	307.00
	SMC	43.40	0	153.40	280.00
	XYZ	0.00	4	0.00	0.00

```
A 8709131427 30.50 35N39.17 108W16.30
     LAZ      57.50      1      173.00      143.00
     BMT      58.40      1      178.60      149.00
     XYZ       0.00      4        0.00        0.00
A 8803092011 40.11 35N49.76 106W48.64
     MLM      58.20      0      116.70      195.00
     LAZ      64.40      1      161.20      191.00
     XYZ       0.00      4        0.00        0.00
```

APPENDIX III: Pn Data

A 6712101930	00.10	36N40.68	107W12.48		
	LAD	38.82	1	246.80	176.00
	ALQ	33.48	1	204.20	161.00
	WTX	44.18	1	290.10	175.00
	XYZ	0.00	4	0.00	0.00
A 7512031012	22.80	32N49.80	108W39.78		
	MLM	60.46	1	261.10	33.00
	ALQ	66.14	1	310.60	41.00
	LPM	58.44	1	250.10	49.00
	XYZ	0.00	4	0.00	0.00
A 7601290804	28.46	32N55.14	108W42.60		
	DM	61.55	0	220.50	53.00
	SC	58.61	0	193.10	51.00
	CC	61.05	0	210.40	49.00
	WTX	60.37	0	207.90	52.00
	TA	61.22	0	219.20	55.00
	CM	59.00	0	199.10	55.00
	XYZ	0.00	4	0.00	0.00
A 7601300845	01.55	34N30.42	109W53.46		
	CC	40.68	2	270.00	98.00
	CM	41.30	0	276.50	102.00
	TA	43.30	0	290.60	99.00
	DM	42.84	0	286.40	98.00
	SC	39.65	0	263.70	102.00
	XYZ	0.00	4	0.00	0.00
A 7602040004	58.10	34N39.30	112W30.00		
	SC	128.29	0	501.60	97.00
	WTX	129.62	0	513.50	96.00
	CC	129.12	0	509.20	95.00
	DM	131.28	0	525.50	95.00
	LPM	133.02	0	538.70	92.00
	LAD	128.29	1	500.40	91.00
	MLM	127.00	1	491.00	88.00
	ALQ	134.74	1	553.80	87.00
	XYZ	0.00	4	0.00	0.00
A 7602282053	58.50	35N54.60	111W47.28		
	MLM	121.37	1	439.00	106.00
	ALQ	128.30	1	495.90	103.00
	XYZ	0.00	4	0.00	0.00
A 7606241527	32.00	35N37.08	103W16.68		
	MLM	83.83	1	363.30	256.00
	ALQ	76.52	1	298.80	255.00
	XYZ	0.00	4	0.00	0.00
A 7607121925	54.10	32N48.06	108W04.25		
	NG	82.05	0	163.40	38.00
	GM	82.60	0	168.10	28.00
	WTX	83.35	0	175.60	37.00
	XYZ	0.00	4	0.00	0.00
A 7608042231	35.44	33N03.78	109W20.10		
	WTX	73.70	2	254.40	63.00
	SC	71.93	2	239.70	63.00
	GM	71.55	2	234.20	60.00
	XYZ	0.00	4	0.00	0.00
A 7608161839	42.66	33N05.41	109W21.55		
	GM	78.35	0	229.30	59.00
	SC	78.60	0	234.10	64.00
	NG	79.50	0	240.30	66.00
	WTX	80.55	0	249.10	64.00
	XYZ	0.00	4	0.00	0.00
A 7608161933	09.24	32N48.06	108W04.25		
	NG	37.10	0	163.40	38.00
	GM	37.75	0	168.10	28.00
	WTX	38.45	0	175.60	37.00
	XYZ	0.00	4	0.00	0.00
A 7608162103	16.66	32N39.13	108W22.13		
	SC	47.85	0	192.00	38.00
	NG	48.00	0	193.90	41.00
	GM	48.55	0	196.40	33.00
	WTX	49.45	0	205.70	40.00
	XYZ	0.00	4	0.00	0.00
A 7608232154	30.36	33N05.41	109W21.55		
	GM	65.75	0	229.30	59.00
	SC	66.25	0	234.10	64.00
	NG	67.05	0	240.30	66.00
	WTX	68.25	0	249.10	64.00
	XYZ	0.00	4	0.00	0.00
A 7702142110	50.14	32N48.06	108W04.25		
	CM	78.10	0	164.20	39.00
	IC	78.50	0	165.20	37.00
	WTX	79.35	0	175.60	37.00
	CC	79.90	0	180.10	34.00
	DM	80.65	0	186.50	39.00
	XYZ	0.00	4	0.00	0.00
A 7702142229	28.36	33N05.41	109W21.55		
	SC	64.50	0	234.10	64.00
	IC	65.25	0	241.00	66.00
	CM	65.30	0	242.70	67.00
	WTX	66.25	0	249.10	64.00
	CC	66.00	0	249.80	62.00
	DM	67.70	0	262.30	65.00
	XYZ	0.00	4	0.00	0.00
A 7702142250	28.31	32N39.13	108W22.13		
	SC	59.75	0	192.00	38.00
	CM	59.65	0	194.90	42.00
	IC	59.70	0	195.60	41.00
	WTX	61.10	0	205.70	40.00
	CC	61.65	0	209.90	38.00
	DM	62.50	0	217.10	42.00
	XYZ	0.00	4	0.00	0.00
A 7704112014	42.25	32N39.13	108W22.13		
	SC	73.55	0	192.00	38.00
	CM	73.60	0	194.90	42.00
	GM	74.00	0	196.40	33.00
	CC	75.65	0	209.90	38.00
	DM	76.45	0	217.10	42.00
	XYZ	0.00	4	0.00	0.00
A 7704252157	08.51	33N05.41	109W21.55		
	GM	44.00	0	229.30	59.00
	SC	44.55	0	234.10	64.00
	CM	45.35	0	242.70	67.00
	WTX	46.40	0	249.10	64.00
	CC	46.25	0	249.80	62.00

	DM	47.95	0	262.30	65.00
	XYZ	0.00	4	0.00	0.00
A	7705022014	49.93	32N39.13	108W22.13	
	SC	81.35	0	192.00	38.00
	CM	81.30	0	194.90	42.00
	GM	81.85	0	196.40	33.00
	CC	83.30	0	209.90	38.00
	DM	84.05	0	217.10	42.00
	XYZ	0.00	4	0.00	0.00
A	7705022031	35.67	32N48.06	108W04.25	
	CM	63.65	0	164.20	39.00
	GM	64.15	0	168.10	28.00
	CC	65.45	0	180.10	34.00
	DM	66.15	0	186.50	39.00
	XYZ	0.00	4	0.00	0.00
A	7706081309	07.40	31N01.44	109W13.62	
	WTX	65.02	0	400.50	32.00
	LPM	69.65	0	438.20	33.00
	GM	64.53	0	393.80	28.00
	DM	66.13	0	410.80	33.00
	SC	63.76	0	387.60	31.00
	ALQ	78.00	0	505.60	30.00
	MLM	73.17	1	463.30	25.00
	LAD	69.23	1	432.70	28.00
	XYZ	0.00	4	0.00	0.00
A	7707200740	49.49	35N37.62	109W00.00	
	CC	83.69	0	231.10	131.00
	CM	85.50	0	248.40	134.00
	GM	81.25	0	215.50	131.00
	SC	84.10	0	234.90	131.00
	XYZ	0.00	4	0.00	0.00
A	7806161146	53.20	33N01.20	100W43.20	
	LPM	131.38	1	566.70	285.00
	WTX	134.08	1	590.20	281.00
	XYZ	0.00	4	0.00	0.00
A	7903051300	02.70	36N22.62	106W10.44	
	LPM	40.89	1	233.70	170.00
	LAD	40.10	2	227.10	160.00
	XYZ	0.00	4	0.00	0.00
A	8105032254	09.37	32N16.22	108W56.32	
	LAD	52.07	0	300.30	36.00
	LPM	53.55	0	312.10	43.00
	XYZ	0.00	4	0.00	0.00
A	8105041055	32.17	32N16.22	108W56.32	
	LPM	76.15	0	312.10	43.00
	LAD	74.75	0	300.30	36.00
	XYZ	0.00	4	0.00	0.00
A	8105070138	20.57	32N16.22	108W56.32	
	LAD	63.38	1	300.30	36.00
	LPM	64.71	2	312.10	43.00
	XYZ	0.00	4	0.00	0.00
A	8105112328	12.87	32N16.22	108W56.32	
	LAD	55.55	1	300.30	36.00
	LPM	57.04	2	312.10	43.00
	XYZ	0.00	4	0.00	0.00
A	8210212231	53.82	33N03.78	109W20.10	
	LPM	96.69	0	297.20	60.00
	BAR	95.61	0	289.90	64.00
	WTX	92.04	0	259.90	63.00
	BMT	91.10	0	245.30	57.00
	XYZ	0.00	4	0.00	0.00
A	8210232014	37.06	36N32.40	110W23.16	
	CAR	96.98	1	432.00	130.00
	LPM	94.96	0	413.50	125.00
	BAR	96.64	1	425.50	127.00
	BMT	89.58	1	372.00	131.00
	WTX	94.76	2	408.50	130.00
	XYZ	0.00	4	0.00	0.00
A	8211031754	11.57	35N10.50	108W43.32	
	CAR	45.77	1	237.00	126.00
	BAR	45.13	1	232.00	120.00
	SMC	44.75	0	231.50	134.00
	LPM	43.73	0	221.50	116.00
	WTX	42.53	1	213.50	126.00
	ALQ	42.60	0	208.10	97.00
	SB	41.70	0	205.30	136.00
	XYZ	0.00	4	0.00	0.00
A	8211280236	53.19	33N34.68	100W52.26	
	SMC	131.08	0	570.90	86.00
	LPM	126.08	2	541.80	80.00
	CAR	127.54	1	546.00	84.00
	XYZ	0.00	4	0.00	0.00
A	8301272048	48.49	32N48.06	108W04.25	
	WTX	77.70	1	175.60	37.00
	CAR	78.00	0	178.20	44.00
	BMT	78.70	1	180.00	25.00
	LAZ	80.90	0	197.50	26.00
	BAR	80.60	1	200.20	42.00
	LPM	82.40	1	214.30	38.00
	MLM	86.10	1	239.20	21.00
	XYZ	0.00	4	0.00	0.00
A	8302172050	26.21	36N44.46	108W04.98	
	BMT	68.68	0	283.70	165.00
	SB	72.93	0	317.60	165.00
	XYZ	0.00	4	0.00	0.00
A	8304262234	17.63	35N37.45	109W05.11	
	LAZ	52.40	2	219.30	126.00
	BMT	52.90	2	224.10	132.00
	SB	56.90	2	252.70	136.00
	XYZ	0.00	4	0.00	0.00
A	8306300212	18.53	35N58.44	104W40.56	
	BAR	59.76	0	270.10	138.00
	CAR	62.90	0	292.60	139.00
	XYZ	0.00	4	0.00	0.00
A	8309152325	35.24	35N03.75	104W20.65	
	ALQ	66.70	1	193.50	266.00
	LPM	70.70	2	225.70	248.00
	BAR	71.60	0	233.10	244.00
	CAR	73.90	0	251.70	241.00
	SMC	77.60	2	284.20	240.00
	SB	78.20	0	287.10	245.00
	XYZ	0.00	4	0.00	0.00

A 8309290744	10.45	35N05.41	104W27.31	
LPM	44.70	1	217.40	247.00
BAR	45.10	0	225.40	242.00
CAR	47.30	1	244.40	239.00
BMT	51.10	2	272.50	251.00
XYZ	0.00	4	0.00	0.00
A 8404271005	54.41	32N44.74	109W20.85	
SB	91.20	1	243.40	56.00
SMC	90.90	0	245.20	62.00
MAG	91.70	0	251.70	51.00
WTX	93.70	0	267.50	57.00
SNM	94.00	0	267.60	57.00
CAR	94.70	0	277.70	61.00
LPM	98.30	2	306.30	55.00
XYZ	0.00	4	0.00	0.00
A 8501290537	59.96	35N27.43	111W42.31	
MLM	120.80	2	421.90	100.00
LAZ	121.70	2	433.40	106.00
WTX	125.20	2	461.90	109.00
CAR	127.90	2	485.10	110.00
XYZ	0.00	4	0.00	0.00
A 8506051036	00.00	32N32.55	106W56.44	
CAR	25.20	0	157.50	7.00
BAR	28.40	0	179.80	9.00
MAG	28.60	0	181.70	351.00
LPM	30.30	1	198.40	8.00
LAZ	31.80	0	199.00	1.00
XYZ	0.00	4	0.00	0.00
A 8507230044	49.17	36N37.12	108W28.00	
ALQ	89.30	0	260.00	136.00
LAZ	91.00	1	273.90	154.00
MAG	93.50	1	294.70	158.00
LEM	94.70	2	304.10	154.00
LPM	95.10	2	305.10	147.00
SB	96.40	1	315.70	158.00
XYZ	0.00	4	0.00	0.00
A 8508010144	16.57	36N38.40	110W16.50	
MLM	68.10	0	348.30	126.00
LAZ	71.10	0	377.60	131.00
LPM	76.60	2	419.30	128.00
BAR	78.10	2	431.90	130.00
XYZ	0.00	4	0.00	0.00
A 8509060522	46.10	32N32.55	106W56.44	
CAR	71.40	2	157.50	7.00
BAR	74.50	1	179.80	9.00
MAG	74.70	2	181.70	351.00
XYZ	0.00	4	0.00	0.00
A 8509302021	29.31	32N48.06	108W04.25	
WTX	58.60	0	175.60	37.00
CAR	58.80	0	178.20	44.00
LEM	59.60	0	182.40	34.00
LAZ	61.50	0	197.50	26.00
BAR	61.60	1	200.20	42.00
MLM	66.80	1	239.20	21.00
XYZ	0.00	4	0.00	0.00
A 8512150714	52.43	35N25.69	104W37.58	
ALQ	80.80	0	175.30	252.00
LPM	86.20	0	221.30	236.00
BAR	87.70	1	232.20	232.00
MLM	88.50	0	239.50	253.00
CAR	90.10	0	253.20	230.00
LAZ	90.10	0	256.40	244.00
SB	94.30	2	284.20	235.00
SMC	94.40	0	285.80	230.00
XYZ	0.00	4	0.00	0.00
A 8603272236	35.54	36N27.74	110W07.50	
MLM	83.40	0	326.10	124.00
LAZ	86.20	0	354.70	130.00
LPM	91.60	2	396.80	127.00
XYZ	0.00	4	0.00	0.00
A 8604032032	10.11	32N35.55	108W03.39	
SB	38.80	2	177.00	27.00
MAG	40.80	2	193.70	23.00
CAR	41.40	0	197.60	39.00
LEM	42.20	1	201.40	30.00
BAR	44.30	1	220.20	37.00
LAZ	44.30	0	221.40	23.00
LJY	45.30	2	224.80	29.00
LPM	45.90	1	235.30	34.00
XYZ	0.00	4	0.00	0.00
A 8604172104	29.40	32N32.55	106W56.44	
BAR	57.60	2	179.80	9.00
LAZ	60.90	1	199.00	1.00
XYZ	0.00	4	0.00	0.00
A 8605141503	3.60	37N20.68	110W15.97	
MLM	58.50	0	397.30	135.00
LAZ	62.30	0	431.60	139.00
ALQ	62.70	0	434.40	128.00
LEM	66.30	1	461.50	140.00
XYZ	0.00	4	0.00	0.00
A 8605221642	44.81	35N44.80	108W57.87	
LAZ	80.10	0	223.50	132.00
LEM	83.70	0	252.60	134.00
BAR	86.90	1	278.00	130.00
SMC	87.10	2	281.70	141.00
CAR	87.30	1	285.10	134.00
XYZ	0.00	4	0.00	0.00
A 8605240014	31.76	32N59.21	109W30.93	
SMC	67.50	0	248.30	69.00
MAG	67.50	1	248.90	58.00
WTX	70.00	0	267.40	63.00
LEM	70.10	0	266.80	60.00
LAZ	70.40	2	270.50	55.00
CAR	71.20	0	279.70	67.00
BAR	73.80	1	297.10	64.00
XYZ	0.00	4	0.00	0.00
A 8606120352	16.37	33N04.97	109W28.81	
SB	51.20	0	235.50	65.00
MAG	51.80	0	240.60	60.00
SMC	51.90	0	241.60	71.00
WTX	54.40	2	259.60	65.00
LAZ	54.60	0	261.70	56.00

```
      LEM      54.30      0      261.80      63.00
      CAR      55.40      0      272.80      69.00
      MLM      58.30      2      289.00      48.00
      LPM      58.70      1      297.10      63.00
      XYZ       0.00      4        0.00       0.00
A 8608271727 48.41 32N39.13 108W22.13
      SMC      78.10      0      177.30      45.00
      SB       79.20      1      183.80      37.00
      MAG      80.70      0      198.10      32.00
      WTX      81.40      2      205.70      40.00
      CAR      81.70      0      209.70      47.00
      LEM      82.30      0      212.10      38.00
      LAZ      83.90      0      225.20      30.00
      BAR      84.50      0      231.40      44.00
      LJY      85.20      1      231.60      36.00
      LPM      86.00      0      244.80      41.00
      XYZ       0.00      4        0.00       0.00
A 8608271806 58.46 35N07.10 105W10.64
      CAR      89.00      2      192.80     228.00
      LEM      88.90      1      195.80     237.00
      LAZ      88.90      1      196.40     246.00
      MAG      91.60      2      216.30     241.00
      SB       92.80      1      223.50     235.00
      SMC      92.70      0      225.30     229.00
      XYZ       0.00      4        0.00       0.00
A 8608271834 45.01 33N05.41 109W21.55
      SB       80.20      1      225.00      64.00
      MAG      80.50      0      230.50      59.00
      SMC      80.70      1      230.70      71.00
      WTX      82.90      2      249.10      64.00
      LEM      83.10      0      251.50      62.00
      LAZ      84.00      0      252.10      55.00
      CAR      84.20      0      262.00      69.00
      BAR      86.60      1      279.10      65.00
      LPM      87.40      2      286.80      62.00
      XYZ       0.00      4        0.00       0.00
A 8609081940  5.74 35N46.30 108W49.99
      LAZ      39.30      2      216.70     135.00
      ALQ      43.00      2      234.60     113.00
      SB       43.10      2      250.10     143.00
      SMC      46.90      2      276.50     143.00
      CAR      46.90      1      278.40     136.00
      XYZ       0.00      4        0.00       0.00
A 8612230320 36.10 30N56.49 109W09.23
      SMC      90.70      0      373.20      33.00
      SB       92.30      0      384.10      29.00
      CAR      94.50      0      404.10      34.00
      WTX      94.30      1      404.50      31.00
      LEM      95.50      0      412.00      30.00
      BAR      97.40      2      427.00      34.00
      XYZ       0.00      4        0.00       0.00
A 8612272156 04.51 33N05.41 109W21.55
      SB       39.70      0      225.00      64.00
      MAG      40.20      0      230.50      59.00
      SMC      40.20      0      230.70      71.00
      WTX      42.40      0      249.10      64.00
      LEM      42.70      0      251.50      62.00
      LAZ      43.40      1      252.10      55.00
      CAR      43.80      0      262.00      69.00
      LJY      45.40      1      267.00      59.00
      BAR      46.40      0      279.10      65.00
      LPM      46.90      2      286.80      62.00
      XYZ       0.00      4        0.00       0.00
A 8702011926 55.18 35N39.83 108W57.83
      LAZ      89.20      2      217.60     130.00
      LEM      92.50      1      246.40     132.00
      SMC      96.50      2      274.70     140.00
      XYZ       0.00      4        0.00       0.00
A 8703191220 49.49 35N02.69 109W50.14
      MLM      85.90      1      247.30      96.00
      LAZ      86.40      0      257.10     106.00
      LEM      89.10      0      280.00     110.00
      SMC      90.90      1      294.60     118.00
      LPM      92.40      1      304.40     105.00
      XYZ       0.00      4        0.00       0.00
A 8704012002 15.63 33N08.45 109W33.67
      SB       51.90      0      239.60      67.00
      MAG      52.40      0      243.90      62.00
      SMC      52.60      0      246.60      73.00
      WTX      55.40      0      263.80      67.00
      LAZ      55.70      1      264.30      58.00
      LEM      54.90      0      265.40      65.00
      CAR      56.00      0      277.70      71.00
      BAR      58.00      0      294.00      68.00
      LPM      59.40      2      300.90      64.00
      XYZ       0.00      4        0.00       0.00
A 8704211719 21.91 32N39.13 108W22.13
      SMC      50.90      1      177.30      45.00
      SB       52.40      0      183.80      37.00
      MAG      54.30      0      198.10      32.00
      WTX      54.70      1      205.70      40.00
      CAR      54.80      1      209.70      47.00
      LEM      55.50      1      212.10      38.00
      LAZ      57.20      0      225.20      30.00
      BAR      58.00      0      231.40      44.00
      LPM      59.10      1      244.80      41.00
      MLM      62.70      3      265.30      25.00
      XYZ       0.00      4        0.00       0.00
A 8704212156 08.31 33N05.41 109W21.55
      SB       43.50      0      225.00      64.00
      MAG      44.00      0      230.50      59.00
      SMC      44.00      0      230.70      71.00
      LEM      46.50      0      251.50      62.00
      LAZ      47.20      2      252.10      55.00
      CAR      47.50      1      262.00      69.00
      BAR      50.30      0      279.10      65.00
      MLM      50.40      3      280.00      47.00
      LPM      50.70      2      286.80      62.00
      XYZ       0.00      4        0.00       0.00
A 8704291336 31.14 32N38.26 105W56.20
      BAR      59.00      0      178.80     339.00
      SB       61.20      2      188.20     322.00
```

LPM	60.90	0	196.80	341.00
XYZ	0.00	4	0.00	0.00
A 8706012127	31.50	32N23.64	106W52.09	
BAR	61.40	2	195.10	7.00
LEM	61.60	2	196.70	357.00
XYZ	0.00	4	0.00	0.00
A 8707041357	53.29	33N43.69	108W48.09	
LEM	81.10	0	175.80	74.00
CAR	83.50	1	193.00	83.00
MLM	84.00	1	194.30	52.00
BAR	85.20	1	206.20	77.00
LPM	86.00	2	210.50	72.00
XYZ	0.00	4	0.00	0.00
A 8709101416	23.27	32N22.62	109W02.80	
SMC	60.20	0	245.60	49.00
SB	60.70	0	249.60	43.00
BMT	62.80	0	270.00	37.00
WTX	63.00	0	272.60	45.00
CAR	63.60	0	278.40	50.00
LAZ	64.80	0	287.90	37.00
BAR	66.20	0	299.40	48.00
LPM	67.90	0	311.80	45.00
MLM	70.00	0	324.90	32.00
XYZ	0.00	4	0.00	0.00
A 8709131427	30.50	35N39.17	108W16.30	
SB	62.40	0	211.20	152.00
CAR	64.70	2	235.30	143.00
XYZ	0.00	4	0.00	0.00
A 8710020715	12.46	37N10.39	107W52.15	
MLM	50.10	0	269.80	166.00
LAZ	55.40	2	314.50	168.00
XYZ	0.00	4	0.00	0.00
A 8710021002	50.46	37N10.39	107W52.15	
MLM	87.90	0	269.80	166.00
LAZ	93.30	2	314.50	168.00
XYZ	0.00	4	0.00	0.00
A 8710022050	19.41	37N10.39	107W52.15	
MLM	57.10	0	269.80	166.00
XYZ	0.00	4	0.00	0.00
A 8801310924	36.18	29N53.68	105W11.07	
SMC	100.70	0	464.40	338.00
CAR	102.00	0	473.20	342.00
BAR	104.50	0	490.30	344.00
SB	104.80	0	490.30	337.00
WTX	105.20	0	492.20	340.00
LEM	106.60	2	502.90	340.00
LPM	106.40	1	508.60	344.00
BMT	108.80	0	523.70	338.00
LAZ	110.00	0	532.80	340.00
MLM	116.00	0	575.80	341.00
XYZ	0.00	4	0.00	0.00
A 8802140739	52.61	36N09.96	111W01.10	
BMT	107.10	2	401.40	122.00
LAZ	108.20	0	403.50	119.00
LEM	111.20	1	430.00	121.00
WTX	112.10	1	438.00	122.00
SMC	112.90	0	451.00	126.00
XYZ	0.00	4	0.00	0.00
A 8803182356	39.33	36N27.05	108W41.33	
MLM	75.60	0	229.30	142.00
LAZ	80.00	0	267.40	148.00
BMT	81.20	0	274.10	152.00
LPM	84.10	2	301.90	142.00
SB	85.60	2	307.10	153.00
BAR	86.20	2	317.40	144.00
CAR	88.10	3	329.40	147.00
SMC	88.70	3	333.30	153.00
XYZ	0.00	4	0.00	0.00
A 8803261808	10.71	32N39.13	108W22.13	
SMC	40.00	0	177.30	45.00
SB	41.20	0	183.80	37.00
WTX	43.50	1	205.70	40.00
BMT	44.00	0	207.40	30.00
CAR	43.80	1	209.70	47.00
LAZ	46.00	0	225.20	30.00
BAR	46.60	0	231.40	44.00
LJY	47.20	0	231.60	36.00
LPM	47.90	1	244.80	41.00
MLM	51.10	2	265.30	25.00
XYZ	0.00	4	0.00	0.00
A 8803261827	33.69	32N48.06	108W04.25	
WTX	62.90	1	175.60	37.00
CAR	63.30	1	178.20	44.00
BMT	63.80	0	180.00	25.00
LAZ	65.80	0	197.50	26.00
BAR	65.70	1	200.20	42.00
LJY	66.70	1	202.20	33.00
LPM	67.10	1	214.30	38.00
MLM	71.10	1	239.20	21.00
XYZ	0.00	4	0.00	0.00
A 8803262105	48.18	36N34.00	108W25.93	
LAZ	89.40	1	267.30	154.00
BMT	90.40	1	275.60	157.00
LPM	93.40	1	298.70	147.00
WTX	94.20	3	308.00	154.00
SB	94.70	2	309.20	158.00
BAR	95.40	2	315.00	149.00
SMC	98.20	3	335.00	157.00
XYZ	0.00	4	0.00	0.00
A 8806110858	35.50	30N47.34	109W24.96	
SMC	92.10	0	401.10	34.00
SB	93.90	1	411.20	31.00
SNM	96.00	1	431.80	33.00
WTX	95.90	1	431.90	33.00
CAR	96.00	0	432.10	36.00
BMT	97.00	0	436.50	28.00
LAZ	99.00	0	454.10	28.00
BAR	98.60	0	454.80	35.00
LJY	100.10	2	459.10	31.00
LPM	100.20	1	470.00	34.00
MLM	104.30	0	494.50	25.00
XYZ	0.00	4	0.00	0.00

APPENDIX IV: Velocity Gradient with Depth

APPENDIX IV

The general equation for Z_1, the maximum depth of penetration of a ray emerging at a distance X_1, is (Officer, 1958),

$$Z_1 = \frac{1}{\pi}\int_0^{X_1} \cosh^{-1}\left(\frac{c_1}{\bar{c}}\right) dX, \tag{1}$$

where

$\bar{c}$ is the inverse slope to the T-X plot along the plot from 0 to X_1, and

c_1 is the slope at the distance X_1.

Using the relationship $\operatorname{sech}^{-1}(x) = \cosh^{-1}\left(\frac{1}{x}\right)$, the general equation becomes

$$Z_1 = \frac{1}{\pi}\int_0^{X_1} \operatorname{sech}^{-1}\left(\frac{\bar{c}}{c_1}\right) dX. \tag{2}$$

Given a linear increase in velocity with distance (i.e. $V = V_0 + W_1 X$), a specific equation can now be written:

$$Z_1 = \frac{1}{\pi}\int_0^{X_1} \operatorname{sech}^{-1}\left[\frac{V_0 + W_1 X}{V_0 + W_1 X_1}\right] dX. \tag{3}$$

The general solution to this integral is of the form:

$$\int \operatorname{sech}^{-1}\left(\frac{x}{a}\right) dx = x\operatorname{sech}^{-1}\left(\frac{x}{a}\right) + a\sin^{-1}\left(\frac{x}{a}\right) \quad \text{for } \operatorname{sech}^{-1}\left(\frac{x}{a}\right) > 0. \tag{4}$$

Specifically then, the solution to the equation of interest is:

$$Z_1 = \frac{1}{\pi}\left\{ (V_0 + W_1 X)\operatorname{sech}^{-1}\left[\frac{V_0 + W_1 X}{V_0 + W_1 X_1}\right] + (V_0 + W_1 X_1)\sin^{-1}\left[\frac{V_0 + W_1 X}{V_0 + W_1 X_1}\right]\right\}, \tag{5}$$

evaluated from 0 to X_1. Thus, given a distance X_1 and values for V_0 and W_1,

the maximum depth of penetration of a ray can be computed.

APPENDIX V: Computer Programs

```
      PROGRAM ATIMTER
      DIMENSION B(899),W(899),A(899,97),X(97),DX(97),
     1WB(899),C(97,97),E(899)
      DIMENSION COL(97)
      CHARACTER *5 STA,COLUMN(97),U(97),SRC
      CHARACTER *10 ELIST,FILIN,FILOUT
C      CALL NOTRAP
      WRITE(6,1000)
1000  FORMAT(' TYPE IN NAME OF DATA FILE: '$)
      READ(5,1001)FILIN
1001  FORMAT(A10)
      WRITE(6,1002)
1002  FORMAT(' TYPE IN NAME OF EVENT LIST: '$)
      READ(5,1001)ELIST
      WRITE(6,1003)
1003  FORMAT(' TYPE IN NAME OF OUTPUT FILE: '$)
      READ(5,1001)FILOUT
      OPEN(FILE=FILOUT,UNIT=3)
      REWIND 3
      OPEN(FILE=ELIST,UNIT=1)
      REWIND 1
      I=1
20    READ(1,'(A5)',END=10)COLUMN(I)
      MM=I
      I=I+1
      GOTO 20
10    CLOSE(1)
        DO 9900 I=1,MM
           U(I)=COLUMN(I)
9900    CONTINUE
        I=1
        II=MM
9904    L=I+1
9905    DO 9906 J=L,II
           IF (U(J).EQ.U(I)) GO TO 9907
9906    CONTINUE
        I=I+1
        IF (I.EQ.II) GO TO 9908
        GO TO 9904
9907    II=II-1
        DO 9901 K=J,II
           U(K)=U(K+1)
9901    CONTINUE
        L=J
        GO TO 9905
9908    M=II
      DO 2 K=1,899
      B(K)=0.
      W(K)=0.
      WB(K)=0.
      E(K)=0.
      DO 2 L=1,97
      A(K,L)=0.
2     CONTINUE
      DO 3 I=1,97
      X(I)=0.
```

```
      DX(I)=0.
      DO 3 J=1,97
      C(I,J)=0.
 3    CONTINUE
      I=1
      OPEN(FILE=FILIN,UNIT=1)
      REWIND 1
      DO 100 J=1,MM
      IF (COLUMN(J) (1:1).EQ.'Z')THEN
          READ(1,500)EVTIME
500       FORMAT(13X,F5.2)
60        READ(1,501,END=100)STA,TIME,NUMBER,DIST,AZIM
501       FORMAT(5X,A5,3X,F6.2,5X,I1,5X,F7.2,5X,F7.2)
c          WRITE(6,501)STA,TIME,NUMBER,DIST,AZIM
          IF(STA.EQ.'XYZ')THEN
          GOTO 100
          ENDIF
                SRC=COLUMN(J)
                JJ=J
                DO 9913 K=1,M
                   IF (SRC.EQ.U(K)) THEN
                   JJ=K
                   GO TO 9914
                   ENDIF
9913               CONTINUE
9914      DO 40 L=1,M
          IF (STA.EQ.U(L))THEN
          LL=L
          GOTO 50
          ENDIF
40        CONTINUE
          GOTO 60
50        B(I)=TIME-EVTIME
          GOTO (110,120,130,140,150) NUMBER+1
110       W(I)=1./.03
          GOTO 160
120       W(I)=1./.06
          GOTO 160
130       W(I)=1./.15
          GOTO 160
140       W(I)=1./.3
          GOTO 160
150       W(I)=1./.5
160       A(I,JJ)=1.0
          A(I,LL)=1.0
          A(I,M+1)=DIST
          I=I+1
          GOTO 60
      ENDIF
100   CONTINUE
      CLOSE(1)
      N=I-1
      M=M+1
      WRITE(3,*)N,M
      IF (M.GE.N)THEN
      WRITE(3,201)M,N
```

```
201   FORMAT(' UNDERDETERMINED MATRIX M,N = ',I3,3X,I3)
      CLOSE(3)
      STOP
      ENDIF
      DO 199 I=1,M
199   COL(I)=0.
      DO 198 I=1,M
      DO 198 J=1,N
198   COL(I)=A(J,I)+COL(I)
      DO 197 I=1,M
      IF (COL(I).EQ.0.)THEN
      WRITE(3,196)U(I)
196   FORMAT(' NO ARRIVALS FOR ',A5)
      CLOSE(3)
      STOP
      ENDIF
197   CONTINUE
      DO 200 I=1,N
      WB(I)=W(I)*B(I)
      DO 200 J=1,M
      A(I,J)=W(I)*A(I,J)
200   CONTINUE
      DO 210 J=1,M
      DO 210 I=1,N
      X(J)=A(I,J)*WB(I)+X(J)
210   CONTINUE
      DO 220 I=1,M
      DO 220 J=1,M
      DO 220 K=1,N
      C(I,J)=A(K,I)*A(K,J)+C(I,J)
220   CONTINUE
      CALL INVR(C,M,X,1,DETERM,97,97)
      DO 230 I=1,N
      E(I)=B(I)
      DO 230 J=1,M
      E(I)=E(I)-A(I,J)*X(J)/W(I)
230   CONTINUE
      ERR=0.
      DO 240 I=1,N
240   ERR=ERR+(E(I)*W(I))**2
      WRITE(3,*)ERR
      ERR=ERR/(N-M)
      sds=sqrt(err)
      write(3,241)sds
241   format(/' std. dev. soln.= ',e12.6/)
      DO 250 I=1,M
250   DX(I)=SQRT(ERR*C(I,I))
      X(M)=1./X(M)
      DX(M)=X(M)**2*DX(M)
      U(M)='VEL'
      WRITE(3,504)(U(K),X(K),DX(K),K=1,M)
504   FORMAT(A5,5X,F10.2,5X,F10.2)
      CLOSE(3)
      STOP
      END
      SUBROUTINE INVR(A,N,B,M,DETERM,ISIZE,JSIZE)
```

```
C   INVR - UW MATRIX INVERSION AND SYSTEM OF EQUATION SOLVER
C        INVR SOLVES THE MATRIX EQUATION AX=B AND RETURNS THE INVERSE
C             OF A IN THE STORAGE LOCATIONS OF A
C        SEE UW COMPUTER CENTER WRITEUP W00042 FOR DETAILS OF USAGE,
C             AVAILABLE AT THE COMPUTER CENTER LIBRARY
      DIMENSION IPIVOT(200), A(ISIZE,JSIZE), B(ISIZE,M), INDEX(200,2),
     $ PIVOT(200)
      EQUIVALENCE (IROW,JROW), (ICOLUM,JCOLUM), (AMAX,T,SWAP)
C
  100 DETERM = 1.0
      DO 110 J=1,N
  110 IPIVOT(J) = 0
      DO 300 I=1,N
C
C     SEARCH FOR PIVOT ELEMENT
C
        AMAX = 0.0
        DO 160 J=1,N
          IF (IPIVOT(J)-1) 120,160,120
  120     DO 150 K=1,N
            IF (IPIVOT(K)-1) 130,150,340
  130       IF (ABS(AMAX)-ABS(A(J,K))) 140,150,150
  140       IROW = J
            ICOLUM = K
            AMAX = A(J,K)
  150     CONTINUE
  160   CONTINUE
        IPIVOT(ICOLUM) = IPIVOT(ICOLUM)+1
C
C     INTERCHANGE ROWS TO PUT PIVOT ELEMENT ON DIAGONAL
C
        IF (IROW-ICOLUM) 170,210,170
  170   DETERM = -DETERM
        DO 180 L=1,N
          SWAP = A(IROW,L)
          A(IROW,L) = A(ICOLUM,L)
  180   A(ICOLUM,L) = SWAP
        IF (M) 210,210,190
  190   DO 200 L=1,M
          SWAP = B(IROW,L)
          B(IROW,L) = B(ICOLUM,L)
  200   B(ICOLUM,L) = SWAP
  210   INDEX(I,1) = IROW
        INDEX(I,2) = ICOLUM
        PIVOT(I) = A(ICOLUM,ICOLUM)
        DETERM = DETERM*PIVOT(I)
C
C     DIVIDE PIVOT ROW BY PIVOT ELEMENT
C
        A(ICOLUM,ICOLUM) = 1.0
        DO 220 L=1,N
  220   A(ICOLUM,L) = A(ICOLUM,L)/PIVOT(I)
        IF (M) 250,250,230
  230   DO 240 L=1,M
  240   B(ICOLUM,L) = B(ICOLUM,L)/PIVOT(I)
C
```

```
C     REDUCE NON-PIVOT ROWS
C
 250    DO 300 L1=1,N
          IF (L1-ICOLUM) 260,300,260
 260      T = A(L1,ICOLUM)
          A(L1,ICOLUM) = 0.0
          DO 270 L=1,N
 270      A(L1,L) = A(L1,L)-A(ICOLUM,L)*T
          IF (M) 300,300,280
 280      DO 290 L=1,M
 290      B(L1,L) = B(L1,L)-B(ICOLUM,L)*T
 300  CONTINUE
C
C     INTERCHANGE COLUMNS
C
      DO 330 I=1,N
        L = N+1-I
        IF (INDEX(L,1)-INDEX(L,2)) 310,330,310
 310    JROW = INDEX(L,1)
        JCOLUM = INDEX(L,2)
        DO 320 K=1,N
          SWAP = A(K,JROW)
          A(K,JROW) = A(K,JCOLUM)
          A(K,JCOLUM) = SWAP
 320    CONTINUE
 330  CONTINUE
 340  RETURN
      END
```

```
      PROGRAM ATIMAZI
      DIMENSION B(899),W(899),A(899,97),X(97),DX(97),
     1WB(899),C(97,97),E(899)
      DIMENSION COL(97)
      CHARACTER *5 STA,COLUMN(97),u(97),src
      CHARACTER *10 ELIST,FILIN,FILOUT
C      CALL NOTRAP
      WRITE(6,1000)
1000  FORMAT(' TYPE IN NAME OF DATA FILE: '$)
      READ(5,1001)FILIN
1001  FORMAT(A10)
      WRITE(6,1002)
1002  FORMAT(' TYPE IN NAME OF EVENT LIST: '$)
      READ(5,1001)ELIST
      WRITE(6,1003)
1003  FORMAT(' TYPE IN NAME OF OUTPUT FILE: '$)
      READ(5,1001)FILOUT
      OPEN(FILE=FILOUT,UNIT=3)
      REWIND 3
      OPEN(FILE=ELIST,UNIT=1)
      REWIND 1
      WRITE(6,1004)
1004  FORMAT(' TYPE IN OFFSET DISTANCE: '$)
      READ(5,*)F
      write(3,666)F
 666  format(' Offset Distance: ',f5.2)
      I=1
20    READ(1,'(A5)',END=10)COLUMN(I)
      MM=I
      I=I+1
      GOTO 20
10    CLOSE(1)
        DO 9900 I=1,MM
           U(I)=COLUMN(I)
9900    CONTINUE
        I=1
        II=MM
9904    L=I+1
9905    DO 9906 J=L,II
           IF (U(J).EQ.U(I)) GO TO 9907
9906    CONTINUE
        I=I+1
        IF (I.EQ.II) GO TO 9908
        GO TO 9904
9907    II=II-1
        DO 9901 K=J,II
           U(K)=U(K+1)
9901    CONTINUE
        L=J
        GO TO 9905
9908    M=II
      DO 2 K=1,899
      B(K)=0.
      W(K)=0.
      WB(K)=0.
      E(K)=0.
```

```
      DO 2 L=1,97
      A(K,L)=0.
2     CONTINUE
      DO 3 I=1,97
      X(I)=0.
      DX(I)=0.
      DO 3 J=1,97
      C(I,J)=0.
3     CONTINUE
      I=1
      OPEN(FILE=FILIN,UNIT=1)
      REWIND 1
      DO 100 J=1,MM
      IF (COLUMN(J) (1:1).EQ.'Z')THEN
          READ(1,500)EVTIME
500       FORMAT(13X,F5.2)
60        READ(1,501,END=100)STA,TIME,NUMBER,DIST,AZIM
501       FORMAT(5X,A5,3X,F6.2,5X,I1,5X,F7.2,5X,F7.2)
          IF(STA.EQ.'XYZ')THEN
          GOTO 100
          ENDIF
                SRC=COLUMN(J)
                JJ=J
                DO 9913 K=1,M
                   IF (SRC.EQ.U(K)) THEN
                   JJ=K
                   GO TO 9914
                   ENDIF
9913            CONTINUE
9914      DO 40 L=1,M
          IF (STA.EQ.U(L))THEN
          LL=L
          GOTO 50
          ENDIF
40        CONTINUE
          GOTO 60
50        B(I)=TIME-EVTIME
          GOTO (110,120,130,140,150) NUMBER+1
110       W(I)=1./.03
          GOTO 160
120       W(I)=1./.06
          GOTO 160
130       W(I)=1./.15
          GOTO 160
140       W(I)=1./.3
          GOTO 160
150       W(I)=1./.5
160       A(I,JJ)=1.0
          A(I,LL)=1.0
          A(I,M+1)=DIST
          A(I,M+2)=(2*F-DIST)*SIN(2*AZIM/57.3)
          A(I,M+3)=(2*F-DIST)*COS(2*AZIM/57.3)
          A(I,M+4)=(2*F-DIST)*SIN(4*AZIM/57.3)
          A(I,M+5)=(2*F-DIST)*COS(4*AZIM/57.3)
          I=I+1
          GOTO 60
```

```
      else
          goto 101
      ENDIF
100   CONTINUE
101   CLOSE(1)
      M=M+5
      N=I-1
      WRITE(3,*)N,M
      IF (M.GE.N)THEN
      WRITE(3,201)M,N
201   FORMAT('UNDERDETERMINED MATRIX M,N = ',I3,3X,I3)
      CLOSE(3)
      STOP
      ENDIF
      DO 199 I=1,M
199   COL(I)=0.
      DO 198 I=1,M
      DO 198 J=1,N
198   COL(I)=A(J,I)+COL(I)
      DO 197 I=1,M
      IF (COL(I).EQ.0.)THEN
      WRITE(3,196)U(I)
196   FORMAT('NO ARRIVALS FOR ',A5)
      CLOSE(3)
      STOP
      ENDIF
197   CONTINUE
      DO 200 I=1,N
      WB(I)=W(I)*B(I)
      DO 200 J=1,M
      A(I,J)=W(I)*A(I,J)
200   CONTINUE
      DO 210 J=1,M
      DO 210 I=1,N
      X(J)=A(I,J)*WB(I)+X(J)
210   CONTINUE
      DO 220 I=1,M
      DO 220 J=1,M
      DO 220 K=1,N
      C(I,J)=A(K,I)*A(K,J)+C(I,J)
220   CONTINUE
      CALL INVR(C,M,X,1,DETERM,97,97)
      DO 230 I=1,N
      E(I)=B(I)
      DO 230 J=1,M
      E(I)=E(I)-A(I,J)*X(J)/W(I)
230   CONTINUE
      ERR=0.
      DO 240 I=1,N
240   ERR=ERR+(E(I)*W(I))**2
      WRITE(3,*)ERR
      ERR=ERR/(N-M)
      sds=sqrt(err)
      write(3,241)sds
241   format(/' std. dev. soln.= ',e12.6/)
      DO 250 I=1,M
```

```
250   DX(I)=SQRT(ERR*C(I,I))
      U(M-4)='VEL'
      U(M-3)=' A '
      U(M-2)=' B '
      U(M-1)=' C '
      U(M)=' D '
      WRITE(3,504)(U(K),X(K),DX(K),K=1,M-5)
504   FORMAT(A5,5X,F10.2,5X,F10.2)
      WRITE(3,509) (U(K),X(K),DX(K),K=M-4,M)
509   FORMAT(A5,5X,G11.5,5X,G11.5)
      DO 300 I=M-4,M-1
      DO 300 J=I+1,M
      WRITE(3,511)I,J,ERR*C(I,J)
511   FORMAT(I3,5X,I3,5X,G11.5)
300   CONTINUE
      X(M-4)=1/X(M-4)
      DX(M-4)=X(M-4)**2*DX(M-4)
      DO 310 K=M-3,M
      DX(K)=SQRT(X(M-4)**4*DX(K)**2+4*(X(M-4)*X(K)*DX(M-4))**2+
     14*X(M-4)**3*X(K)*ERR*C(M-4,K))
310   X(K)=X(M-4)**2*X(K)
      WRITE(3,509) (U(K),X(K),DX(K),K=M-4,M)
      CLOSE(3)
      STOP
      END
      SUBROUTINE INVR(A,N,B,M,DETERM,ISIZE,JSIZE)
C   INVR - UW MATRIX INVERSION AND SYSTEM OF EQUATION SOLVER
C        INVR SOLVES THE MATRIX EQUATION AX=B AND RETURNS THE INVERSE
C             OF A IN THE STORAGE LOCATIONS OF A
C        SEE UW COMPUTER CENTER WRITEUP W00042 FOR DETAILS OF USAGE,
C             AVAILABLE AT THE COMPUTER CENTER LIBRARY
      DIMENSION IPIVOT(200), A(ISIZE,JSIZE), B(ISIZE,M), INDEX(200,2),
     $ PIVOT(200)
      EQUIVALENCE (IROW,JROW), (ICOLUM,JCOLUM), (AMAX,T,SWAP)
C
 100  DETERM = 1.0
      DO 110 J=1,N
 110  IPIVOT(J) = 0
      DO 300 I=1,N
C
C     SEARCH FOR PIVOT ELEMENT
C
        AMAX = 0.0
        DO 160 J=1,N
          IF (IPIVOT(J)-1) 120,160,120
 120      DO 150 K=1,N
            IF (IPIVOT(K)-1) 130,150,340
 130        IF (ABS(AMAX)-ABS(A(J,K))) 140,150,150
 140        IROW = J
            ICOLUM = K
            AMAX = A(J,K)
 150      CONTINUE
 160    CONTINUE
        IPIVOT(ICOLUM) = IPIVOT(ICOLUM)+1
C
C     INTERCHANGE ROWS TO PUT PIVOT ELEMENT ON DIAGONAL
```

```
C
      IF (IROW-ICOLUM) 170,210,170
 170  DETERM = -DETERM
      DO 180 L=1,N
        SWAP = A(IROW,L)
        A(IROW,L) = A(ICOLUM,L)
 180  A(ICOLUM,L) = SWAP
      IF (M) 210,210,190
 190  DO 200 L=1,M
        SWAP = B(IROW,L)
        B(IROW,L) = B(ICOLUM,L)
 200  B(ICOLUM,L) = SWAP
 210  INDEX(I,1) = IROW
      INDEX(I,2) = ICOLUM
      PIVOT(I) = A(ICOLUM,ICOLUM)
      DETERM = DETERM*PIVOT(I)
C
C     DIVIDE PIVOT ROW BY PIVOT ELEMENT
C
      A(ICOLUM,ICOLUM) = 1.0
      DO 220 L=1,N
 220  A(ICOLUM,L) = A(ICOLUM,L)/PIVOT(I)
      IF (M) 250,250,230
 230  DO 240 L=1,M
 240  B(ICOLUM,L) = B(ICOLUM,L)/PIVOT(I)
C
C     REDUCE NON-PIVOT ROWS
C
 250  DO 300 L1=1,N
        IF (L1-ICOLUM) 260,300,260
 260    T = A(L1,ICOLUM)
        A(L1,ICOLUM) = 0.0
        DO 270 L=1,N
 270    A(L1,L) = A(L1,L)-A(ICOLUM,L)*T
        IF (M) 300,300,280
 280    DO 290 L=1,M
 290    B(L1,L) = B(L1,L)-B(ICOLUM,L)*T
 300  CONTINUE
C
C     INTERCHANGE COLUMNS
C
      DO 330 I=1,N
        L = N+1-I
        IF (INDEX(L,1)-INDEX(L,2)) 310,330,310
 310    JROW = INDEX(L,1)
        JCOLUM = INDEX(L,2)
        DO 320 K=1,N
          SWAP = A(K,JROW)
          A(K,JROW) = A(K,JCOLUM)
          A(K,JCOLUM) = SWAP
 320    CONTINUE
 330  CONTINUE
 340  RETURN
      END
```

```
      PROGRAM ATIMDIS
      DIMENSION B(899),W(899),A(899,97),X(97),DX(97),
     1WB(899),C(97,97),E(899)
      DIMENSION COL(97)
      CHARACTER *5 STA,COLUMN(97),u(97),src
      CHARACTER *10 ELIST,FILIN,FILOUT
c      CALL NOTRAP
      WRITE(6,1000)
1000  FORMAT(' TYPE IN NAME OF DATA FILE: '$)
      READ(5,1001)FILIN
1001  FORMAT(A10)
      WRITE(6,1002)
1002  FORMAT(' TYPE IN NAME OF EVENT LIST: '$)
      READ(5,1001)ELIST
      WRITE(6,1003)
1003  FORMAT(' TYPE IN NAME OF OUTPUT FILE: '$)
      READ(5,1001)FILOUT
      OPEN(FILE=FILOUT,UNIT=3)
      REWIND 3
      OPEN(FILE=ELIST,UNIT=1)
      REWIND 1
      WRITE(6,1004)
1004  FORMAT(' TYPE IN OFFSET DISTANCE: '$)
      READ(5,*)F
      write(3,666)F
 666  format(' Offset Distance: ',f5.2)
      I=1
20    READ(1,'(A5)',END=10)COLUMN(I)
      MM=I
      I=I+1
      GOTO 20
10    CLOSE(1)
        DO 9900 I=1,MM
           U(I)=COLUMN(I)
9900    CONTINUE
        I=1
        II=MM
9904    L=I+1
9905    DO 9906 J=L,II
           IF (U(J).EQ.U(I)) GO TO 9907
9906    CONTINUE
        I=I+1
        IF (I.EQ.II) GO TO 9908
        GO TO 9904
9907    II=II-1
        DO 9901 K=J,II
           U(K)=U(K+1)
9901    CONTINUE
        L=J
        GO TO 9905
9908    M=II
      DO 2 K=1,899
      B(K)=0.
      W(K)=0.
      WB(K)=0.
      E(K)=0.
```

```
      DO 2 L=1,97
      A(K,L)=0.
2     CONTINUE
      DO 3 I=1,97
      X(I)=0.
      DX(I)=0.
      DO 3 J=1,97
      C(I,J)=0.
3     CONTINUE
      I=1
      OPEN(FILE=FILIN,UNIT=1)
      REWIND 1
      DO 100 J=1,MM
      IF (COLUMN(J) (1:1).EQ.'Z')THEN
          READ(1,500)EVTIME
500       FORMAT(13X,F5.2)
60        READ(1,501,END=100)STA,TIME,NUMBER,DIST,AZIM
501       FORMAT(5X,A5,3X,F6.2,5X,I1,5X,F7.2,5X,F7.2)
          IF(STA.EQ.'XYZ')THEN
          GOTO 100
          ENDIF
                SRC=COLUMN(J)
                JJ=J
                DO 9913 K=1,M
                   IF (SRC.EQ.U(K)) THEN
                   JJ=K
                   GO TO 9914
                   ENDIF
9913            CONTINUE
9914      DO 40 L=1,M
          IF (STA.EQ.U(L))THEN
          LL=L
          GOTO 50
          ENDIF
40        CONTINUE
          GOTO 60
50        B(I)=TIME-EVTIME
          GOTO (110,120,130,140,150) NUMBER+1
110       W(I)=1./.03
          GOTO 160
120       W(I)=1./.06
          GOTO 160
130       W(I)=1./.15
          GOTO 160
140       W(I)=1./.3
          GOTO 160
150       W(I)=1./.5
160       A(I,JJ)=1.0
          A(I,LL)=1.0
          A(I,M+1)=DIST
          A(I,M+2)=(2*F-DIST)*DIST
          I=I+1
          GOTO 60
      else
          goto 101
      ENDIF
```

```
100   CONTINUE
101   CLOSE(1)
      M=M+2
      N=I-1
      WRITE(3,*)N,M
      IF (M.GE.N)THEN
      WRITE(3,201)M,N
201   FORMAT('UNDERDETERMINED MATRIX M,N = ',I3,3X,I3)
      CLOSE(3)
      STOP
      ENDIF
      DO 199 I=1,M
199   COL(I)=0.
      DO 198 I=1,M
      DO 198 J=1,N
198   COL(I)=A(J,I)+COL(I)
      DO 197 I=1,M
      IF (COL(I).EQ.0.)THEN
      WRITE(3,196)U(I)
196   FORMAT('NO ARRIVALS FOR ',A5)
      CLOSE(3)
      STOP
      ENDIF
197   CONTINUE
      DO 200 I=1,N
      WB(I)=W(I)*B(I)
      DO 200 J=1,M
      A(I,J)=W(I)*A(I,J)
200   CONTINUE
      DO 210 J=1,M
      DO 210 I=1,N
      X(J)=A(I,J)*WB(I)+X(J)
210   CONTINUE
      DO 220 I=1,M
      DO 220 J=1,M
      DO 220 K=1,N
      C(I,J)=A(K,I)*A(K,J)+C(I,J)
220   CONTINUE
      CALL INVR(C,M,X,1,DETERM,97,97)
      DO 230 I=1,N
      E(I)=B(I)
      DO 230 J=1,M
      E(I)=E(I)-A(I,J)*X(J)/W(I)
230   CONTINUE
      ERR=0.
      DO 240 I=1,N
240   ERR=ERR+(E(I)*W(I))**2
      WRITE(3,*)ERR
      ERR=ERR/(N-M)
      sds=sqrt(err)
      write(3,241)sds
241   format(/' std. dev. soln.= ',e12.6/)
      DO 250 I=1,M
250   DX(I)=SQRT(ERR*C(I,I))
      U(M-1)='VEL'
      U(M)='V1 '
```

```
      WRITE(3,504)(U(K),X(K),DX(K),K=1,M-2)
504   FORMAT(A5,5X,F10.2,5X,F10.2)
      WRITE(3,507) (U(K),X(K),DX(K),K=M-1,M)
507   FORMAT(A5,5X,G11.5,5X,G11.5)
      WRITE(3,508) ERR*C(M-1,M)
508   FORMAT('COV = ',G11.5)
      X(M-1)=1/X(M-1)
      DX(M-1)=X(M-1)**2*DX(M-1)
      DX(M)=SQRT(X(M-1)**4*DX(M)**2+4*(X(M-1)*X(M)*DX(M-1))**2+
     14*X(M-1)**3*X(M)*ERR*C(M-1,M))
      X(M)=X(M-1)**2*X(M)
      WRITE(3,507) (U(K),X(K),DX(K),K=M-1,M)
      CLOSE(3)
      STOP
      END
      SUBROUTINE INVR(A,N,B,M,DETERM,ISIZE,JSIZE)
C    INVR - UW MATRIX INVERSION AND SYSTEM OF EQUATION SOLVER
C         INVR SOLVES THE MATRIX EQUATION AX=B AND RETURNS THE INVERSE
C              OF A IN THE STORAGE LOCATIONS OF A
C         SEE UW COMPUTER CENTER WRITEUP W00042 FOR DETAILS OF USAGE,
C              AVAILABLE AT THE COMPUTER CENTER LIBRARY
      DIMENSION IPIVOT(200), A(ISIZE,JSIZE), B(ISIZE,M), INDEX(200,2),
     $ PIVOT(200)
      EQUIVALENCE (IROW,JROW), (ICOLUM,JCOLUM), (AMAX,T,SWAP)
C
 100  DETERM = 1.0
      DO 110 J=1,N
 110  IPIVOT(J) = 0
      DO 300 I=1,N
C
C     SEARCH FOR PIVOT ELEMENT
C
        AMAX = 0.0
        DO 160 J=1,N
          IF (IPIVOT(J)-1) 120,160,120
 120      DO 150 K=1,N
            IF (IPIVOT(K)-1) 130,150,340
 130        IF (ABS(AMAX)-ABS(A(J,K))) 140,150,150
 140        IROW = J
            ICOLUM = K
            AMAX = A(J,K)
 150      CONTINUE
 160    CONTINUE
        IPIVOT(ICOLUM) = IPIVOT(ICOLUM)+1
C
C     INTERCHANGE ROWS TO PUT PIVOT ELEMENT ON DIAGONAL
C
        IF (IROW-ICOLUM) 170,210,170
 170    DETERM = -DETERM
        DO 180 L=1,N
          SWAP = A(IROW,L)
          A(IROW,L) = A(ICOLUM,L)
 180    A(ICOLUM,L) = SWAP
        IF (M) 210,210,190
 190    DO 200 L=1,M
          SWAP = B(IROW,L)
```

```
            B(IROW,L) = B(ICOLUM,L)
  200       B(ICOLUM,L) = SWAP
  210       INDEX(I,1) = IROW
            INDEX(I,2) = ICOLUM
            PIVOT(I) = A(ICOLUM,ICOLUM)
            DETERM = DETERM*PIVOT(I)
C
C     DIVIDE PIVOT ROW BY PIVOT ELEMENT
C
            A(ICOLUM,ICOLUM) = 1.0
            DO 220 L=1,N
  220       A(ICOLUM,L) = A(ICOLUM,L)/PIVOT(I)
            IF (M) 250,250,230
  230       DO 240 L=1,M
  240       B(ICOLUM,L) = B(ICOLUM,L)/PIVOT(I)
C
C     REDUCE NON-PIVOT ROWS
C
  250       DO 300 L1=1,N
              IF (L1-ICOLUM) 260,300,260
  260         T = A(L1,ICOLUM)
              A(L1,ICOLUM) = 0.0
              DO 270 L=1,N
  270         A(L1,L) = A(L1,L)-A(ICOLUM,L)*T
              IF (M) 300,300,280
  280         DO 290 L=1,M
  290         B(L1,L) = B(L1,L)-B(ICOLUM,L)*T
  300   CONTINUE
C
C     INTERCHANGE COLUMNS
C
        DO 330 I=1,N
          L = N+1-I
          IF (INDEX(L,1)-INDEX(L,2)) 310,330,310
  310     JROW = INDEX(L,1)
          JCOLUM = INDEX(L,2)
          DO 320 K=1,N
            SWAP = A(K,JROW)
            A(K,JROW) = A(K,JCOLUM)
            A(K,JCOLUM) = SWAP
  320     CONTINUE
  330   CONTINUE
  340   RETURN
        END
```

```
      PROGRAM TIMTERM
      DIMENSION B(899),W(899),A(899,97),X(97),DX(97),
     1WB(899),C(97,97),E(899)
      DIMENSION COL(97)
      CHARACTER *5 STA,COLUMN(97),U(97),SRC
      CHARACTER *10 ELIST,FILIN,FILOUT
C      CALL NOTRAP
      WRITE(6,1000)
1000  FORMAT(' TYPE IN NAME OF DATA FILE: '$)
      READ(5,1001)FILIN
1001  FORMAT(A10)
      WRITE(6,1002)
1002  FORMAT(' TYPE IN NAME OF EVENT LIST: '$)
      READ(5,1001)ELIST
      WRITE(6,1003)
1003  FORMAT(' TYPE IN NAME OF OUTPUT FILE: '$)
      READ(5,1001)FILOUT
      OPEN(FILE=FILOUT,UNIT=3)
      REWIND 3
      OPEN(FILE=ELIST,UNIT=1)
      REWIND 1
      I=1
20    READ(1,'(A5)',END=10)COLUMN(I)
      MM=I
      I=I+1
      GOTO 20
10    CLOSE(1)
        DO 9900 I=1,MM
           U(I)=COLUMN(I)
9900    CONTINUE
        I=1
        II=MM
9904    L=I+1
9905    DO 9906 J=L,II
           IF (U(J).EQ.U(I)) GO TO 9907
9906    CONTINUE
        I=I+1
        IF (I.EQ.II) GO TO 9908
        GO TO 9904
9907    II=II-1
        DO 9901 K=J,II
           U(K)=U(K+1)
9901    CONTINUE
        L=J
        GO TO 9905
9908    M=II
      DO 2 K=1,899
      B(K)=0.
      W(K)=0.
      WB(K)=0.
      E(K)=0.
      DO 2 L=1,97
      A(K,L)=0.
2     CONTINUE
      DO 3 I=1,97
      X(I)=0.
```

```
      DX(I)=0.
      DO 3 J=1,97
      C(I,J)=0.
3     CONTINUE
      I=1
      OPEN(FILE=FILIN,UNIT=1)
      REWIND 1
      DO 100 J=1,MM
      IF (COLUMN(J) (1:1).EQ.'Z')THEN
          READ(1,500)EVTIME
500       FORMAT(13X,F5.2)
60        READ(1,501,END=100)STA,TIME,NUMBER,DIST,AZIM
501       FORMAT(5X,A5,3X,F6.2,5X,I1,5X,F7.2,5X,F7.2)
c          WRITE(6,501)STA,TIME,NUMBER,DIST,AZIM
          IF(STA.EQ.'XYZ')THEN
          GOTO 100
          ENDIF
                SRC=COLUMN(J)
                JJ=J
                DO 9913 K=1,M
                   IF (SRC.EQ.U(K)) THEN
                   JJ=K
                   GO TO 9914
                   ENDIF
9913               CONTINUE
9914        DO 40 L=1,M
            IF (STA.EQ.U(L))THEN
            LL=L
            GOTO 50
            ENDIF
40          CONTINUE
            GOTO 60
50          B(I)=TIME-EVTIME
            GOTO (110,120,130,140,150) NUMBER+1
110         W(I)=1./.03
            GOTO 160
120         W(I)=1./.06
            GOTO 160
130         W(I)=1./.15
            GOTO 160
140         W(I)=1./.3
            GOTO 160
150         W(I)=1./.5
160         A(I,JJ)=1.0
            IF (LL.NE.M)THEN
            A(I,LL)=1.0
            ENDIF
            A(I,M)=DIST
            I=I+1
            GOTO 60
      ENDIF
100   CONTINUE
      CLOSE(1)
      N=I-1
      WRITE(3,*)N,M
      IF (M.GE.N)THEN
```

```
      WRITE(3,201)M,N
201   FORMAT(' UNDERDETERMINED MATRIX M,N = ',I3,3X,I3)
      CLOSE(3)
      STOP
      ENDIF
      DO 199 I=1,M
199   COL(I)=0.
      DO 198 I=1,M
      DO 198 J=1,N
198   COL(I)=A(J,I)+COL(I)
      DO 197 I=1,M
      IF (COL(I).EQ.0.)THEN
      WRITE(3,196)U(I)
196   FORMAT(' NO ARRIVALS FOR ',A5)
      CLOSE(3)
      STOP
      ENDIF
197   CONTINUE
      DO 200 I=1,N
      WB(I)=W(I)*B(I)
      DO 200 J=1,M
      A(I,J)=W(I)*A(I,J)
200   CONTINUE
      DO 210 J=1,M
      DO 210 I=1,N
      X(J)=A(I,J)*WB(I)+X(J)
210   CONTINUE
      DO 220 I=1,M
      DO 220 J=1,M
      DO 220 K=1,N
      C(I,J)=A(K,I)*A(K,J)+C(I,J)
220   CONTINUE
      CALL INVR(C,M,X,1,DETERM,97,97)
      DO 230 I=1,N
      E(I)=B(I)
      DO 230 J=1,M
      E(I)=E(I)-A(I,J)*X(J)/W(I)
230   CONTINUE
      ERR=0.
      DO 240 I=1,N
240   ERR=ERR+(E(I)*W(I))**2
      WRITE(3,*)ERR
      ERR=ERR/(N-M)
      sds=sqrt(err)
      write(3,241)sds
241   format(/' std. dev. soln.= ',e12.6/)
      DO 250 I=1,M
250   DX(I)=SQRT(ERR*C(I,I))
      X(M)=1./X(M)
      DX(M)=X(M)**2*DX(M)
      WRITE(3,505)U(M)
505   FORMAT(A5,' SET TO ZERO')
      U(M)='VEL'
      WRITE(3,504)(U(K),X(K),DX(K),K=1,M)
504   FORMAT(A5,5X,F10.2,5X,F10.2)
      CLOSE(3)
```

```
      STOP
      END
      SUBROUTINE INVR(A,N,B,M,DETERM,ISIZE,JSIZE)
C   INVR - UW MATRIX INVERSION AND SYSTEM OF EQUATION SOLVER
C        INVR SOLVES THE MATRIX EQUATION AX=B AND RETURNS THE INVERSE
C             OF A IN THE STORAGE LOCATIONS OF A
C        SEE UW COMPUTER CENTER WRITEUP W00042 FOR DETAILS OF USAGE,
C             AVAILABLE AT THE COMPUTER CENTER LIBRARY
      DIMENSION IPIVOT(200), A(ISIZE,JSIZE), B(ISIZE,M), INDEX(200,2),
     $ PIVOT(200)
      EQUIVALENCE (IROW,JROW), (ICOLUM,JCOLUM), (AMAX,T,SWAP)
C
  100 DETERM = 1.0
      DO 110 J=1,N
  110 IPIVOT(J) = 0
      DO 300 I=1,N
C
C     SEARCH FOR PIVOT ELEMENT
C
        AMAX = 0.0
        DO 160 J=1,N
          IF (IPIVOT(J)-1) 120,160,120
  120     DO 150 K=1,N
            IF (IPIVOT(K)-1) 130,150,340
  130       IF (ABS(AMAX)-ABS(A(J,K))) 140,150,150
  140       IROW = J
            ICOLUM = K
            AMAX = A(J,K)
  150     CONTINUE
  160   CONTINUE
        IPIVOT(ICOLUM) = IPIVOT(ICOLUM)+1
C
C     INTERCHANGE ROWS TO PUT PIVOT ELEMENT ON DIAGONAL
C
        IF (IROW-ICOLUM) 170,210,170
  170   DETERM = -DETERM
        DO 180 L=1,N
          SWAP = A(IROW,L)
          A(IROW,L) = A(ICOLUM,L)
  180   A(ICOLUM,L) = SWAP
        IF (M) 210,210,190
  190   DO 200 L=1,M
          SWAP = B(IROW,L)
          B(IROW,L) = B(ICOLUM,L)
  200   B(ICOLUM,L) = SWAP
  210   INDEX(I,1) = IROW
        INDEX(I,2) = ICOLUM
        PIVOT(I) = A(ICOLUM,ICOLUM)
        DETERM = DETERM*PIVOT(I)
C
C     DIVIDE PIVOT ROW BY PIVOT ELEMENT
C
        A(ICOLUM,ICOLUM) = 1.0
        DO 220 L=1,N
  220   A(ICOLUM,L) = A(ICOLUM,L)/PIVOT(I)
        IF (M) 250,250,230
```

```
 230    DO 240 L=1,M
 240    B(ICOLUM,L) = B(ICOLUM,L)/PIVOT(I)
C
C     REDUCE NON-PIVOT ROWS
C
 250    DO 300 L1=1,N
          IF (L1-ICOLUM) 260,300,260
 260      T = A(L1,ICOLUM)
          A(L1,ICOLUM) = 0.0
          DO 270 L=1,N
 270      A(L1,L) = A(L1,L)-A(ICOLUM,L)*T
          IF (M) 300,300,280
 280      DO 290 L=1,M
 290      B(L1,L) = B(L1,L)-B(ICOLUM,L)*T
 300  CONTINUE
C
C     INTERCHANGE COLUMNS
C
      DO 330 I=1,N
        L = N+1-I
        IF (INDEX(L,1)-INDEX(L,2)) 310,330,310
 310    JROW = INDEX(L,1)
        JCOLUM = INDEX(L,2)
        DO 320 K=1,N
          SWAP = A(K,JROW)
          A(K,JROW) = A(K,JCOLUM)
          A(K,JCOLUM) = SWAP
 320    CONTINUE
 330  CONTINUE
 340  RETURN
      END
```

```
      PROGRAM TIMAZI
      DIMENSION B(899),W(899),A(899,97),X(97),DX(97),
     1WB(899),C(97,97),E(899)
      DIMENSION COL(97)
      CHARACTER *5 STA,COLUMN(97),u(97),src
      CHARACTER *10 ELIST,FILIN,FILOUT
C      CALL NOTRAP
      WRITE(6,1000)
1000  FORMAT(' TYPE IN NAME OF DATA FILE: '$)
      READ(5,1001)FILIN
1001  FORMAT(A10)
      WRITE(6,1002)
1002  FORMAT(' TYPE IN NAME OF EVENT LIST: '$)
      READ(5,1001)ELIST
      WRITE(6,1003)
1003  FORMAT(' TYPE IN NAME OF OUTPUT FILE: '$)
      READ(5,1001)FILOUT
      OPEN(FILE=FILOUT,UNIT=3)
      REWIND 3
      OPEN(FILE=ELIST,UNIT=1)
      REWIND 1
      WRITE(6,1004)
1004  FORMAT(' TYPE IN OFFSET DISTANCE: '$)
      READ(5,*)F
      write(3,666)F
 666  format(' Offset Distance: ',f5.2)
      I=1
20    READ(1,'(A5)',END=10)COLUMN(I)
      MM=I
      I=I+1
      GOTO 20
10    CLOSE(1)
        DO 9900 I=1,MM
           U(I)=COLUMN(I)
9900    CONTINUE
        I=1
        II=MM
9904    L=I+1
9905    DO 9906 J=L,II
           IF (U(J).EQ.U(I)) GO TO 9907
9906    CONTINUE
        I=I+1
        IF (I.EQ.II) GO TO 9908
        GO TO 9904
9907    II=II-1
        DO 9901 K=J,II
           U(K)=U(K+1)
9901    CONTINUE
        L=J
        GO TO 9905
9908    M=II
      DO 2 K=1,899
      B(K)=0.
      W(K)=0.
      WB(K)=0.
      E(K)=0.
```

```
      DO 2 L=1,97
      A(K,L)=0.
2     CONTINUE
      DO 3 I=1,97
      X(I)=0.
      DX(I)=0.
      DO 3 J=1,97
      C(I,J)=0.
3     CONTINUE
      I=1
      OPEN(FILE=FILIN,UNIT=1)
      REWIND 1
      DO 100 J=1,MM
      IF (COLUMN(J) (1:1).EQ.'Z')THEN
          READ(1,500)EVTIME
500       FORMAT(13X,F5.2)
60        READ(1,501,END=100)STA,TIME,NUMBER,DIST,AZIM
501       FORMAT(5X,A5,3X,F6.2,5X,I1,5X,F7.2,5X,F7.2)
          IF(STA.EQ.'XYZ')THEN
          GOTO 100
          ENDIF
                SRC=COLUMN(J)
                JJ=J
                DO 9913 K=1,M
                   IF (SRC.EQ.U(K)) THEN
                   JJ=K
                   GO TO 9914
                   ENDIF
9913            CONTINUE
9914      DO 40 L=1,M
          IF (STA.EQ.U(L))THEN
          LL=L
          GOTO 50
          ENDIF
40        CONTINUE
          GOTO 60
50        B(I)=TIME-EVTIME
          GOTO (110,120,130,140,150) NUMBER+1
110       W(I)=1./.03
          GOTO 160
120       W(I)=1./.06
          GOTO 160
130       W(I)=1./.15
          GOTO 160
140       W(I)=1./.3
          GOTO 160
150       W(I)=1./.5
160       A(I,JJ)=1.0
          IF (LL.NE.M)THEN
          A(I,LL)=1.0
          ENDIF
          A(I,M)=DIST
          A(I,M+1)=(2*F-DIST)*SIN(2*AZIM/57.3)
          A(I,M+2)=(2*F-DIST)*COS(2*AZIM/57.3)
          A(I,M+3)=(2*F-DIST)*SIN(4*AZIM/57.3)
          A(I,M+4)=(2*F-DIST)*COS(4*AZIM/57.3)
```

```
          I=I+1
          GOTO 60
        ENDIF
100     CONTINUE
        CLOSE(1)
        M=M+4
        N=I-1
        WRITE(3,*)N,M
        IF (M.GE.N)THEN
        WRITE(3,201)M,N
201     FORMAT(' UNDERDETERMINED MATRIX M,N = ',I3,3X,I3)
        CLOSE(3)
        STOP
        ENDIF
        DO 199 I=1,M
199     COL(I)=0.
        DO 198 I=1,M
        DO 198 J=1,N
198     COL(I)=A(J,I)+COL(I)
        DO 197 I=1,M
        IF (COL(I).EQ.0.)THEN
        WRITE(3,196)U(I)
196     FORMAT(' NO ARRIVALS FOR ',A5)
        CLOSE(3)
        STOP
        ENDIF
197     CONTINUE
        DO 200 I=1,N
        WB(I)=W(I)*B(I)
        DO 200 J=1,M
        A(I,J)=W(I)*A(I,J)
200     CONTINUE
        DO 210 J=1,M
        DO 210 I=1,N
        X(J)=A(I,J)*WB(I)+X(J)
210     CONTINUE
        DO 220 I=1,M
        DO 220 J=1,M
        DO 220 K=1,N
        C(I,J)=A(K,I)*A(K,J)+C(I,J)
220     CONTINUE
        CALL INVR(C,M,X,1,DETERM,97,97)
        DO 230 I=1,N
        E(I)=B(I)
        DO 230 J=1,M
        E(I)=E(I)-A(I,J)*X(J)/W(I)
230     CONTINUE
        ERR=0.
        DO 240 I=1,N
240     ERR=ERR+(E(I)*W(I))**2
        WRITE(3,*)ERR
        ERR=ERR/(N-M)
        sds=sqrt(err)
        write(3,241)sds
241     format(/' std. dev. soln.= ',e12.6/)
        DO 250 I=1,M
```

```
250   DX(I)=SQRT(ERR*C(I,I))
      WRITE(3,505)U(M-4)
505   FORMAT(A5,' SET TO ZERO')
      U(M-4)='VEL'
      U(M-3)=' A '
      U(M-2)=' B '
      U(M-1)=' C '
      U(M)=' D '
      WRITE(3,504)(U(K),X(K),DX(K),K=1,M-5)
504   FORMAT(A5,5X,F10.2,5X,F10.2)
      WRITE(3,509) (U(K),X(K),DX(K),K=M-4,M)
509   FORMAT(A5,5X,G11.5,5X,G11.5)
      DO 300 I=M-4,M-1
      DO 300 J=I+1,M
      WRITE(3,511)I,J,ERR*C(I,J)
511   FORMAT(I3,5X,I3,5X,G11.5)
300   CONTINUE
      X(M-4)=1/X(M-4)
      DX(M-4)=X(M-4)**2*DX(M-4)
      DO 310 K=M-3,M
      DX(K)=SQRT(X(M-4)**4*DX(K)**2+4*(X(M-4)*X(K)*DX(M-4))**2+
     14*X(M-4)**3*X(K)*ERR*C(M-4,K))
310   X(K)=X(M-4)**2*X(K)
      WRITE(3,509) (U(K),X(K),DX(K),K=M-4,M)
      CLOSE(3)
      STOP
      END
      SUBROUTINE INVR(A,N,B,M,DETERM,ISIZE,JSIZE)
C   INVR - UW MATRIX INVERSION AND SYSTEM OF EQUATION SOLVER
C        INVR SOLVES THE MATRIX EQUATION AX=B AND RETURNS THE INVERSE
C             OF A IN THE STORAGE LOCATIONS OF A
C        SEE UW COMPUTER CENTER WRITEUP W00042 FOR DETAILS OF USAGE,
C             AVAILABLE AT THE COMPUTER CENTER LIBRARY
      DIMENSION IPIVOT(200), A(ISIZE,JSIZE), B(ISIZE,M), INDEX(200,2),
     $ PIVOT(200)
      EQUIVALENCE (IROW,JROW), (ICOLUM,JCOLUM), (AMAX,T,SWAP)
C
 100  DETERM = 1.0
      DO 110 J=1,N
 110  IPIVOT(J) = 0
      DO 300 I=1,N
C
C     SEARCH FOR PIVOT ELEMENT
C
        AMAX = 0.0
        DO 160 J=1,N
          IF (IPIVOT(J)-1) 120,160,120
 120      DO 150 K=1,N
            IF (IPIVOT(K)-1) 130,150,340
 130        IF (ABS(AMAX)-ABS(A(J,K))) 140,150,150
 140        IROW = J
            ICOLUM = K
            AMAX = A(J,K)
 150      CONTINUE
 160    CONTINUE
        IPIVOT(ICOLUM) = IPIVOT(ICOLUM)+1
```

```
C
C     INTERCHANGE ROWS TO PUT PIVOT ELEMENT ON DIAGONAL
C
        IF (IROW-ICOLUM) 170,210,170
 170    DETERM = -DETERM
        DO 180 L=1,N
          SWAP = A(IROW,L)
          A(IROW,L) = A(ICOLUM,L)
 180    A(ICOLUM,L) = SWAP
        IF (M) 210,210,190
 190    DO 200 L=1,M
          SWAP = B(IROW,L)
          B(IROW,L) = B(ICOLUM,L)
 200    B(ICOLUM,L) = SWAP
 210    INDEX(I,1) = IROW
        INDEX(I,2) = ICOLUM
        PIVOT(I) = A(ICOLUM,ICOLUM)
        DETERM = DETERM*PIVOT(I)
C
C     DIVIDE PIVOT ROW BY PIVOT ELEMENT
C
        A(ICOLUM,ICOLUM) = 1.0
        DO 220 L=1,N
 220    A(ICOLUM,L) = A(ICOLUM,L)/PIVOT(I)
        IF (M) 250,250,230
 230    DO 240 L=1,M
 240    B(ICOLUM,L) = B(ICOLUM,L)/PIVOT(I)
C
C     REDUCE NON-PIVOT ROWS
C
 250    DO 300 L1=1,N
          IF (L1-ICOLUM) 260,300,260
 260      T = A(L1,ICOLUM)
          A(L1,ICOLUM) = 0.0
          DO 270 L=1,N
 270      A(L1,L) = A(L1,L)-A(ICOLUM,L)*T
          IF (M) 300,300,280
 280      DO 290 L=1,M
 290      B(L1,L) = B(L1,L)-B(ICOLUM,L)*T
 300  CONTINUE
C
C     INTERCHANGE COLUMNS
C
      DO 330 I=1,N
        L = N+1-I
        IF (INDEX(L,1)-INDEX(L,2)) 310,330,310
 310    JROW = INDEX(L,1)
        JCOLUM = INDEX(L,2)
        DO 320 K=1,N
          SWAP = A(K,JROW)
          A(K,JROW) = A(K,JCOLUM)
          A(K,JCOLUM) = SWAP
 320    CONTINUE
 330  CONTINUE
 340  RETURN
      END
```

```
      PROGRAM TIMDIP
      DIMENSION B(899),W(899),A(899,97),X(97),DX(97),
     1WB(899),C(97,97),E(899)
      DIMENSION COL(97)
      CHARACTER *5 STA,COLUMN(97),u(97),src
      CHARACTER *10 ELIST,FILIN,FILOUT
C      CALL NOTRAP
      WRITE(6,1000)
1000  FORMAT(' TYPE IN NAME OF DATA FILE: '$)
      READ(5,1001)FILIN
1001  FORMAT(A10)
      WRITE(6,1002)
1002  FORMAT(' TYPE IN NAME OF EVENT LIST: '$)
      READ(5,1001)ELIST
      WRITE(6,1003)
1003  FORMAT(' TYPE IN NAME OF OUTPUT FILE: '$)
      READ(5,1001)FILOUT
      OPEN(FILE=FILOUT,UNIT=3)
      REWIND 3
      OPEN(FILE=ELIST,UNIT=1)
      REWIND 1
      WRITE(6,1004)
1004  FORMAT(' TYPE IN OFFSET DISTANCE: '$)
      READ(5,*)F
      write(3,666)F
 666  format(' Offset Distance: ',f5.2)
      I=1
20    READ(1,'(A5)',END=10)COLUMN(I)
      MM=I
      I=I+1
      GOTO 20
10    CLOSE(1)
        DO 9900 I=1,MM
           U(I)=COLUMN(I)
9900    CONTINUE
        I=1
        II=MM
9904    L=I+1
9905    DO 9906 J=L,II
           IF (U(J).EQ.U(I)) GO TO 9907
9906    CONTINUE
        I=I+1
        IF (I.EQ.II) GO TO 9908
        GO TO 9904
9907    II=II-1
        DO 9901 K=J,II
           U(K)=U(K+1)
9901    CONTINUE
        L=J
        GO TO 9905
9908    M=II
        iz=0
        do 9 k=1,m
           IF(U(k) (1:1).EQ.'Z')THEN
           IZ=IZ+1
           Endif
```

```
 9      continue
      DO 2 K=1,899
      B(K)=0.
      W(K)=0.
      WB(K)=0.
      E(K)=0.
      DO 2 L=1,97
      A(K,L)=0.
2     CONTINUE
      DO 3 I=1,97
      X(I)=0.
      DX(I)=0.
      DO 3 J=1,97
      C(I,J)=0.
3     CONTINUE
      I=1
      OPEN(FILE=FILIN,UNIT=1)
      REWIND 1
      DO 100 J=1,MM
      IF (COLUMN(J) (1:1).EQ.'Z')THEN
          READ(1,500)EVTIME
500       FORMAT(13X,F5.2)
60        READ(1,501,END=100)STA,TIME,NUMBER,DIST,AZIM
501       FORMAT(5X,A5,3X,F6.2,5X,I1,5X,F7.2,5X,F7.2)
          IF(STA.EQ.'XYZ')THEN
          GOTO 100
          ENDIF
                SRC=COLUMN(J)
                JJ=J
                DO 9913 K=1,M
                   IF (SRC.EQ.U(K)) THEN
                   JJ=K
                   GO TO 9914
                   ENDIF
9913            CONTINUE
9914      DO 40 L=1,M
          IF (STA.EQ.U(L))THEN
          LL=L
          GOTO 50
          ENDIF
40        CONTINUE
          GOTO 60
50        B(I)=TIME-EVTIME
          GOTO (110,120,130,140,150) NUMBER+1
110       W(I)=1./.03
          GOTO 160
120       W(I)=1./.06
          GOTO 160
130       W(I)=1./.15
          GOTO 160
140       W(I)=1./.3
          GOTO 160
150       W(I)=1./.5
160       A(I,JJ)=1.0
          A(I,IZ+1)=DIST
          A(I,IZ+2)=(2*F-DIST)*SIN(AZIM/57.3)
```

```
            A(I,IZ+3)=(2*F-DIST)*COS(AZIM/57.3)
            I=I+1
            GOTO 60
         ENDIF
100      CONTINUE
         CLOSE(1)
         M=IZ+3
         N=I-1
         WRITE(3,*)N,M
         IF (M.GE.N)THEN
         WRITE(3,201)M,N
201      FORMAT('UNDERDETERMINED MATRIX M,N = ',I3,3X,I3)
         CLOSE(3)
         STOP
         ENDIF
         DO 199 I=1,M
199      COL(I)=0.
         DO 198 I=1,M
         DO 198 J=1,N
198      COL(I)=A(J,I)+COL(I)
         DO 197 I=1,M
         IF (COL(I).EQ.0.)THEN
         WRITE(3,196)U(I)
196      FORMAT('NO ARRIVALS FOR ',A5)
         CLOSE(3)
         STOP
         ENDIF
197      CONTINUE
         DO 200 I=1,N
         WB(I)=W(I)*B(I)
         DO 200 J=1,M
         A(I,J)=W(I)*A(I,J)
200      CONTINUE
         DO 210 J=1,M
         DO 210 I=1,N
         X(J)=A(I,J)*WB(I)+X(J)
210      CONTINUE
         DO 220 I=1,M
         DO 220 J=1,M
         DO 220 K=1,N
         C(I,J)=A(K,I)*A(K,J)+C(I,J)
220      CONTINUE
         CALL INVR(C,M,X,1,DETERM,97,97)
         DO 230 I=1,N
         E(I)=B(I)
         DO 230 J=1,M
         E(I)=E(I)-A(I,J)*X(J)/W(I)
230      CONTINUE
         ERR=0.
         DO 240 I=1,N
240      ERR=ERR+(E(I)*W(I))**2
         WRITE(3,*)ERR
         ERR=ERR/(N-M)
         sds=sqrt(err)
         write(3,241)sds
241      format(/' std. dev. soln.= ',e12.6/)
```

```
      DO 250 I=1,M
250   DX(I)=SQRT(ERR*C(I,I))
      WRITE(3,505)U(M-2)
505   FORMAT(A5,' SET TO ZERO')
      U(M-2)='VEL'
      U(M-1)=' A '
      U(M)=' B '
      WRITE(3,504)(U(K),X(K),DX(K),K=1,M-3)
504   FORMAT(A5,5X,F10.2,5X,F10.2)
      WRITE(3,509) (U(K),X(K),DX(K),K=M-2,M)
509   FORMAT(A5,5X,G11.5,5X,G11.5)
      DO 300 I=M-2,M-1
      DO 300 J=I+1,M
      WRITE(3,511)I,J,ERR*C(I,J)
511   FORMAT(I3,5X,I3,5X,G11.5)
300   CONTINUE
      X(M-2)=1/X(M-2)
      DX(M-2)=X(M-2)**2*DX(M-2)
      DO 310 K=M-1,M
      DX(K)=SQRT(X(M-2)**4*DX(K)**2+4*(X(M-2)*X(K)*DX(M-2))**2+
     14*X(M-2)**3*X(K)*ERR*C(M-2,K))
310   X(K)=X(M-2)**2*X(K)
      WRITE(3,509) (U(K),X(K),DX(K),K=M-2,M)
      CLOSE(3)
      STOP
      END
      SUBROUTINE INVR(A,N,B,M,DETERM,ISIZE,JSIZE)
C   INVR - UW MATRIX INVERSION AND SYSTEM OF EQUATION SOLVER
C        INVR SOLVES THE MATRIX EQUATION AX=B AND RETURNS THE INVERSE
C             OF A IN THE STORAGE LOCATIONS OF A
C        SEE UW COMPUTER CENTER WRITEUP W00042 FOR DETAILS OF USAGE,
C             AVAILABLE AT THE COMPUTER CENTER LIBRARY
      DIMENSION IPIVOT(200), A(ISIZE,JSIZE), B(ISIZE,M), INDEX(200,2),
     $ PIVOT(200)
      EQUIVALENCE (IROW,JROW), (ICOLUM,JCOLUM), (AMAX,T,SWAP)
C
 100  DETERM = 1.0
      DO 110 J=1,N
 110  IPIVOT(J) = 0
      DO 300 I=1,N
C
C     SEARCH FOR PIVOT ELEMENT
C
        AMAX = 0.0
        DO 160 J=1,N
          IF (IPIVOT(J)-1) 120,160,120
 120      DO 150 K=1,N
            IF (IPIVOT(K)-1) 130,150,340
 130        IF (ABS(AMAX)-ABS(A(J,K))) 140,150,150
 140        IROW = J
            ICOLUM = K
            AMAX = A(J,K)
 150      CONTINUE
 160    CONTINUE
        IPIVOT(ICOLUM) = IPIVOT(ICOLUM)+1
C
```

```
C      INTERCHANGE ROWS TO PUT PIVOT ELEMENT ON DIAGONAL
C
         IF (IROW-ICOLUM) 170,210,170
 170     DETERM = -DETERM
         DO 180 L=1,N
           SWAP = A(IROW,L)
           A(IROW,L) = A(ICOLUM,L)
 180     A(ICOLUM,L) = SWAP
         IF (M) 210,210,190
 190     DO 200 L=1,M
           SWAP = B(IROW,L)
           B(IROW,L) = B(ICOLUM,L)
 200     B(ICOLUM,L) = SWAP
 210     INDEX(I,1) = IROW
         INDEX(I,2) = ICOLUM
         PIVOT(I) = A(ICOLUM,ICOLUM)
         DETERM = DETERM*PIVOT(I)
C
C      DIVIDE PIVOT ROW BY PIVOT ELEMENT
C
         A(ICOLUM,ICOLUM) = 1.0
         DO 220 L=1,N
 220     A(ICOLUM,L) = A(ICOLUM,L)/PIVOT(I)
         IF (M) 250,250,230
 230     DO 240 L=1,M
 240     B(ICOLUM,L) = B(ICOLUM,L)/PIVOT(I)
C
C      REDUCE NON-PIVOT ROWS
C
 250     DO 300 L1=1,N
           IF (L1-ICOLUM) 260,300,260
 260       T = A(L1,ICOLUM)
           A(L1,ICOLUM) = 0.0
           DO 270 L=1,N
 270       A(L1,L) = A(L1,L)-A(ICOLUM,L)*T
           IF (M) 300,300,280
 280       DO 290 L=1,M
 290       B(L1,L) = B(L1,L)-B(ICOLUM,L)*T
 300   CONTINUE
C
C      INTERCHANGE COLUMNS
C
       DO 330 I=1,N
         L = N+1-I
         IF (INDEX(L,1)-INDEX(L,2)) 310,330,310
 310     JROW = INDEX(L,1)
         JCOLUM = INDEX(L,2)
         DO 320 K=1,N
           SWAP = A(K,JROW)
           A(K,JROW) = A(K,JCOLUM)
           A(K,JCOLUM) = SWAP
 320     CONTINUE
 330   CONTINUE
 340   RETURN
       END
```

```
      PROGRAM TIMDIS
      DIMENSION B(899),W(899),A(899,97),X(97),DX(97),
     1WB(899),C(97,97),E(899)
      DIMENSION COL(97)
      CHARACTER *5 STA,COLUMN(97),u(97),src
      CHARACTER *10 ELIST,FILIN,FILOUT
c      CALL NOTRAP
      WRITE(6,1000)
1000  FORMAT(' TYPE IN NAME OF DATA FILE: '$)
      READ(5,1001)FILIN
1001  FORMAT(A10)
      WRITE(6,1002)
1002  FORMAT(' TYPE IN NAME OF EVENT LIST: '$)
      READ(5,1001)ELIST
      WRITE(6,1003)
1003  FORMAT(' TYPE IN NAME OF OUTPUT FILE: '$)
      READ(5,1001)FILOUT
      OPEN(FILE=FILOUT,UNIT=3)
      REWIND 3
      OPEN(FILE=ELIST,UNIT=1)
      REWIND 1
      WRITE(6,1004)
1004  FORMAT(' TYPE IN OFFSET DISTANCE: '$)
      READ(5,*)F
      write(3,666)F
 666  format(' Offset Distance: ',f5.2)
      I=1
20    READ(1,'(A5)',END=10)COLUMN(I)
      MM=I
      I=I+1
      GOTO 20
10    CLOSE(1)
        DO 9900 I=1,MM
           U(I)=COLUMN(I)
9900    CONTINUE
        I=1
        II=MM
9904    L=I+1
9905    DO 9906 J=L,II
           IF (U(J).EQ.U(I)) GO TO 9907
9906    CONTINUE
        I=I+1
        IF (I.EQ.II) GO TO 9908
        GO TO 9904
9907    II=II-1
        DO 9901 K=J,II
           U(K)=U(K+1)
9901    CONTINUE
        L=J
        GO TO 9905
9908    M=II
      DO 2 K=1,899
      B(K)=0.
      W(K)=0.
      WB(K)=0.
      E(K)=0.
```

```
      DO 2 L=1,97
      A(K,L)=0.
2     CONTINUE
      DO 3 I=1,97
      X(I)=0.
      DX(I)=0.
      DO 3 J=1,97
      C(I,J)=0.
3     CONTINUE
      I=1
      OPEN(FILE=FILIN,UNIT=1)
      REWIND 1
      DO 100 J=1,MM
      IF (COLUMN(J) (1:1).EQ.'Z')THEN
          READ(1,500)EVTIME
500       FORMAT(13X,F5.2)
60        READ(1,501,END=100)STA,TIME,NUMBER,DIST,AZIM
501       FORMAT(5X,A5,3X,F6.2,5X,I1,5X,F7.2,5X,F7.2)
          IF(STA.EQ.'XYZ')THEN
          GOTO 100
          ENDIF
                SRC=COLUMN(J)
                JJ=J
                DO 9913 K=1,M
                   IF (SRC.EQ.U(K)) THEN
                   JJ=K
                   GO TO 9914
                   ENDIF
9913            CONTINUE
9914      DO 40 L=1,M
          IF (STA.EQ.U(L))THEN
          LL=L
          GOTO 50
          ENDIF
40        CONTINUE
          GOTO 60
50        B(I)=TIME-EVTIME
          GOTO (110,120,130,140,150) NUMBER+1
110       W(I)=1./.03
          GOTO 160
120       W(I)=1./.06
          GOTO 160
130       W(I)=1./.15
          GOTO 160
140       W(I)=1./.3
          GOTO 160
150       W(I)=1./.5
160       A(I,JJ)=1.0
          IF (LL.NE.M)THEN
          A(I,LL)=1.0
          ENDIF
          A(I,M)=DIST
          A(I,M+1)=(2*F-DIST)*DIST
          I=I+1
          GOTO 60
      ENDIF
```

```
100   CONTINUE
      CLOSE(1)
      M=M+1
      N=I-1
      WRITE(3,*)N,M
      IF (M.GE.N)THEN
      WRITE(3,201)M,N
201   FORMAT('UNDERDETERMINED MATRIX M,N = ',I3,3X,I3)
      CLOSE(3)
      STOP
      ENDIF
      DO 199 I=1,M
199   COL(I)=0.
      DO 198 I=1,M
      DO 198 J=1,N
198   COL(I)=A(J,I)+COL(I)
      DO 197 I=1,M
      IF (COL(I).EQ.0.)THEN
      WRITE(3,196)U(I)
196   FORMAT('NO ARRIVALS FOR ',A5)
      CLOSE(3)
      STOP
      ENDIF
197   CONTINUE
      DO 200 I=1,N
      WB(I)=W(I)*B(I)
      DO 200 J=1,M
      A(I,J)=W(I)*A(I,J)
200   CONTINUE
      DO 210 J=1,M
      DO 210 I=1,N
      X(J)=A(I,J)*WB(I)+X(J)
210   CONTINUE
      DO 220 I=1,M
      DO 220 J=1,M
      DO 220 K=1,N
      C(I,J)=A(K,I)*A(K,J)+C(I,J)
220   CONTINUE
      CALL INVR(C,M,X,1,DETERM,97,97)
      DO 230 I=1,N
      E(I)=B(I)
      DO 230 J=1,M
      E(I)=E(I)-A(I,J)*X(J)/W(I)
230   CONTINUE
      ERR=0.
      DO 240 I=1,N
240   ERR=ERR+(E(I)*W(I))**2
      WRITE(3,*)ERR
      ERR=ERR/(N-M)
      sds=sqrt(err)
      write(3,241)sds
241   format(/' std. dev. soln.= ',e12.6/)
      DO 250 I=1,M
250   DX(I)=SQRT(ERR*C(I,I))
      WRITE(3,505)U(M-1)
505   FORMAT(A5,' SET TO ZERO')
```

```
      U(M-1)='VEL'
      U(M)='W1 '
      WRITE(3,504)(U(K),X(K),DX(K),K=1,M-2)
504   FORMAT(A5,5X,F10.2,5X,F10.2)
      WRITE(3,507) (U(K),X(K),DX(K),K=M-1,M)
507   FORMAT(A5,5X,G11.5,5X,G11.5)
      WRITE(3,508) ERR*C(M-1,M)
508   FORMAT('COV = ',G11.5)
      X(M-1)=1/X(M-1)
      DX(M-1)=X(M-1)**2*DX(M-1)
      DX(M)=SQRT(X(M-1)**4*DX(M)**2+4*(X(M-1)*X(M)*DX(M-1))**2+
     14*X(M-1)**3*X(M)*ERR*C(M-1,M))
      X(M)=X(M-1)**2*X(M)
      WRITE(3,507) (U(K),X(K),DX(K),K=M-1,M)
      CLOSE(3)
      STOP
      END
      SUBROUTINE INVR(A,N,B,M,DETERM,ISIZE,JSIZE)
C   INVR - UW MATRIX INVERSION AND SYSTEM OF EQUATION SOLVER
C        INVR SOLVES THE MATRIX EQUATION AX=B AND RETURNS THE INVERSE
C             OF A IN THE STORAGE LOCATIONS OF A
C        SEE UW COMPUTER CENTER WRITEUP W00042 FOR DETAILS OF USAGE,
C             AVAILABLE AT THE COMPUTER CENTER LIBRARY
      DIMENSION IPIVOT(200), A(ISIZE,JSIZE), B(ISIZE,M), INDEX(200,2),
     $ PIVOT(200)
      EQUIVALENCE (IROW,JROW), (ICOLUM,JCOLUM), (AMAX,T,SWAP)
C
 100  DETERM = 1.0
      DO 110 J=1,N
 110  IPIVOT(J) = 0
      DO 300 I=1,N
C
C     SEARCH FOR PIVOT ELEMENT
C
        AMAX = 0.0
        DO 160 J=1,N
          IF (IPIVOT(J)-1) 120,160,120
 120      DO 150 K=1,N
            IF (IPIVOT(K)-1) 130,150,340
 130        IF (ABS(AMAX)-ABS(A(J,K))) 140,150,150
 140        IROW = J
            ICOLUM = K
            AMAX = A(J,K)
 150      CONTINUE
 160    CONTINUE
        IPIVOT(ICOLUM) = IPIVOT(ICOLUM)+1
C
C     INTERCHANGE ROWS TO PUT PIVOT ELEMENT ON DIAGONAL
C
        IF (IROW-ICOLUM) 170,210,170
 170    DETERM = -DETERM
        DO 180 L=1,N
          SWAP = A(IROW,L)
          A(IROW,L) = A(ICOLUM,L)
 180    A(ICOLUM,L) = SWAP
        IF (M) 210,210,190
```

```
 190     DO 200 L=1,M
           SWAP = B(IROW,L)
           B(IROW,L) = B(ICOLUM,L)
 200     B(ICOLUM,L) = SWAP
 210     INDEX(I,1) = IROW
         INDEX(I,2) = ICOLUM
         PIVOT(I) = A(ICOLUM,ICOLUM)
         DETERM = DETERM*PIVOT(I)
C
C      DIVIDE PIVOT ROW BY PIVOT ELEMENT
C
         A(ICOLUM,ICOLUM) = 1.0
         DO 220 L=1,N
 220     A(ICOLUM,L) = A(ICOLUM,L)/PIVOT(I)
         IF (M) 250,250,230
 230     DO 240 L=1,M
 240     B(ICOLUM,L) = B(ICOLUM,L)/PIVOT(I)
C
C      REDUCE NON-PIVOT ROWS
C
 250     DO 300 L1=1,N
           IF (L1-ICOLUM) 260,300,260
 260       T = A(L1,ICOLUM)
           A(L1,ICOLUM) = 0.0
           DO 270 L=1,N
 270       A(L1,L) = A(L1,L)-A(ICOLUM,L)*T
           IF (M) 300,300,280
 280       DO 290 L=1,M
 290       B(L1,L) = B(L1,L)-B(ICOLUM,L)*T
 300   CONTINUE
C
C      INTERCHANGE COLUMNS
C
       DO 330 I=1,N
         L = N+1-I
         IF (INDEX(L,1)-INDEX(L,2)) 310,330,310
 310     JROW = INDEX(L,1)
         JCOLUM = INDEX(L,2)
         DO 320 K=1,N
           SWAP = A(K,JROW)
           A(K,JROW) = A(K,JCOLUM)
           A(K,JCOLUM) = SWAP
 320     CONTINUE
 330   CONTINUE
 340   RETURN
       END
```

This dissertation is accepted on behalf of the faculty of the Institute by the following committee:

Advisor

April 25, 1989

Date